Title

Structural Behavior of a Two Span Reinforced Concrete Box Girder Bridge Model, Vol. II -- Reduction, Analysis and Interpretation of Results

Authors

Scordelis, Alex
Bouwkamp, Jack
Wasti, Syed

Publication Date

1971-10-01

REPORT NO.
UC SESM 71-16

STRUCTURES AND MATERIALS RESEARCH
DEPARTMENT OF CIVIL ENGINEERING

STRUCTURAL BEHAVIOR OF A TWO SPAN REINFORCED CONCRETE BOX GIRDER BRIDGE MODEL

VOL. II - REDUCTION, ANALYSIS AND INTERPRETATION OF RESULTS

by
A. C. SCORDELIS
J. G. BOUWKAMP
S. T. WASTI

Report to the Sponsors: Division of Highways, Department of Public Works, State of California, and the Bureau of Public Roads, Federal Highway Administration, United States Department of Transportation.

OCTOBER 1971

COLLEGE OF ENGINEERING
OFFICE OF RESEARCH SERVICES
UNIVERSITY OF CALIFORNIA
BERKELEY CALIFORNIA

Structures and Materials Research
Department of Civil Engineering
Division of Structural Engineering
and
Structural Mechanics

UC-SESM Report No. 71-16

STRUCTURAL BEHAVIOR OF A TWO SPAN REINFORCED CONCRETE BOX GIRDER BRIDGE MODEL

VOL. II - REDUCTION, ANALYSIS AND INTERPRETATION OF RESULTS

by

A. C. Scordelis

J. G. Bouwkamp

Professors of Civil Engineering

and

S. T. Wasti

Assistant Research Engineer

to

the Division of Highways
Department of Public Works
State of California
Under Research Technical Agreement
No. 13945-14423
and
U.S. Department of Transportation
Federal Highway Administration
Bureau of Public Roads

College of Engineering
Office of Research Services
University of California
Berkeley, California

October 1971

ABSTRACT

A detailed presentation of the reduction, analysis and interpretation of the experimental and theoretical results obtained in testing a large scale two span, four cell, reinforced concrete box girder bridge model is given. The various computer programs used in obtaining theoretical results are described and compared. The methods and computer programs used for reduction of experimental data are also presented. Results, in terms of reactions, deflections, strains and moments, for the response of the bridge to dead load, working stress loads and at over load stress levels are given and comparisons between experimental and theoretical values are made. A review of the behavior under sustained dead load during the load history of the model is given with respect to strains, deflections and cracking. The loading to failure, and observations of structural behavior during this final phase are considered in detail.

KEYWORDS

Box girder bridges; bridge model; cellular structures; continuous box girder; model testing; experimental study; harmonic analysis; direct stiffness method; finite element method; computer programs; bridge analysis; bridge design; reinforced concrete.

TABLE OF CONTENTS

Page

LIST OF TABLES

LIST OF FIGURES

1. INTRODUCTION

1.1 General Remarks

The present volume is the second of a three volume sequence on the "Structural Behavior of a Two Span Reinforced Concrete Box Girder Bridge Model". The material included in each volume is as follows:

Vol. I - Design, Construction, Instrumentation and Loading

Vol. II - Reduction, Analysis and Interpretation of Results

Vol. III - Detailed Tables of Experimental and Analytical Results

These volumes deal with the complete experimental and analytical study of a 72 ft. long, 12 ft. wide and 1 ft. 8 9/16 in. deep box girder bridge model built and tested in the Structural Engineering Materials Laboratory (S.E.M.L) of the University of California, Berkeley. Concrete dimensions, location and amounts of reinforcing steel, instrumentation and loading used for the model have been described in detail in Vol. I. For easy reference in the present volume, Figs. 1 and 2 depict the general dimensions of the model and the designation of transverse sections and longitudinal girder lines which are of pertinent interest.

1.2 Scope of Volume II

The present volume comprises the analysis of experimental data from the box girder bridge model. While the main emphasis is placed on the part dealing with load distribution properties of the box girder bridge at working stresses, the dead load and overload cases and the whole history of the bridge are also treated in detail. Experimental data reduction is described, and data is presented for almost all loading cases of interest. Theoretical values obtained from the MUPDI3, FINPLA2 and 1DFRAME computer programs are also given.

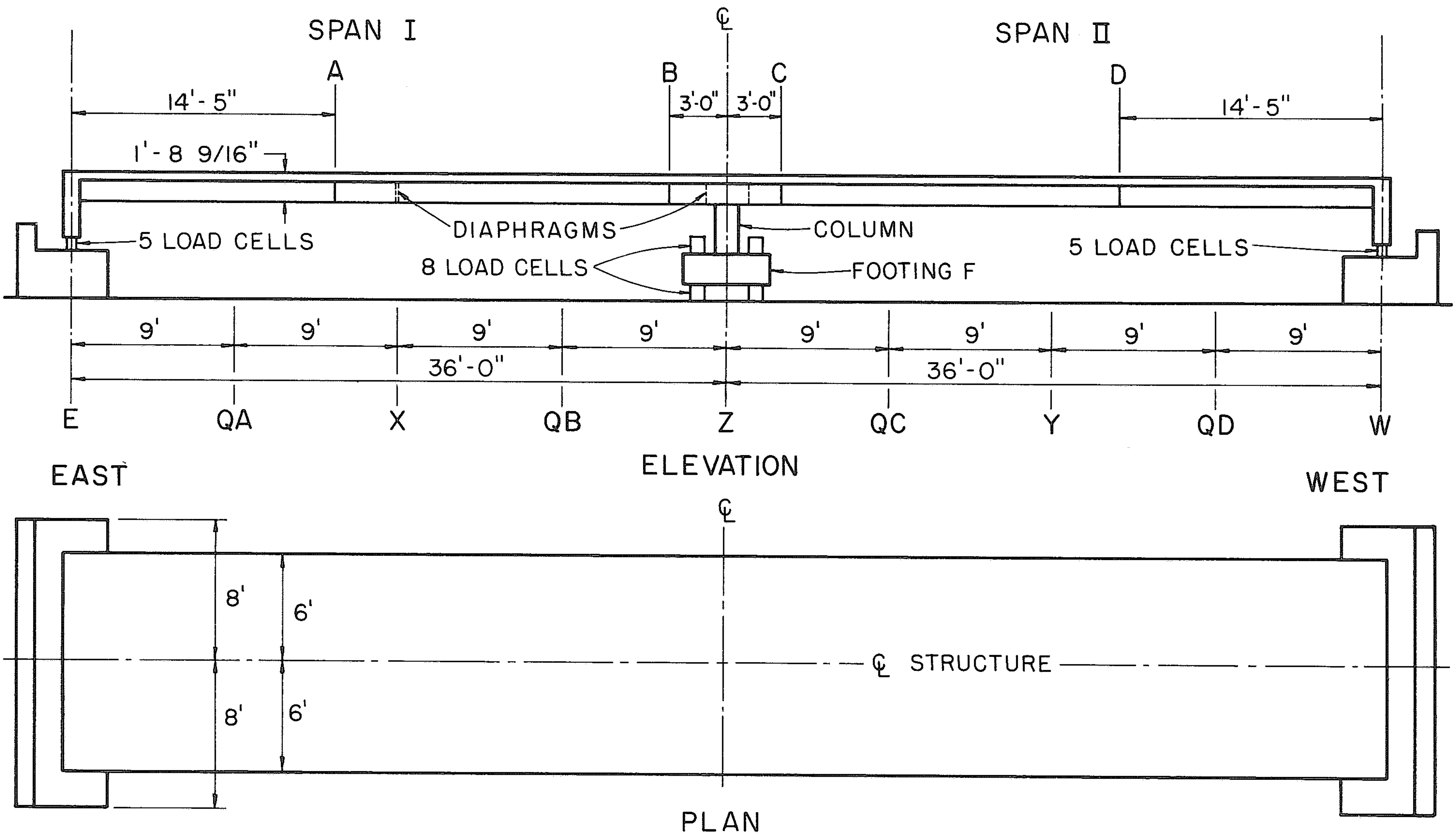

FIG. 1 DIMENSIONS OF BOX GIRDER BRIDGE MODEL WITH TRANSVERSE LOCATIONS

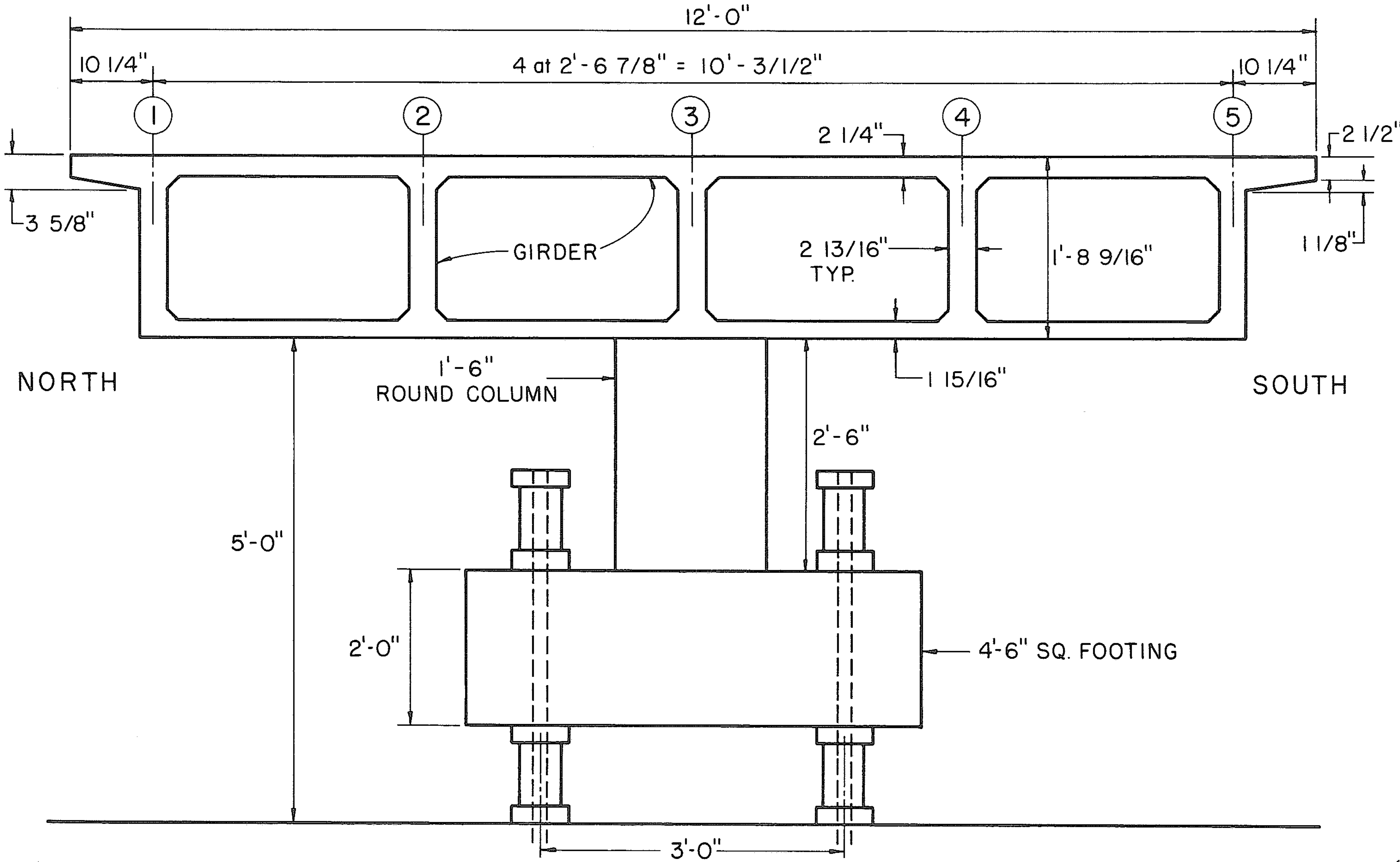

FIG. 2 TYPICAL SECTION OF BOX GIRDER BRIDGE MODEL

Each presentation of theoretical and experimental results is accompanied by interpretation and discussion with special reference to correlations and corroborations between the sets of results, checks for superposition and symmetry, and evaluation of the effect of the midspan diaphragm. Where possible, implications of the results with regard to design are considered.

Of particular interest from a load distribution standpoint at the working stress level is how accurate the proposed theoretical methods predict the results found in the experimental study with respect to the following two important items for a load anywhere on the bridge.

1. The total moment at the midspan Sections A and D and at the support Sections B and C.

2. The transverse distribution of these total moments at a section across the width of the bridge.

General tables comparing theoretical and experimental results for reactions, deflections, strains, longitudinal stresses and moments are given in Volume III for all load cases considered. Selected typical cases are taken from these tables and discussed in detail in the present volume. Results for dead load and for live loads producing a working stress of 30 ksi in the steel reinforcement are considered at length. Response of the bridge at and after overload stresses of 40, 50 and 60 ksi in the reinforcement is also examined. The linearity of the structural response during the overloading as well as afterwards is studied.

Attention is paid to the interpretation and applicability of theoretical results given by different analytical models. The relative merits of the folded plate and finite element approaches are discussed, and comparisons are also made with results obtained by idealizing the box girder bridge model as a planar longitudinal frame composed of one dimensional members.

In addition, the whole scheme of cataloguing, classifying and editing experimental data in four specially prepared computer programs giving normalized results for comparison with theoretical values is also treated in Volume II. These comparisons are made mainly for reactions, deflections, strains and moments. In most cases, pertinent theoretical and experimental data are presented in the text.

A study is also made of the history of strains at different locations in the box girder bridge model. The deterioration of the structure after the completion of each succeeding load phase and as indicated by cracking patterns for each load phase is presented.

The loading to failure and observations of structural behavior during this final phase are considered in detail.

Lastly, a critical evaluation of the entire experimental study, incorporating conclusions reached and recommendations for implementation is presented.

2. INTERPRETATION OF THEORETICAL RESULTS FOR BRIDGE MODEL

2.1 General Remarks

Three different analytical methods were used in various phases of the theoretical studies for the model. The computer programs associated with these three analytical solutions are entitled: (1) MUPDI3; (2) FINPLA2; (3) 1DFRAME. A brief description of these programs is given below.

MUPDI3 Program

This program can be utilized to analyse open or cellular folded plate structures simply supported at the two ends and having up to twelve interior diaphragms or supports between the two ends. Diaphragms may be defined by flexible beams and supports may be defined by two dimensional planar rigid frame bents. Options permit evaluation of internal forces in the frame bents as well as in the bridge. A direct stiffness harmonic analysis based on the elasticity theory is used for the folded plate system. Compatibility at the interior diaphragms or supports is accomplished by a force method of analysis. Loads and redundant forces may be approximated by up to 100 non-zero terms of the appropriate Fourier series.

FINPLA2 Program

This program can analyze general non-prismatic cellular structures of varying width and depth and may have an integrated three-dimensional frame. The structure is discretized by dividing it longitudinally into a certain number of structure segments by vertical sections, and by subdividing each such segment into finite elements. The structure alignment is described by a longitudinal reference line which may be a straight line, a circular curve or an arbitrary planar string polygon and cross-sections are defined with respect to this line. Orthotropic plate properties and arbitrary loadings and boundary conditions can be treated. Automatic element and coordinate generation options minimize the required input data.

1DFRAME Program

This program can analyze simple planar frames made up of one dimensional members such as beams and columns. A direct stiffness analysis is used to determine displacements and member forces due to any desired loading on the frame.

MUPDI3 and FINPLA2 represent the latest available versions of the original programs MUPDI and FINPLA which have been briefly described in Vol. I and in detail in [1, 2, 5].

For the MUPDI3 analysis, 100 harmonics were used to approximate the applied loading in each case. This program treats the center single column bent as a transverse planar rigid frame, and therefore it cannot account for the longitudinal bending moment developed at the base of the column under unsymmetrical loadings in the two spans. For symmetrical loadings it yields a very accurate solution. The program analyzes a single load case for each input.

For the FINPLA2 analysis, the bridge was subdivided transversely by selecting nodal points at the top and bottom of each web and at the edges of the cantilever overhangs. This resulted in 15 finite elements transversely. Longitudinally the bridge was subdivided into 30 segments. Due account was taken of the variation in modulus of elasticity throughout the bridge and the flares in the web thicknesses. Because the center single column bent is assumed to be a three dimensional frame, the longitudinal bending stiffness of the column is included and therefore FINPLA2 can be used for unsymmetrical as well as symmetrical loads in the two spans. The program can treat multiple load cases for each input.

For the 1D FRAME analysis, the bridge is assumed to be a simple planar longitudinal frame made up of three members. Two of these are horizontal members each having a length equal to 36 ft. and a moment of inertia of 2.64 $ft.^4$, which is obtained by considering the entire bridge cross-section, Fig. 2, to be an uncracked beam section. The third member is the vertical circular column, Figs. 1 and 2, which has a length from the top of the footing to the centroid of the bridge cross-section of 3.43 ft. and a moment of inertia of 0.249 ft^4. The modulus of elasticity is assumed constant in this analysis. It is obvious that 1DFRAME can only be used to give an indication of the longitudinal distrubution of total reactions and moments, but gives no information on the transverse distribution of these quantities or the internal membrane forces and plate bending moments in each plate element which are obtained from the more complex MUPDI3 and FINPLA2 programs.

In order to give some idea of the computer times involved on a CDC 6400 for solutions of the bridge model by these programs, a summary is given below in Table 1. CP time stands for central computer processing time and PP time stands for peripheral unit processing time which has a cost charged at about 0.8 CP time for large problems of

TABLE 1 - CDC 6400 COMPUTER TIMES FOR BRIDGE MODEL ANALYSES

Computer Program	CP Time (Seconds)	PP Time (Seconds)
MUPDI3 (1 load case)	225	112
FINPLA2 (9 load cases)		
Compilation	50	
Input Setup	53	
Load matrix	7	
Structure stiffness	54	
Solution of equations	229	
Output generation	295	
Total	688	1531
1DFRAME (1 load case)	3	15

this type. For the times given for FINPLA2, about 1/3 to 1/2 of the total cost can be assigned to the first load case with the remainder being spread among the other eight load cases.

In the remainder of this Chapter, selected theoretical results obtained by the three programs will be presented and compared. The extent to which deflection and strains predicted by the above theories, which are based on an uncracked homogeneous bridge model, can be used to provide a realistic comparison with resultsobtained experimentally on a cracked model will be discussed. Methods of modifying theoretical results to account for cracking will be suggested.

2.2 Theoretical Results For 1DFRAME Analysis

Results obtained by 1DFRAME Program for reactions, deflections, and moments are shown in Figs 3, 4, 5 and 6. Loading cases considered are a uniform dead load of 2.44 kips/ft; a midspan load of 100 kips in Span I; a midspan load of 100 kips in Span II; and midspan loads of 100 kips in both Spans I and II. The values given form a useful reference and it will be of particular interest to study whether this simple analysis can be used to accurately predict the total reactions and moments found from the more complete analyses of MUPDI3 and FINPLA2 as well as from the experimental results. Results from 1DFRAME are completely independent of the transverse position of the load on the bridge model. The 1DFRAME solution gives internal moments that are in exact agreement with external moments computed from reactions.

2.3 Comparison of Theoretical Results

2.3.1 Loads at Both Midspans

For this longitudinally symmetrical loading in the two spans, Fig. 7 shows theoretical results for total internal moments at various

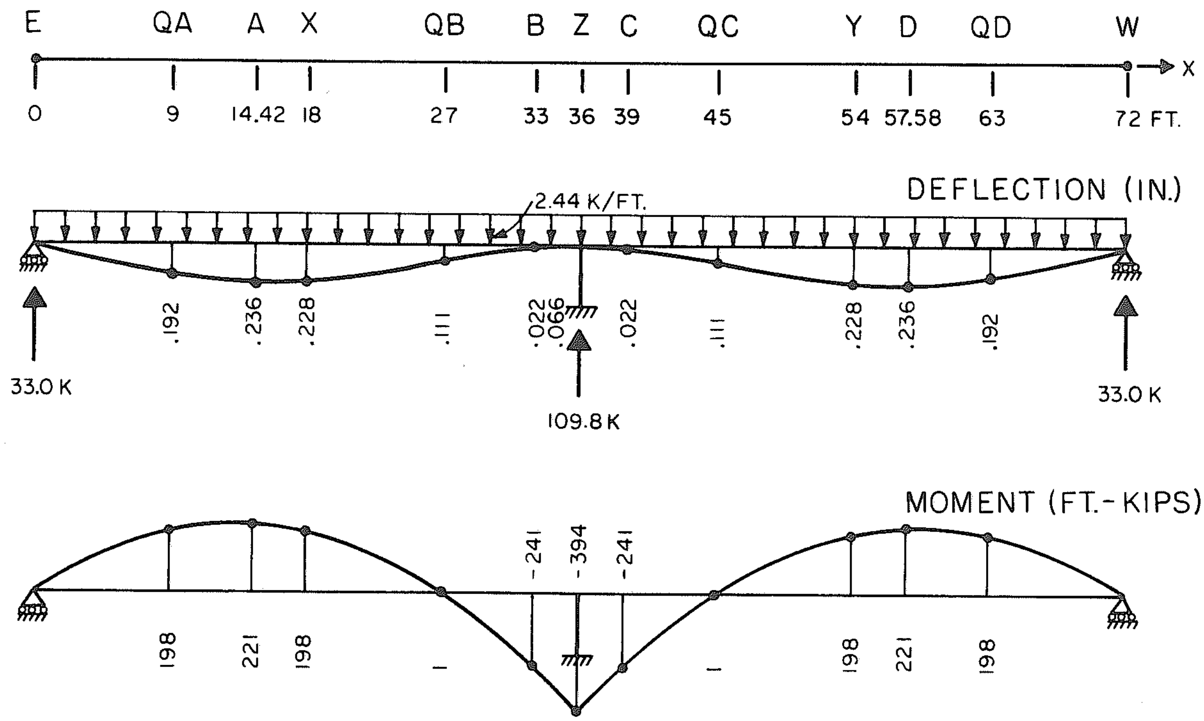

FIG. 3 1DFRAME RESULTS FOR DEAD LOAD OF 2.44 KIPS PER FT.

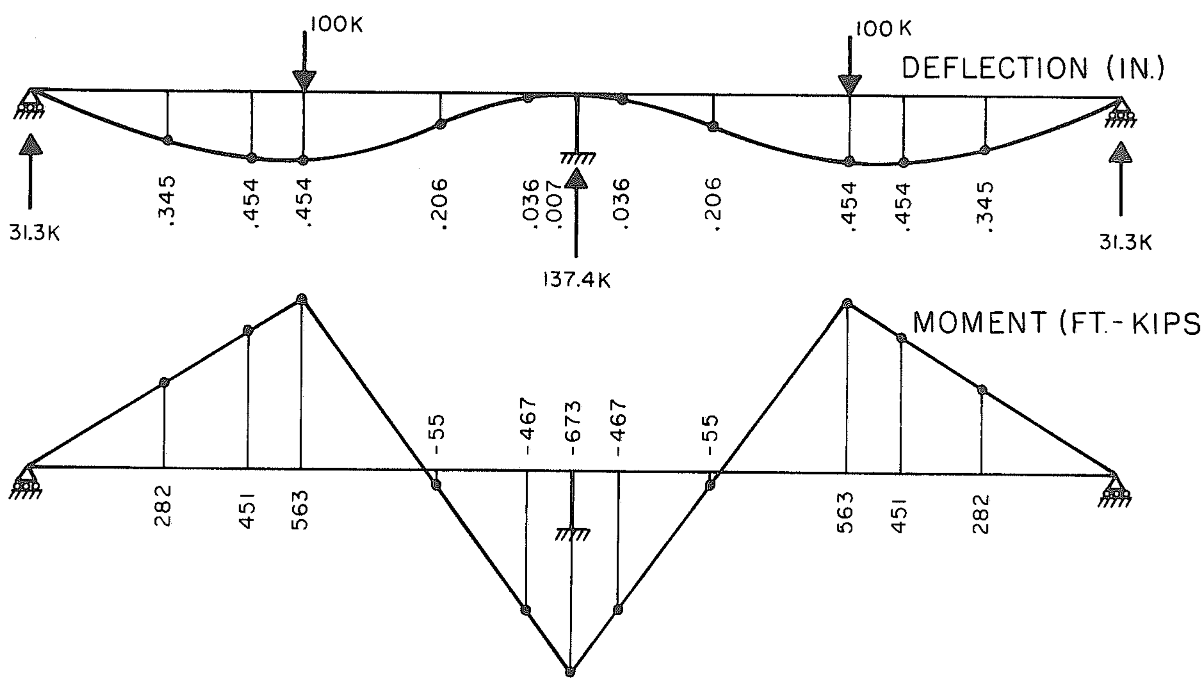

FIG. 4 1DFRAME RESULTS FOR 100 KIP MIDSPAN LOADS IN SPANS I AND II

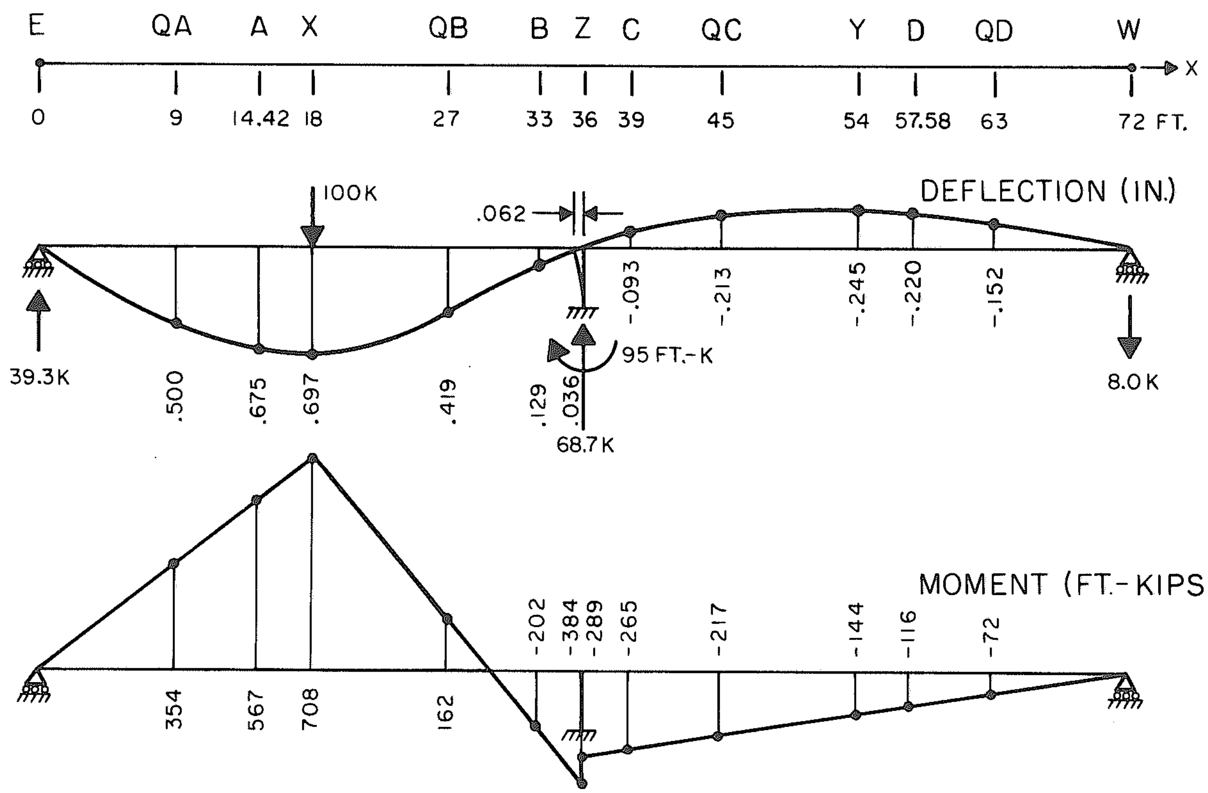

FIG. 5 1DFRAME RESULTS FOR 100 KIP MIDSPAN LOAD IN SPAN I

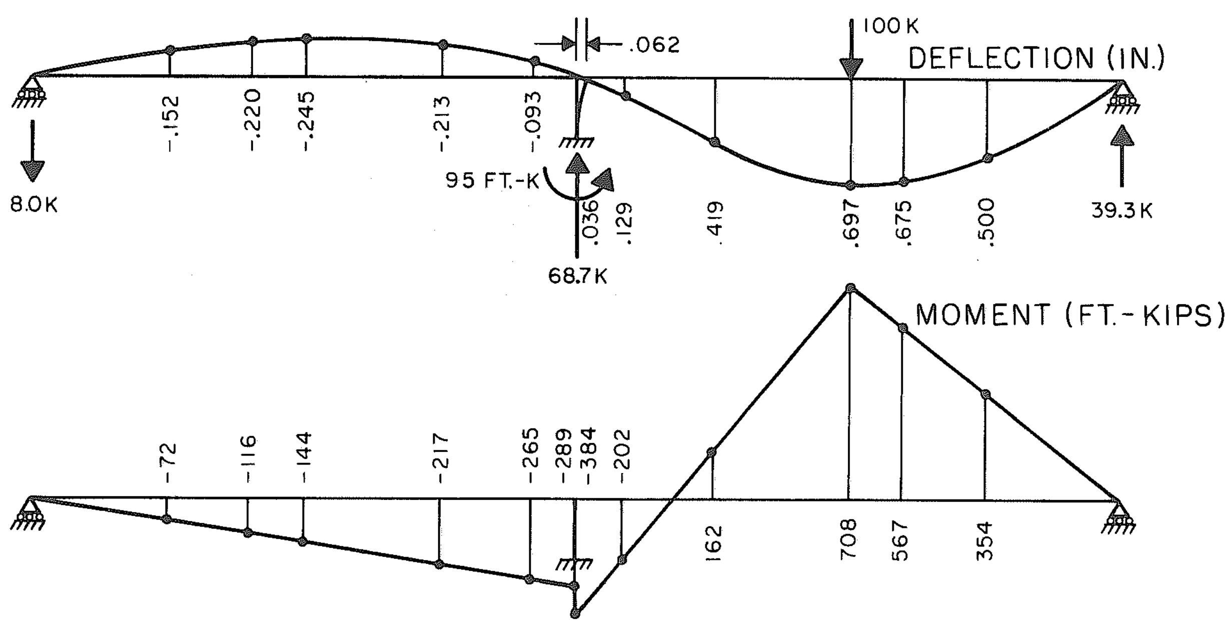

FIG. 6 1DFRAME RESULTS FOR 100 KIP MIDSPAN LOAD IN SPAN II sections by 1DFRAME, MUPDI3 and FINPLA2 and for total reactions by 1DFRAME and FINPLA2. MUPDI3 does not print out values for reactions. Results are given for MUPDI3 or FINPLA2 for transverse load positions on girders 1, 2 or 3.

The total internal moment at a section and its distribution to each girder are found in MUPDI3 and FINPLA2 by automatic subroutines which perform the operations described below.

The actual box girder bridge cross-section is first divided into a number of similar interior I girders plus two exterior girders. Each interior girder consists of a web and a top and bottom flange equal in width to the web spacing while each exterior girder consists of an exterior web with a top flange extending from the midpoint between girder webs to the edge of the cantilever overhang and the bottom flange being equal in width to half of the web spacing. Thus the bridge model, shown in Fig. 2,has three interior girders 2, 3 and 4 and two exterior girders 1 and 5.

The girder moment at any section taken by an individual girder can be found by integrating the longitudinal membrane stresses, over the proper slab and web areas to obtain forces and then multiplying these forces by their respective lever arms to the neutral axis of the gross uncracked section. The small contribution of the longitudinal slab moments is also included. The girder moments, at a particular section, can then be summed to determine the total moment on an entire cross-section. This was done for the sections indicated in Fig. 7. Each girder moment can then be divided by the total moment at a section to determine the percentage distribution to each girder.

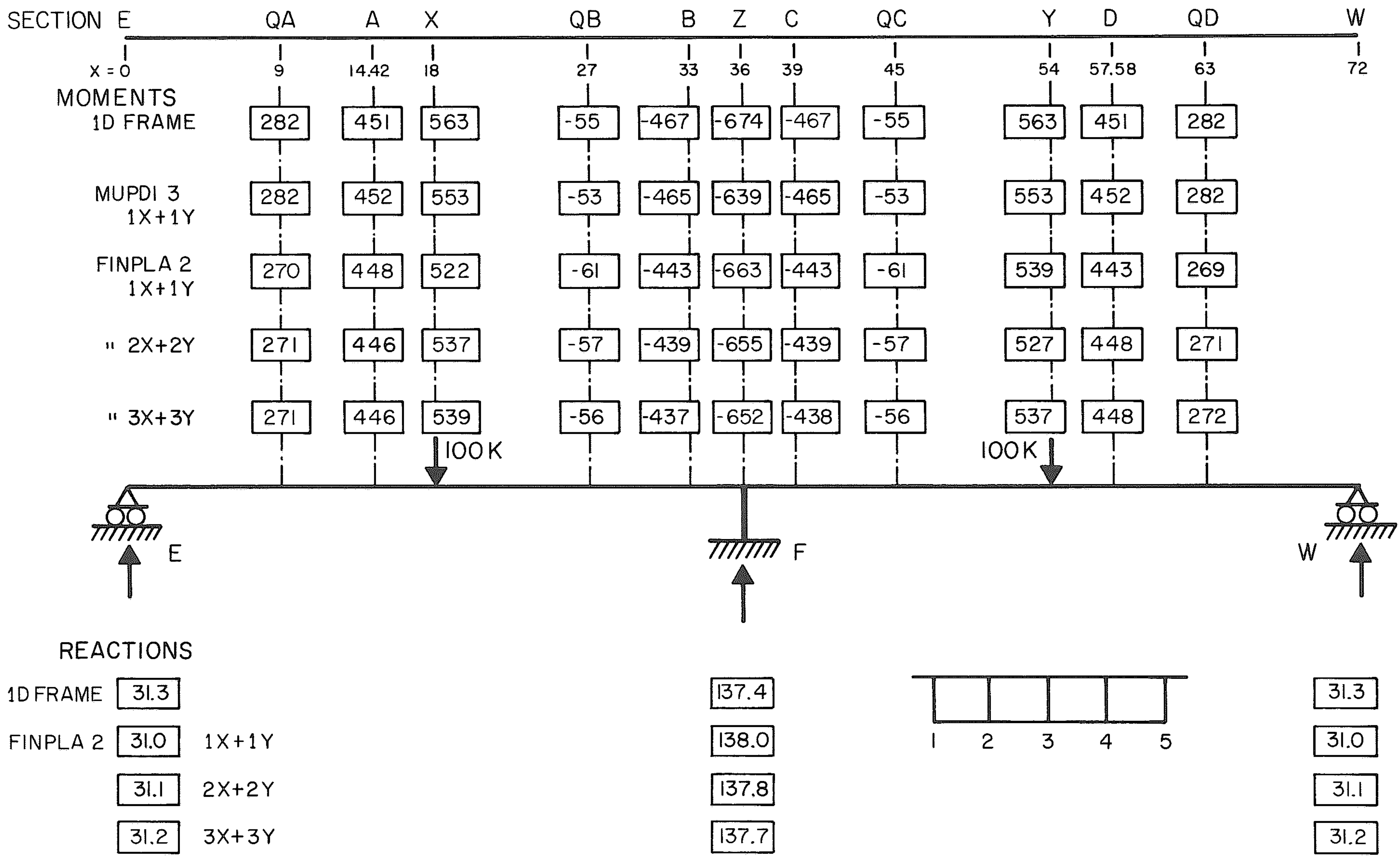

FIG. 7 REACTIONS (KIPS) AND TOTAL INTERNAL MOMENTS (FT-KIPS) AT A SECTION DUE TO 100 KIP LOADS AT MIDSPANS I AND II

Unlike 1DFRAME, the results in Fig. 7 from FINPLA2 for internal moments do not agree exactly with the external moments computed from the reactions, however the agreement is good and could be improved even further by using a finer finite element mesh.

An immediate conclusion from Fig. 7, is that irrespective of the transverse position of the loads, the reactions from the 1DFRAME and FINPLA2 solutions are in close agreement. The total internal moments at a section found by the three programs are also in good agreement generally within less than 5%

The theoretical deflections as calculated by the three programs are summarized in Table 2 for loads at both midspans at the extreme transverse eccentric positions, 1X + 1Y.

TABLE 2 - DEFLECTION (IN.) OF GIRDERS AT MIDSPAN SECTIONS X AND Y FOR 100 KIP LOADS AT 1X +1Y

Girder	Section X			Section Y		
	MUPDI3	FINPLA2	1DFRAME	MUPDI3	FINPLA2	1DFRAME
1	0.78	0.74	same	0.88	0.86	same
2	0.57	0.57	for	0.59	0.57	for
3	0.43	0.42	all	0.39	0.37	all
4	0.30	0.29	girders	0.26	0.24	girders
5	0.19	0.17		0.17	0.15	
ave	0.45	0.44	0.45	0.46	0.44	0.45

Several conclusions can be drawn from Table 2: (1) the agreement between FINPLA2 and MUPDI3 is excellent; (2) 1DFRAME accurately predicts the average deflection of the five girders; (3) as expected, the deflection under the load is greater at the midspan section without a transverse diaphragm 1Y, than at 1X which has a diaphragm

As a final comparison, the distribution of the total internal moment at the instrumented Sections A, B, C and D to the individual girders as predicted by MUPDI3 and FINPLA2 is given in Table 3.

TABLE 3 - DISTRIBUTION OF MOMENTS TO GIRDERS (FT-KIPS AND %) FOR 100 KIP LOADS AT 1X + 1Y

SECTION	GIRDER	Load Case 1X + 1Y			
		MUPDI3		FINPLA2	
		K-Ft.	%	K-Ft.	%
SECTION A	1	92.8	20.4	88.5	19.8
	2	115.8	25.6	115.7	25.9
	3	97.8	21.6	98.7	22.0
	4	85.1	18.8	86.1	19.2
	5	61.4	13.6	58.6	13.1
	Σ	452.4	100.0	447.6	100.0
SECTION B	1	-93.5	20.1	-83.5	18.8
	2	-117.1	25.2	-110.3	24.9
	3	-104.1	22.4	-101.0	22.8
	4	-92.1	19.8	-91.3	20.6
	5	-57.9	12.5	-57.1	12.9
	Σ	-464.8	100.0	-443.1	100.0
SECTION C	1	-97.4	21.0	-92.3	20.8
	2	-119.0	25.6	-113.9	25.7
	3	-103.3	22.2	-97.7	22.1
	4	-89.8	19.3	-85.9	19.4
	5	-55.3	11.9	-53.2	12.0
	Σ	-464.8	100.0	-442.9	100.0
SECTION D	1	98.0	21.7	93.9	21.2
	2	124.4	27.5	123.8	28.0
	3	96.7	21.4	96.2	21.7
	4	78.7	17.4	78.0	19.6
	5	54.6	12.0	51.1	11.5
	Σ	452.3	100.0	443.0	100.0

The table shows that both the ft-kip values of moments and the percentage distribution given by MUPDI3 and FINPLA2 agree closely with each other.

From the preceeding comparisons, for this symmetric loading in the two spans, it can be concluded that either MUPDI3 or FINPLA2 can be used to obtain detailed transverse and longitudinal distributions of theoretical results of interest. Also 1DFRAME yields an accurate theoretical picture of the longitudinal distribution of total reactions or moments and average deflections, irrespective of the transverse positions of the loads on the bridge.

2.3.2 Load at One Midspan

For this longitudinally unsymmetrical loading in the two spans, Fig. 8 shows theoretical results for moments and reactions. For this case MUPDI3, which assumes the center bent support to be a planar frame, cannot account for the longitudinal moment M_F at the base of the column and thus will not give accurate results for the internal moments.

From Fig. 8, it is apparent again as in the case for loads in both spans, that the reactions from 1DFRAME and FINPLA2 are in close agreement. Both of these solutions account for the longitudinal moment at the base of the column. The total internal moments at various sections found by these two programs, at the instrumented Sections A, C and D are in excellent agreement, within 2%. However, directly under the load and at the instrumented Section B near the support the differences are greater, being respectively about 3-5% and 10% lower by FINPLA2. The moment at Section B is particularly sensitive to small changes in the reactions, because it is related to the difference of two large numbers.

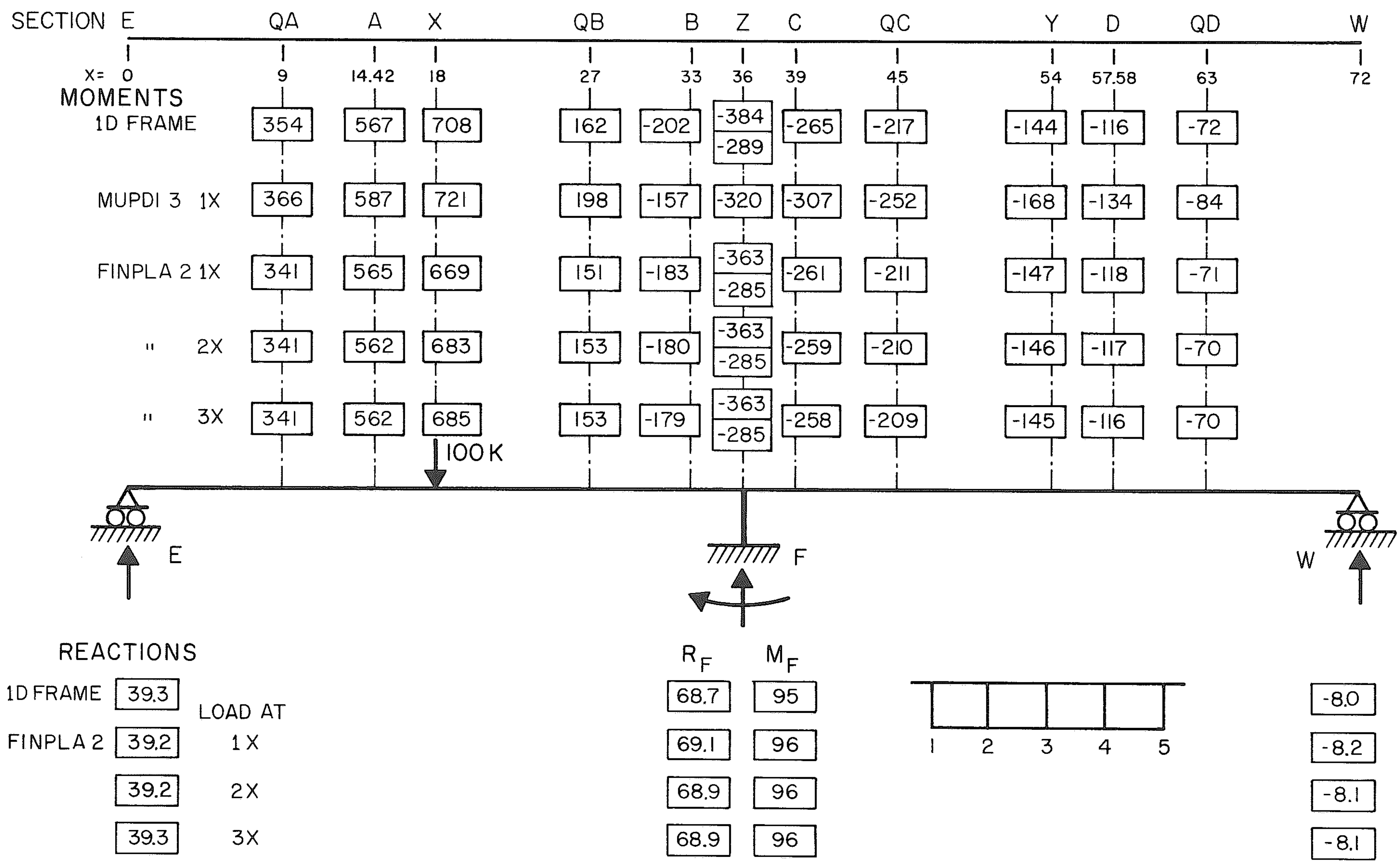

FIG. 8 REACTIONS (KIPS) AND TOTAL INTERNAL MOMENTS (FT-KIPS) AT A SECTION DUE TO 100 KIP LOAD AT MIDSPAN I

At Section Z, FINPLA2 prints only the average value of the moment on the two sides of the section, therefore extrapolated values for the two sides are given in Fig. 8.

The theoretical deflections as calculated by the three programs are summarized in Table 4 for a load at the extreme transverse position 1X.

TABLE 4 - DEFLECTION (IN.) OF GIRDERS AT MIDSPAN SECTIONS X AND Y FOR 100 KIP LOAD AT 1X

Girder	Section X			Section Y		
	MUPDI3	FINPLA2	1DFRAME	MUPDI3	FINPLA2	1DFRAME
1	0.97	0.89	Same	-0.19	-0.15	Same
2	0.81	0.75	for	-0.22	-0.18	for
3	0.68	0.63	all	-0.25	-0.21	all
4	0.55	0.53	girders	-0.27	-0.25	girders
5	0.50	0.45		-0.30	-0.27	
ave	0.70	0.65	0.70	-0.25	-0.21	-0.25

Deflections by FINPLA2 are slightly lower than those by MUPDI3 due to the lack of longitudinal moment restraint in the column in the latter solution. 1DFRAME gives a fairly good estimate of the average deflection across the width of the bridge.

2.4 Modification of Theoretical Values for Deflection and Strains.

Analytical methods used for comparison with experimental results, e.g. the folded plate theory with the associated MUPDI3 computer program, the finite element approach with the associated FINPLA2 program, or the 1DFRAME approach, are based on the linear elastic behavior of an uncracked, homogeneous, isotropic structure. The values given by these theories for the deflection of a box girder bridge at a certain point or the strain at a cross-section are not immediately applicable to those experimentally obtained from the cracked reinforced concrete box girder bridge model. It is clear that the assumption of a completely uncracked section as made in the theories would result in underestimation of the actual deflection of the box girder bridge model. Again, the strain values predicted by the theories in the part of the box girder cross-section subject to tension can not directly be compared with the experimental case where, due to concrete cracking, most of the stress was concentrated in the steel reinforcement.

2.4.1 Modification of Theoretical Deflections

Theoretical deflections based on an uncracked section should form a lower bound on the actual deflections in the model. An upper bound should be formed by assuming a fully cracked transformed section throughout, since it neglects participation of the concrete between cracks. The new ACI Code (1971) recommends a method for interpolating between these two bounds in calculating beam deflections. It states an effective moment of inertia should be used based on the following equations

$$I_{eff} = \left(\frac{M_{cr}}{M_{max}}\right)^3 I_g + \left[1 - \left(\frac{M_{cr}}{M_{max}}\right)^3\right] I_{cr} \qquad (2.1)$$

$$M_{cr} = \frac{f_r I_g}{y_t} \qquad (2.2)$$

$$f_r = 7.5 \sqrt{f'_c} \qquad (2.3)$$

I_{eff}, I_g, and I_{cr} are respectively the effective, uncracked gross, and fully cracked moments of inertia of the beam section. M_{cr} and M_{max} are the cracking moment and the maximum moment in the beam at the stage for which the deflection is being computed. f_r is the modulus of rupture.

Table 5 summarizes the above calculations considering the entire midspan bridge cross-sections at Section A and B. M_{max} is the total dead load plus live load moment existing under the full conditioning load at the beginning of each phase. f'_c is taken from the material properties, given in Vol. I, for the concrete in the bottom slab at each midspan section. A study of Table 5, indicates that the ACI equations give an I_{eff} very close to the fully cracked value for the Phase II loads producing a working stress of 30 ksi. However for the dead load case I_{eff} is much larger. Hereafter, in each case where experimental deflections are compared to theoretical deflections based on an uncracked section their ratio will be tabulated and may be compared to the ratio I_g/I_{eff} given in Table 5, to see how closely the ACI recommendations account for the cracking in the concrete. Note that the results are highly dependent on M_{cr} which is directly dependent on f_r, the modulus of rupture, which is hard to predict accurately.

2.4.2 Modification of Theoretical Strains

Direct comparisons between the strains predicted by the MUPDI3 and FINPLA2 programs, with their analytical models of homogeneous linear elastic material without cracking, and the actual experimental strains measured in the concrete and steel of the cracked box girder bridge model are difficult to make. If it is assumed that the force distribution

TABLE 5 - VALUES OF THE MOMENT ON INERTIA (FT^4) OF THE BOX GIRDER BRIDGE MODEL

SECTION	PHASE	I_g FT^4	I_{cr} FT^4	f'_c PSI	$f_r=7.5\sqrt{f'_c}$ PSI	M_{cr} K-FT	M_{max} K-FT	I_{eff} FT^4	I_g/I_{eff}
A	0 DEAD LOAD	2.64	1.16	3200	425	173	222	1.87	1.42
	I 24 KSI	2.64	1.10	3500	445	181	439	1.20	2.19
	II 30 KSI	2.64	1.10	3500	445	181	543	1.16	2.28
	III 40 KSI	2.64	1.06	3500	445	181	716	1.09	2.42
	IV 50 KSI	2.64	1.06	3500	445	181	890	1.08	2.45
	V 60 KSI	2.64	1.06	3500	445	181	1062	1.07	2.47
D	0 DEAD LOAD	2.64	1.16	5000	530	215	222	2.50	1.06
	I 24 KSI	2.64	1.10	5000	530	215	439	1.28	2.05
	II 30 KSI	2.64	1.10	5000	530	215	543	1.20	2.21
	III 40 KSI	2.64	1.06	5000	530	215	716	1.10	2.39
	IV 50 KSI	2.64	1.06	5000	530	215	890	1.08	2.44
	V 60 KSI	2.64	1.06	5000	530	215	1062	1.07	2.46

over the width of the box girder model given by the MUPDI3 and FINPLA2 programs is representative of the actual force distribution, then bearing in mind that each girder of the box girder bridge model essentially behaves like an I-beam with the T-C couple acting in the flanges, approximate expressions for the strains in the girders can be derived.

Thus, for comparison with experimental values, compressive strains were obtained from the theoretical results by dividing the values for the longitudinal compressive force N_x per unit length at each gaged location by the respective plate thickness and the concrete elastic modulus E_c. Theoretical steel strains were obtained by considering a fully cracked section and dividing the total longitudinal tensile force N_x per girder by the product of the steel area of the girder and the steel elastic modulus E_s.

As the contribution of the transverse membrane force N_y to the strains was found to be negligible it was ignored in the calculations.

Hereafter, comparisons for strains are based on theoretical strain values derived as above.

3. REDUCTION OF EXPERIMENTAL DATA

3.1 General Remarks

In order to process the large volume of data obtained from the experimental program, so as to evaluate the reactions, forces, moments, etc., four computer programs were developed. The programs, which will be considered in detail below, were designated as DATAMAN, ADJSTRN, MOMENT and REACTION. Data as obtained from the S.E.S.M Low Speed Scanner for each loading step on the box girder bridge model were handled by these four computer programs in succession, or separately as instructed, and all calculations necessary for theoretical comparisons, equilibrium checks and important quantities were made and printed in desired formats.

3.2 DATAMAN Program

DATAMAN, representing Data management, was an extremely versatile program able to handle all kinds of data as well as to help the editing of "raw" data. In the form used to reduce data pertaining to the box girder bridge model, DATAMAN performed the following functions for each loading step:

1. The data output of the 237 monitored channels was arranged under the categories of standard resistor, applied jack loads, weldable gage readings, concrete strain meter readings, clip gage readings, potentiometer readings and load cell reactions, and the data was punched out in the form of punched cards.

2. The difference of the readings for the load step considered from the pre-load condition readings was taken to obtain net readings for the load step. To facilitate comparisons, the net readings were normalized to a load of 100 kips in the span loaded. All strains were rounded off to the nearest micro in/in., all loads and reactions to the nearest hundredth of a kip and all deflections to the nearest ten-thousandths of an inch.

3. All strain readings coming from overrange (i.e. unbalanced) or faulty gages were screened by the DATAMAN program and replaced by known quantities of high magnitude. All illegible or garbled readings were replaced by known readings of low magnitude. The above substitutions were separately catalogued by the DATAMAN program in a list of "diagnostics" for each loading case. An example of a typical Dataman output is shown in Fig. 9, the diagnostics comprise Fig. 10.

3.3 Editing of Experimental Data

After the data for a particular loading case was obtained from DATAMAN, faulty or garbled readings as catalogued by DATAMAN were replaced in the printed output and in the punched card deck by readings of symmetrical gages at the same instrumented section under comparable complementary loading. Thus, in general, a gage reading in the main tensile reinforcement below girder 2 at section A under a point load above girder 5 at section X in span I, if found to be faulty, would be replaced by the reading of the gage in the main tensile reinforcement below girder 4 at section A under a point load above girder 1 at section X in span I. The editing scheme was extended to include gage

SEP/7/70

BOX GIRDER BRIDGE EXPERIMENTAL DATA, PROJECT S-10582, DEPARTMENT OF CIVIL ENGINEERING, UNIVERSITY OF CALIFORNIA

DATA FROM PAPER TAPE INTO PUNCHED CARDS

CASE 1076 --- LOAD CASE 11 2 1 4 7/27/70
M TAKE ZERO DIFFERENCES

SERIAL	NAME	CH.NO.	TYPE	CASE 1076
STANDARD RESISTORS				
1	STDR1	63	0	-.9999090E-01
2	STDR2	127	0	+.1201172E+00
3	STDR3	191	0	+.1611328E-01
4	STDR4	255	0	-.6005859E-01
APPLIED LOADS IN KIPS				
5	R000J1	184	3	-.1397270E-01
6	R000J2	185	3	-.2328277E-02
WELDABLE GAGE STRAINS IN MICRO-INCH PER INCH				
7	W100A	0	1	+.3117675E+00
8	W125A	1	1	+.4445798E+00
9	W150A	2	1	+.4621072E+01
10	W175A	3	1	+.3554686E+00
11	W200A	4	1	+.2226562E+00
12	W225A	5	1	+.2663573E+00
13	W250A	6	1	+.4445798E+00
14	W275A	7	1	+.3111266E+00
15	W300A	8	1	+.1782226E+00
16	W350A	9	1	+.8888694E+00
17	W400A	10	1	+.7600039E+01
18	W450A	11	1	+.3999022E+00
19	W500A	12	1	-.1757813E+00
20	L100A12	13	1	+.4467773E-01
21	L100A34	14	1	+.3554686E+00
22	L200A12	15	1	-.2695313E+00
23	L200A34	16	1	+.3085936E+00
24	L300A12	17	1	-.8437507E+00
25	L300A34	18	1	+.2219238E+00
26	M100A12	19	1	+.2656249E+00
27	M100A34	20	1	+.1328125E+00
28	M200A12	21	1	+.3107909E+00
29	M200A34	22	1	+.9765616E+00
30	M300A12	23	1	+.2226562E+00
31	M300A34	24	1	+.2226562E+00
32	M400A12	25	1	+.1796875E+00
33	M400A34	26	1	+.3124999E+00
34	M500A12	27	1	+.8000482E+00
35	M500A34	28	1	+.8984375E-01
36	W000B	29	1	+.4023436E+00
37	W100B	30	1	+.3554686E+00
38	W150B	31	1	-.4516602E-01
39	W200B	32	1	+.1782226E+00
40	W250B	33	1	+.2666015E+00

SERIAL	NAME	CH.NO.	TYPE	CASE 1076
41	W300B	34	1	+.2656249E+00
42	W350B	35	1	+.4445798E+00
43	W400B	36	1	+.2226562E+00
44	W450B	37	1	+.1782226E+00
45	W500B	38	1	+.4453123E+00
46	W600B	39	1	+.3085936E+00
47	W000C	40	1	+.7099604E+00
48	W100C	41	1	+.2695311E+00
49	W125C	42	1	+.3110350E+00
50	W150C	43	1	+.3547362E+00
51	W175C	44	1	+.1328125E+00
52	W200C	45	1	+.2187500E+00
53	W225C	46	1	+.3555601E+00
54	W250C	47	1	+.2226562E+00
55	W275C	48	1	+.1772460E+00
56	W300C	49	1	+.3100585E+00
57	W350C	50	1	+.4414060E+00
58	W400C	51	1	+.3110350E+00
59	W450C	52	1	+.4888608E+00
60	W500C	53	1	+.4001463E+00
61	W600C	54	1	+.4892310E+00
62	U100C12	64	1	+.2663573E+00
63	U200C34	65	1	+.3554686E+00
64	U200C12	66	1	+.1779783E+00
65	U200C34	67	1	+.3554686E+00
66	U300C12	68	1	+.8837890E-01
67	U300C34	69	1	+.2219238E+00
68	M100C12	70	1	+.1777801E+00
69	M100C34	71	1	+.2695311E+00
70	M200C12	72	1	+.7109370E+00
71	M200C34	73	1	+.1392932E+02
72	M300C12	74	1	+.6210933E+00
73	M300C34	75	1	+.1367187E+00
74	M400C12	76	1	-.4296875E-01
75	M400C34	77	1	+.8007806E+00
76	M500C12	78	1	-.8000494E+00
77	M500C34	79	1	+.8892822E-01
78	M100D12	80	1	+.2226562E+00
79	M100D34	81	1	+.4001463E+00
80	M200D12	82	1	+.8837890E-01
81	M200D34	83	1	+.1335442E+00
82	M300D12	84	1	+.3984373E+00
83	M300D34	85	1	+.4023436E+00
84	M400D12	86	1	+.3984373E+00
85	M400D34	87	1	+.2219238E+00
86	M500D12	88	1	+.7553705E+00
87	M500D34	89	1	+.3984373E+00
88	L100D12	90	1	+.3555601E+00
89	L100D34	91	1	+.1796875E+00

FIG. 9 TYPICAL OUTPUT FROM DATAMAN PROGRAM

SEP/7/70

BOX GIRDER BRIDGE EXPERIMENTAL DATA, PROJECT S-20680, DEPARTMENT OF CIVIL ENGINEERING, UNIVERSITY OF CALIFORNIA

DATA FROM PAPER TAPE INTO PUNCHED CARDS

SERIAL	NAME	CH.NO.	TYPE	CASE 1076
90	L200D12	92	1	+.3562010E+00
91	L200D34	93	1	+.5312497E+00
92	L300D12	94	1	-.8984380E-01
93	L300D34	95	1	+.4023436E+00
94	T100D12	96	1	+.3999022E+00
95	T100D34	97	1	+.0000000E+00
96	T150D12	98	1	+.8886718E-01
97	T150D34	99	1	-.1777344E+00
98	T200D12	100	1	+.2226562E+00
99	T200D34	101	1	+.1782226E+00
100	T250D12	102	1	-.1243897E+01
101	T250D34	103	1	+.7148432E+00
102	T300D12	104	1	+.5351550E+00
103	T300D34	105	1	+.4445798E+00
104	U100D12	106	1	+.4882810E+00
105	U100D34	107	1	+.4438474E+00
106	U200D12	108	1	+.2226562E+00
107	U200D34	109	1	+.4453123E+00
108	U300D12	110	1	+.5334012E+00
109	U300D34	111	1	+.3085936E+00
110	W100D	112	1	+.6044396E+01
111	W125D	113	1	+.2187500E+00
112	W150D	114	1	+.2226562E+00
113	W175D	115	1	+.3124999E+00
114	W200D	116	1	-.8886724E-01
115	W225D	117	1	+.8837890E-01
116	W250D	118	1	+.1796875E+00
117	W275D	119	1	+.2656249E+00
118	W300D	120	1	+.5334470E+00
119	W350D	121	1	+.4445798E+00
120	W400D	122	1	+.1796875E+00
121	W450D	123	1	+.4687500E-01
122	W500D	124	1	+.1644528E+01
CONCRETE METER STRAINS			IN MICRO-INCH PER INCH	
123	K000A	128	2	+.9301763E-01
124	K100A	129	2	-.3198242E-01
125	K125A	130	2	+.9326177E-01
126	K150A	131	2	-.3125000E-01
127	K175A	132	2	+.1586914E+00
128	K200A	133	2	+.6372076E-01
129	K225A	134	2	+.0000000E+00
130	K250A	135	2	+.0000000E+00
131	K275A	136	2	-.6352239E-01
132	K300A	137	2	-.1247559E+00
133	K350A	138	2	+.3051758E-01
134	K400A	139	2	+.3140259E-01
135	K450A	140	2	+.1228027E+00
136	K500A	141	2	+.1257324E+00

SERIAL	NAME	CH.NO.	TYPE	CASE 1076
137	K600A	142	2	+.6274420E-01
138	K100B	143	2	+.3100586E-01
139	K150B	144	2	+.6274420E-01
140	K200B	145	2	-.6396490E-01
141	K300B	146	2	+.3140259E-01
142	K350B	147	2	-.1945683E+02
143	K400B	148	2	+.9594732E-01
144	K450B	149	2	+.1907806E+00
145	K500B	150	2	+.9301763E-01
146	K100C	151	2	+.9423834E-01
147	K125C	152	2	+.0000000E+00
148	K150C	153	2	-.6274420E-01
149	K175C	154	2	+.6278997E-01
150	K200C	155	2	+.0000000E+00
151	K225C	156	2	+.1572266E+00
152	K250C	157	2	+.1562500E+00
153	K275C	158	2	+.6347662E-01
154	K300C	159	2	+.3134155E-01
155	K350C	160	2	+.0000000E+00
156	K400C	161	2	-.1562500E+00
157	K450C	162	2	+.1276856E+00
158	K500C	163	2	-.6176758E-01
159	K100D	164	2	+.2222138E+00
160	K150D	165	2	+.9375005E-01
161	K175D	166	2	+.9331327E-01
162	K200D	167	2	+.3036499E-01
163	K225D	168	2	+.9477239E-01
164	K250D	169	2	-.1906738E+00
165	K275D	170	2	+.1269531E+00
166	K300D	171	2	-.6250005E-01
167	K350D	172	2	+.6250005E-01
168	K400D	173	2	+.3182983E-01
169	K450D	174	2	+.6347662E-01
170	K500D	175	2	+.3149414E-01
171	K600D	176	2	+.3125000E-01
172	K000D	177	2	+.1906738E+00
173	K125D	178	2	+.1633301E+00
174	VOID	179	2	-.9390264E-01
LOAD CELL REACTIONS IN KIPS				
175	R100A1	192	3	+.7255928E-01
176	R200A1	193	3	+.1855860E-02
177	R300A1	194	3	+.9210592E-02
178	R400A1	195	3	-.3729820E-02
179	R500A1	196	3	+.7433897E-02
180	R100D1	197	3	+.3725006E-02
181	R200D1	198	3	-.2807617E-02
182	R300D1	199	3	-.9307867E-03
183	R400D1	200	3	+.1349175E-02

FIG. 9 TYPICAL OUTPUT FROM DATAMAN PROGRAM

BOX GIRDER BRIDGE EXPERIMENTAL DATA, PROJECT S-20680, DEPARTMENT OF CIVIL ENGINEERING, UNIVERSITY OF CALIFORNIA SEP/7/70

DATA FROM PAPER TAPE INTO PUNCHED CARDS

SERIAL	NAME	CH.NO.	TYPE	CASE 1076
184	R500D1	201	3	+.1858711E-02
185	R000S1	202	3	+.3111267E-01
186	R000S2	203	3	+.1165772E-01
187	R000S3	204	3	+.3850474E-02
188	RC00S4	205	3	+.0000000E+00
189	R000S5	206	3	+.3906250E-02
190	R000S6	207	3	+.7720953E-02
191	RC00S7	208	3	+.0000000E+00
192	R000S8	209	3	-.7812505E-02
POTENTIOMETER DEFLECTIONS IN INCHES				
193	P100A	210	3	-.1201630E-03
194	P200A	211	3	-.2880097E-03
195	P300A	212	3	-.2384186E-04
196	P400A	213	3	-.9536749E-04
197	P500A	214	3	-.1916885E-03
198	P100E	215	3	+.4768372E-04
199	P200E	216	3	+.4768372E-04
200	P300E	217	3	-.1201630E-03
201	P400F	218	3	-.2479553E-04
202	P500E	219	3	-.4768372E-04
203	P100F	220	3	+.5760193E-03
204	P200F	221	3	+.5044937E-03
205	P300F	222	3	+.3347397E-03
206	P400F	223	3	+.4768372E-04
207	P500F	224	3	+.4863739E-04
208	P100D	225	3	+.2384186E-04
209	P200D	226	3	-.4768372E-04
210	P300D	227	3	+.4768372E-04
211	P400D	228	3	+.0000000E+00
212	P500D	229	3	-.4863739E-04
213	P100X	230	3	+.2384186E-04
214	P200X	231	3	+.4768372E-04
215	P300X	232	3	+.4768372E-04
216	P400X	233	3	+.2384186E-04
217	P500X	234	3	+.0000000E+00
STEEL CLIP GAGE STRAINS IN MICRO-INCHES PER INCH				
218	G100A	235	3	-.9140625E+00
219	G200A	236	3	+.0000000E+00
220	G300A	237	3	-.1949219E+01
221	G400A	238	3	-.7539063E+00
222	G500A	239	3	+.7500000E+01
223	G100B	240	3	+.0000000E+00
224	G200B	241	3	+.1562500E-01
225	G300B	242	3	-.8610840E+00
226	G400B	243	3	+.0000000E+00
227	G500B	244	3	+.7414551E+00
228	G100C	245	3	+.9047852E+00

SERIAL	NAME	CH.NO.	TYPE	CASE 1076
229	G200C	246	3	+.1023437E+01
230	G300C	247	3	+.9062500E+00
231	G400C	248	3	+.0000000E+00
232	G500C	249	3	-.9726563E+00
233	G100D	250	3	-.8515625E+00
234	G200D	251	3	+.8242188E+00
235	G300D	252	3	+.8242188E+00
236	G400D	253	3	-.2285156E+01
237	G500D	254	3	+.1199219E+01
SUM OF APPLIED LOADS AND REACTIONS IN KIPS				
238	SLOAD	260	-1	000000000000000
239	SREAC	261	-1	000000000000000
240	EREAC	262	-1	000000000000000
241	CREAC	263	-1	000000000000000
242	WREAC	264	-1	000000000000000
TOTAL MOMENTS IN FT-KIPS AT SECTIONS A, B, C, D, CALCULATED FROM MEASURED LOADS AND REACTIONS				
243	MOMA	265	-1	000000000000000
244	MOMB	266	-1	000000000000000
245	MOMC	267	-1	000000000000000
246	MOMD	268	-1	000000000000000
MISCELLANEOUS INFORMATION				
247	SPACE1	269	-1	000000000000000
248	SPACE2	270	-1	000000000000000
249	SPACE3	271	-1	000000000000000
250	SPACE4	272	-1	000000000000000
251	SPACE5	273	-1	000000000000000
252	SPACE6	274	-1	000000000000000
253	SPACE7	275	-1	000000000000000
254	SPACE8	276	-1	000000000000000
255	SPACE9	277	-1	000000000000000
256	SPACE10	278	-1	000000000000000
257	SPACE11	279	-1	000000000000000
258	SPACE12	280	-1	000000000000000
259	SPACE13	281	-1	000000000000000
260	SPACE14	282	-1	000000000000000
261	SPACE15	283	-1	000000000000000

FIG. 9 TYPICAL OUTPUT FROM DATAMAN PROGRAM

```
$ JOB PRESET NOTAPE DATE SEP/7/70

BEGIN
________________________________________________________________________
READ TITLE

. BOX GIRDER BRIDGE EXPERIMENTAL DATA, PROJECT S-20680, DEPARTMENT OF
CIVIL ENGINEERING, UNIVERSITY OF CALIFORNIA
________________________________________________________________________

READ SUBTITLE

. DATA FROM PAPER TAPE INTO PUNCHED CARDS
________________________________________________________________________

TRANSFER WORDS TO CARDS WITH CHECK AND PRINT IN PRESET FORM

. 1076  LOAD CASE  II 2 1 A  7/27/70  M ,
________________________________________________________________________
TAKE ZERO DIFFERENCES

    CASE NUMBER 1076          NUMBER OF INPUT RECORDS REGISTERED  237
    WITH POSSIBLE MISSING DATA OF FOLLOWING ELEMENTS, IF ANY..

           260  261  262  263  264  265  266  267  268  269  270  271
________________________________________________________________________
           272  273  274  275  276  277  278  279  280  281  282  283

________________________________________________________________________
END
```

FIG. 10 TYPICAL SET OF DIAGNOSTICS OBTAINED FROM DATAMAN PROGRAM readings (not catalogued by DATAMAN) which were obviously grossly inconsistent; however, the total number of gage readings replaced for any loading case never exceeded about 7 channels out of a total of 237 channels. The punched card decks after editing were fed into the ADJSTRN program.

3.4 ADJSTRN Program

At each instrumented section of the box girder bridge model, Fig. 11, the strains in the top slab, bottom slab and girder webs were treated separately. The top slab was divided into six regions, four regions corresponding to the four cell bays of the box girder model and two regions corresponding to the cantilever overhangs on either side. The bottom slab was divided into four regions corresponding to the four cell bays of the box girder model.

Each cell bay of the top or bottom slab whether in tension or in compression was instrumented either at 3 points (i.e. girders and midbay) or at 5 points (i.e. girders, midbay and quarter bays), the girder locations being common to contiguous bays. The cantilever overhangs were instrumented at 2 points (i.e. exterior girder and edge of overhang). The girder webs were instrumented at a maximum of 3 points over the depth and were not instrumented in certain cases. The arrangement of gages and measuring devices can be seen in Fig. 11.

The operation of the ADJSTRN program at an instrumented section was as follows:

1. Averages of observed i. e. measured strain values were taken at necessary instrumented locations.

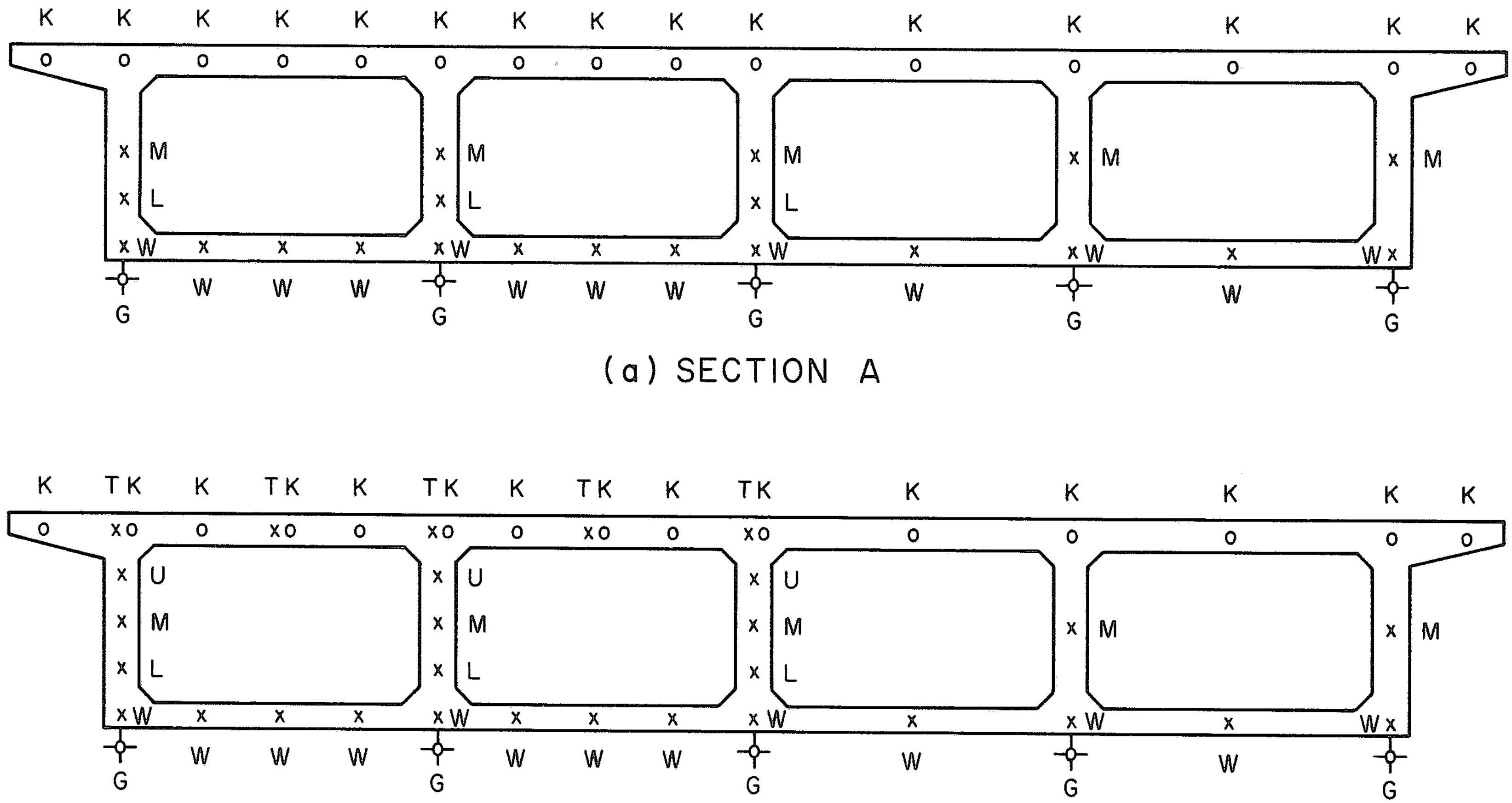

(a) SECTION A

(b) SECTION D

G - CLIP GAGE
K - CONCRETE STRAIN METER
U - UPPER WELDABLE GAGE
M - MIDDLE WELDABLE GAGE
L - LOWER WELDABLE GAGE
W - WELDABLE GAGE IN SLAB
T - TRANSVERSE WELDABLE GAGE

FIG. 11 BOX GIRDER BRIDGE MODEL INSTRUMENTATION

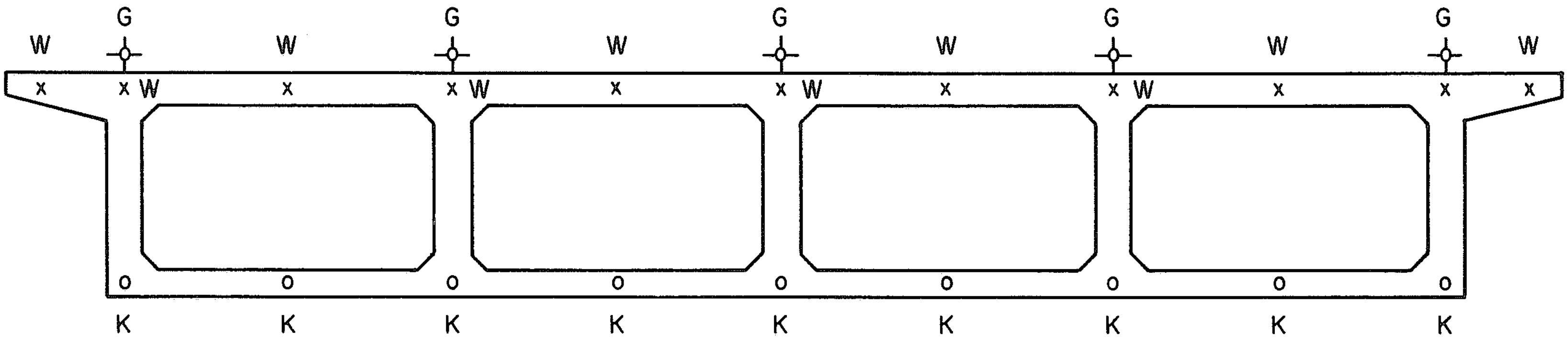

(c) SECTION B

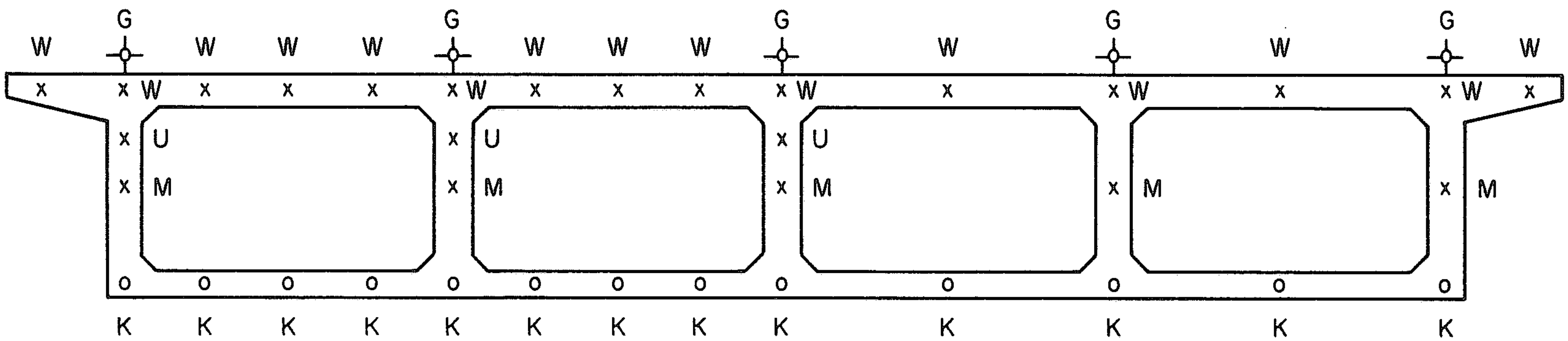

(d) SECTION C

G - CLIP GAGE
K - CONCRETE STRAIN METER
U - UPPER WELDABLE GAGE
M - MIDDLE WELDABLE GAGE
L - LOWER WELDABLE GAGE
W - WELDABLE GAGE IN SLAB

FIG. 11 BOX GIRDER BRIDGE MODEL INSTRUMENTATION

2. The top and bottom slabs were treated first and the number of gaged locations in a bay was established, i.e. 5 or 3.

3. The gages were checked for tension or compression readings and the strain values compared with ceiling values of strain, the yield strain of 2070 μ in./in. for steel and the crushing strain of 1000 μ in./in. for concrete. Any weldable gage reading in excess of the yield strain or any concrete strain meter reading in excess of the crushing strain was discarded. [In practice, because of the editing procedure, it was not necessary to use this option].

4. Depending on the number of strain values in a bay, a 5 point adjustment or a 3 point adjustment was made.

   The 5 point adjustment called for the passing of a least-squares parabola to fit the five points. At each gaged location, the ratio of the adjusted ordinate of the parabola was compared with the observed value. If a ratio did not lie between 0.8 and 1.2, the violating strain value was discarded and a least squares parabola was passed to fit the remaining four points. The ordinates of the second parabola were then printed out at several locations to facilitate integration of strains, stresses, etc. If two ratios did not satisfy the requirement, the two violating strain values were discarded and a simple parabola was passed through the remaining three points. If all ratios lay between the prescribed limits, the first least squares parabola was taken as the curve for strain distribution in the bay and ordinates of this parabola at several locations were printed out at several locations to facilitate integration of strains, stresses, etc.

The 3 point adjustment commenced with the calculation of the average of the three observed strain ordinates. The absolute value of the difference between this average and each of the observed values was then compared with the average. If this difference was smaller than the average for all three strain values, a parabola was passed through the three observed strain points and ordinates of this parabola were printed. An observed strain ordinate violating the criterion was discarded, and in this case a straight line was passed through the remaining two points.

5. The strain values at the cantilever edges of the top slab were compared with those at the girders nearest them. If a cantilever edge strain value did not lie between 0.5 and 1.5 times the strain value for the adjacent girder, it was replaced by the strain value at the girder; otherwise, it was retained as the actual value. A straight line was passed through the two points.

6. The girder web strains were treated together with the appropriate adjusted strains at the top and bottom of the girder web in each case. For the maximum case where the girder webs were instrumented at three points, a total of five strain values was considered -- i.e. the three strain values in the girder web, the top slab strain as adjusted by the 5 point or 3 point adjustment, and the bottom slab strain as adjusted by the 5 point or 3 point adjustment. A least squares straight line was drawn to fit these five values. For cases where a girder web was instrumented at one or two points only,

a total of three or four strains was considered, and the least squares line drawn. Where the girder web was not instrumented, a straight line was drawn through the top and bottom slab adjusted strains.

In all cases where the least squares line was passed through the measured strain values, the ratios of the measured and adjusted values were specified to lie between 0.8 and 1.20. A measured value violating this criterion was discarded and subsequently a second least squares line was passed through the remaining values. Finally, relevant strain values and the location of the neutral axis for the girder in question were printed in the computer output. An example of a typical output is shown in Fig. 12.

3.5 MOMENT Program

At each instrumented section the MOMENT program first calculated from the adjusted strains the compressive forces in the slab concrete and steel and the girder web concrete and steel and the tensile forces in the slab and girder web steel for the case of each girder separately. All these quantities were classified and then girder moments were calculated in terms of kip-ft. and as percentages of the total moment at the section about four axes: the compression flange mid-depth; the line of main tensile reinforcement; the neutral axis of the box girder uncracked cross-section and the individual neutral axis of each girder as determined from measured strains by the ADJSTRN program. An example of a typical output is shown in Fig. 13.

```
STEP NO. II.2.10 (NORMALIZED) - AFTER 30 KSI CONDITIONING LOAD
STRAIN ADJUSTMENTS (ALL STRAINS IN MICRO-IN/IN)

SECTION A

---------------------------------------------------------------------------------------------------------------------------------------------------
OBSERVED STRAINS           267.   270.   212.   215.   190.   157.   195.   190.   246.   228.          201.          199.          170.          177.   196.

FIRST ADJUSTED                    262.   232.   205.   182.   163.
                                                              158.   188.   210.   226.   235.
---------------------------------------------------------------------------------------------------------------------------------------------------
ADJUSTED STRAINS           267.   270.                        158.   188.   210.   226.   235.                        199.   180.   170.   169.   177.
                                  262.   232.   205.   182.   163.                        228.   211.   201.   197.   199.                        177.   196.

RATIOS (OBS./ADJ.)         1.00   1.00                        1.00   1.04    .90   1.09    .97                        1.00          1.00          1.00
                                  1.03    .91   1.05   1.04    .97                        1.00          1.00          1.00                        1.00   1.00
---------------------------------------------------------------------------------------------------------------------------------------------------
                              ***********************************************************************************************************************
                                     *                           *                           *                           *                           *
                                     *                           *                           *                           *                           *
OBS=D WEB STRAINS                 262.                        158.                        228.                        199.                        177.
ADJ=D WEB STRAINS                 411.                         43.                        160.                        192.                        171.
RATIO (OBS./ADJ.)                  .64                        3.64                        1.42                        1.04                        1.03
---------------------------------------------------------------------------------------------------------------------------------------------------
                                     *                           *                           *                           *                           *
OBS=D WEB STRAINS
ADJ=D WEB STRAINS                 -16.                        -227.                       -124.                        -72.                        -16.
RATIO (OBS./ADJ.)
                                     *                           *                           *                           *                           *
OBS=D WEB STRAINS                -227.                        -597.                       -376.                       -351.                       -214.
---------------------------------------------------------------------------------------------------------------------------------------------------
ADJ=D WEB STRAINS                -443.                        -498.                       -408.                       -336.                       -203.
RATIO (OBS./ADJ.)                  .51                        1.20                         .92                        1.05                        1.05
                                     *                           *                           *                           *                           *
OBS=D WEB STRAINS                -706.                       -1028.                      -1027.
ADJ=D WEB STRAINS                -871.                        -769.                       -692.                       -599.                       -390.
RATIO (OBS./ADJ.)                  .81                        1.34                        1.48
---------------------------------------------------------------------------------------------------------------------------------------------------
                                     *                           *                           *                           *                           *
OBS=D WEB STRAINS               -1529.                        -795.                       -740.                       -855.                       -572.
ADJ=D WEB STRAINS               -1298.                       -1039.                       -975.                       -863.                       -578.
RATIO (OBS./ADJ.)                 1.18                         .77                         .76                         .99                         .99
                                     *                           *                           *                           *                           *
                                     *********************************************************************************************************
---------------------------------------------------------------------------------------------------------------------------------------------------

OBSERVED STRAINS                -1569.-1002.  -919.-1047.  -764.  -996.  -882.  -877.  -740.         -805.         -855.         -431.         -572.

FIRST ADJUSTED                  -1484.-1161.  -949.  -848.  -858.
                                                             -795.  -914.  -942.  -880.  -728.
---------------------------------------------------------------------------------------------------------------------------------------------------
ADJUSTED STRAINS                                             -795.  -914.  -942.  -880.  -728.                       -855.  -573.  -431.  -431.  -572.
                                -1529.-1107.  -840.  -730.  -777.                        -740.  -774.  -805.  -832.  -855.

RATIOS (OBS./ADJ.)                                             .96   1.09    .94   1.00   1.02                        1.00          1.00          1.00
                                  1.03    .91   1.09   1.43    .98                        1.00          1.00          1.00
---------------------------------------------------------------------------------------------------------------------------------------------------
```

FIG. 12 TYPICAL OUTPUT FOR AN INSTRUMENTED SECTION OBTAINED FROM ADJSTRN PROGRAM

BOX GIRDER BRIDGE MODEL - CALCULATION OF GIRDER FORCES AND MOMENTS

STEP NO. II.2.10 (NORMALIZED) - AFTER 30 KSI CONDITIONING LOAD

SECTION A

	GIRDER 1	GIRDER 2	GIRDER 3	GIRDER 4	GIRDER 5	ALL GIRDERS
LOCATION OF GIRDER EXPERIMENTAL NEUTRAL AXIS (INCHES)						
DISTANCE OF N.A. FROM LINE OF COMP. METERS	4.40	.73	2.58	3.33	4.19	
DISTANCE OF N.A. FROM LINE OF TENSILE STEEL	13.91	17.58	15.73	14.98	14.12	
DETAILED SUMMARY OF INTERNAL FORCES (KIPS)						
COMPRESSIVE FORCES						
CONCRETE IN FLANGE	-61.96	-49.08	-58.09	-50.41	-44.19	
STEEL IN FLANGE	-4.64	-4.02	-4.91	-4.27	-3.26	
TOTAL IN FLANGE	-66.60	-53.09	-63.00	-54.68	-47.45	
CONCRETE IN WEB	-4.22	0.	0.	-1.51	-1.62	
STEEL IN WEB	0.	0.	0.	0.	0.	
TOTAL IN WEB	-4.22	0.	0.	-1.51	-1.62	
TOTAL COMPRESSIVE FORCE	-70.81	-53.09	-63.00	-56.19	-49.07	-292.16
TENSILE FORCES						
STEEL IN FLANGE	46.11	62.39	63.95	54.65	18.25	
STEEL IN WEB	1.01	2.35	1.57	2.39	1.36	
TOTAL TENSION FORCE	47.12	64.75	65.52	57.03	19.61	254.03
NET AXIAL FORCE	-23.70	11.66	2.52	.85	-29.46	-38.13
RATIO OF COMP. FORCE TO TENSILE FORCE	1.50	.82	.96	.99	2.50	1.15
DETAILED SUMMARY OF INTERNAL MOMENTS (KIP-FT)						
ABOUT COMPRESSION FLANGE MID-DEPTH						
STEEL IN TENSION FLANGE	69.87	94.55	96.92	82.81	27.66	
STEEL IN TENSION WEB	.96	1.45	1.08	2.30	1.43	
CONCRETE IN COMPRESSION WEB	-.89	0.	0.	-.24	-.33	
STEEL IN COMPRESSION WEB	0.	0.	0.	0.	0.	
TOTAL MOMENT ABOUT COMPRESSION FLANGE	69.94	96.00	98.00	84.88	28.76	377.57
PERCENT OF TOTAL MOMENT TAKEN BY GIRDERS	(18.52)	(25.43)	(25.95)	(22.48)	(7.62)	(100.00)
ABOUT TENSION FLANGE STEEL						
CONCRETE IN COMPRESSION FLANGE	93.89	74.37	88.03	76.40	66.97	
STEEL IN COMPRESSION FLANGE	7.03	6.08	7.44	6.47	4.94	
CONCRETE IN COMPRESSION WEB	5.55	0.	0.	1.98	2.14	
STEEL IN COMPRESSION WEB	0.	0.	0.	0.	0.	
STEEL IN TENSION WEB	-.57	-2.12	-1.30	-1.31	-.63	
TOTAL MOMENT ABOUT TENSION FLANGE	105.90	78.34	94.18	83.53	73.42	435.35
PERCENT OF TOTAL MOMENT TAKEN BY GIRDERS	(24.32)	(17.99)	(21.63)	(19.19)	(16.86)	(100.00)
ABOUT ENTIRE GROSS SECTION NEUTRAL AXIS (DISTANCE FROM TOP DECK FACE = 9.37 IN.)						
STEEL IN TENSION FLANGE	38.20	51.70	52.99	45.28	15.12	
STEEL IN TENSION WEB	.26	-.17	.00	.66	.49	
CONCRETE IN COMPRESSION FLANGE	42.56	33.72	39.91	34.63	30.36	
STEEL IN COMPRESSION FLANGE	3.19	2.76	3.37	2.93	2.24	
CONCRETE IN COMPRESSION WEB	2.38	0.	0.	.86	.93	
STEEL IN COMPRESSION WEB	0.	0.	0.	0.	0.	
TOTAL MOMENT ABOUT GROSS SECTION N.A.	86.60	88.00	96.28	84.37	49.14	404.38
PERCENT OF TOTAL MOMENT TAKEN BY GIRDERS	(21.41)	(21.76)	(23.81)	(20.86)	(12.15)	(100.00)
ABOUT GIRDER EXPERIMENTAL NEUTRAL AXIS						
STEEL IN TENSION FLANGE	53.43	91.40	93.81	68.22	21.48	
STEEL IN TENSION WEB	.60	1.33	.76	1.67	.97	
CONCRETE IN COMPRESSION FLANGE	22.09	2.48	11.90	13.46	14.96	
STEEL IN COMPRESSION FLANGE	1.65	.20	1.01	1.14	1.10	
CONCRETE IN COMPRESSION WEB	.62	0.	0.	.15	.22	
STEEL IN COMPRESSION WEB	-0.	-0.	-0.	-0.	-0.	
TOTAL MOMENT ABOUT EXPERIMENTAL N.A.	78.39	95.41	97.48	84.64	38.73	394.65
PERCENT OF TOTAL MOMENT TAKEN BY GIRDERS	(19.86)	(24.18)	(24.70)	(21.45)	(9.81)	(100.00)
INTERNAL FORCES USING CLIP-GAGE STEEL STRAINS (KIPS)						
STEEL IN FLANGE	42.87	69.72	52.96	44.36	23.45	233.36
RATIO OF STEEL FLANGE FORCES (CLIP/MICRODOT)	.93	1.12	.83	.81	1.29	.95
INTERNAL MOMENTS USING CLIP-GAGE STEEL STRAINS (KIP-FT) INSTEAD OF MICRO-DOT STEEL STRAINS FOR FLANGE ONLY						
TOTAL MOMENT ABOUT COMPRESSION FLANGE	65.04	107.10	81.33	69.29	36.64	359.40
PERCENT OF TOTAL MOMENT TAKEN BY GIRDERS	(18.10)	(29.80)	(22.63)	(19.28)	(10.20)	(100.00)
TOTAL MOMENT ABOUT GROSS-SECTION N.A.	83.92	94.07	87.16	75.85	53.45	394.45
PERCENT OF TOTAL MOMENT TAKEN BY GIRDERS	(21.27)	(23.85)	(22.10)	(19.23)	(13.55)	(100.00)
TOTAL MOMENT ABOUT EXPERIMENTAL N.A.	74.64	106.13	83.07	71.80	44.86	380.50
PERCENT OF TOTAL MOMENT TAKEN BY GIRDERS	(19.62)	(27.89)	(21.83)	(18.87)	(11.79)	(100.00)

FIG. 13 TYPICAL OUTPUT FOR AN INSTRUMENTED SECTION OBTAINED FROM MOMENT PROGRAM

BOX GIRDER BRIDGE MODEL - SUMMARY OF GIRDER FORCES AND MOMENTS

STEP NO. II.2.10 (NORMALIZED) - AFTER 30 KSI CONDITIONING LOAD

SECTION A

	GIRDER 1	GIRDER 2	GIRDER 3	GIRDER 4	GIRDER 5	ALL GIRDERS
LOCATION OF GIRDER EXPERIMENTAL NEUTRAL AXIS (INCHES)						
(1) DISTANCE OF N.A. FROM LINE OF COMP. METERS	4.40	.73	2.58	3.33	4.19	
(2) DISTANCE OF N.A. FROM LINE OF TENSILE STEEL	13.91	17.58	15.73	14.98	14.12	

SUMMARY BASED ON CARLSON STRAINS IN CONCRETE AND MICRODOT STRAINS IN STEEL

	GIRDER 1	GIRDER 2	GIRDER 3	GIRDER 4	GIRDER 5	ALL GIRDERS
TOTAL INTERNAL FORCES (KIPS)						
(3) COMPRESSIVE FORCES	-70.81	-53.09	-63.00	-56.19	-49.07	-292.16
(4) TENSILE FORCE	47.12	64.75	65.52	57.03	19.61	254.03
(5) NET AXIAL FORCE	-23.70	11.66	2.52	.85	-29.46	-38.13
(6) RATIO OF COMP. FORCE TO TENSILE FORCE	1.50	.82	.96	.99	2.50	1.15
TOTAL INTERNAL MOMENTS (KIP-FT)						
(7) ABOUT COMPRESSION FLANGE MID-DEPTH	69.94	96.00	98.00	84.88	28.76	377.57
(8) ABOUT TENSION FLANGE STEEL	105.90	78.34	94.18	83.53	73.42	435.35
(9) ABOUT ENTIRE GROSS-SECTION N.A.	86.60	88.00	96.28	84.37	49.14	404.38
(10) ABOUT GIRDER EXPERIMENTAL N.A.	78.39	95.41	97.48	84.64	38.73	394.65
MOMENT PERCENTAGES TAKEN BY EACH GIRDER						
(11) ABOUT COMPRESSION FLANGE MID-DEPTH	18.52	25.43	25.95	22.48	7.62	(100.00)
(12) ABOUT TENSION FLANGE STEEL	24.32	17.99	21.63	19.19	16.86	(100.00)
(13) ABOUT ENTIRE GROSS-SECTION N.A.	21.41	21.76	23.81	20.86	12.15	(100.00)
(14) ABOUT GIRDER EXPERIMENTAL N.A.	19.86	24.18	24.70	21.45	9.81	(100.00)

TOTAL SECTION MOMENTS
(15) CALCULATED FROM EXPERIMENTAL LOADS AND REACTIONS = 433.36
(16) RATIO (7) TO (15) = .87
(17) RATIO (8) TO (15) = 1.00
(18) RATIO (9) TO (15) = .93
(19) RATIO (10) TO (15) = .91

BOX GIRDER BRIDGE MODEL - SUMMARY OF GIRDER FORCES AND MOMENTS

STEP NO. II.2.10 (NORMALIZED) - AFTER 30 KSI CONDITIONING LOAD

SECTION A

	GIRDER 1	GIRDER 2	GIRDER 3	GIRDER 4	GIRDER 5	ALL GIRDERS
LOCATION OF GIRDER EXPERIMENTAL NEUTRAL AXIS (INCHES)						
(1) DISTANCE OF N.A. FROM LINE OF COMP. METERS	4.40	.73	2.58	3.33	4.19	
(2) DISTANCE OF N.A. FROM LINE OF TENSILE STEEL	13.91	17.58	15.73	14.98	14.12	

SUMMARY BASED ON CARLSON STRAINS IN CONCRETE,
CLIP-GAGE STRAINS FOR MAIN TENSILE STEEL,
AND MICRODOT STRAINS FOR OTHER STEEL

	GIRDER 1	GIRDER 2	GIRDER 3	GIRDER 4	GIRDER 5	ALL GIRDERS
TOTAL INTERNAL FORCES (KIPS)						
(3) COMPRESSIVE FORCES	-70.81	-53.09	-63.00	-56.19	-49.07	-292.16
(4) TENSILE FORCE	43.88	72.07	54.53	46.75	24.81	242.04
(5) NET AXIAL FORCE	-26.93	18.98	-8.47	-9.44	-24.26	-50.12
(6) RATIO OF COMP. FORCE TO TENSILE FORCE	1.61	.74	1.16	1.20	1.98	1.21
TOTAL INTERNAL MOMENTS (KIP-FT)						
(7) ABOUT COMPRESSION FLANGE MID-DEPTH	65.04	107.10	81.33	69.29	36.64	359.40
(8) ABOUT TENSION FLANGE STEEL	105.90	78.34	94.18	83.53	73.42	435.35
(9) ABOUT ENTIRE GROSS-SECTION N.A.	83.92	94.07	87.16	75.85	53.45	394.45
(10) ABOUT GIRDER EXPERIMENTAL N.A.	74.64	106.13	83.07	71.80	44.86	380.50
MOMENT PERCENTAGES TAKEN BY EACH GIRDER						
(11) ABOUT COMPRESSION FLANGE MID-DEPTH	18.10	29.80	22.63	19.28	10.20	(100.00)
(12) ABOUT TENSION FLANGE STEEL	24.32	17.99	21.63	19.19	16.86	(100.00)
(13) ABOUT ENTIRE GROSS-SECTION N.A.	21.27	23.85	22.10	19.23	13.55	(100.00)
(14) ABOUT GIRDER EXPERIMENTAL N.A.	19.62	27.89	21.83	18.87	11.79	(100.00)

TOTAL SECTION MOMENTS
(15) CALCULATED FROM EXPERIMENTAL LOADS AND REACTIONS = 433.36
(16) RATIO (7) TO (15) = .83
(17) RATIO (8) TO (15) = 1.00
(18) RATIO (9) TO (15) = .91
(19) RATIO (10) TO (15) = .88

FIG. 13 TYPICAL OUTPUT FOR AN INSTRUMENTED SECTION OBTAINED FROM MOMENT PROGRAM

3.6 REACTION Program

The REACTION program printed the experimental reactions at the east and west abutments and center column footing of the box girder bridge model, compared the results with the applied loads and with reactions calculated from continuous beam formulas for each loading case. External moments of all experimental loads and reactions were calculated, first, about the N-S centerline and then about E-W centerline of the bridge, to provide additional external static checks on the experimental reaction values. Moments at the instrumented sections and the midspans were also computed from the experimental reactions and compared with analytical values. An example of a typical output is shown in Fig. 14.

3.7 Partial Modification of Data at Section D

After the scheme of data reduction described in the earlier sections was implemented for several loading cases, it was observed that, even under fully symmetric loading conditions, the compressive strains registered at the instrumented section D in the northern half (near girders 1 and 2) of the box girder bridge model were significantly higher than those registered in the southern half of the same section. As the latter strains agreed closely, for cases of symmetrical loading conditions, with those observed in the compressive strain meters at the instrumented section A, the discrepancy was not immediately explicable. However, during the demolition of the box girder bridge model, which took place shortly afterwards, it was decided to observe the positions of the concrete strain meters, and it was found that far more lead wires of instrumentation emerged from the north side of the slab in the region of section D than from the south side. Although effort had been made

STEP NO. II.2.10 (NORMALIZED) - AFTER 30 KSI CONDITIONING LOAD

SUMMARY OF MEASURED APPLIED LOADS AND REACTIONS (KIPS)

LOADS APPLIED AT X=18.00 FT ON GIRDERS- 1
LOADS APPLIED AT X=54.00 FT ON GIRDERS- 1

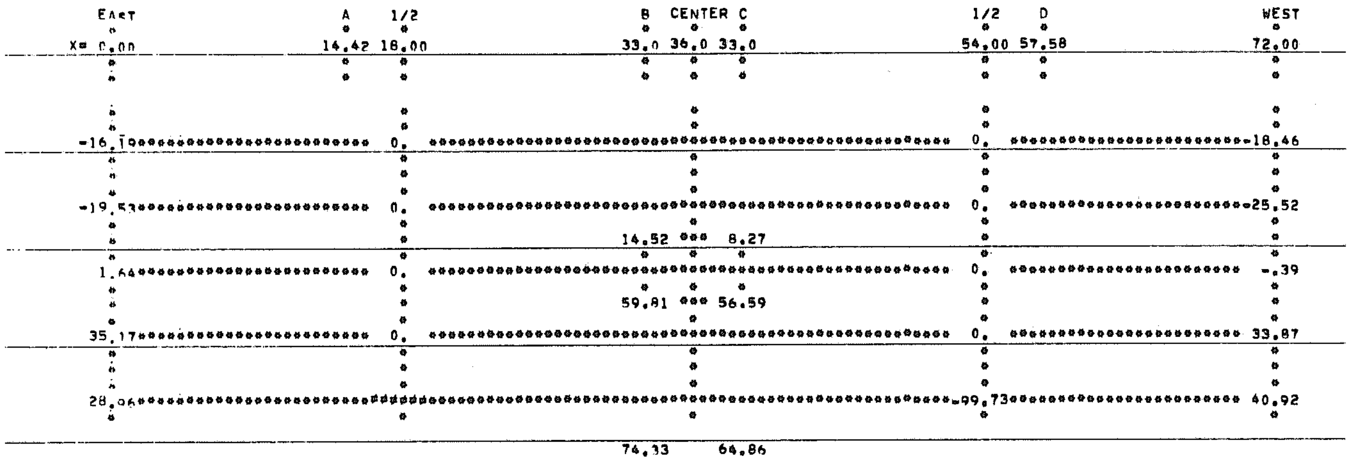

30.05	TOTALS	MEASURED		-100.00	TOTALS	MEASURED		139.19	TOTALS	MEASURED		-99.73	TOTALS	MEASURED		30.42			
31.28	TOTALS	THEORETICAL		-100.00	TOTALS	THEORETICAL		137.32	TOTALS	THEORETICAL		-99.73	TOTALS	THEORETICAL		31.14			
.96	RATIO	MEAS/THEOR		1.00	RATIO	MEAS/THEOR		1.01	RATIO	MEAS/THEOR		1.00	RATIO	MEAS/THEOR		.98			

STATICS CHECK OF MEASURED APPLIED LOADS AND REACTIONS (KIPS AND KIP-FT)

SUM OF APPLIED LOADS = -199.73 SUM OF REACTIONS = 199.66
SUM OF VERTICAL FORCES = -.07

SUM OF MOMENTS ABOUT N-S CENTER LINE = 5871.86 -5875.66 = -3.80
SUM OF MOMENTS ABOUT E-W CENTER LINE = 1061.97 -925.45 = 136.52

TOTAL STATICAL MOMENTS (KIP FT) CALCULATED FROM APPLIED LOADS AND REACTIONS

			MEASURED	THEORETICAL	RATIO M/T
AT SECTION A,	X = 14.42 FT	MOMENT =	433.36	450.99	.961
AT MIDSPAN I,	X = 18.00 FT	MOMENT =	540.95	562.95	.961
AT SECTION B,	X = 33.00 FT	MOMENT =	-508.25	-467.92	1.086
AT CENTER (FROM EAST FORCES),	X = 36.00 FT	MOMENT =	-718.09	-674.09	1.065
AT CENTER (FROM WEST FORCES),	X = 36.00 FT	MOMENT =	-700.09	-674.09	1.039
AT SECTION C,	X = 39.00 FT	MOMENT =	-492.15	-468.32	1.051
AT MIDSPAN II,	X = 54.00 FT	MOMENT =	547.54	560.54	.977
AT SECTION D,	X = 57.58 FT	MOMENT =	438.64	449.05	.977

FIG. 14 TYPICAL OUTPUT OBTAINED FROM REACTION PROGRAM

at all the instrumented sections to fan the lead wires out over an adequate area, the large number of lead wires emerging from the north side of the slab at section D had apparently decreased the stiffness of the concrete section there, causing the strain meters over half the section to register considerably higher strains even under symmetric loading than the identical instrumentation on the south side.

It was therefore decided to modify the compressive strains in the northern half of the slab at section D at the girder and midbay locations only, replacing the values by strains registered at mirror-image locations in the southern half of the slab at section D for cases of symmetrical loading, and by suitable complementary values for other cases.

All experimental results presented in this volume for section D only have the major strain values or, by extension, moment values in the northern half of the slab, i.e. for girders 1, 2 and one edge of girder 3 modified as above.

4. RESULTS FOR DEAD LOAD

4.1 General Remarks

The measurements for dead load, i.e. the self weight of the bridge and the extra weight of the steel billets added for proper simulation of prototype dead load behavior, were taken manually for each gage separately by means of a strain indicator box and a switching unit. The manual reading provided a check on the response of each individual gage as opposed to the sum of strain readings subsequently recorded by the Data Acquisition System.

For the dead load case, the clip gages for the measurement of tensile strains at Sections A and D were not attached because of the likelihood of damage ensuing to them during the removal of the shoring.

Theoretical results used for comparison with experimental values in the dead load case have been obtained from MUPDI3 and 1DFRAME; however, modified theoretical values for deflections and strains based on a cracked cross-section have also been employed.

Results for the dead load case of the box girder bridge model can be divided into results for reactions, deflections, longitudinal forces, strains and moments. Each is discussed below.

4.2 Reactions

The density of plain concrete used in the box girder bridge model was found as 141 pcf. Taking a value of 150 pcf for reinforced concrete, the weight of the bridge model for the dead load case was calculated as in the Table below:

TABLE 6 - TOTAL DEAD WEIGHT OF BOX GIRDER MODEL

	Volume cu. ft.	Weight kips
Cellular portion of bridge	399.5	59.93
Two end diaphragms	79.0	11.85
Center bent diaphragm	36.8	5.52
Bent footing	40.5	6.08
Bent column	4.8	0.72
Midspan diaphragm	3.1	0.47
Total self weight of bridge model		84.57
Weight of steel billets and sand		113.10
Total Dead Load		197.67

Weights are shown to the nearest 0.01 kip only for convenience of comparison with computer output results. Accuracy for each value is probably limited to three significant figures.

After insertion of the load cells, their adjustment, and then the removal of the shoring, the five load cells at each end abutment and the load cells at the center footing gave values for the reactions as shown in Table 7, column 4. The sum of all these reactions is 196.97 k, which when added to the small reactions in the load cells incurred during their placement before the removal of the shoring (given in column 3) give a figure of 199.09 k as the total dead load.

The theoretical values for the total reactions at E, F and W in column 2 are based on those obtained from 1DFRAME taking into consideration only the uniformly distributed weights of the cellular portion of the bridge and the steel billets and sand. The cellular portion is taken as 69 ft in length, and the steel billets and sand are assumed distributed over the whole length of the bridge giving a total uniformly distributed load of 2.44 kips per ft.

The total theoretical reactions at the ends from 1DFRAME are further sub-divided among the five load cells by considering the five load cells to be the supports for the transverse diaphragm analyzed as a uniformly loaded four span continuous beam. The center reaction is allocated equally to the four supports at the central footing.

For purposes of comparison, the experimental reactions in column 7 have the weights of the end diaphragms and center bent column with footing deducted from the actually measured values. Here again, each end diaphragm has been treated as being a continuous beam on the five load cell supports, and the weight of the center bent column with footing has been deducted equally from the four measured reactions.

As can be seen by comparing columns 1 and 7 in Table 7, not only does the total sum of the reactions agree remarkably well with the total applied load, but the total reactions at either end and at the center footing also agree with the theoretical values very closely. The reaction at the center footing is shared almost equally by the load cells at the four locations; however, there are some discrepancies in the distribution of the reaction at each end. Reaction 3 at the east abutment (Section E) appears to be larger at the expense of reactions 4 and 5, and the northern half of the bridge model seems to have a bigger reaction than the southern half.

This difference between experiment and theory for the transverse distribution of the total reaction to each of the five load cells at the two ends of the bridge was undoubtedly due to the manner in which the

TABLE 7: SUMMARY OF REACTIONS (KIPS) FOR DEAD LOAD CASE

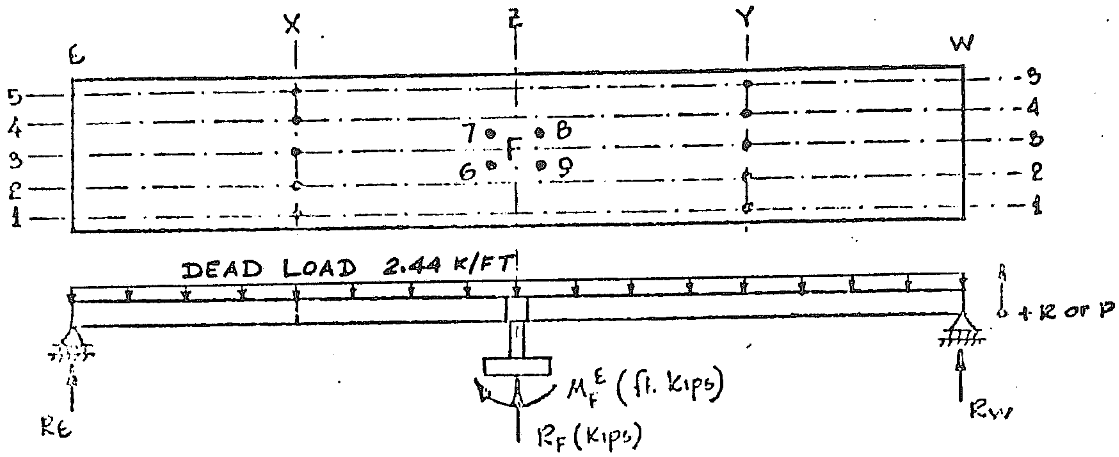

REACTION or LOAD	THEORETICAL NET REACTIONS (KIPS)	REACTIONS DUE TO LOAD CELL PLACEMENT (KIPS)	REACTIONS DUE TO REMOVAL OF SHORES (KIPS)	TOTAL REACTIONS (KIPS)	WEIGHT OF DIAPH., COL. AND FTG. (KIPS)	EXPERIMENTAL NET REACTIONS (KIPS)
1E	3.24	0.12	4.62	4.74	0.58	4.16
2E	9.41	0.18	11.04	11.22	1.69	9.53
3E	7.65	0.24	10.38	10.62	1.37	9.25
4E	9.41	0.24	8.22	8.46	1.69	6.77
5E	3.24	0.12	3.30	3.42	0.58	2.84
ΣE	32.95	0.90	37.56	38.46	5.91	32.55
6F	27.45	0.13	29.75	29.88	3.08	26.80
7F	27.45	0.12	30.74	30.86	3.08	27.78
8F	27.45	0.13	30.75	30.88	3.08	27.80
9F	27.45	0.12	30.25	30.37	3.08	27.29
ΣF	109.80	0.50	121.49	121.99	12.32	109.67
1W	3.24	0.24	4.20	4.44	0.58	3.86
2W	9.41	0.12	11.10	11.22	1.69	9.53
3W	7.65	0.24	8.52	8.76	1.37	7.39
4W	9.41	0.06	10.56	10.62	1.69	8.93
5W	3.24	0.06	3.54	3.60	0.58	3.02
ΣW	32.95	0.72	37.92	38.64	5.91	32.73
ΣR	175.70	2.12	196.97	199.09	24.14	174.95
ΣP	-173.03					-173.03
ΣR/ΣP	1.01					1.01

load cells were placed under the bridge, before the shoring was removed. An attempt was made, by jacking and the placement of metal shims of different thicknesses at each of the five support points, to obtain approximately equal initial readings in all the load cells. Subsequently, because of the different compressibility of the various shim thicknesses, this gave a situation where a very deep rigid end diaphragm rested on essentially five supports with slightly different spring constants. This caused the difference between the experimental and theoretical transverse distributions of the five reactions at each end of the bridge. However, the expermental and theoretical total reactions at each end were in close agreement and these totals were distributed by the rigid end diaphragms into the bridge in a similar way, thus not affecting the overall response of the bridge differently. The above comments point out the sensitivity of the distribution of end reactions to the manner in which reactions supports are placed in prototype structures as well as in models.

4.3 Deflections

Theoretical and experimental results for the deflections at instrumented Sections A and D and at quarter spans are given in Table 8 for the case of total dead load. Experimental deflections, for this case only, had to be measured prior to the placement of the deflection potentiometers by means of precise level measurements on a ruler graduated to 1/16 in. Theoretical results in column 2 are those given by MUPDI3, which considers a homogeneous uncracked cross-section. The ratio of experimental to theoretical deflections are given in column 4 where it can be seen that experimental deflections are considerably higher than those predicted by theory based on an uncracked section.

TABLE 8: SUMMARY OF DEFLECTIONS (INCHES) FOR DEAD LOAD CASE

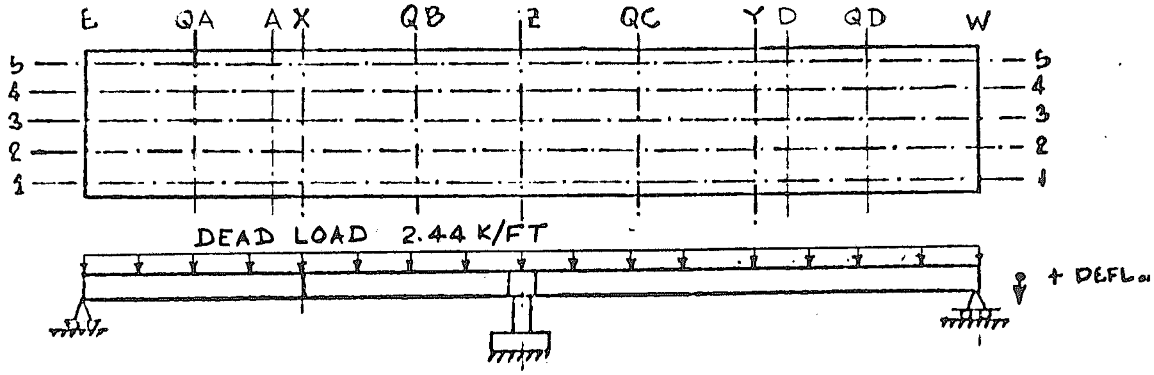

DEFLECTION	THEORETICAL RESULTS	EXPERIMENTAL RESULTS	$\frac{E}{T}$	$\frac{I_G}{I_{EFF}}$
1 QA	0.20	0.19	0.95	
5 QA	0.20	0.19	0.95	
1 A	0.25	0.38	1.52	1.42
2 A	0.25	0.38	1.52	1.42
3 A	0.25	0.38	1.52	1.42
4 A	0.25	0.31	1.24	1.42
5 A	0.25	0.38	1.52	1.42
1 QB	0.13	0.13	1.00	
5 QB	0.13	0.13	1.00	
1 QC	0.13	0.19	1.46	
5 QC	0.13	0.19	1.46	
1 D	0.25	0.44	1.76	1.06
2 D	0.25	0.44	1.76	1.06
3 D	0.25	0.44	1.76	1.06
4 D	0.25	0.44	1.76	1.06
5 D	0.25	0.44	1.76	1.06
1 QD	0.20	0.31	1.55	
5 QD	0.20	0.31	1.55	

In column 5 the ratio of I_g/I_{eff} taken from Table 5 for this load phase are shown and can be compared with column 4 to indicate how accurately the use of I_{eff} predicts the effect of cracking.

The values for deflection as given in Table 8 indicate that Span I with the midspan diaphragm experienced smaller deflections than the undiaphragmed span.

It should also be kept in mind when comparing values in Table 8 that the dead load experimental deflections were measured by means of a graduated rule having a least count of 1/16 in. [$\simeq$ 0.06 in.]. The maximum deflection measured was only 0.44 in. A change of 0.06 in. in the experimental values recorded could significantly reduce the discrepancy between Sections A and D or between experimental and theoretical values.

It is of interest to note that the maximum measured dead load deflection of 0.44 in. is 1/982 of the 36 ft. span and because of similitude this same ratio could be expected in a prototype structure.

4.4 Strains and Longitudinal Forces at a Section

The summary of dead load strains in microinches per inch at the instrumented Sections A, B. C and D comprises Tables 9A and 9B. Theoretical results are based on the procedure described in Section 2.4.2.

Tensile and compressive forces over the cross-section at each instrumented section are shown in Table 10. Theoretical values were obtained automatically from MUPDI3 by separately integrating the forces at a section in the flanges and web on each side of the gross uncracked section neutral axis. Experimental values were obtained from the MOMENT program into which the relevant data were fed.

Although the reactions to the dead load as measured by the load cells, Table 8, were in close agreement with theoretical values, it is seen that experimental strains at the instrumented sections, Tables 9A and 9B, are much higher than those predicted by theory. This is probably due to cracking in the model and the unknown internal stress state prior to the removal of shores and formwork.

Table 10 shows that the conditions of statics are not satisfied at the instrumented sections, the experimental compressive forces being greater in every case than the experimental tensile forces. The latter, however, are in fairly good agreement with the values given by theory.

The dead load case was unique in that it represented the removal of the constraints of shoring and formwork from the bridge model. The exact forces and stresses in the bridge model, formwork and shoring prior to the release of shoring are impossible to assess. The fact that the top slab of the box girder bridge model was placed several weeks after the bottom slab could have caused stresses in the bridge model due to differential shrinkage and bending action may have resulted. Thus prior to the removal of the forms, an internal section of the bridge model could have had longitudinal forces acting on it. What was measured during the removal of the forms was the transition from an initial unknown internal stress state under the constraints of shoring, etc. to another state under dead load alone. Unlike the internal stresses, the reactions due to dead load could be measured accurately since their values under the initial state were known. The external load cells measure the total values existing, while the internal strain gages can only be used to measure changes in strains in going from one load state to another.

TABLE 9A: SUMMARY OF STRAINS (MICRO IN/INCH) FOR DEAD LOAD CASE

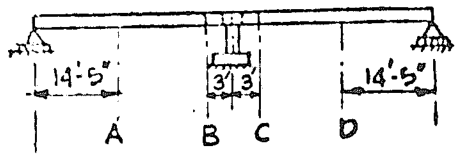

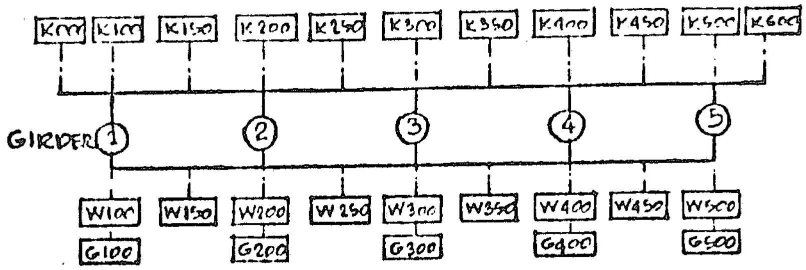

TENSION +

GAGE TYPE	GAGE LOCATION	LONGITUDINAL STRAINS					
		SECTION A			SECTION D		
		THEORY	EXPERIMENTAL MEAS.	EXPERIMENTAL ADJUSTED	THEORY	EXPERIMENTAL MEAS.	EXPERIMENTAL ADJUSTED
CONCRETE STRAIN GAGES	K000	-111	-174	-174	-111	-137	-141
	K100	-113	-177	-174	-113	-166	-166
	K150	-115	-162	-155	-115	-199	-183
	K200	-117	-151	-152	-117	-237	-195
	K250	-117	-153	-158	-117	-238	-186
	K300	-118	-186	-181	-118	-122	-122
	K350	-117	-170	-170	-117	-186	-186
	K400	-117	-172	-172	-117	-195	-195
	K450	-115	-162	-162	-115	-183	-183
	K500	-113	-172	-172	-113	-166	-166
	K600	-111	-166	-166	-111	-141	-141
WELDABLE GAGES	W100	550	800	793	550	670	425
	W150		590	542		490	470
	W200	461	685	675	461	540	520
	W250		530	515		480	660
	W300	460	570	570	460	565	565
	W350		480	480		660	660
	W400	461	625	625	461	520	520
	W450		450	450		470	470
	W500	550	805	805	550	425	425

TABLE 9B: SUMMARY OF STRAINS (MICRO·IN/INCH) FOR DEAD LOAD CASE

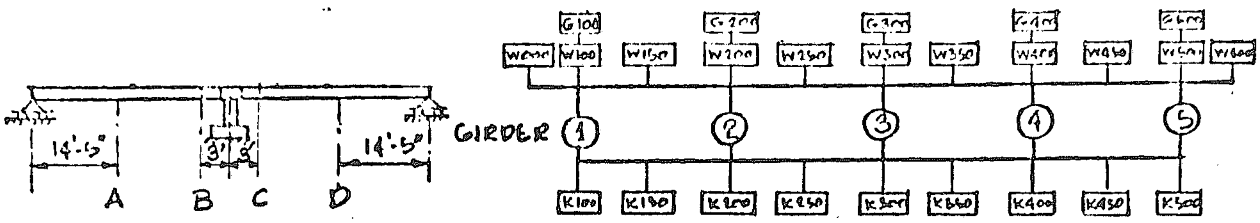

GAGE TYPE	GAGE LOCATION	LONGITUDINAL STRAINS SECTION B THEORY	SECTION B EXPERIMENTAL MEAS.	SECTION B EXPERIMENTAL ADJUSTED	SECTION C THEORY	SECTION C EXPERIMENTAL MEAS.	SECTION C EXPERIMENTAL ADJUSTED
CONCRETE STRAIN GAGES	K 100	-174	-194	-194	-174	-153	-152
	K 150	-181	-230	-230	-181	-217	-221
	K 200	-187	-207	-207	-187	-171	-171
	K 250	-189		-212	-189	-154	-332
	K 300	-191	-217	-217	-191	-198	-198
	K 350	-189	-250	-250	-189	-232	-232
	K 400	-187	-213	-213	-187	-173	-173
	K 450	-181	-296	-296	-181	-238	-238
	K 500	-174	-193	-193	-174	-149	-149
WELDABLE GAGES	W 000	360	300	300	360	290	290
	W 100	360	360	360	360	450	450
	W 150		365	365		440	443
	W 200	330	385	385	330	430	435
	W 250		360	360		370	369
	W 300	346	320	320	346	400	400
	W 350		290	290		440	440
	W 400	330	290	290	330	430	430
	W 450		335	335		350	350
	W 500	360	360	360	360	435	435
	W 600	360	310	310	360	370	370

TABLE 10: LONGITUDINAL FORCES (KIPS) AT INSTRUMENTED SECTIONS FOR DEAD LOAD CASE

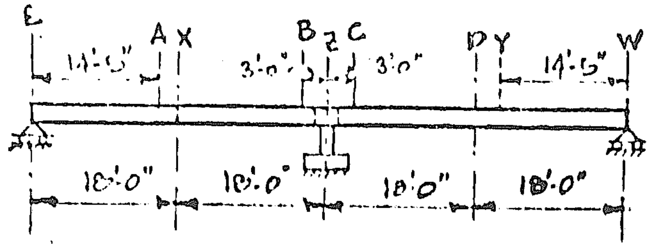

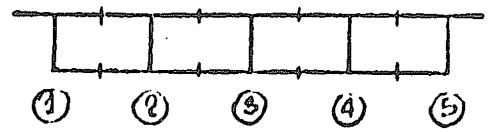

SECTION	GIRDER	COMPRESSIVE FORCE		TENSILE FORCE	
		THEORY	EXPT.	THEORY	EXPT.
SECTION A	1	-29.4	-45.5	22.4	25.9
	2	-31.7	-43.5	36.6	45.5
	3	-32.1	-48.4	36.5	40.5
	4	-31.7	-47.7	36.6	41.1
	5	-29.5	-43.7	22.4	25.7
	Σ	-154.4	-228.8	154.5	178.7
SECTION B	1	-22.7	-22.0	29.4	29.8
	2	-39.2	-40.0	34.4	39.9
	3	-39.8	-45.1	36.2	34.7
	4	-39.2	-47.3	34.4	32.1
	5	-22.7	-25.6	29.4	29.5
	Σ	-163.6	-180.0	163.8	166.0
SECTION C	1	-22.7	-21.3	29.4	34.3
	2	-39.2	-45.5	34.4	42.2
	3	-39.8	-52.0	36.2	41.1
	4	-39.2	-39.9	34.4	43.3
	5	-22.8	-21.1	29.4	32.2
	Σ	-163.7	-179.8	163.8	193.1
SECTION D	1	-29.5	-45.1	22.4	18.4
	2	-31.7	-56.7	36.6	43.4
	3	-32.1	-53.8	36.5	43.9
	4	-31.7	-56.7	36.6	43.4
	5	-29.5	-45.1	22.4	18.4
	Σ	-154.5	-257.4	154.5	167.5

4.5 Moments

Figure 15 gives the total moments at midspans X and Y, quarter spans QA, QB, QC, and QD and instrumented Sections A, B, C and D, all based on theoretical internal moments from MUPDI3, and on external moments determined from experimental reactions. It can be seen that these experimental and theoretical values are in close agreement. In addition, Fig. 15 shows values of experimental internal moments about the gross-section neutral axis at the instrumented Sections A, B, C and D as determined from the internal forces at these Sections. These are not in good agreement with theoretical values at Sections A and D, being considerably higher, but are in much better agreement at Sections B and C.

Table 11 gives a detailed break down of the distribution of the internal moments to each girder. Theoretical results are by MUPDI3, while experimental results obtained by the MOMENT program are given about four different axes for comparison. The different experimental values obtained for the four axes are due to the fact that the longitudinal compressive and tensile forces acting on each girder, Table 10, are not equal. Fig. 16 compares theoretical and experimental per centage distributions to each girder for moment, about the gross section neutral axis. It can be seen that while the absolute values, Table 11, are sometimes not in good agreement, the percentage distributions, Fig. 16, are quite good being within 1-2% of each other. It is of interest to note that for a uniform distribution of stresses accross the section one would expect that each girder would take a percentage of the total moment in direct proportion to the ratio of the individual girder to the total section moment of inertia. A calculation of these values

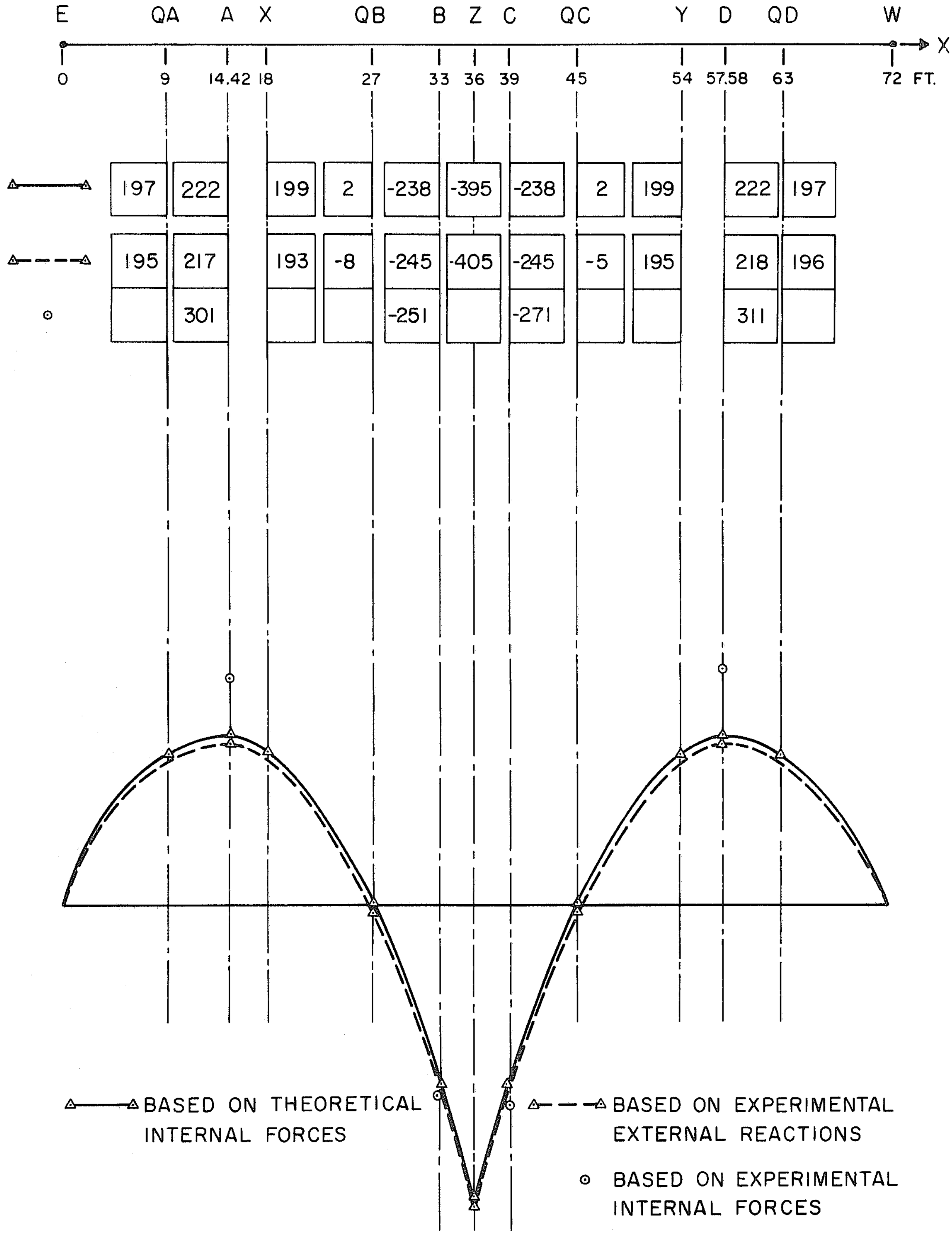

FIG. 15 TOTAL DEAD LOAD MOMENTS (FT-KIPS)

TABLE 11: DISTRIBUTION OF MOMENTS (KIP-FT AND %) TO EACH GIRDER FOR DEAD LOAD CASE

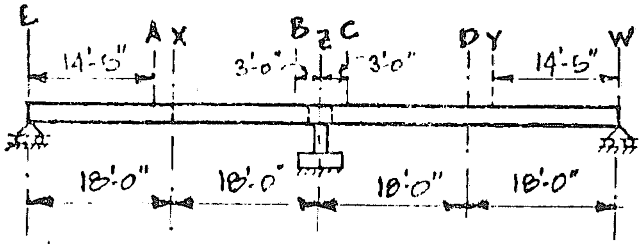

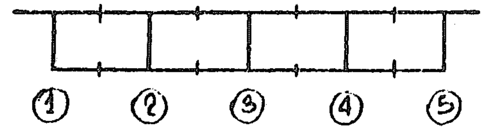

SECTION	GIRDER	ANALYTICAL RESULTS THEORY		DISTRIBUTION OF MOMENTS BASED ON FOLLOWING AXIS: COMPRESSION FLANGE MID-DEPTH		TENSION FLANGE STEEL		ENTIRE GROSS CROSS-SECTION NEUTRAL AXIS		EACH GIRDER EXPERIMENTAL NEUTRAL AXIS	
		K-FT	%	K-FT	%	K-FT	%	K-FT	%	K-FT	%
SECTION A	1	36	16.2	38	14.4	68	19.9	52	17.3	46	16.3
	2	50	22.5	68	25.6	65	19.0	67	22.2	67	23.7
	3	50	22.5	61	22.8	73	21.2	66	22.0	63	22.2
	4	50	22.5	61	23.0	71	20.8	66	21.9	64	22.4
	5	36	16.3	38	14.2	65	19.1	50	16.6	44	15.4
	Σ	222	100.0	266	100.0	342	100.0	301	100.0	284	100.0
SECTION B	1	-37	15.4	-44	17.9	-34	12.2	-36	14.4	-40	15.6
	2	-54	22.8	-59	24.1	-61	22.2	-58	23.1	-59	23.2
	3	-56	23.5	-51	20.9	-69	25.1	-59	23.4	-57	22.5
	4	-54	22.8	-47	19.3	-72	26.3	-59	23.5	-57	22.3
	5	-37	15.5	-44	17.8	-39	14.2	-39	15.6	-42	16.4
	Σ	-238	100.0	-245	100.0	-275	100.0	-251	100.0	-255	100.0
SECTION C	1	-37	15.4	-51	18.0	-33	12.0	-40	14.6	-43	15.4
	2	-54	22.8	-62	22.1	-70	25.3	-65	24.0	-65	23.1
	3	-56	23.5	-60	21.4	-80	28.9	-69	25.5	-68	24.3
	4	-54	22.8	-63	22.2	-61	22.1	-60	22.2	-63	22.3
	5	-37	15.5	-46	16.3	-32	11.7	-37	13.7	-42	14.9
	Σ	-238	100.0	-282	100.0	-276	100.0	-271	100.0	-281	100.0
SECTION D	1	36	16.2	27	10.9	67	17.5	45	14.5	39	13.6
	2	50	22.5	64	25.8	84	22.0	74	23.8	70	24.3
	3	50	22.5	66	26.6	80	21.0	73	23.4	70	24.2
	4	50	22.5	64	25.8	84	22.0	74	23.8	70	24.3
	5	37	16.3	27	10.9	67	17.5	45	14.5	39	13.6
	Σ	223	100.0	248	100.0	382	100.0	311	100.0	288	100.0

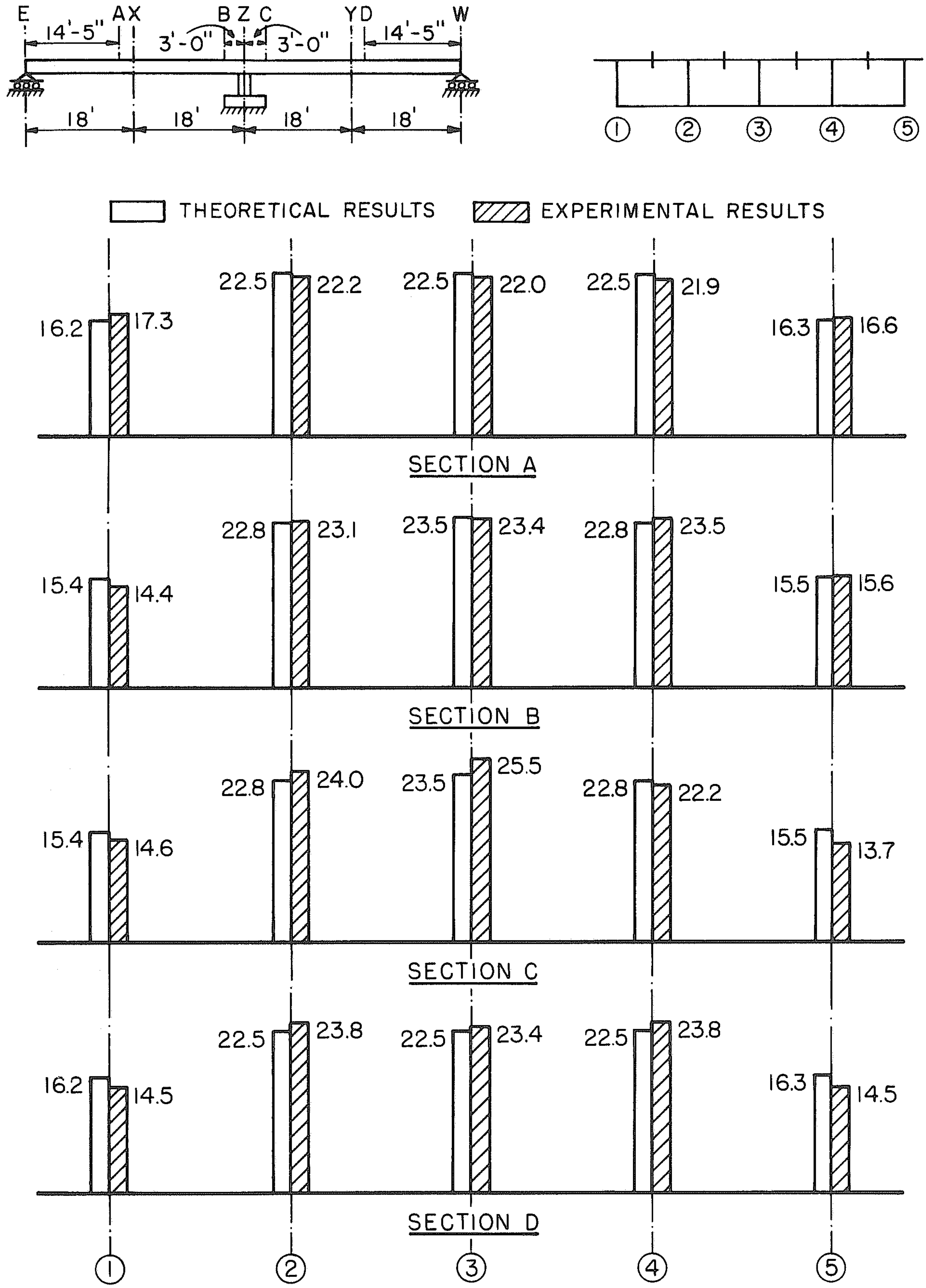

FIG. 16 PERCENTAGES OF TOTAL MOMENT AT A SECTION CARRIED BY EACH GIRDER FOR DEAD LOAD

based on uncracked sections taken about the gross-section neutral axis gives the following percentage distributions for girders 1 to 5 respectively: 16.5, 22.4, 22.4, 22.4, 16.5. The values shown in Fig. 16 closely approximate these percentages.

4.6 Summary

Experimental measurements of response due to dead load are more difficult to evaluate than those due to live load, because they are dependent on the sequence and manner of construction, placing of instrumentation, placing of reaction supports and removal of shoring. Nevertheless after comparing theoretical and experimental results the following conclusions can be made with respect to the dead load case.

1. Distribution of the total reactions between the east, center and west supports is accurately predicted by theory.

2. As a result of 1 the total external moment at any section can also be found with confidence.

3. The transverse distribution of the total reactions at each end to the five reaction supports is highly dependent on the manner of installation of these supports. The placement of the reaction supports after the bridge has been cast and the insertion of compressible metal shims to equalize reactions prior to the removal of forms gives reaction supports having slightly different spring constants. This results in an experimental transverse distribution of the total reaction at each end support which differs somewhat from theory. In future tests, the bridge should be cast directly on the supports, which should be made up of hard machined surfaces.

4. Experimental deflections at midspans I and II were approximately 50% and 75% higher than theoretical values based on an uncracked section.

5. Transverse distributions of deflection were uniform by both theory and experiment as expected for this loading.

6. The experimental values of strains and internal longitudinal forces and moments at a section in several cases were not in good agreement with theory or statics. This was probably due to the fact that it was impossible to measure the actual external and internal forces and stresses existing in the model prior to the removal of the forms. For subsequent live loadings, to be discussed later, the agreement was much better.

7. The agreement between theory and experiment for the percentage of the total moment at any section taken by each girder was very good, within 1-2%.

5. RESULTS FOR WORKING STRESS LOADS

5.1 General Remarks

As described in Volume I the loading program was divided into several phases in which initial conditioning loads were applied to create total maximum tensile stresses in the reinforcement of 24, 30, 40, 50 and 60 ksi. Each of these initial conditioning loads was then followed by a detailed sequence of point loads on the bridge.

One of the prime objectives of the test program was to determine the bridge response at working stress levels. The loading phase involving the initial application of conditioning loads to produce a maximum tensile stress of 30 ksi was chosen to be representative of response at working stress from the point of view of assessing actual box girder bridge behavior for design purposes. An advantage of using the 30 ksi stress level instead of the 24 ksi stress level was that 50% higher values of live load stresses could be registered for a total increase in the bridge model tensile stresses of only 6 ksi. All subsequent point loads in this phase, however, were chosen to produce maximum stresses, where applied, of the order of the working stresses, i.e. 24 to 30 ksi total maximum tensile stress in the reinforcement.

The 30 ksi working load phase contained the most complete and detailed loading schedule of any phase (See Vol. I). In this chapter a presentation and evaluation of results will be made for this phase for the following loadings and conditions.

(1) Point loads on girder webs at midspan.

(2) Effect of support restraints.

(3) Trucks and construction vehicle loads.

(4) Moving fork lift truck load.

5.2 Point Loads on Girder Webs at Midspans

Detailed tabulations of theoretical and experimental results related to reactions, deflections,strains and moments for each of the 19 point load combinations used are given in Vol. III (Tables 1 to 7 inclusive). All theoretical and experimental values have been normalized for purposes of comparison to loads of 100 kips per span. Theoretical values for these point load cases have been obtained from computer analyses using FINPLA2.

Because of the voluminous amount of data, only three typical point load cases will be treated in detail in the text of the present volume. These cases are: point load at location 5X; point load at location at 5Y; point loads at 5X + 5Y simultaneously. These cases have been chosen as typical of the 19 point load combinations, and comprise cases of the most eccentric loading at the diaphragmed and undiaphragmed midspans, producing maximum positive moments in the case of 5X or 5Y and maximum negative moments at the center bent in the case of 5X + 5Y. Furthermore, these loading cases lend themselves to comparisons of superposition which can be used as a check on the reliability of the experimental data.

In addition to the detailed study of reactions, deflections, strains and moments for cases 5X, 5Y and 5X + 5Y, a complete summary and discussion of theoretical and experimental moments for all 19 point load cases is given in Section 5.4.

5.2.1 Reactions

Figure 17 compares theoretical and experimental reactions for normalized 100 kip loads at 5X, 5Y, and 5X + 5Y. Fig. 17a shows the total vertical reactions at the end supports and at the central footing, while Fig. 17b depicts the transverse distribution of the total reaction at the east end to the five individual girder reaction supports.

In order to check superposition, Fig. 17, line (3), gives the sum of the results for loads placed separately at 5X, line (1), and at 5Y, line (2). This sum, line (3), can then be compared directly with line (4) which gives the results for loads at 5X + 5Y applied simultaneously. These comparisons show that superposition of theoretical results is perfect and for experimental results superposition is valid within a range of 1-5% for the larger significant reaction values.

Agreement between theoretical and experimental total reactions, Fig. 17a, at both ends and the central footing is excellent. The total reactions for a load at 5X are symmetric with those for a symmetric load at 5Y.

Comparing the theoretical and experimental transverse distribution of the total reaction at the east support, Fig. 17b, the agreement at girder 5 which has the largest reaction is good. While individual values at girder 1 and 2 differ, the sum of these two reactions indicates a good agreement between theory and experiment. As explained in Section 4.2, differences between theoretical and experimental reactions at individual supports is probably due to the slightly different stiffnesses (spring constants) of the individual reaction assemblies.

5.2.2 <u>Deflections</u>

Deflections for load cases 5X, 5Y and 5X + 5Y are shown in Fig. 18 and 19. In each case curves are given based on 1.0 and 1.5 times the theoretical values obtained from FINPLA2, which assumes an uncracked section. These may be compared with the individually plotted experimental points.

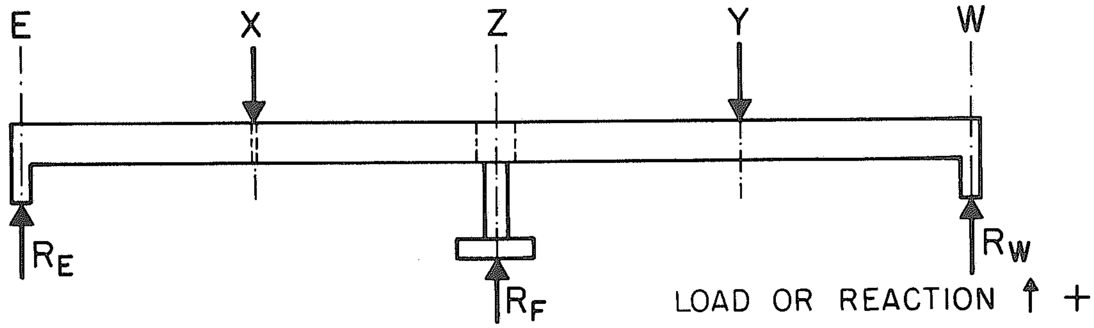

LOAD	R_E THEO.	R_E EXPT.	R_F THEO.	R_F EXPT.	R_W THEO.	R_W EXPT.
(1) 5X	39.2	37.9	69.1	69.5	-8.2	-8.3
(2) 5Y	-8.2	-8.4	69.0	69.7	39.2	39.0
(3) (1)+(2)	31.0	29.5	138.0	139.2	31.0	30.7
(4) 5X+5Y	31.0	30.3	138.0	140.2	31.0	31.5

(a) TOTAL REACTIONS AT END AND CENTER SUPPORTS

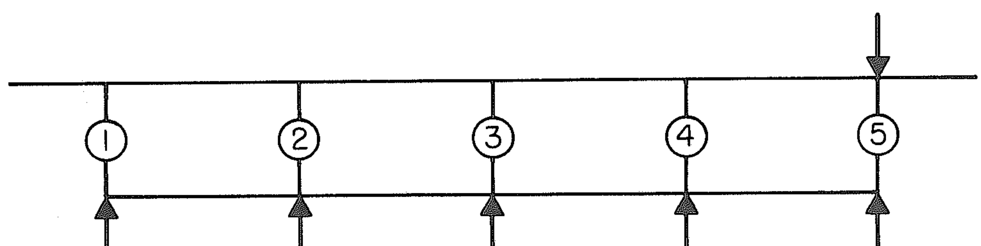

LOAD	R_1 THEO.	R_1 EXPT.	R_2 THEO.	R_2 EXPT.	R_3 THEO.	R_3 EXPT.	R_4 THEO.	R_4 EXPT.	R_5 THEO.	R_5 EXPT.
(1) 5X	-14.8	-5.2	1.7	-17.8	5.8	6.1	11.9	18.8	39.5	36.0
(2) 5Y	-9.8	-2.9	-2.8	-10.4	-1.6	-4.0	-0.4	3.8	6.4	5.2
(3) (1)+(2)	-29.6	-8.1	-1.1	-28.2	4.2	2.1	11.5	22.6	45.9	41.2
(4) 5X+5Y	-29.6	-6.7	-1.1	-29.0	4.2	0.4	11.5	22.2	45.9	43.4

(b) TRANSVERSE DISTRIBUTION OF REACTIONS AT EAST SUPPORT

FIG. 17 REACTIONS (KIPS) FOR NORMALIZED 100 KIP LOADS AT 5X, 5Y, 5X + 5Y

Figure 18 shows the longitudinal variation of the deflection along the loaded girder 5 and Fig. 19 shows the transverse distribution of deflections at the loaded sections. A study of Figs. 18 and 19 indicates that the principle of superposition is valid for both theoretical and experimental results. Comparing results from theory with experiment, it can be seen that the theory predicts the general distribution of deflections quite well if the theoretical values based on an uncracked section are multiplied by a factor of about 1.5 to account for cracking at this stress level. This factor of 1.5 can be compared with the value of approximately 2.2 given in Section 2.4.1 which is the calculated ratio of I_g/I_{eff} for the 30 ksi stress level. It is evident that this latter factor greatly overestimates the effect of cracking on deflections.

5.2.3 Strains

Comparisons of the transverse distributions of theoretical and experimental longitudinal strains in the top and bottom slabs at the instrumented sections under loading case 5X + 5Y are given in Fig. 20. While there is general agreement, substantial differences exist at certain points. Theoretical strains have been obtained using the modifying procedure described in Section 2.4.2 which only gives values at the top and bottom of each web and thus straight lines are drawn between these points. Experimental values are adjusted as described in Section 3.4, however, only values at and halfway between the webs have been plotted and connected by straight lines.

5.2.4 Moments

The longitudinal distribution of total moments at a section are given in Fig. 21. At almost all sections good agreement is obtained

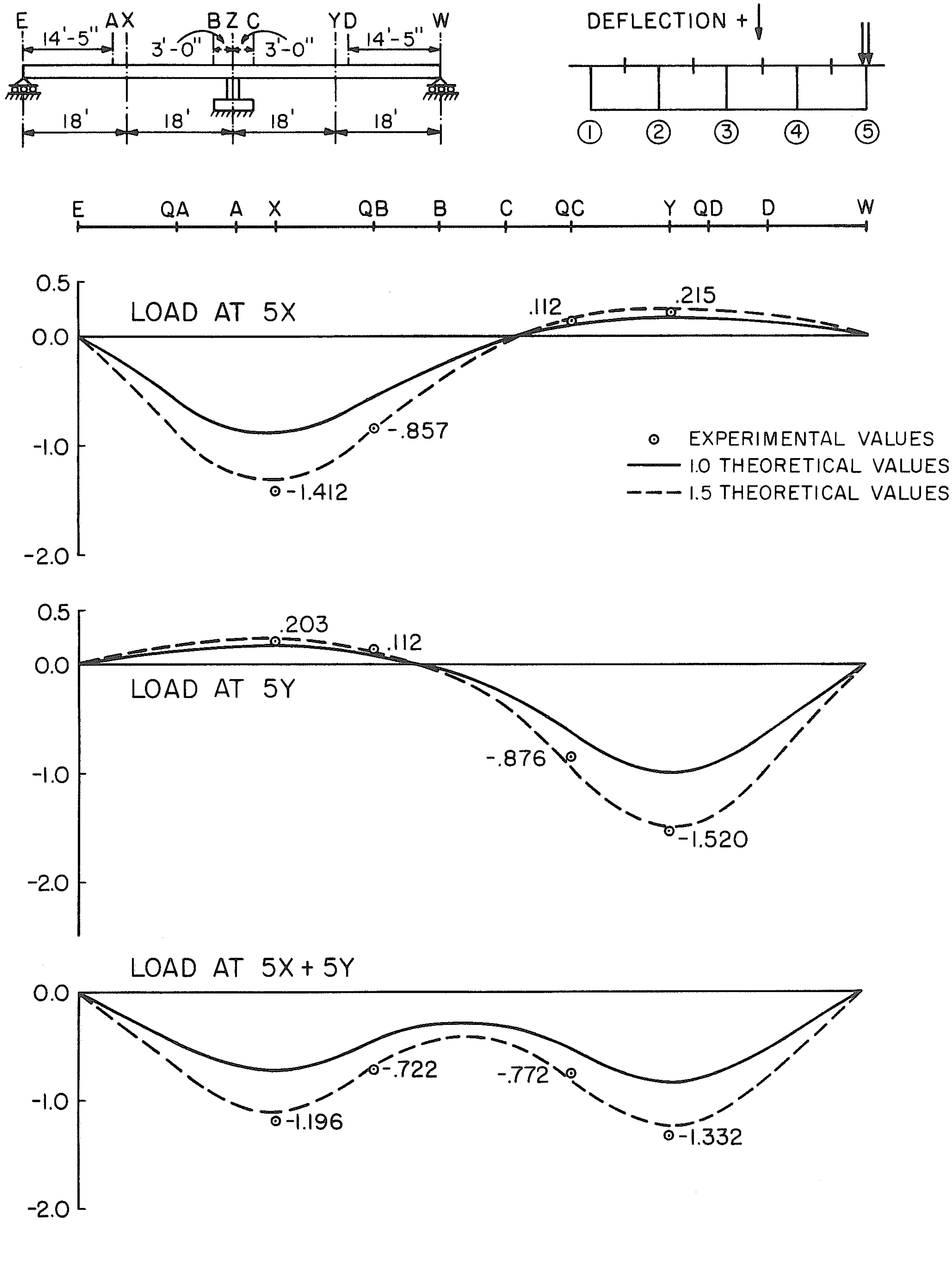

FIG. 18 VERTICAL DEFLECTIONS (INCHES) ALONG GIRDER 5 FOR 100 KIP LOADS AT 5X, 5Y, 5X + 5Y

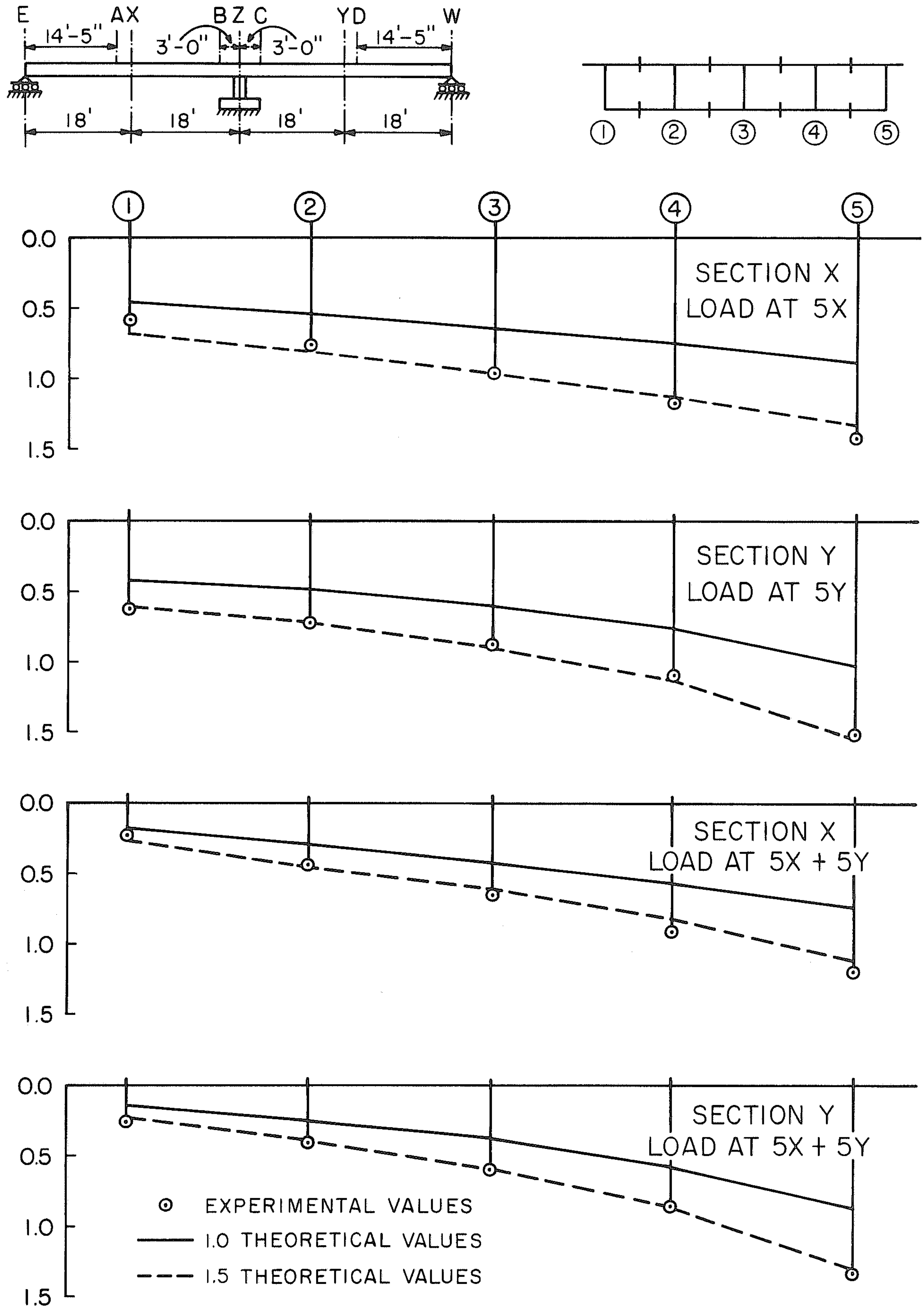

FIG. 19 VERTICAL DEFLECTIONS (INCHES) AT TRANSVERSE SECTIONS FOR 100 KIP LOADS AT 5X, 5Y, 5X + 5Y

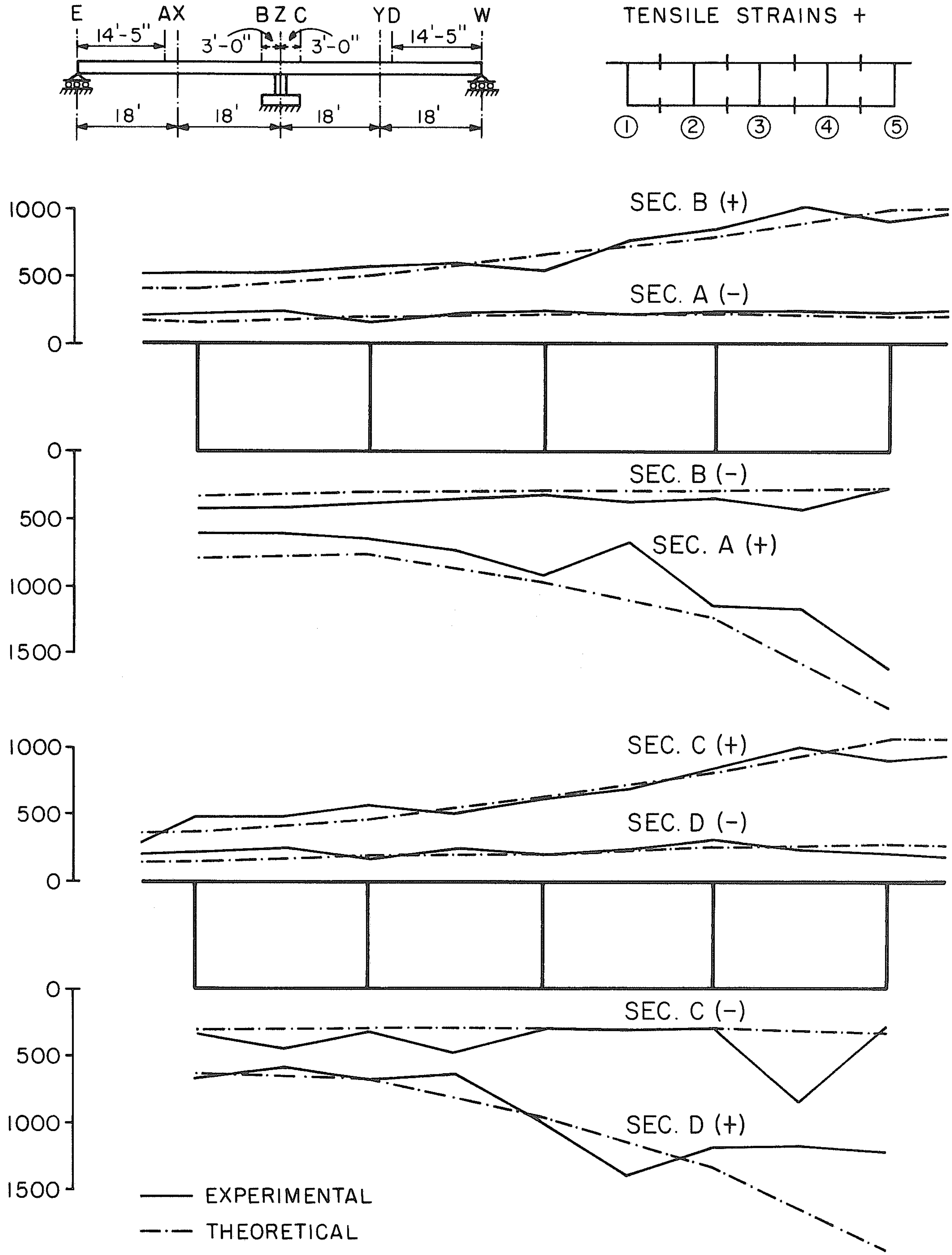

FIG. 20 LONGITUDINAL STRAINS (MICRO–INCH/INCH) AT TRANSVERSE SECTIONS FOR 100 KIP LOADS AT 5X + 5Y

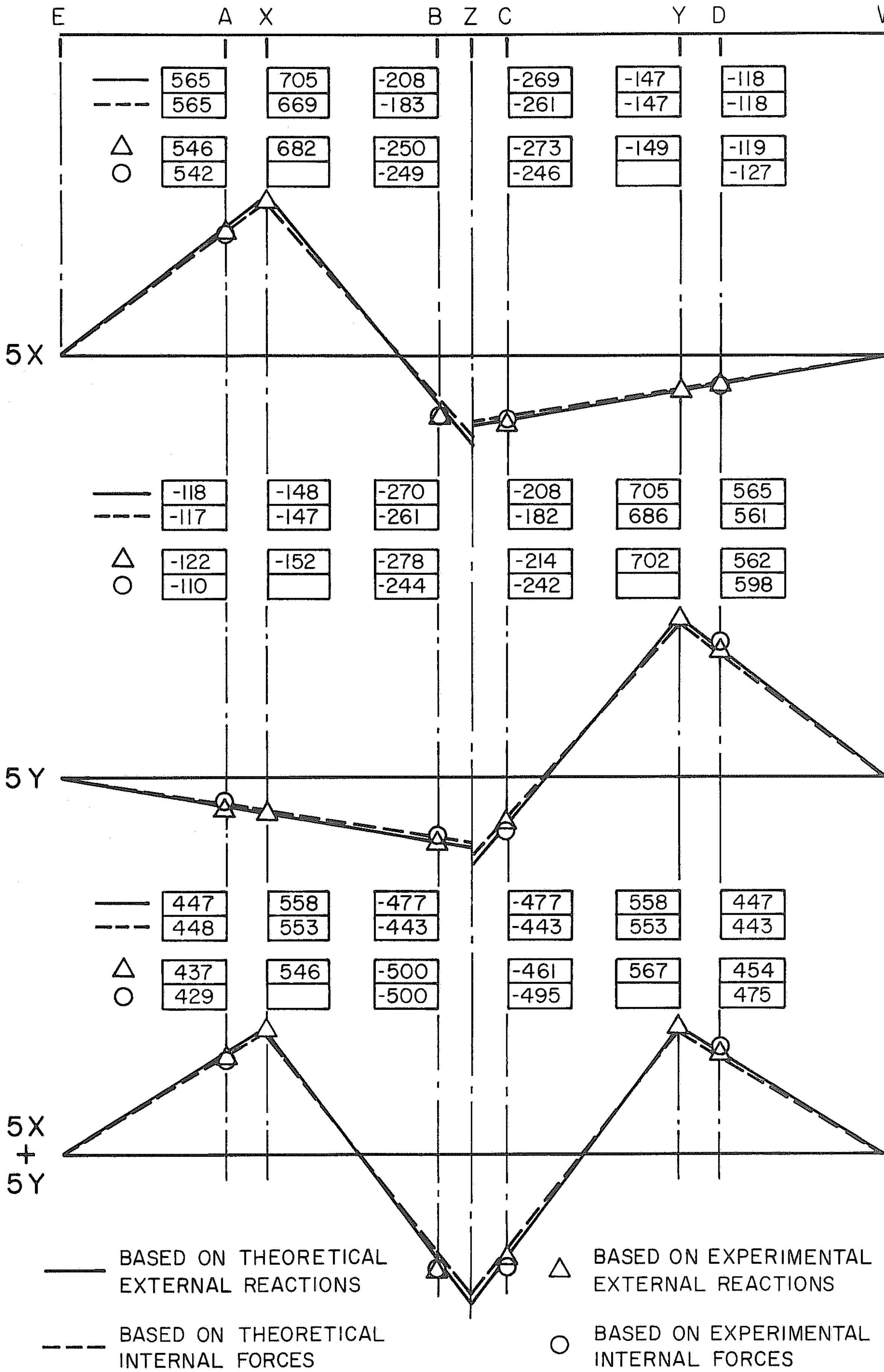

FIG. 21 TOTAL MOMENTS (FT-KIPS) AT A SECTION FOR NORMALIZED 100 KIP POINT LOADS AT 5X, 5Y, 5X + 5Y

between theoretical values and experimental values both for moments determined by experimental external reactions and by internal longitudinal forces at instrumented sections. Only at support sections in the loaded spans do some differences occur. The principle of superposition is also satisfied for almost all theoretical and experimental values shown.

The transverse distributions of the total moments at the instrumented Sections A, B, C and D are illustrated in Figs.22, 23 and 24. The percentages shown are for 100 kip point loads at the most eccentric positions 5X, 5Y and 5X + 5Y and may be compared with the best possible distributions of 16.5, 22.4, 22.4, 22.4 and 16.5% for girders 1 to 5 respectively which would be obtained for a uniform distribution of stress across the entire section. The closer one gets to these optimum values, the better are the load distribution properties of the bridge.

From Figs. 22, 23, 24 several observations may be made.

(1) The agreement between theory and experiment is generally good with differences in most cases being of the order of 1-2%. Only at girder 5 at Section B under loading 5X, and at Sections C and D under loading 5Y and 5X + 5Y do the theoretical values exceed the experimental values by larger amounts.

(2) Comparing results for a load at 5X, Fig. 22, with those for a load at 5Y, Fig. 23, it can be seen that the distributions at sections in the unloaded spans approach the optimum values associated with a uniform stress distribution mentioned above. For sections in the loaded spans a slightly higher concentration of moments in girders 4 and 5 is found for a load in the undiaphragmed span, 5Y, than for a load in the diaphragmed span, 5X.

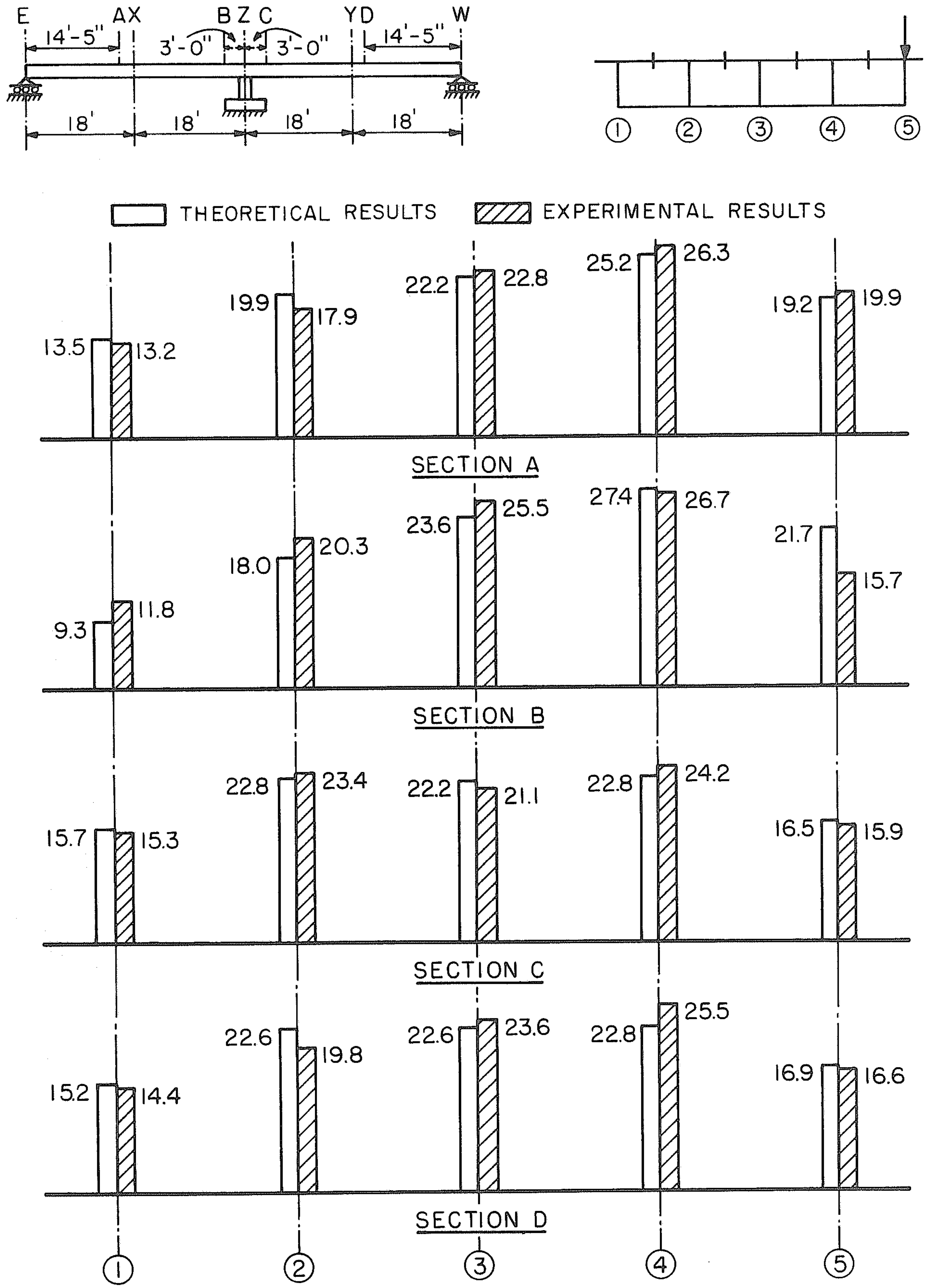

FIG. 22 PERCENTAGES OF TOTAL MOMENT AT A SECTION CARRIED BY EACH GIRDER FOR 100 KIP LOAD AT 5X

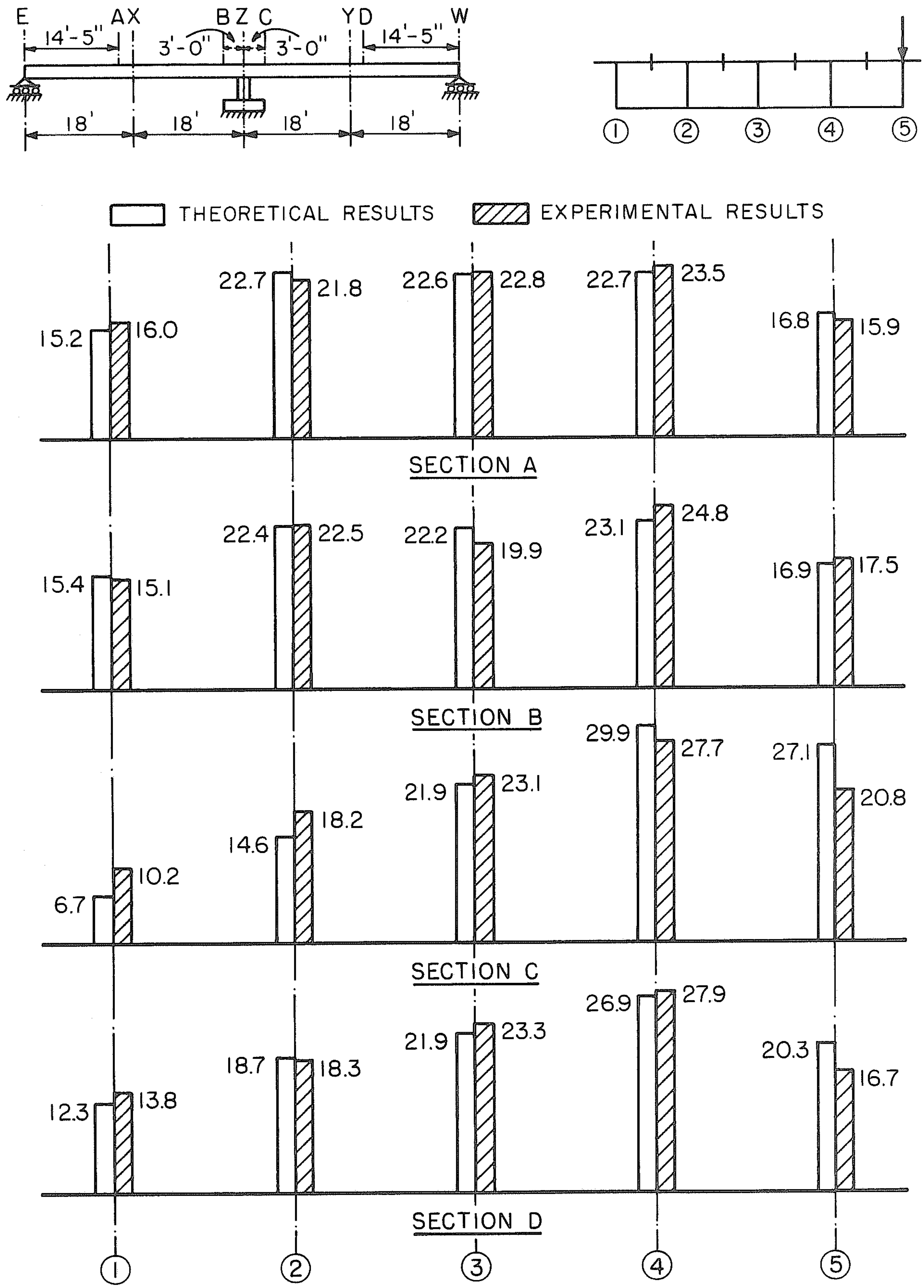

FIG. 23 PERCENTAGES OF TOTAL MOMENT AT A SECTION CARRIED BY EACH GIRDER FOR 100 KIP LOAD AT 5Y

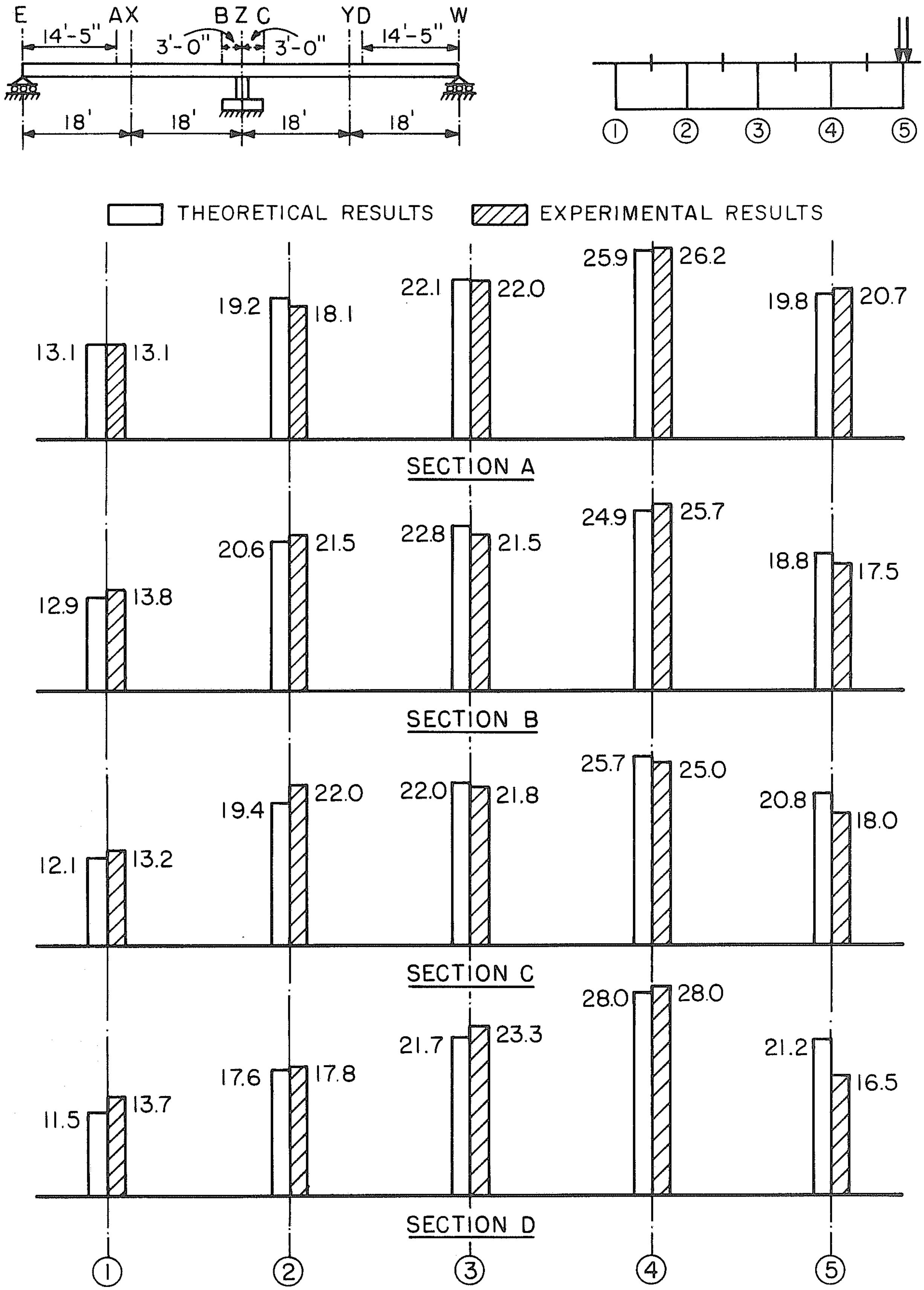

FIG. 24 PERCENTAGES OF TOTAL MOMENT AT A SECTION CARRIED BY EACH GIRDER FOR 100 KIP LOADS AT 5X + 5Y

(3) For the loading 5X + 5Y, Fig. 24, the distribution is almost identical at Sections A, B and C while at D, near the undiaphragmed midspan section, a slightly higher concentration of moment exists in girder 4.

5.3 Effect of Support Restraints

As described in detail in Vol. I, most of the experimental program was carried out for the bridge model with what will hereafter be termed normal support restraints. These consisted of simply supported end abutments and the center bent being supported by a single central column as shown in Figs. 1 and 2. However, in order to investigate the effect of torsional restraint at the center bent and longitudinal restraint at the two end diaphragms, all 19 point load cases were repeated for the 30 ksi working stress phase for each of these two support conditions.

Torsional restraint at the center bent was provided by adding vertical supports under girders 1 and 5 at center Section Z. Longitudinal restraint at the end diaphragms was provided by adding three horizontal reaction supports at each end in line with girders 1, 3, 5. The horizontal reactions were located at a vertical distance of 3.42 ft. below the top surface of the bridge, which is equivalent to 2.73 ft. below the gross neutral axis of the bridge. Details of these support conditions are given in Figs. 24 and 25 of Vol. I.

Detailed tabulation of experimental results only for selected point load cases for the torsional and longitudinal restraint cases are given in Vol. III (Tables 8 to 13 inclusive). In this section comparisons in general of experimental results only will be made for the three support conditions: (1) normal restraint; (2) torsional restraint; and (3) longitudinal restraint. Load cases 5X, 5Y and 5X + 5Y will be considered as typical cases.

5.3.1 Reactions

Figure 25 compares experimental reactions for each of the three support restraints under normalized 100 kip loads at 5X + 5Y. Comparisons with the normal support restraint case can then be made.

Figure 25a shows that the torsional restraint has little effect on the two end reactions, while the reaction at the center footing R_F decreases by the amount which is transferred to the vertical supports under girder 1 and 5 at the center bent, which are not recorded. The longitudinal restraint increases the end reactions and decreases the reaction under the center footing, while the total sum of all the reactions equals 197.3 kips compared to the total applied load of 200.0 kips. This small difference was probably resisted by the vertical friction at the horizontal reaction supports at each end. The increase in the vertical end reactions for the longitudinal restraint case is due to the negative moment developed at the two ends of the bridge under this condition.

Figure 25b shows a substantial decrease in reactions R_4 and R_5 for the torsional restraint case due to the fact that a greater portion of the total torque of the bridge is being taken at the center bent for this case compared to the normal support case. For the longitudinal restraint case, the increase in the total east reaction is being taken primarily at R_2 and R_4 with little change in the other reactions compared to the normal support case.

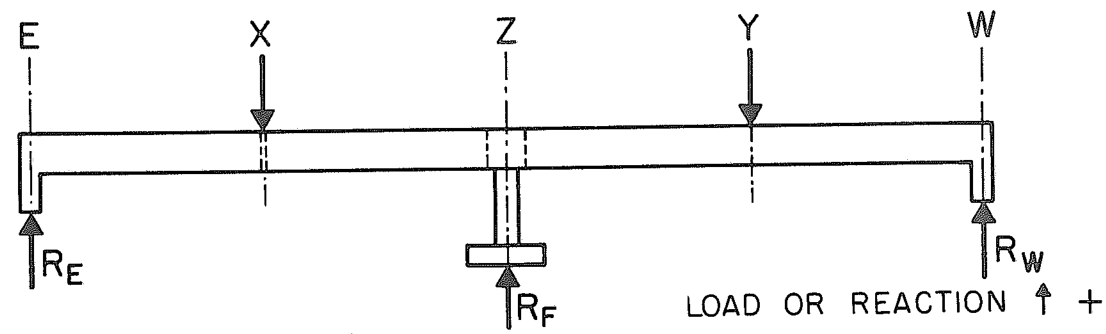

RESTRAINT	R_E	R_F	R_W
(1) NORMAL	31.0	138.0	31.0
(2) TORSIONAL	30.2	83.4	31.6
(3) LONGIT.	39.3	119.2	38.8

(a) TOTAL REACTIONS AT END SUPPORTS AND COLUMN FOOTING

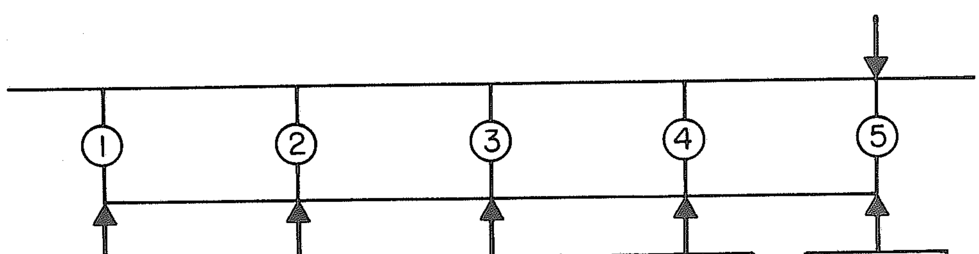

RESTRAINT	R_1	R_2	R_3	R_4	R_5
(1) NORMAL	-6.7	-28.2	2.1	22.6	41.2
(2) TORSIONAL	-5.6	-18.6	4.1	18.0	32.3
(3) LONGIT.	-5.5	-24.8	3.0	25.0	41.6

(b) TRANSVERSE DISTRIBUTION OF REACTIONS AT EAST SUPPORT

FIG. 25 EXPERIMENTAL REACTIONS (KIPS) FOR DIFFERENT SUPPORT RESTRAINTS UNDER 100 KIP LOADS AT 5X + 5Y

5.3.2 Deflections

Transverse distributions of experimental deflections at Sections X and Y are shown in Fig. 26 for the three support conditions under the loading 5X + 5Y. Comparing the torsional restraint case to the normal restraint case it can be seen that the deflections at center girder 3 are almost identical, while the deflections at the loaded girder 5 are slightly smaller indicating, as would be expected, that less twist occurred in the torsional restraint case. The longitudinal restraint case has the smallest deflections of the three cases due to the decrease in positive midspan moments for this case. However, it has a transverse deflected shape almost identical to the normal restraint cases. Comparing the undiaphragmed span Section Y to the diaphragmed span Section X it is evident there is a greater concentration of deflection in the former case directly under loaded girder 5.

5.3.3 Strains

Comparisons of the transverse distributions of experimental longitudinal strains for the different support conditions are given in Figs. 27 and 28 for loads at 5X + 5Y. The type of support restraint appears to have very little effect on the compressive strains at all sections except that at support Sections B and C there is a slight increase near the loaded girder for the torsional restraint case as should be expected.

For the tensile strains, the magnitudes and distributions for the normal and torsional restraint cases are similar except for a few isolated points. Curves for the longitudinal restraint case, while similar in shape to the other restraint cases, have values which are substantially smaller in magnitude. This is due to the combined

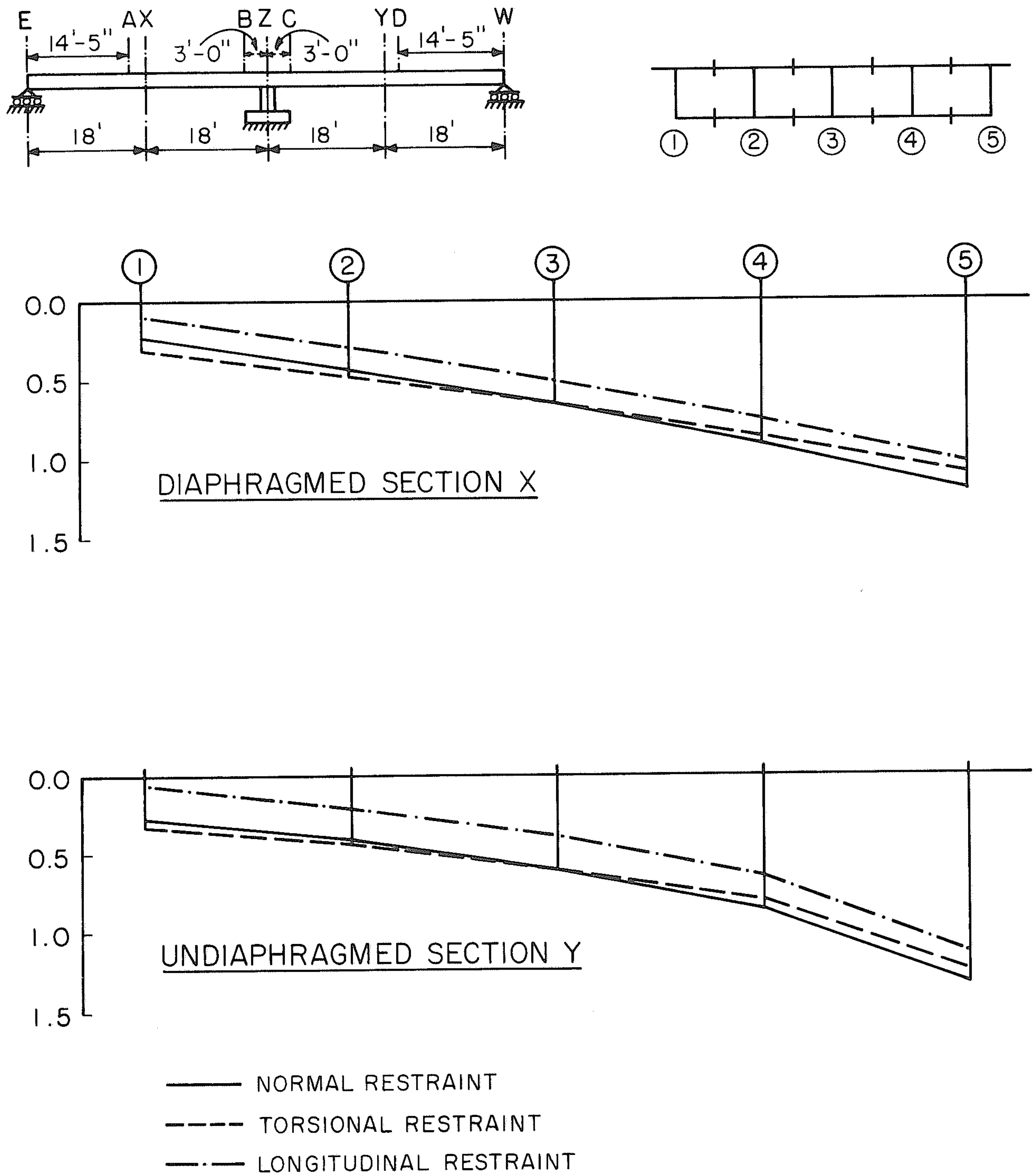

FIG. 26 EXPERIMENTAL DEFLECTIONS (INCHES) AT TRANSVERSE SECTIONS FOR DIFFERENT SUPPORT RESTRAINTS UNDER 100 KIP LOADS AT 5X + 5Y

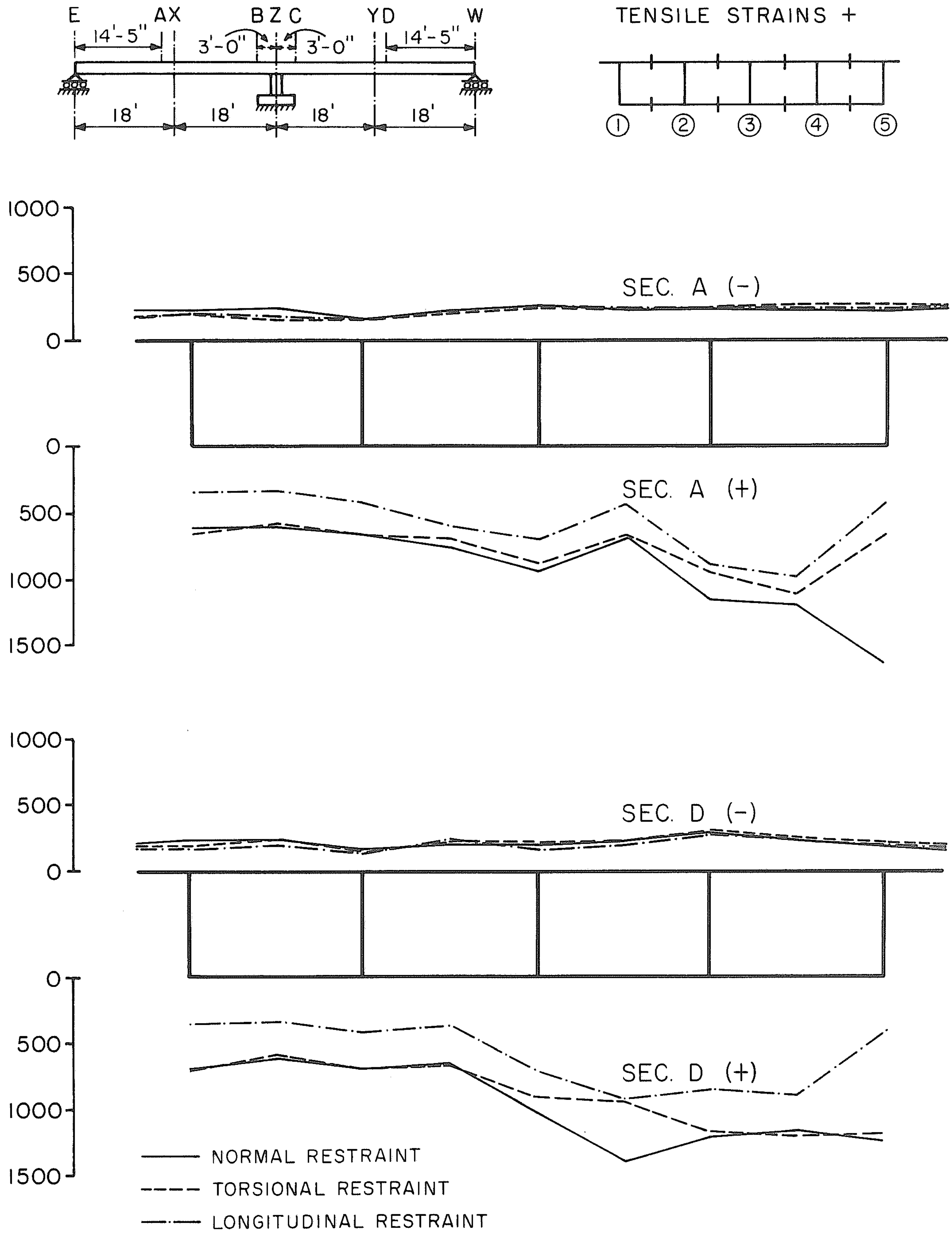

FIG. 27 EXPERIMENTAL LONGITUDINAL STRAINS (MICRO-INCH/INCH) IN TOP AND BOTTOM SLABS AT SECTIONS A AND D FOR DIFFERENT SUPPORT RESTRAINTS UNDER 100 KIP LOADS AT 5X + 5Y

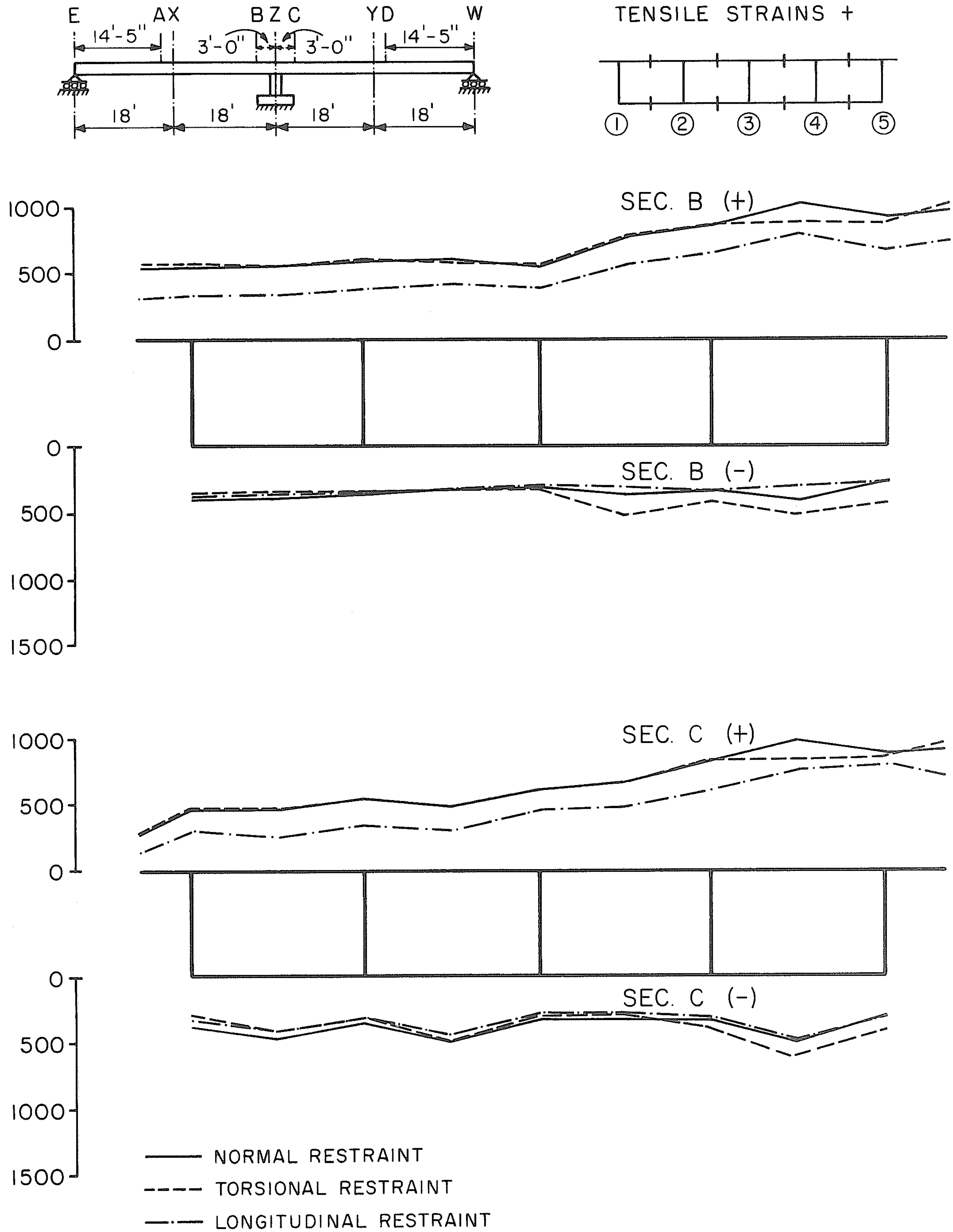

FIG. 28 EXPERIMENTAL LONGITUDINAL STRAINS (MICRO-INCH/INCH) IN TOP AND BOTTOM SLABS AT SECTIONS B AND C FOR DIFFERENT SUPPORT RESTRAINTS UNDER 100 KIP LOADS AT 5X + 5Y

additive effects at each section of a decrease in moment and the introduction of a longitudinal compressive axial force produced by the longitudinal reactions at the supports. Note that for the compressive strains these effects tend to cancel each other resulting in little change as mentioned above.

5.3.4 Moments

The longitudinal distributions of the total moments at a section for different support restraints are shown in Fig. 29 for 100 kip loads at 5X, 5Y and 5X + 5Y. Curves for theoretical values were obtained from 1DFRAME for cases both with and without longitudinal end restraints. Experimental points and numerical values for moments based on internal forces are given at Sections A, B, C and D for each of the three support restraint conditions.

Comparing these experimental results for the three loadings for a particular restraint it can be found that the principle of superposition is satisfied with maximum discrepancies of approximately 2, 4, 6 and 3% at Sections A, B, C and D respectively.

For the normal and torsional restraint cases agreement between experimental values and the theoretical curve without longitudinal restraint is generally very good except at support sections in the loaded spans where some differences occur. It should be observed that these latter sections are in regions of steep moment gradients where a shift of section of only 1 ft. on the bridge changes the moment by 30 to 60 ft. kips depending on the load case.

For the longitudinal restraint case, the theoretical curve can only be taken as a bounding curve since the full longitudinal restraint considered to exist across the width of the bridge in the

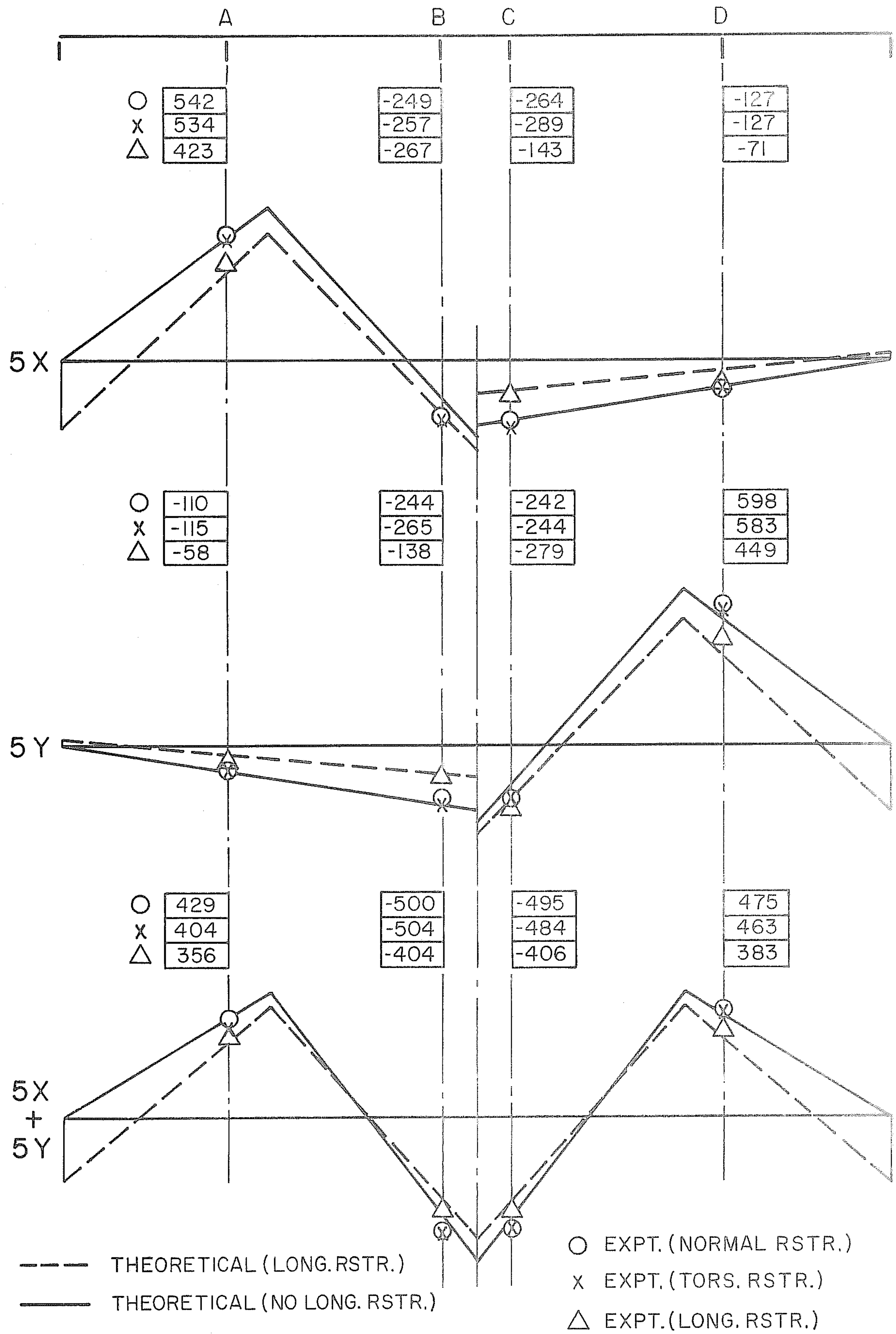

FIG. 29 TOTAL MOMENTS (FT-KIPS) AT A SECTION FOR DIFFERENT SUPPORT RESTRAINTS UNDER 100 KIP LOADS AT 5X, 5Y AND 5X + 5Y

1DFRAME analysis cannot be realized in the experimental case where point restraints were applied at only three points opposite girder 1, 3 and 5. However, agreement between theory and experiment is again generally good.

Comparing now only experimental values at Sections A, B, C and D in Fig. 29 to ascertain the effect of support restraints, the results for the normal and torsional restraints are quite similar. There is a very slight trend for a small drop in the positive midspan moments in the loaded spans for the torsional restraint case, but for practical design purposes, the difference would be considered negligible. Results for the longitudinal restraint case indicate considerably lower moments than the other cases indicating that the effect of such restraints, where they exist, should be taken into account.

The transverse distribution of the experimental moments at Sections A, B, C and D for the different support restraints are illustrated in Figs. 30, 31 and 32. The percentages shown are for 100 kip point loads at the most eccentric positions 5X, 5Y and 5X + 5Y and may be compared with the best possible distributions of 16.5, 22.4, 22.4, 22.4 and 16.5% for girders 1 to 5 respectively which would be obtained for a uniform distribution of stress across the entire section.

From Figs. 30, 31 and 32 several observations may be made in comparing results of the three support restraints.

(1) At Section A, near the diaphragmed midspan, the distribution of moments is practically independent of support restraint for all three load cases 5X, 5Y and 5X + 5Y.

(2) At Section D, near the undiaphragmed midspan, differences depending on support restraint are slightly larger than at Section A, but still no greater than 2.7% of the total section moment at any point. In general a slightly greater concentration of moment occurs in girder 3 at Section D as compared to Section A.

(3) At support Sections B and C, the differences depending on support restraint are somewhat more pronounced. Comparing the torsional to the normal restraint case a greater percentage of the moment is carried by girders 4 and 5 near the load. For the longitudinal restraint case a large drop occurs in the moment taken by girder 3 in the loaded span under loads 5X or 5Y.

5.4 Summary of Moments for all Point Load Cases

As described in Vol. I a total of 19 different point load combinations were applied to the bridge. Detailed tabulations of theoretical and experimental result for reactions, deflections, strains and moments for each of these cases is given in Vol III (Tables 1 to 7 inclusive). All results have been normalized for purposes of comparison to loads of 100 kips per span. Theoretical values were obtained using F1NPLA2. In this section, the total moments at instrumented Sections A, B, C, D and the transverse distribution of these total moments will be summarized and discussed for all 19 point load cases.

5.4.1 Total Moments at a Section

Table 12 summarizes total moments at Sections A and D near midspans I and II for each of the 19 point load cases. Theoretical and

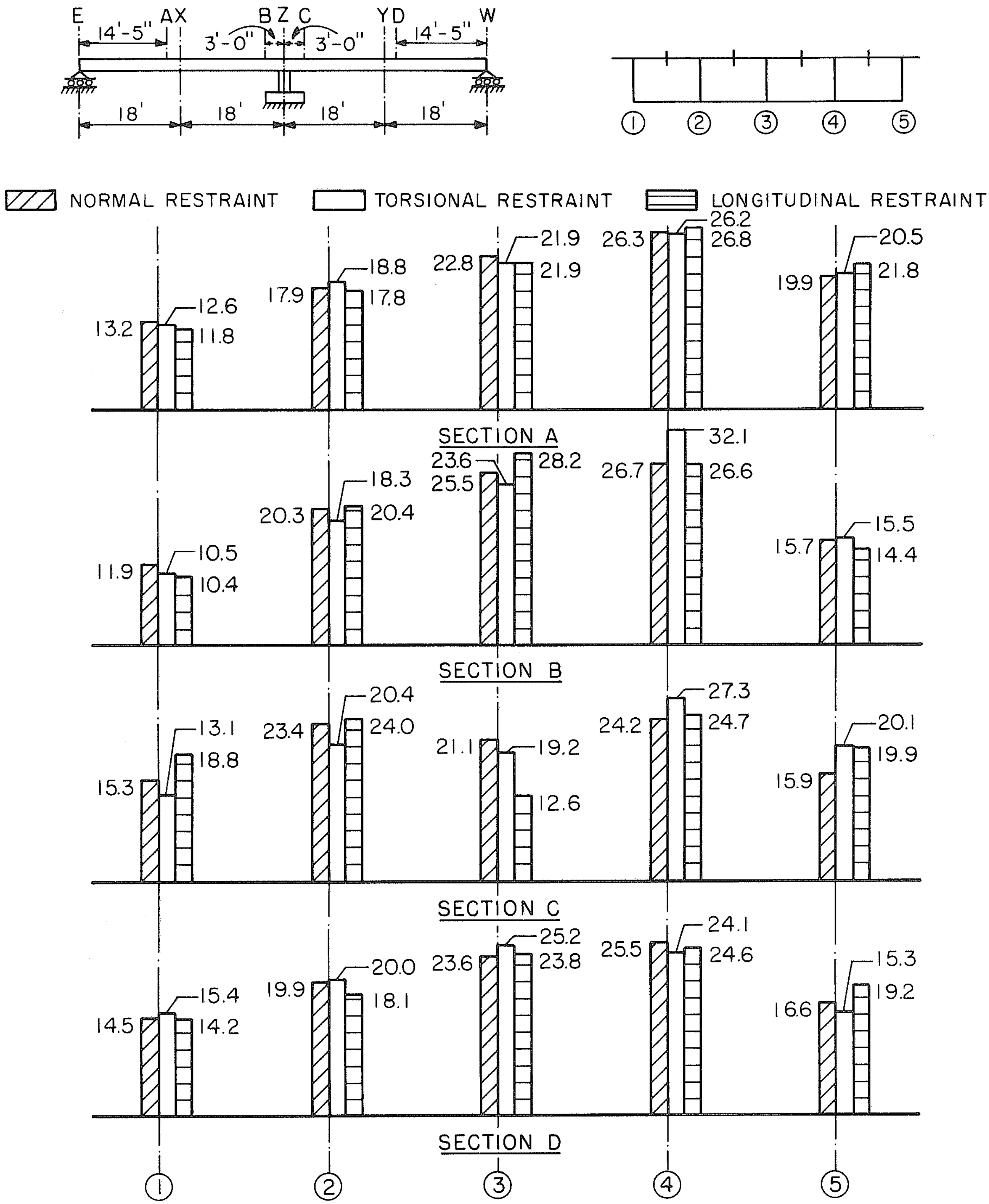

FIG. 30 EXPERIMENTAL PERCENTAGES OF TOTAL MOMENT AT A SECTION CARRIED BY EACH GIRDER FOR DIFFERENT SUPPORT RESTRAINTS UNDER 100 KIP LOAD AT 5X

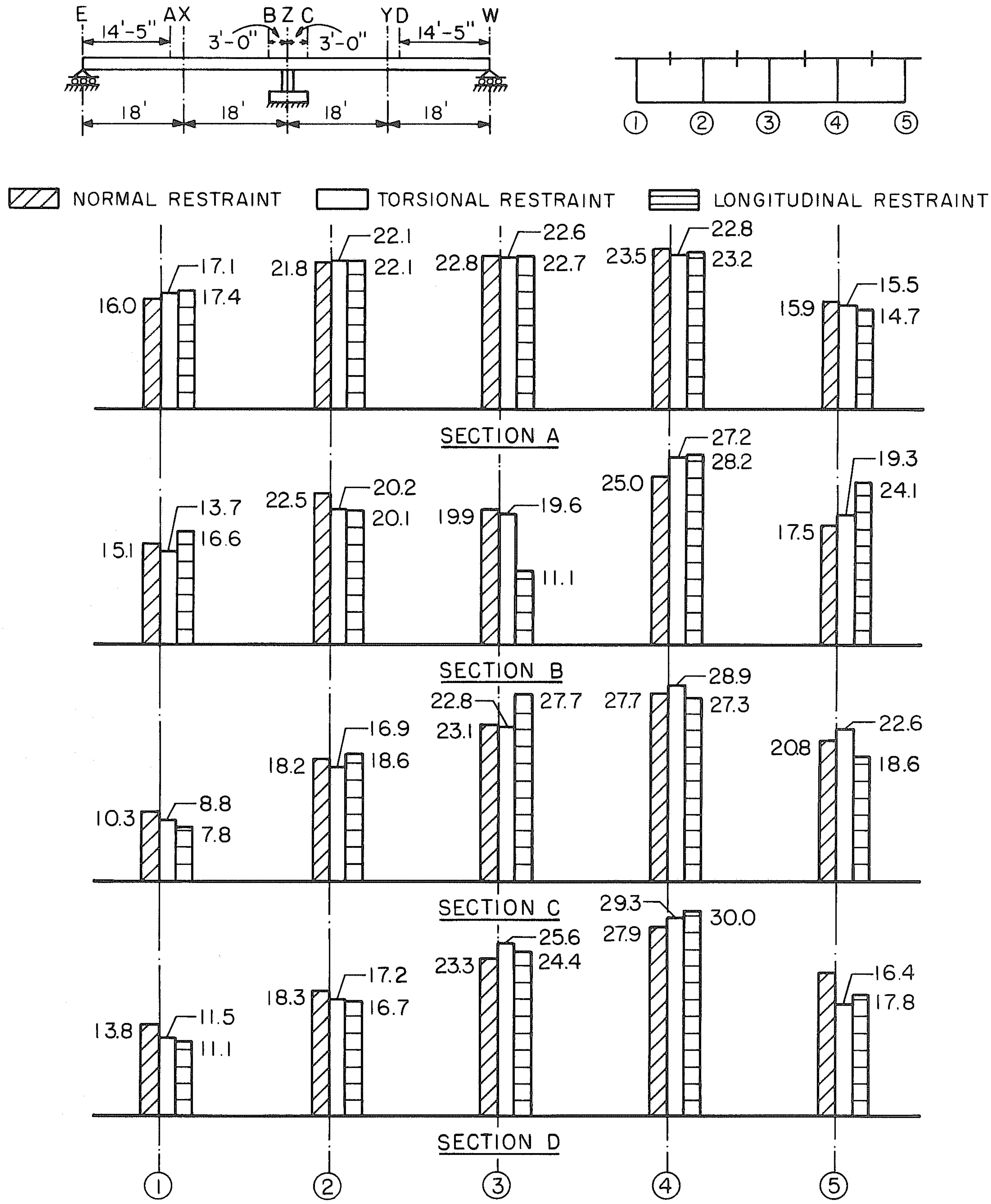

FIG. 31 EXPERIMENTAL PERCENTAGES OF TOTAL MOMENT AT A SECTION CARRIED BY EACH GIRDER FOR DIFFERENT SUPPORT RESTRAINTS UNDER 100 KIP LOAD AT 5Y

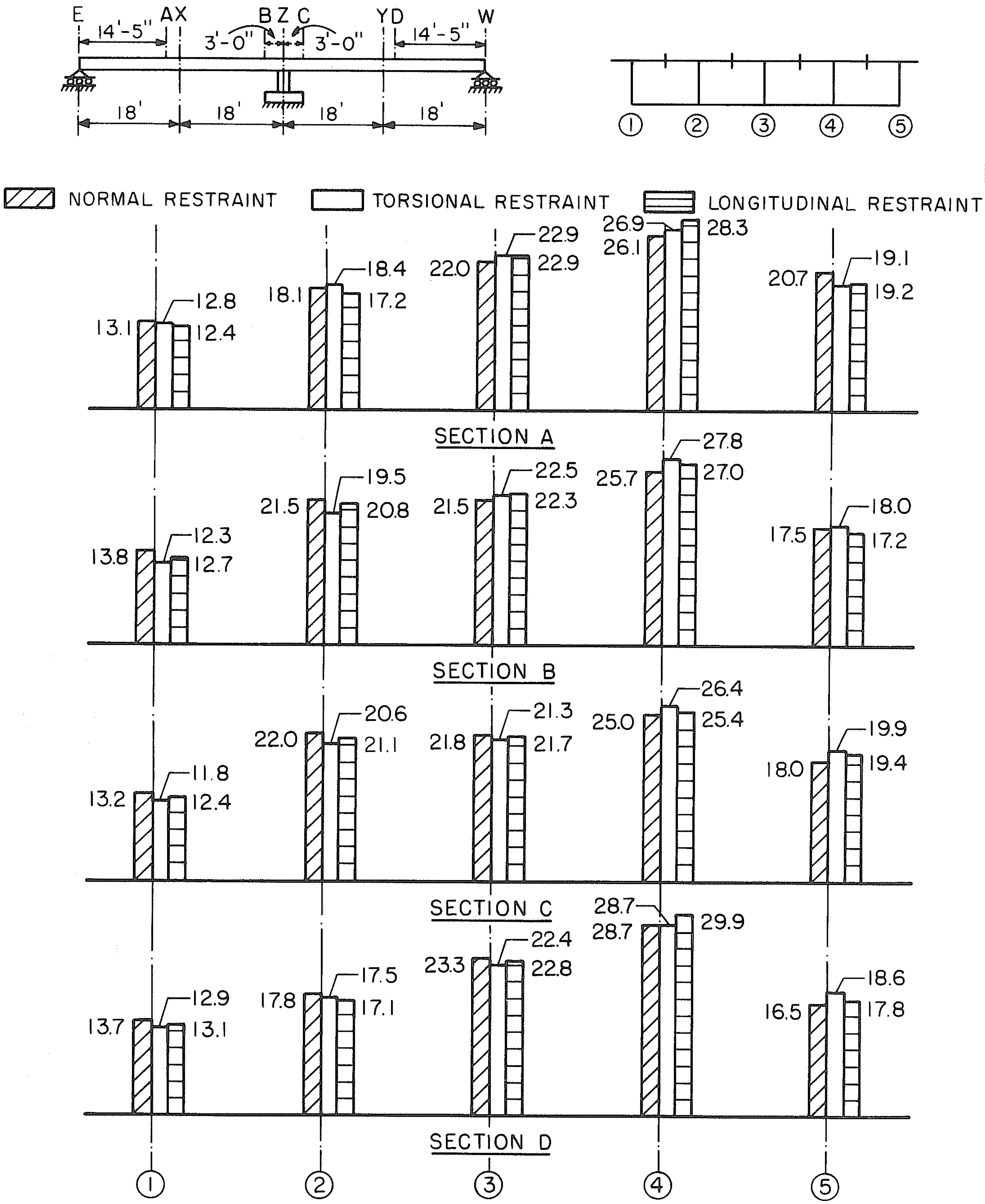

FIG. 32 EXPERIMENTAL PERCENTAGES OF TOTAL MOMENT AT A SECTION CARRIED BY EACH GIRDER FOR DIFFERENT SUPPORT RESTRAINTS UNDER 100 KIP LOADS AT 5X + 5Y

experimental moments are given, first, based on the external reactions, and second, based on an integration of the internal longitudinal forces at the section times the appropriate lever arm to the gross-section neutral axis. A study of Table 12 reveals a number of important points.

(1) The total moment at a section is essentially independent of the transverse position of the point loads.

(2) Agreement between theory and experiment for moments based on external reactions is very good generally within 2 or 3%, with experimental values being usually slightly lower.

(3) For internal moments, experimental values are generally slightly lower than theoretical values (4 to 8%) at Section A and slightly higher (4 to 6%) at Section D. Such differences could easily be due to variations in actual material properties, cracking, internal gage locations etc. in the bridge from those assumed in converting experimental data to moments.

(4) Comparing external and internal moments, the check between theoretical values is almost perfect. For experimental values, the internal moments are slightly lower (2 to 6%) at Section A and slightly higher (2 to 6%) at Section D than corresponding external moments.

Table 13 summarizes total moments at Section B and C near the center bent support. A study of this table reveals the following.

(1) Again the total moment is generally independent of the transverse position of the point loads.

TABLE 12 - SUMMARY OF THEORETICAL AND EXPERIMENTAL TOTAL MOMENTS (FT-KIPS) AT SECTIONS A AND D FOR ALL POINT LOAD (100 KIPS) POSITIONS

SECTION A					SECTION D				
100 K LOAD AT	BASED ON EXTERNAL REACTIONS		BASED ON INTERNAL FORCES		100 K LOAD AT	BASED ON EXTERNAL REACTIONS		BASED ON INTERNAL FORCES	
	THEO.	EXPT.	THEO.	EXPT.		THEO.	EXPT.	THEO.	EXPT.
1X	565	548	565	524	1Y	565	553	561	572
2X	568	547	562	525	2Y	566	544	565	586
3X	566	550	562	535	3Y	566	553	565	574
4X	568	547	562	532	4Y	566	558	565	581
5X	565	546	565	542	5Y	565	562	561	598
1Y	-118	-115	-117	-109	1X	-118	-120	-118	-125
2Y	-117	-122	-116	-119	2X	-117	-120	-117	-123
3Y	-117	-115	-116	-121	3X	-116	-119	-116	-123
4Y	-117	-112	-116	-110	4X	-117	-120	-117	-123
5Y	-118	-122	-117	-110	5X	-118	-119	-118	-127
1X + 1Y	447	433	448	404	1X + 1Y	447	439	443	461
2X + 2Y	449	435	446	417	2X + 2Y	449	456	448	468
3X + 3Y	449	428	446	406	3X + 3Y	449	440	448	443
4X + 4Y	449	438	446	410	4X + 4Y	449	448	448	474
5X + 5Y	447	437	448	429	5X + 5Y	447	454	443	475
1X + 5Y	447	437	448	421	1Y + 5X	447	437	443	455
2X + 4Y	451	429	446	407	2Y + 4X	449	453	448	458
1Y + 5X	447	441	448	423	1X + 5Y	447	441	443	451
2Y + 4X	451	433	446	405	2X + 4Y	449	450	448	454

TABLE 13 - SUMMARY OF THEORETICAL AND EXPERIMENTAL TOTAL MOMENTS (FT-KIPS) AT SECTIONS B AND C FOR ALL POINT LOAD (100 KIPS) POSITIONS

SECTION B					SECTION C				
100 K LOAD AT	BASED ON EXTERNAL REACTIONS		BASED ON INTERNAL FORCES		100 K LOAD AT	BASED ON EXTERNAL REACTIONS		BASED ON INTERNAL FORCES	
	THEO.	EXPT.	THEO.	EXPT.		THEO.	EXPT.	THEO.	EXPT.
1X	-208	-246	-183	-263	1Y	-208	-235	-182	-261
2X	-205	-249	-180	-263	2Y	-205	-254	-180	-253
3X	-205	-241	-179	-256	3Y	-206	-234	-180	-246
4X	-205	-249	-180	-264	4Y	-205	-224	-180	-248
5X	-208	-250	-183	-249	5Y	-208	-214	-182	-242
1Y	-270	-263	-261	-282	1X	-269	-275	-261	-288
2Y	-268	-280	-259	-273	2X	-267	-275	-259	-292
3Y	-267	-264	-258	-259	3X	-266	-273	-258	-275
4Y	-268	-257	-259	-255	4X	-267	-275	-259	-293
5Y	-270	-278	-261	-244	5X	-269	-273	-261	-264
1X + 1Y	-477	-508	-443	-500	1X + 1Y	-477	-496	-443	-500
2X + 2Y	-473	-503	-439	-519	2X + 2Y	-473	-457	-439	-540
3X + 3Y	-471	-521	-437	-498	3X + 3Y	-471	-494	-438	-490
4X + 4Y	-473	-498	-439	-517	4X + 4Y	-473	-474	-439	-498
5X + 5Y	-477	-500	-443	-500	5X + 5Y	-477	-461	-443	-495
1X + 5Y	-477	-500	-443	-494	1Y + 5X	-477	-491	-443	-539
2X + 4Y	-473	-518	-439	-514	2Y + 4X	-472	-463	-439	-533
1Y + 5X	-477	-492	-443	-519	1X + 5Y	-477	-500	-443	-482
2Y + 4X	-473	-509	-439	-514	2X + 4Y	-472	-471	-439	-519

(2) Experimental external and internal moments in regions of steep moment gradients, therefore in loaded spans, are generally higher than corresponding theoretical values. However, in the unloaded spans, where the moment gradient is not steep, the agreement is excellent. If the total statical moment in a span, positive plus negative, is accounted for in a design, differences such as the above are not critical.

(3) Comparing external and internal moments, the check between experimental values is better than the check between theoretical values. For theoretical values, internal moments in loaded spans are lower than external moments, indicating that in this region of steep moment gradient a refined finite element mesh should be used.

5.4.2 Transverse Distribution of Total Moments

Theoretical and experimental percentages of the total moments at Sections A, D, B, C carried by each girder are given in Tables 14, 15, 16, 17 respectively for all 19 point load combinations. These tables are essentially influence tables, which at a glance enable one to determine the load distributing properties of the bridge. It should be kept in mind that for a uniform stress distribution across the entire section, the percentage distributions to girders 1 to 5 respectively would be 16.5, 22.4, 22.4, 22.4 and 16.5%.

Maximum total moments are produced at Section A for loads in Span I at Section X only; at Section D for loads in Span II at Section Y only; and at Sections B and C near the center bent for loads in both

Spans I and II at Sections X and Y. Restricting attention in Tables 14, 15, 16, 17 to these critical loading cases the following observations may be made.

(1) Differences between theoretical and experimental values in almost all cases is from 0 to 2% of the total moment at the section.

(2) The maximum percentages found in the tables for single loads over any girder at Sections X and/or Y for the critical loading cases are as follows.

	Theoretical		Experimental	
	Interior girder	Exterior girder	Interior girder	Exterior girder
Section A	25	19	26	21
Section B	27	20	28	17
Section C	25	19	27	18
Section D	26	21	26	19

As can be seen above, except at Section D, experimental values are slightly larger than theoretical values for the interior girder, while the reverse is true for the exterior girder.

(3) Actual design live loads consist of two or three lanes of trucks on the bridge and for such conditions the average percentage taken by an individual girder would approach the uniform stress distribution values of 22.4% and 16.5% for interior and exterior girders respectively.

TABLE 14 - SUMMARY OF THEORETICAL AND EXPERIMENTAL PERCENTAGE DISTRIBUTION OF THE TOTAL MOMENT AT SECTION A FOR ALL POINT LOAD POSITIONS.

LOAD AT	THEORETICAL % TO GIRDERS					EXPERIMENTAL % TO GIRDERS				
	1	2	3	4	5	1	2	3	4	5
1X	19	25	22	20	14	21	24	23	21	12
2X	17	24	23	21	14	18	23	23	22	13
3X	15	23	23	23	15	17	22	23	23	15
4X	14	21	23	24	17	14	20	23	25	18
5X	14	20	22	25	19	13	18	23	26	20
1Y	17	23	23	23	15	17	22	23	24	14
2Y	16	23	23	23	16	17	22	22	23	15
3Y	16	23	23	23	16	16	20	25	21	17
4Y	16	23	23	23	16	16	22	23	23	16
5Y	15	23	23	23	17	16	22	23	24	16
1X + 1Y	20	26	22	19	13	21	22	24	21	12
2X + 2Y	17	25	23	21	14	18	23	24	22	13
3X + 3Y	15	23	24	23	15	15	22	25	24	15
4X + 4Y	14	21	23	25	17	15	20	24	26	16
5X + 5Y	13	19	22	26	20	13	18	22	26	21
1X + 5Y	20	26	22	19	13	21	24	24	20	11
2X + 4Y	18	25	23	21	14	19	23	24	23	11
1Y + 5X	13	19	22	26	20	14	18	23	28	18
2Y + 4X	14	21	23	25	18	14	20	24	26	16

TABLE 15 - SUMMARY OF THEORETICAL AND EXPERIMENTAL PERCENTAGE DISTRIBUTION OF THE TOTAL MOMENT AT SECTION D FOR ALL POINT LOAD POSITIONS

LOAD AT	THEORETICAL % TO GIRDERS					EXPERIMENTAL % TO GIRDERS				
	1	2	3	4	5	1	2	3	4	5
1Y	20	27	22	19	12	16	29	23	20	12
2Y	19	25	23	20	13	16	25	27	21	11
3Y	15	23	23	23	15	13	25	24	25	13
4Y	13	20	23	25	19	11	22	26	25	16
5Y	12	19	22	27	20	14	18	23	28	17
1X	17	23	23	23	15	17	26	25	23	10
2X	16	23	23	23	16	15	24	25	24	11
3X	16	23	23	23	16	13	25	26	25	13
4X	16	23	23	23	16	11	24	25	24	15
5X	15	23	23	23	17	14	20	24	25	17
1X + 1Y	21	28	22	18	12	17	30	22	19	12
2X + 2Y	19	26	23	19	12	16	26	25	21	12
3X + 3Y	15	23	24	23	15	17	22	23	25	14
4X + 4Y	12	19	23	26	19	14	19	25	26	16
5X + 5Y	12	18	22	28	21	14	18	23	29	16
1Y + 5X	22	28	22	18	11	17	30	24	20	10
2Y + 4X	19	26	23	19	12	20	24	25	21	10
1X + 5Y	11	18	22	28	22	10	20	24	30	17
2X + 4Y	12	19	23	26	19	12	18	25	27	18

TABLE 16 - SUMMARY OF THEORETICAL AND EXPERIMENTAL PERCENTAGE DISTRIBUTION OF THE TOTAL MOMENT AT SECTION B FOR ALL POINT LOAD POSITIONS

LOAD AT	THEORETICAL % TO GIRDERS					EXPERIMENTAL % TO GIRDERS				
	1	2	3	4	5	1	2	3	4	5
1X	22	27	23	18	9	17	23	22	27	12
2X	18	26	25	20	11	15	22	23	28	12
3X	14	23	26	23	14	13	21	24	29	13
4X	11	20	25	26	18	12	20	24	30	14
5X	9	18	24	27	22	12	20	25	27	16
1Y	17	23	22	22	15	16	23	21	25	15
2Y	17	23	22	22	15	16	23	22	25	15
3Y	16	23	22	23	16	15	21	22	26	16
4Y	15	22	22	23	17	15	22	20	26	18
5Y	15	22	22	23	17	15	23	20	25	18
1X + 1Y	19	25	23	21	13	17	24	21	23	15
2X + 2Y	17	24	23	21	14	16	23	21	25	14
3X + 3Y	15	23	24	23	15	15	23	23	25	15
4X + 4Y	14	21	23	24	17	14	21	22	28	16
5X + 5Y	13	21	23	25	19	14	21	21	26	18
1X + 5Y	18	24	23	21	14	16	23	21	24	16
2X + 4Y	16	24	23	22	15	15	22	21	27	15
1Y + 5X	12	19	22	26	20	15	22	22	27	15
2Y + 4X	15	22	23	24	16	15	22	22	27	14

TABLE 17 - SUMMARY OF THEORETICAL AND EXPERIMENTAL PERCENTAGE DISTRIBUTION OF THE TOTAL MOMENT AT SECTION C FOR ALL POINT LOAD POSITIONS

LOAD AT	THEORETICAL % TO GIRDERS					EXPERIMENTAL % TO GIRDERS				
	1	2	3	4	5	1	2	3	4	5
1Y	27	30	22	15	7	22	26	23	18	11
2Y	20	30	25	17	8	16	27	26	20	11
3Y	13	23	28	23	13	12	24	28	23	14
4Y	8	17	25	30	20	10	19	27	27	17
5Y	7	15	22	30	27	10	18	23	28	21
1X	16	23	22	23	16	15	23	19	25	18
2X	16	23	22	23	16	14	22	20	26	18
3X	16	23	22	23	16	14	23	19	25	19
4X	16	23	22	23	16	14	22	20	26	18
5X	16	23	22	23	16	15	23	21	24	16
1X + 1Y	21	26	22	19	12	18	26	21	20	14
2X + 2Y	18	26	23	20	13	15	25	22	22	15
3X + 3Y	15	23	25	23	15	14	24	23	23	15
4X + 4Y	13	20	23	26	18	13	23	20	25	19
5X + 5Y	12	19	22	26	21	13	22	22	25	18
1Y + 5X	18	24	23	21	14	18	25	21	22	15
2Y + 4X	18	26	23	21	13	15	25	22	22	15
1X + 5Y	12	19	22	26	20	13	23	22	24	18
2X + 4Y	13	21	23	26	18	13	22	22	26	18

5.4.3 Maximum Number of Wheel Loads Carried by an Interior or Exterior Girder

As described in Vol. I, the AASHO Specifications require that each girder be designed as a separate member by applying to it a certain fraction of a single longitudinal line of wheels from a standard AASHO HS 20-44 truck. This fraction known as the number of wheel loads N_{WL}, is given by the relations

$$N_{WL} = S/7 \text{ for interior girders}$$
$$N_{WL} = S_1/7 \text{ for exterior girders}$$

S is the flange width in feet of the interior girder, which is also equal to the average width of the cell, and S_1 is the top flange width in feet of the exterior girder, which is also equal to half the cell width plus the cantilever overhang. For the prototype of the bridge model, $S = 7.25$ ft. and $S_1 = 6.12$ ft., which gives N_{WL} values of 1.04 and 0.88 for interior and exterior girders. Because of similitude, these same values of N_{WL} are applicable to the model. The most important variable unaccounted for in the AASHO formulas is the number of traffic lanes on the bridge.

To study this problem, Table 18 has been prepared to give the maximum number of wheel loads to be carried by an interior girder or an exterior girder at Sections A, B, C and D. Line (1) gives the AASHO values from above. The remaining lines give values for two lanes of trucks (total of 4 wheel lines on bridge) and for three lanes of trucks (total of 6 wheel lines on bridge). The uniform stress values, lines (2) and (5) are obtained by multiplying the total number of wheel lines on the bridge by 22.4 and 16.5% for an interior and exterior girder respectively. Lines

(3), (4), (6) and (7) are found by using the values in Tables 14 to 17 as influence ordinates. Each truck is assumed to occupy a 10 ft. traffic lane and has wheels spaced transversely at 6 ft. For simplicity, only a single transverse series of wheels at midspan are considered. These are shifted laterally to give maximum effects. Finally lines (8), (9) and (10) are given since AASHO specifies a 10% reduction for three lanes of loading. It is important to note in using the S/7 AASHO empirical formula, no reduction should be made for more than two lanes of loading, since this is assumed to have been already included in the development of the formula.

A study of Table 18 reveals several interesting facts for the bridge under consideration.

(1) The AASHO formulas are conservative for the two lane truck loading, but unconservative for the three lane truck loading on the bridge. The latter is especially true for interior girders, even with the 10% reduction, where AASHO underestimates the load by about 18 to 23%.

(2) Comparing theoretical and experimental values, experimental values are 2 to 3% higher for interior girders and 6 to 7% higher for exterior girders.

(3) Comparing both theoretical and experimental values with the uniform stress values, the former are generally 2 to 8% higher than the latter, with the three lane truck loading being the closest.

TABLE 18 - MAXIMUM NUMBER OF WHEEL LOADS TO BE CARRIED BY AN INTERIOR OR AN EXTERIOR GIRDER.

GIRDER	LOAD CASE	SECTION			
		A	B	C	D
INTERIOR	AASHO Specifications.	1.04	1.04	1.04	1.04
	Two Lane (Uniform Stress)	0.90	0.90	0.90	0.90
	Two Lane (Theoretical)	0.96	0.95	0.99	0.99
	Two Lane (Experimental)	0.98	1.06	1.00	1.04
	Three Lane (Uniform Stress)	1.34	1.34	1.34	1.34
	Three Lane (Theoretical)	1.37	1.38	1.40	1.39
	Three Lane (Experimental)	1.42	1.54	1.45	1.47
	.90 x Three Lane (Unif. Stress)	1.21	1.21	1.21	1.21
	.90 x Three Lane (Theor.)	1.23	1.24	1.26	1.25
	.90 x Three Lane (Exper.)	1.27	1.39	1.31	1.32
EXTERIOR	AASHO Specifications.	0.88	0.88	0.88	0.88
	Two Lane (Uniform Stress)	0.66	0.66	0.66	0.66
	Two Lane (Theoretical)	0.67	0.67	0.71	0.71
	Two Lane (Experimental)	0.73	0.65	0.70	0.61
	Three Lane (Uniform Stress)	0.99	0.99	0.99	0.99
	Three Lane (Theoretical)	0.96	0.95	0.97	0.97
	Three Lane (Experimental)	1.02	0.94	0.99	0.84
	.90 x Three Lane (Unif. Stress)	0.89	0.89	0.89	0.89
	.90 x Three Lane (Theor.)	0.86	0.86	0.87	0.87
	.90 x Three Lane (Exper.)	0.92	0.84	0.89	0.76

5.5 Truck and Construction Vehicle Loads

As described in Vol. I, the model was loaded by scaled down versions of the standard AASHO HS 20-44 truck (total load = 72 kips) and a proposed overload construction vehicle class II (total load = 330 kips). All linear dimensions were reduced by the scale factor 1:2.82 and details of wheel positions in the model vehicles can be found in Vol. I. Simulitude required that the loads be reduced by a factor of 1:8 to produce the same stresses in the model as in the prototype. Thus for the model the total load for each truck was 9.0 kips and for each construction vehicle was 41.25 kips. Using these loads, a study could be made of the bridge response due to actual design truck live loads placed at various positions on the bridge.

Figure 33 shows the positions and directions of the truck and and construction vehicle loads on the bridge. As described in Vol. I, a total of 11 combinations of two lane truck loadings, 3 combinations of three lane truck loadings, and 7 combinations of construction vehicle loading were used. Because each vehicle had six wheels and the front wheels had smaller loads than the rear wheels, exact symmetry of loading about the bridge longitudinal and transverse centerlines was not maintained, Fig. 33.

Detailed tabulations of theoretical and experimental results related to reactions, deflections, strains and moments for these loading are given in Vol. III (Tables 14 to 19 inclusive). Theoretical values were obtained from computer analyses using FINPLA2. Selected results will be discussed in the following sections.

5.5.1 Loadings for Maximum Girder Moments

Table 19 summarizes the experimental girder moments for a variety of load combinations on the bridge involving 1, 2, 3, 4 or 6

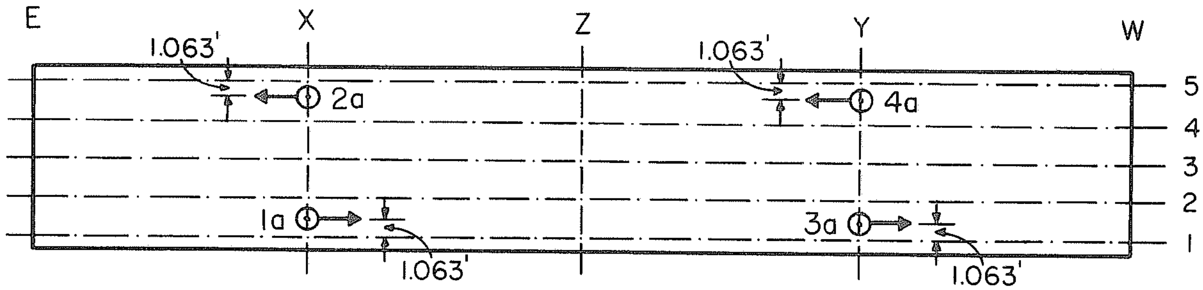

(a) TWO LANE TRUCK LOADING (EACH TRUCK 9.0 KIPS NOMINAL)

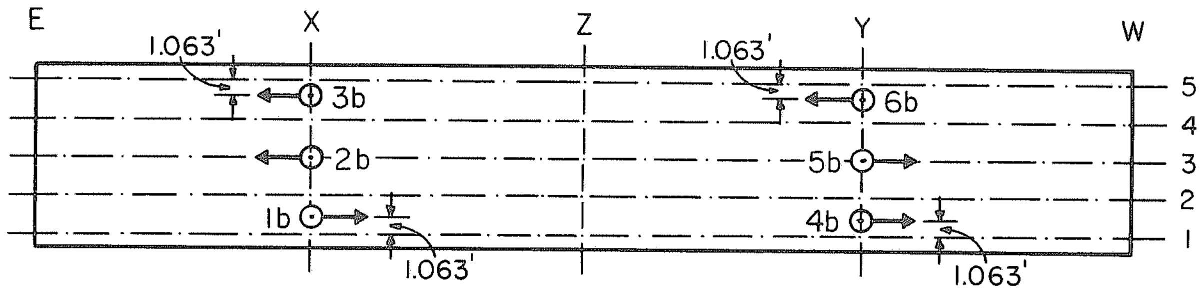

(b) THREE LANE TRUCK LOADING (EACH TRUCK 9.0 KIPS NOMINAL)

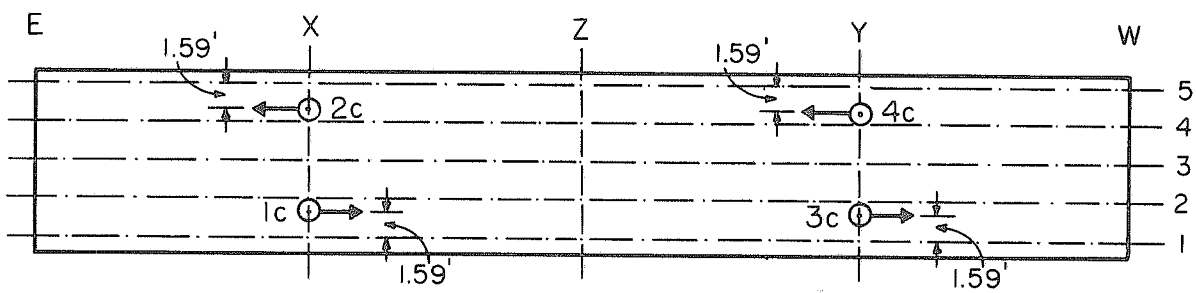

(c) CONSTRUCTION VEHICLE LOADING (EACH TRUCK 41.25 KIPS NOMINAL)

FIG. 33 POSITIONS AND DIRECTIONS OF TRUCK (9.0K) AND CONSTRUCTION VEHICLE (41.25K) LOADS ON THE BRIDGE vehicles on the bridge. Vehicle locations can be identified from Fig. 33. If one searches Table 19 for maximum moments in interior girders 2, 3, 4 and exterior girders 1, 5 certain conclusions can be immediately reached regarding critical design loadings.

(1) As would be expected the maximum moments get progressively larger as one proceeds from the two lane truck, to the three lane truck to the construction vehicle loading.

(2) Considering positive moment Sections A and D maximum moments are produced when loading only one span with as many vehicles as possible across the width of the bridge. Single vehicles in one span in an extreme eccentric position do not produce maximum effects.

(3) Considering negative moment Sections B and C maximum moments are produced when both spans are loaded, again with as many vehicles as possible across the width of the bridge.

(4) Considering two lane truck, three lane truck and construction vehicle loadings respectively, the ratios of the maximum moment for an exterior girder 1, 5 to an interior girder 2, 3, 4 for the critical loadings are as follows:

Section A - .76, .70, .67

Section B - .62, .63, .62

Section C - .62, .69, .62

Section D - 1.00, .68, .61

Except for the 1.00 value at Section D, which is questionable, it can be seen that for this bridge, Section A, near the diaphragmed midspan section, has the highest ratios and the best

TABLE 19 - EXPERIMENTAL GIRDER MOMENTS (FT-KIPS) UNDER CRITICAL TRUCK (9.0 KIPS) AND CONSTRUCTION VEHICLE (41.25 KIPS) LOADS (MOMENTS ABOUT GROSS-SECTION NEUTRAL AXIS)

SECTION	GIRDER	TWO LANE TRUCK LOADING				THREE LANE TRUCK LOADING		CONSTRUCTION VEHICLE LOADING		
		2a	1a+2a	1a+4a	1a+2a +3a+4a	1b+2b+3b	1b+2b+3b +4b+5b+6b	2c	1c+4c	1c+3c
A	1	6	16	7	12	21	18	25	24	24
	2	8	20	9	15	27	23	34	35	30
	3	10	20	8	15	29	24	44	30	31
	4	12	21	7	16	30	25	54	27	28
	5	8	15	4	12	18	15	36	16	16
	Σ	44	92	34	70	126	105	193	133	128
		2a+4a	1a+2a	1a+4a	1a+2a +3a+4a	1b+2b+3b	1b+2b+3b +4b+5b+6b	2c	1c+4c	1c+3c
B	1	-6	-7	-7	-11	-8	-19	-9	-29	-31
	2	-9	-10	-9	-18	-13	-29	-16	-40	-42
	3	-9	-11	-9	-18	-14	-29	-22	-38	-38
	4	-11	-11	-10	-21	-15	-32	-25	-41	-42
	5	-7	-6	-7	-13	-8	-20	-16	-26	-25
	Σ	-41	-44	-42	-81	-58	-128	-88	-173	-178
		2a+4a	3a+4a	1a+4a	1a+2a +3a+4a	4b+5b+6b	1b+2b+3b +4b+5b+6b	4c	1c+4c	1c+3c
C	1	-5	-6	-5	-13	-9	-19	-7	-24	-31
	2	-9	-10	-9	-20	-15	-29	-15	-40	-48
	3	-9	-12	-9	-19	-16	-27	-19	-38	-42
	4	-10	-11	-10	-18	-14	-29	-24	-42	-40
	5	-7	-6	-7	-13	-9	-20	-20	-31	-25
	Σ	-39	-45	-40	-83	-63	-123	-86	-174	-186
		4a	3a+4a	1a+4a	1a+2a +3a+4a	4b+5b+6b	1b+2b+3b +4b+5b+6b	4c	1c+4c	1c+3c
D	1	7	24	5	14	25	28	29	20	28
	2	9	21	7	16	30	25	39	28	38
	3	11	20	9	17	33	26	44	37	32
	4	15	24	12	19	37	29	49	40	31
	5	9	19	8	12	21	21	30	23	17
	Σ	51	108	41	77	146	130	191	149	146

distributions. It is of interest to compare the above ratios with the theoretical distribution for a uniform stress across the width of the bridge which gives a ratio of moment carried by an exterior girder to that by an interior girder of 16.5/22.4 = .74.

5.5.2 Reactions

A summary of experimental reactions is given in Table 20 for various vehicle loadings. Theoretical solutions were obtained by FINPLA2 for only a selected number of cases and these are also shown in Table 20 where they exist.

First,considering experimental results only, it is evident that excellent static checks are obtained with ratios of the sum of the reactions to the sum of the applied loads varying from 0.97 to 1.01. Superposition is also satisfied indicating a reliability in the experimental results.

Second, comparing theoretical and experimental results, the agreement is very good. It should be noted in Table 13 that the theoretical truck loads were 9.0 kips per truck and 41.25 kips per construction vehicle for all analyses run, while experimental values were slightly larger or smaller than the theoretical values in some cases. The good agreement between theoretical and experimental reactions indicates that the theory can also be used to accurately predict the total moment at any section of the bridge based on the external reactions.

5.5.3 Deflections

Experimental deflections are shown in Fig. 34 for vehicle loadings producing maximum values at diaphragmed Section X and undiaphragmed Section Y. For the two and three lane truck cases, the

TABLE 20 - COMPARISON OF THEORETICAL AND EXPERIMENTAL REACTIONS (KIPS) UNDER TRUCK (9 KIPS) AND CONSTRUCTION VEHICLE (41.25 KIPS) LOADS.

TWO LANE TRUCK LOADING

POSITION	1a+2a		3a+4a		1a+2a+3a+4a	
P or R	THEO.	EXPT.	THEO.	EXPT.	THEO.	EXPT.
P_X	No Theoretical Results	-18.0	0.0	0.0	-18.0	-18.1
P_Y		0.0	-18.0	-18.3	-18.0	-18.2
ΣP		-18.0	-18.0	-18.3	-36.0	-36.4
R_E		6.8	-1.4	-1.4	5.7	5.4
R_F		12.2	12.3	12.6	24.6	24.3
R_W		-1.4	7.1	7.1	5.7	5.7
ΣR		17.6	18.0	18.3	36.0	35.4
$\Sigma R/\Sigma P$		0.98	1.00	1.00	1.00	0.97

THREE LANE TRUCK LOADING

POSITION	1b+2b+3b		4b+5b+6b		1b+2b+3b+4b+5b+6b	
P or R	THEO.	EXPT.	THEO.	EXPT.	THEO.	EXPT.
P_X	No Theoretical Results	-25.1	0.0	0.0	-27.0	-26.8
P_Y		0.0	-27.0	-26.9	-27.0	-27.1
ΣP		-25.1	-27.0	-26.9	-54.0	-53.9
R_E		9.5	-2.1	-2.0	8.6	8.2
R_F		17.0	18.4	18.8	36.8	36.8
R_W		-2.0	10.7	10.5	8.6	8.6
ΣR		24.5	27.0	27.2	54.0	53.6
$\Sigma R/\Sigma P$		0.98	1.00	1.01	1.00	0.99

CONSTRUCTION VEHICLE LOADING

POSITION	2c		1c+4c		1c+3c	
P or R	THEO.	EXPT.	THEO.	EXPT.	THEO.	EXPT.
P_X	No Theoretical Results	-41.4	No Theoretical Results	-40.8	No Theoretical Results	-40.0
P_Y		0.0		-41.3		-41.3
ΣP		-41.4		-82.1		-81.3
R_E		16.2		13.2		12.7
R_F		28.0		55.7		54.8
R_W		-3.1		13.5		13.6
ΣR		41.1		82.3		81.2
$\Sigma R/\Sigma P$		0.99		1.00		1.00

loading is relatively uniform across the width of the bridge, Fig. 33, resulting in a uniform distribution of deflection also. For the construction vehicle, only one lane is loaded, Fig. 33, resulting in a larger deflection under girder 5. By comparing results at Sections X and Y, these loadings also demonstrate the effect of the diaphragm.

It is of interest to compute the maximum deflection to span ratios for each of these design live loadings, since they would be the same in a full scale prototype structure because of similitude. For the two lane truck, three lane truck, and construction vehicle loading the maximum deflections are respectively 0.17, 0.25, and 0.51 in. which when divided by the span of 432 in. (36 ft.) give deflection to span ratios of 1/2600, 1/1770, and 1/870, all of which are quite small.

5.5.4 Strains and Maximum Stresses

Transverse distributions of experimental longitudinal strains for vehicle loadings producing maximum effects are shown in Figs. 35 and 36. Again for the relatively uniform two and three lane truck loadings across the width of the bridge the strain distributions are also fairly uniform. For the construction vehicle case, with only one lane loaded, strains are not uniform across the width.

An estimate of the maximum design live load stresses can be obtained by multiplying the maximum strain values from Figs. 35 and 36 by the appropriate modulus of elasticity values from Vol. I for this loading phase. A summary of these stresses in the concrete and the steel is given in Table 21.

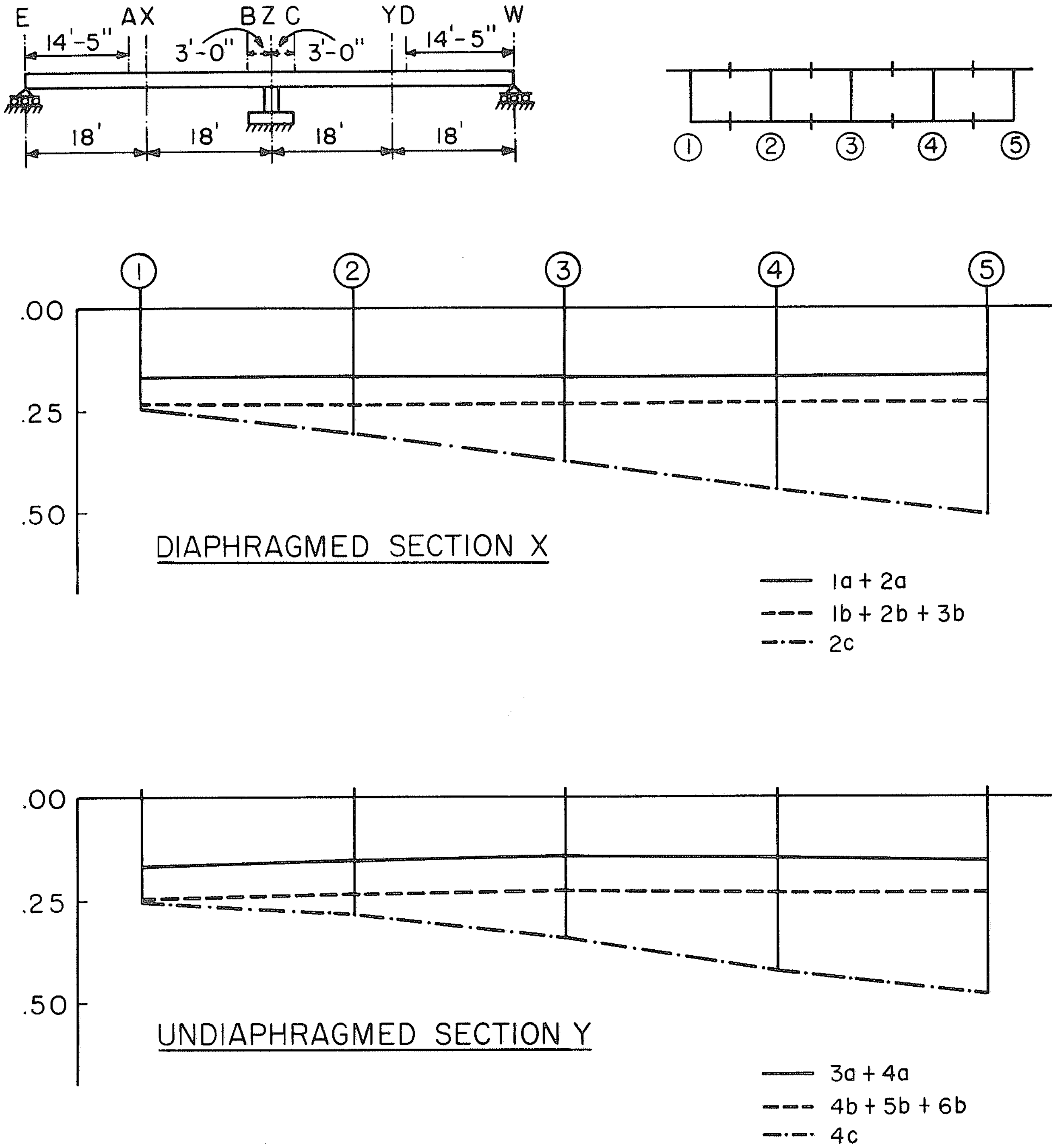

FIG. 34 EXPERIMENTAL DEFLECTIONS (INCHES) AT TRANSVERSE SECTIONS FOR DIFFERENT VEHICLE LOADINGS

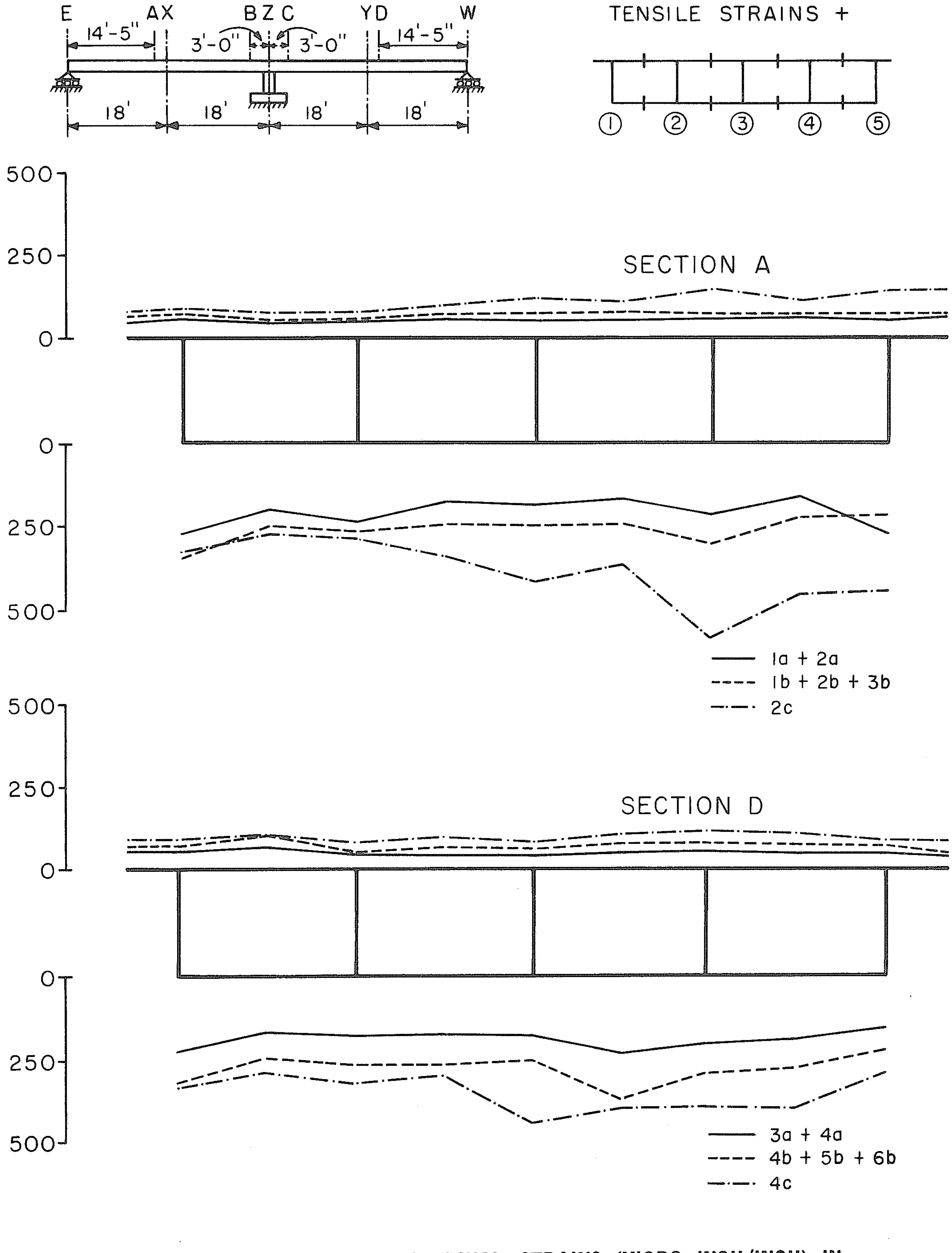

FIG. 35 EXPERIMENTAL LONGITUDINAL STRAINS (MICRO-INCH/INCH) IN TOP AND BOTTOM SLABS AT SECTIONS A AND D FOR DIFFERENT VEHICLE LOADINGS

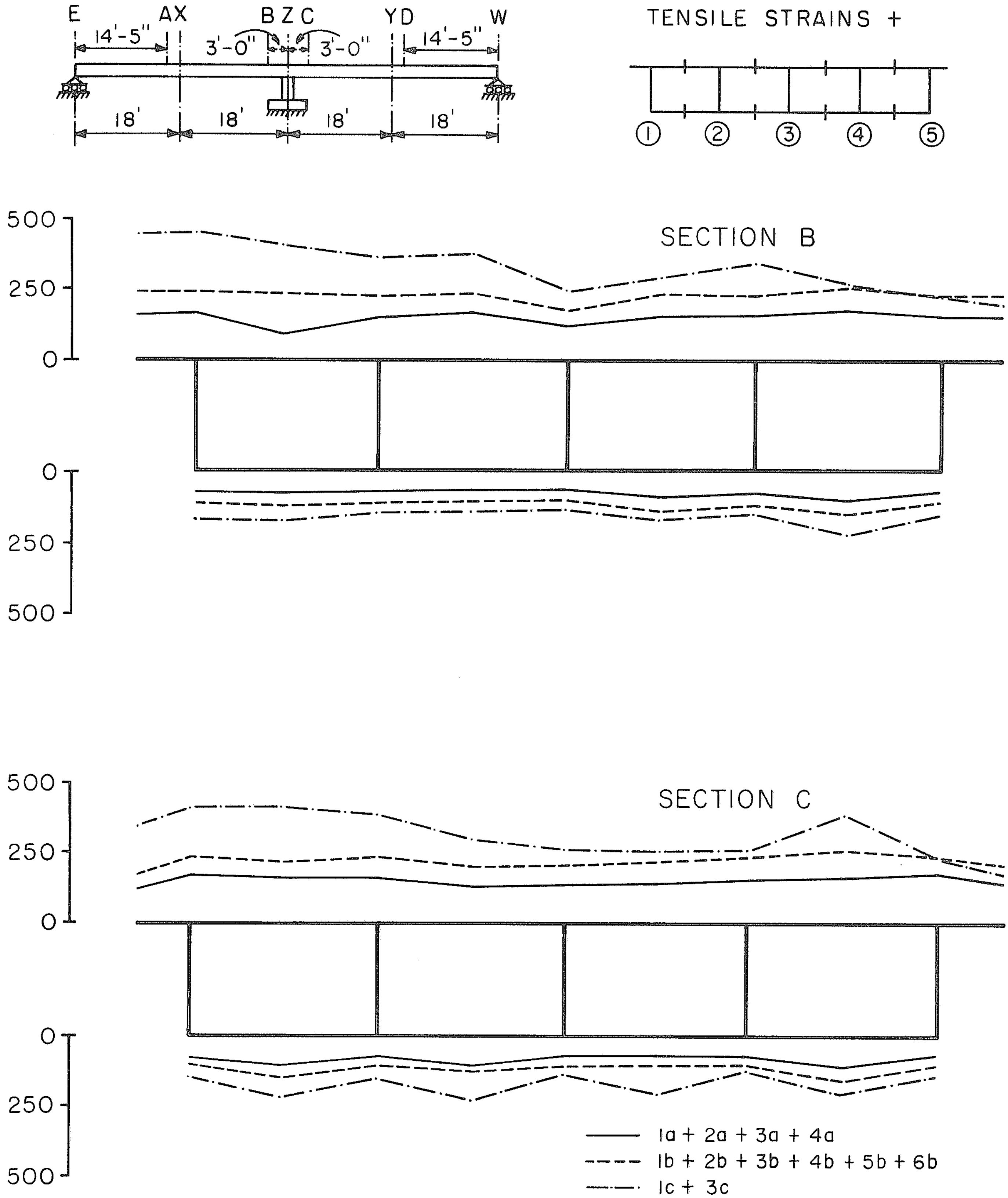

FIG. 36 EXPERIMENTAL LONGITUDINAL STRAINS (MICRO-INCH/INCH) IN TOP AND BOTTOM SLABS AT SECTIONS B AND C FOR DIFFERENT VEHICLE LOADINGS

TABLE 21 - MAXIMUM LIVE LOAD EXPERIMENTAL STRESSES (PSI) UNDER TRUCK AND CONSTRUCTION VEHICLE LOADS.

MATERIAL	SECTION	TWO LANE TRUCK LOADING	THREE LANE TRUCK LOADING	CONSTRUCTION VEHICLE LOADING
CONCRETE	A	207	276	516
	B	235	351	510
	C	241	346	514
	D	249	383	440
STEEL	A	8,030	9,980	17,000
	B	3,710	5,850	10,200
	C	3,860	5,830	9,370
	D	6,640	10,700	13,000

If one adds to the live load stresses for the steel in Table 21, the nominal calculated dead load steel stresses of 12,800 psi at Sections A and D and 8,800 psi at Sections B and C it can be seen that the total steel stresses for the two lane and three lane truck loadings would be below the allowable value of 24,000 psi. For the construction vehicle loading a maximum calculated total steel stress of about 30,000 psi occurs.

It should be recognized that total stresses at midspan Sections X and Y would be about 10% higher than those at Sections A and D, each of which are 3.55 ft. away from midspan Sections X and Y respectively, Likewise the total stresses near the edge of the center bent diaphragm would be about 30% higher than those at Sections B and C which are 3 ft. away from the centerline of the center bent diaphragm.

Live load concrete stresses in Table 21 are quite low and would be well within the allowable when added to the nominal dead load stresses.

5.6 Moving Fork Lift Truck Load

A fork lift truck with two concrete blocks on the fork was used as a total moving load of about 9.3 kips. Three longitudinal passes were made from east to west and static readings were taken at 19 different transverse sections, in order to obtain an approximately continuous record from which experimental influence ordinates could be determined. Details on the truck dimensions, wheel loads, loading paths and transverse sections at which measurements were taken may be found in Vol. I.

5.6.1 Influence Lines

Figures 37 and 38 show theoretical influence lines obtained using the 1DFRAME program and plotted experimental points for a center pass directly over girder 3 and also for a pass near girder 5 at the edge of the bridge. In each case the experimental influence ordinates are given for the position of the center of gravity of the fork lift truck load at a given location on the bridge. The theoretical curves are obtained by taking the results from 1DFRAME for a single unit load placed at the same locations as above and then scaling all values so that the experimental and theoretical ordinates at a selected location are identical. In this way a comparison between the shapes of the experimental and theoretical influence lines can be made directly.

For the total reaction at the west support, Fig. 37, the agreement between theory and experiment is excellent. Comparing the results for the two different passes of the moving load, it is evident that the total reaction is independent of the transverse position of the load.

For the deflection at 5Y, Fig. 37, the agreement for loads in Span II is again very good. For loads in Span I some differences between experiment and theory exist for the pass near girder 5, reflecting the torsional effect produced by this eccentric loading which cannot be captured by the one dimensional 1DFRAME theoretical analysis. For the center pass, which gives a symmetrical loading with respect to the longitudinal centerline, the agreement in Span I is much better.

In Fig. 38, experimental concrete strains at the top and steel strains at the bottom of girder 5 at Section D are compared with theoretical influence lines for moment at Section D obtained from the 1DFRAME analysis. It can be seen that there is general agreement between the shapes of the experimental and theoretical influence lines except when the load is very close to Section D. For these points the transverse distributing properties of the actual bridge, which are not reflected in the one dimensional 1DFRAME theoretical analysis, become important. Thus for the pass near girder 5 over the instrumented location a peaking occurs with experimental strains at 5D being larger than theoretical values. On the contrary for the center pass which is not near the instrumented location, a rounding off of the experimental influence line occurs, causing experimental strains at 5D to be smaller than theoretical values.

5.7 Summary

A detailed discussion of the results for working stress loads has been presented. The most important conclusions under various categories are summarized below.

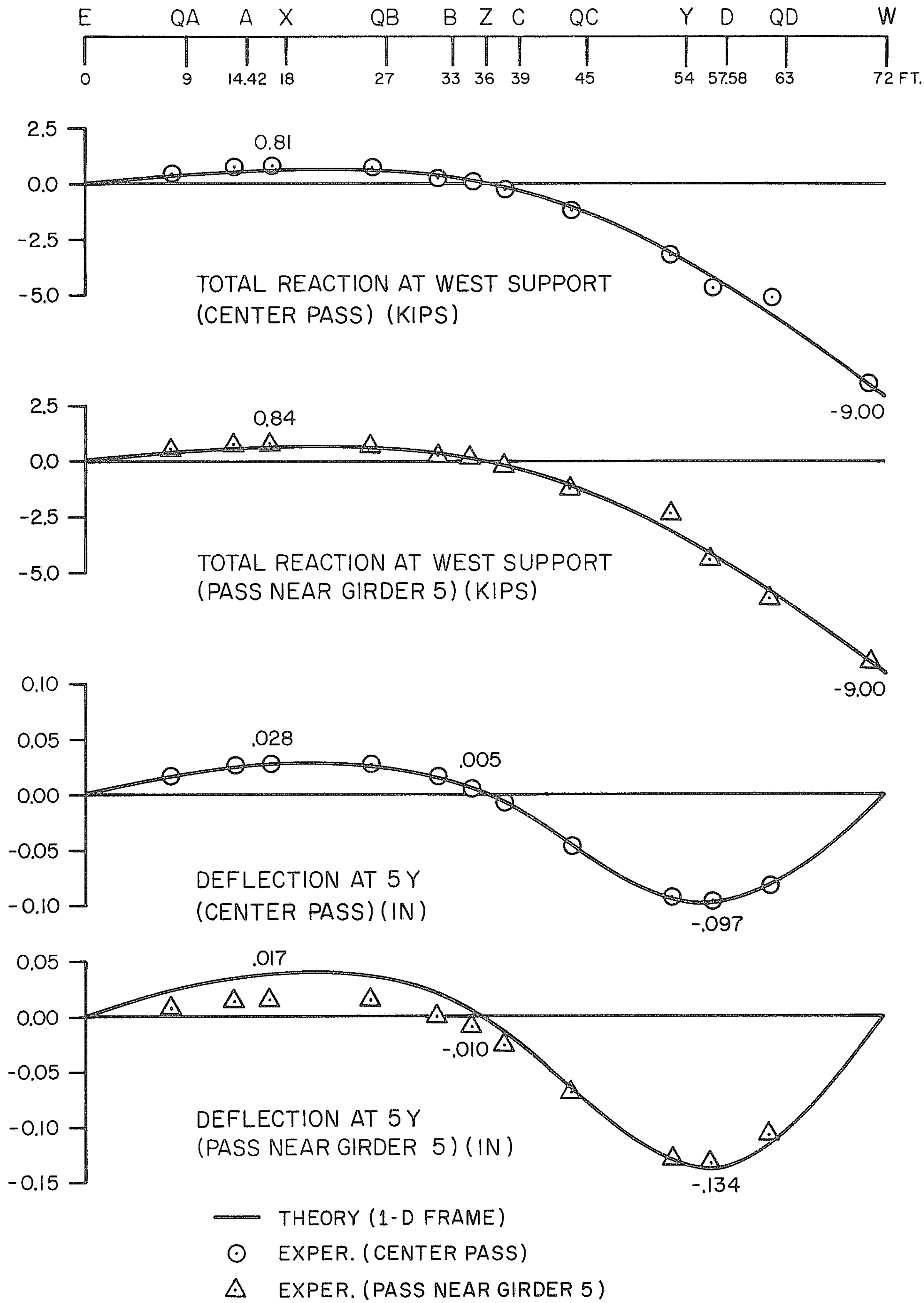

FIG. 37 INFLUENCE LINES FOR EXPERIMENTAL WEST REACTION (KIPS) AND DEFLECTION (INCHES) AT 5Y UNDER MOVING FORK LIFT TRUCK LOAD

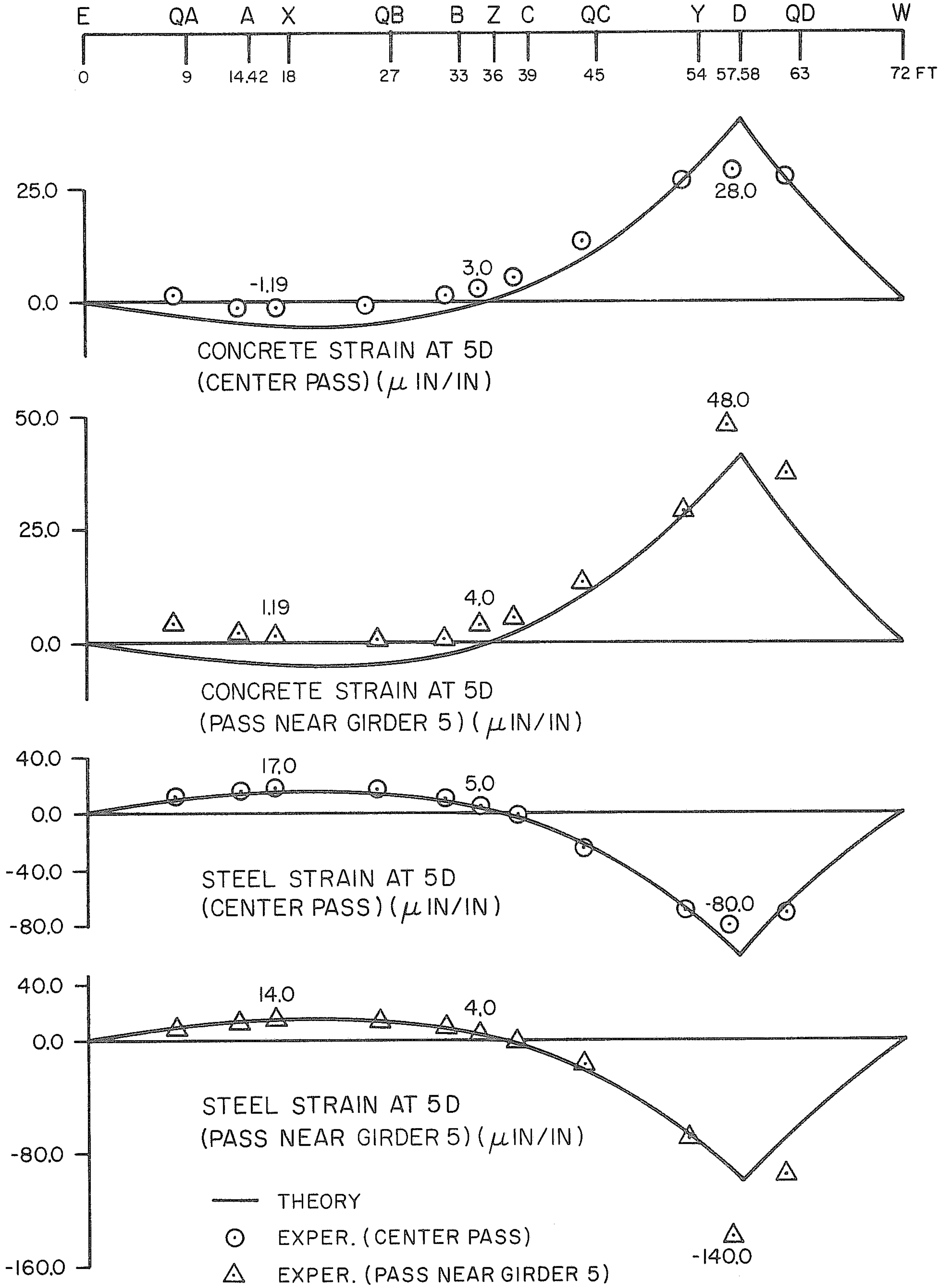

FIG. 38 INFLUENCE LINES FOR EXPERIMENTAL LONGITUDINAL CONCRETE AND STEEL STRAINS (MICRO-INCH/INCH) AT 5D UNDER MOVING FORK LIFT TRUCK LOAD

1. Comparison of theoretical results from FINPLA2 with experimental results.

   a. Distribution of total reactions between the east, center and west supports is accurately predicted by theory. As a consequence the total external moment at any section can be found with confidence.

   b. Theory predicts the distribution and magnitude of deflections quite well if theoretical values based on an uncracked section are multiplied by a factor of 1.5 to account for cracking at this stress level.

   c. While theory predicts the general distribution of strains, substantial differences can exist with experimental values at certain points.

   d. The longitudinal distribution of the total moments at a section as computed from external reactions or the integration of internal stresses are adequately predicted by theory for design purposes.

   e. For the transverse distribution of the total moment, in terms of percentage to each girder, the maximum differences between theoretical and experimental values in almost all cases are only from 0 to 2% of the total moment at the section.

2. Effect of support restraints.

   a. Comparing results from the case where torsional restraint at the center bent exists with those from the normal restraint case, the differences are small and could be ignored in a practical design problem.

b. Comparing results from the case where longitudinal restraint exists at the end diaphragm with those from the normal restraint case, the differences are larger and should be considered in a practical design problem.

3. From the study of 19 different midspan point load combinations it can be concluded that the total moment at any section is essentially independent of the transverse position of the point loads.

4. Both theoretical and experimental results show that the AASHO empirical formula $N_{WL} = S/7$ overestimates the actual value slightly for a two lane truck loading, but underestimates by as much as 23%, the actual value for a three lane truck loading on the bridge.

5. Nominal calculated dead load steel stresses plus experimentally measured live load steel stresses extrapolated to critical midspan sections had the following approximate maximum total values for design vehicles placed to produce maximum effects.

   a. Two lanes of HS 20-44 trucks, 18,000 psi.

   b. Three lanes of HS 20-44 trucks, 23,000 psi.

   c. One lane of construction vehicles, 30,000 psi.

6. RESPONSE AT OVERLOAD STRESS LEVELS

6.1 General Remarks

As described in Vol. I, the experimental program was divided into two parts to study the response of the bridge under the following loadings:

Part 1 - Dead load and working loads

Part 2 - Overloads and loading to failure.

Responses to dead load and working loads have been discussed in Chapters 4 and 5. Response to overloads will be discussed in this Chapter and loading to failure will be discussed in Chapter 8.

The overload sequence was divided into several phases, in each of which initial conditioning loads were applied to create total maximum tensile stresses in the reinforcement of 40, 50 and 60 ksi. Each of these was then followed by a detailed sequence of 19 point load cases, having magnitudes in all cases identical to those used after the 30 ksi working stress conditioning load. These point load magnitudes were chosen to produce total maximum stresses of the order of 24 to 30 ksi in the reinforcement. In this manner, the response of the bridge at working stress level could be studied assuming it had been subjected to an overload of increasing magnitude, which would accentuate the maximum amount of cracking, deflection and stress in the bridge.

Of particular interest was how much, if any, would these overloads change the distribution and magnitude of reactions, deflections, strains, total moments at a section and percentage distribution of the total moment at a section to each girder. Of additional interest was the degree of linearity of response and the change in stiffness of the bridge during and after each of the conditioning overloads.

In this chapter the results for the above will be discussed and compared for the following cases: (1) during each of the conditioning loads to bring the stress level to 24, 30, 40, 50 and 60 ksi; (2) for a working stress point load at 1Y or 5Y after each of the conditioning loads to bring the stress level to 30, 40, 50 and 60 ksi was applied.

6.2 Results for Conditioning Loads

Detailed tabulations of theoretical and experimental results related to reactions, deflections, strains and moments for each of the conditioning loads are given in Vol. III (Table 20). Conditioning loads were obtained by applying equal loads over each of the five girders at both midspan Sections X and Y. All theoretical and experimental values have been normalized for purposes of comparison to total loads of 100 kips per span. Theoretical values have been obtained from computer analyses using FINPLA2.

During each of the conditioning load cases a specific sequence of loading as follows was used.

(1) Take zero readings on all gages and meters.

(2) Apply load in several increments to reach the full conditioning load and take readings after each increment.

(3) Remove load in several increments to reach zero load and take readings after each increment.

(4) Cycle eight times from zero to full load to zero.

(5) Take zero readings on all gages and meters.

(6) Apply full load in one increment and take readings.

(7) Unload to zero in one increment and take readings.

A series of graphs are given in Figs. 39 to 44 for the total west reaction, deflection at 5Y, and steel and concrete strains at 5D. Figs. 39, 40, 42, 43 depict for each conditioning load separately the response for the first complete load cycle (zero, full load, zero) as dotted lines, together with the response during the final load cycles as solid lines. These plots enable one to study the linearity of response and the permanent sets encountered in each conditioning load sequence. Figs. 41 and 44 superimpose on single plots the response for the final load cycle only, for all conditioning loads. These plots permit an evaluation of change in response for load for increasing values of maximum conditioning load.

6.2.1 Total West Reaction

Figure 39 indicates that this reaction is linearly related to load for all load levels and little difference exists between the first and last cycle of loading.

Figure 41 shows that there is hardly any change in the reaction per unit load response under increasing load levels all the way to the 60 ksi conditioning load case. It is also seen that theory accurately predicts this reaction response.

6.2.2 Deflection at 5Y

Figure 40 indicates that some residual deflection exists after the first cycle of loading in each case due to an increased level of cracking. However, for all cases, except the 60 ksi conditioning load, comparing the unloading path during the first cycle with the loading

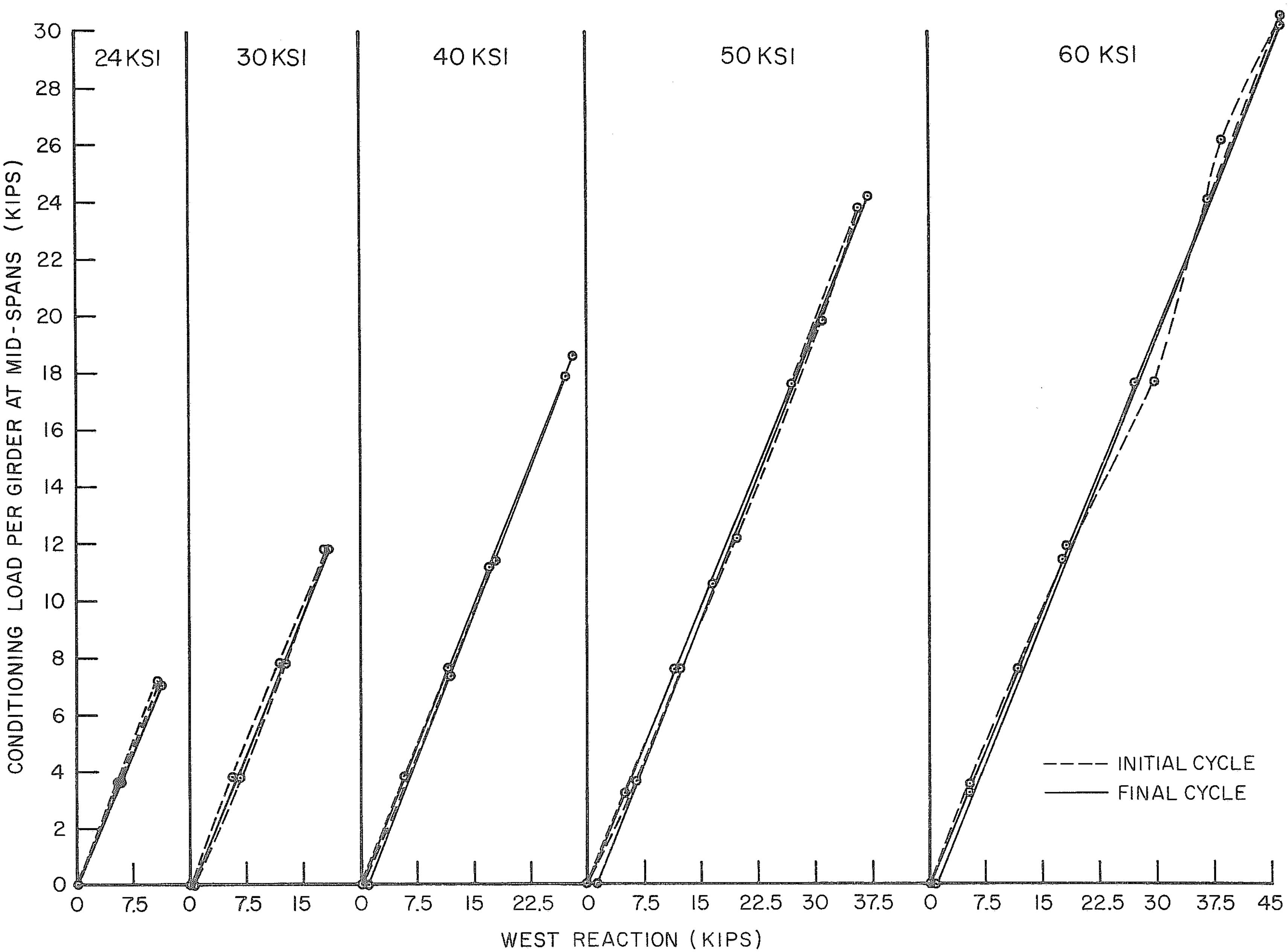

FIG. 39 EXPERIMENTAL TOTAL WEST REACTIONS (KIPS) DURING CONDITIONING LOAD CYCLES

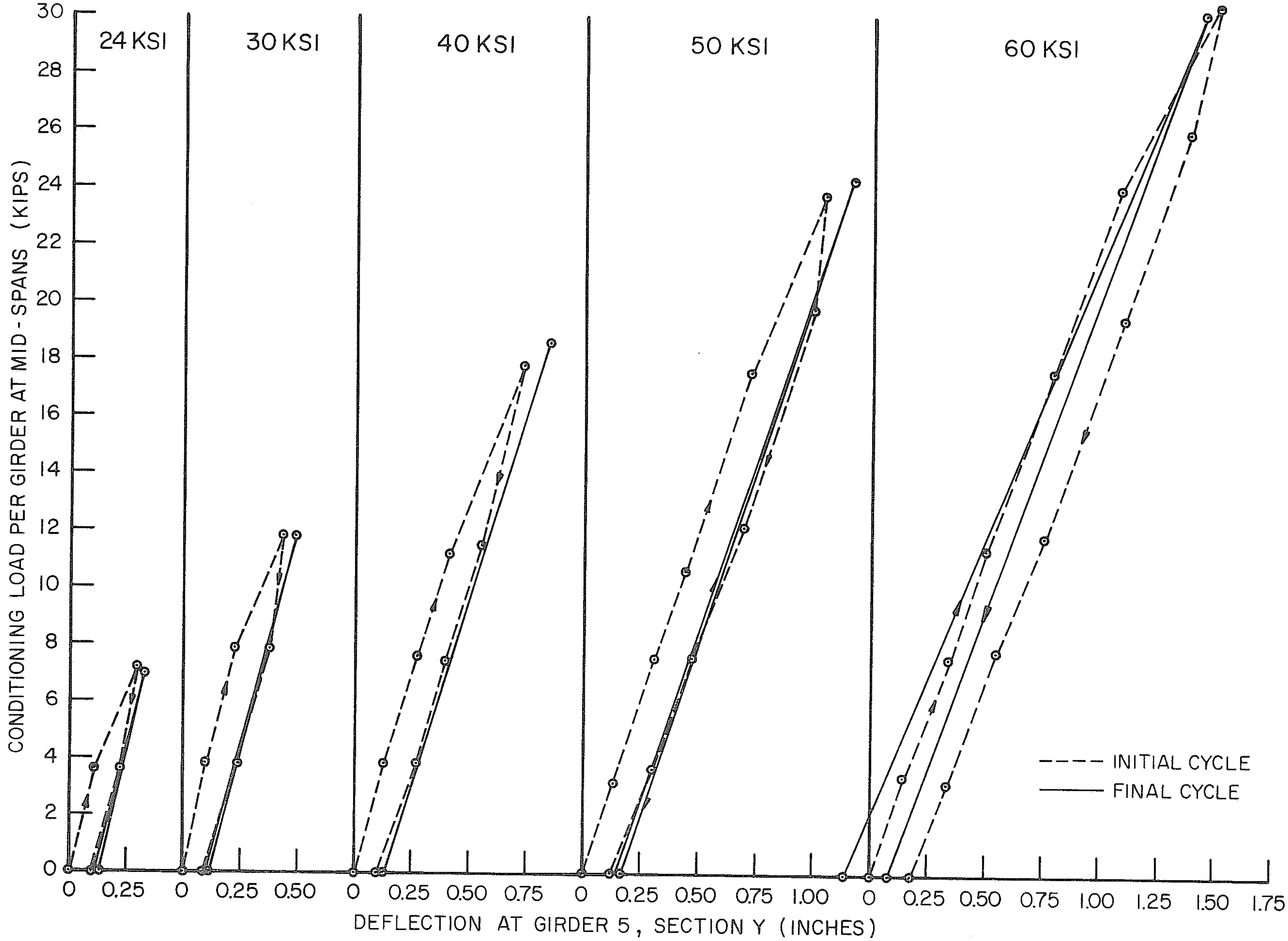

FIG. 40 EXPERIMENTAL DEFLECTIONS (INCHES) AT 5Y DURING CONDITIONING LOAD CYCLES

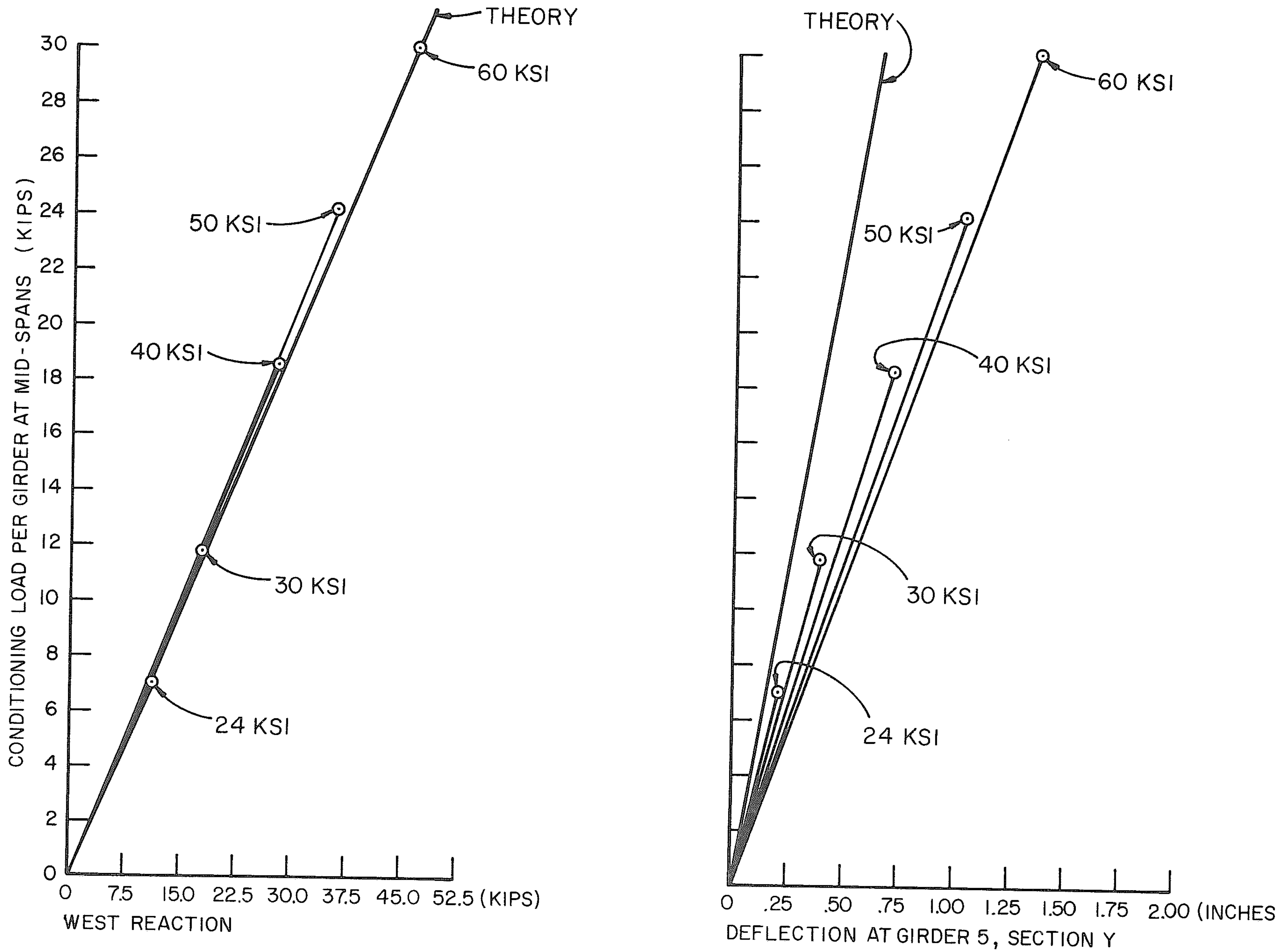

FIG. 41 TOTAL WEST REACTIONS (KIPS) AND DEFLECTIONS (INCHES) AT 5Y DURING CONDITIONING LOAD CYCLES

path during the final cycle of loading, it is seen that the slopes are almost identical and little additional permanent deflection occurs between the first cycle and the last (tenth) cycle of loading.

Figure 41 shows that a decreasing stiffness of the structure occurs under increasing conditioning loads due to the larger amount of cracking. Comparing the experimental values with that of theory based on an uncracked section, one finds that experimental values range from about 1.4 to 2.1 times the theoretical values respectively for the 24 and 60 ksi conditioning loads.

6.2.3 Steel and Concrete Strains at 5D

As indicated in Figs. 42 and 43, steel and concrete strains exhibit a similar response to that of deflection with respect to linearity and residual deformation. Linearity appears to be quite good even at high load levels.

Figure 44 shows that an increase in steel strain per unit load occurs for higher levels of conditioning loads while just the reverse is true for concrete strains. These changes are much smaller for concrete strains than for steel strains.

6.2.4 Moments

The experimental longitudinal variation of the total moments at a section for each conditioning load normalized to 100 kips per span are compared to theoretical values in Fig. 45. Moments obtained from both external reactions and integration of internal forces at the sections are given.

First, comparing experimental values with theoretical values, the agreement for moments based on external reactions is very good for

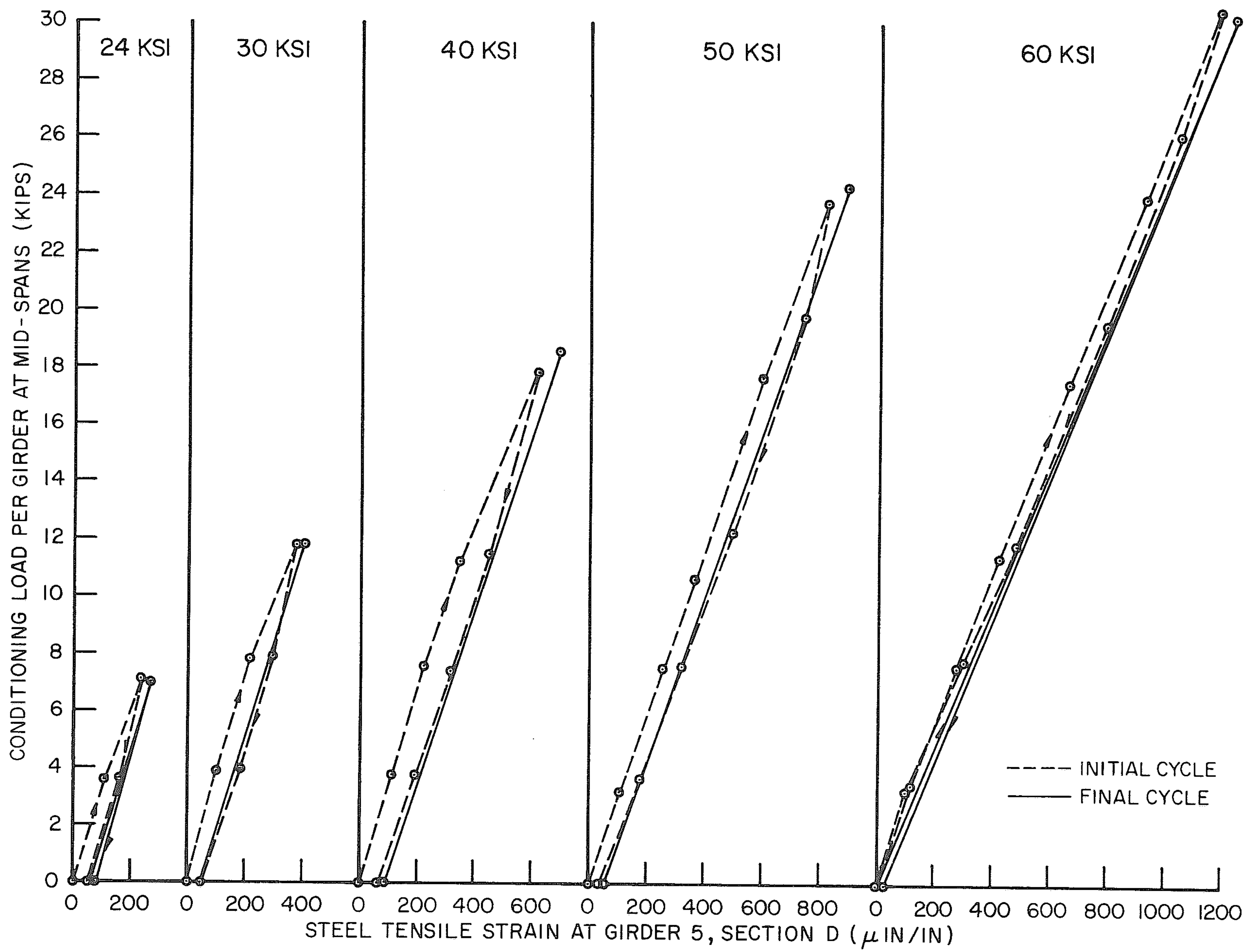

FIG. 42 EXPERIMENTAL LONGITUDINAL STEEL TENSILE STRAINS (MICRO-INCH/INCH) AT 5D DURING CONDITIONING LOAD CYCLES

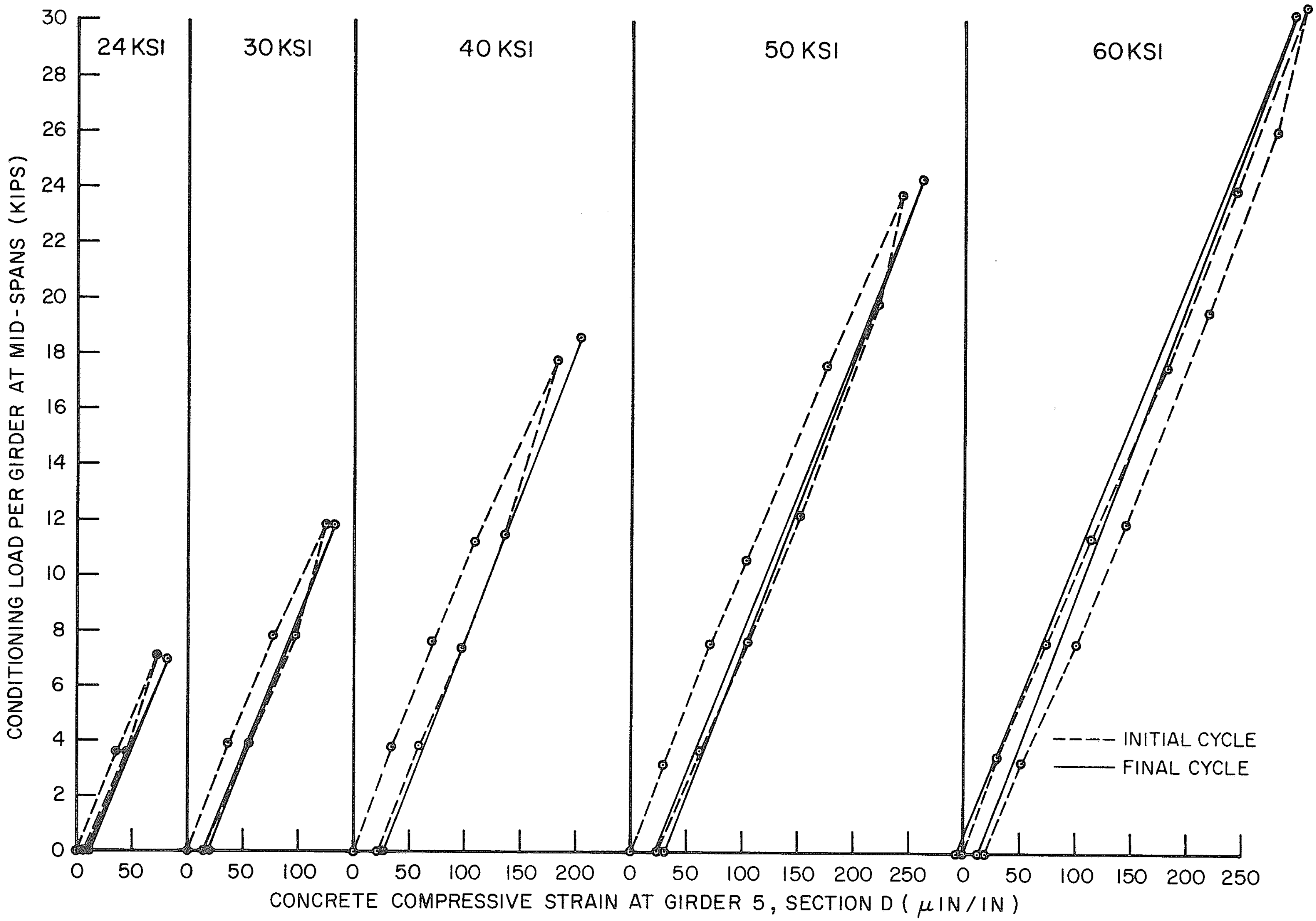

FIG. 43 EXPERIMENTAL LONGITUDINAL CONCRETE COMPRESSIVE STRAINS (MICRO-INCH/INCH) AT 5D DURING CONDITIONING LOAD CYCLES

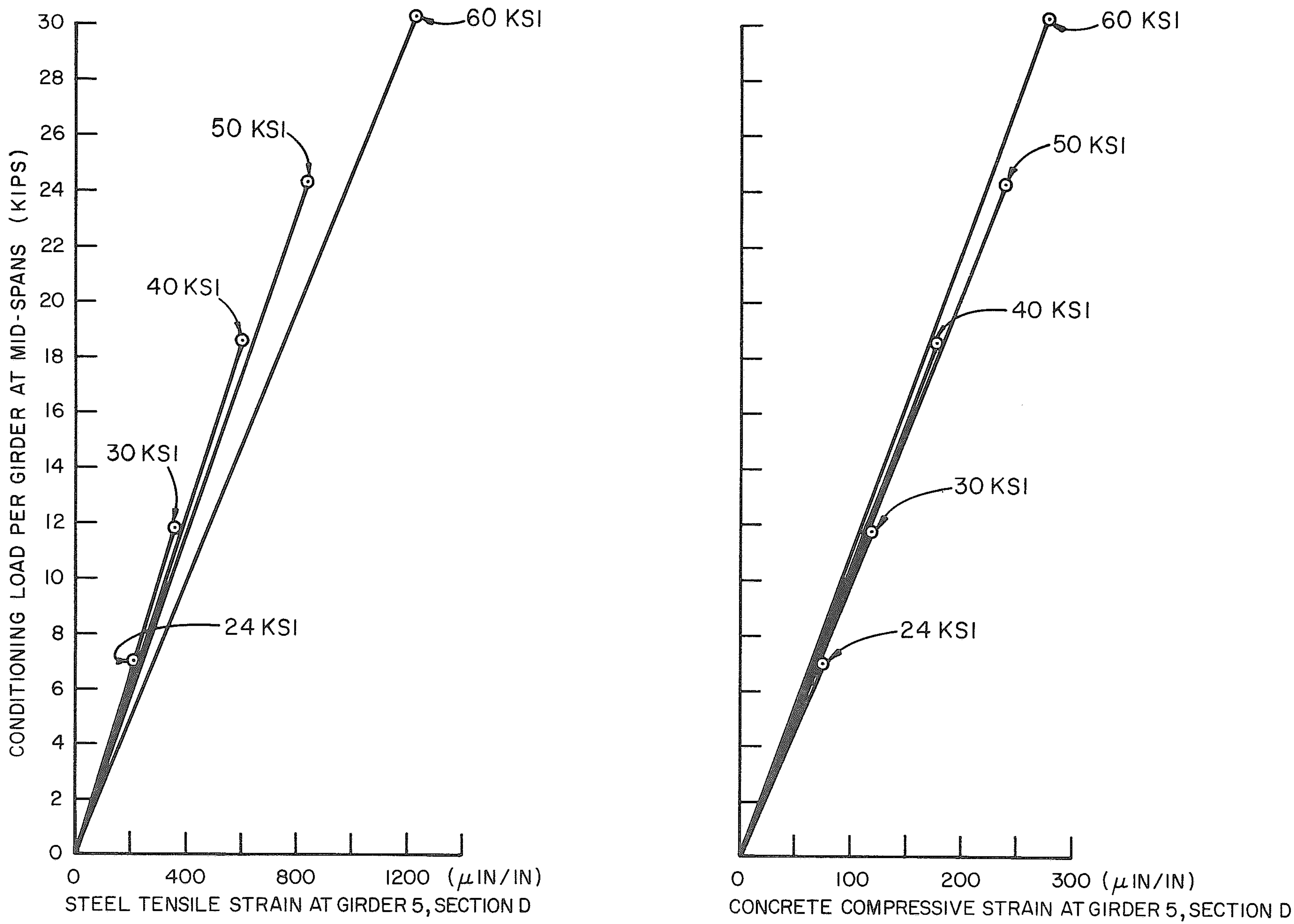

FIG. 44 EXPERIMENTAL LONGITUDINAL STEEL AND CONCRETE STRAINS (MICRO-INCH/INCH) AT 5D DURING CONDITIONING LOAD CYCLES

all load levels, the values being generally within 1 to 5% of each other. The agreement between experiment and theory for moments based on internal forces is excellent at positive moment Sections A and D, being generally within 1 to 3% for all load levels. At negative moment Sections B and C the differences are somewhat greater, with experimental values exceeding theoretical values by increasing margins as the load level is increased.

Second, comparing moments based on internal forces to those based on external reactions, which should give identical results, it is seen that at Sections A and D the agreement is within 1% for theoretical values and within 1 to 8% for experimental values at all load levels, except at Section D for the 50 and 60 ksi conditioning loads, where the difference reaches 11%. At Sections B and C, for theoretical values, internal moments are 7% less than external moments, once again indicating that a finer finite element mesh is needed in this region of steep moment gradient to get accurate theoretical results. At Sections B and C, for experimental values, internal and external moments agree within 1% for the 24 and 30 ksi conditioning loads, while for the 40, 50 and 60 ksi conditioning loads, the internal moments are larger than the external moments by amounts ranging from 5 to 17%. At the higher load levels, with increasing cracking the accuracy of the measurement of internal moments, expecially in regions of steep moment gradient such as at Sections B and C probably decreases. These internal moments are calculated from experimentally determined internal strains as described in Section 3.5. Thus, for these higher load levels, it is believed more reliability should be placed on the experimental moments at a section determined from the external reactions than from the internal forces.

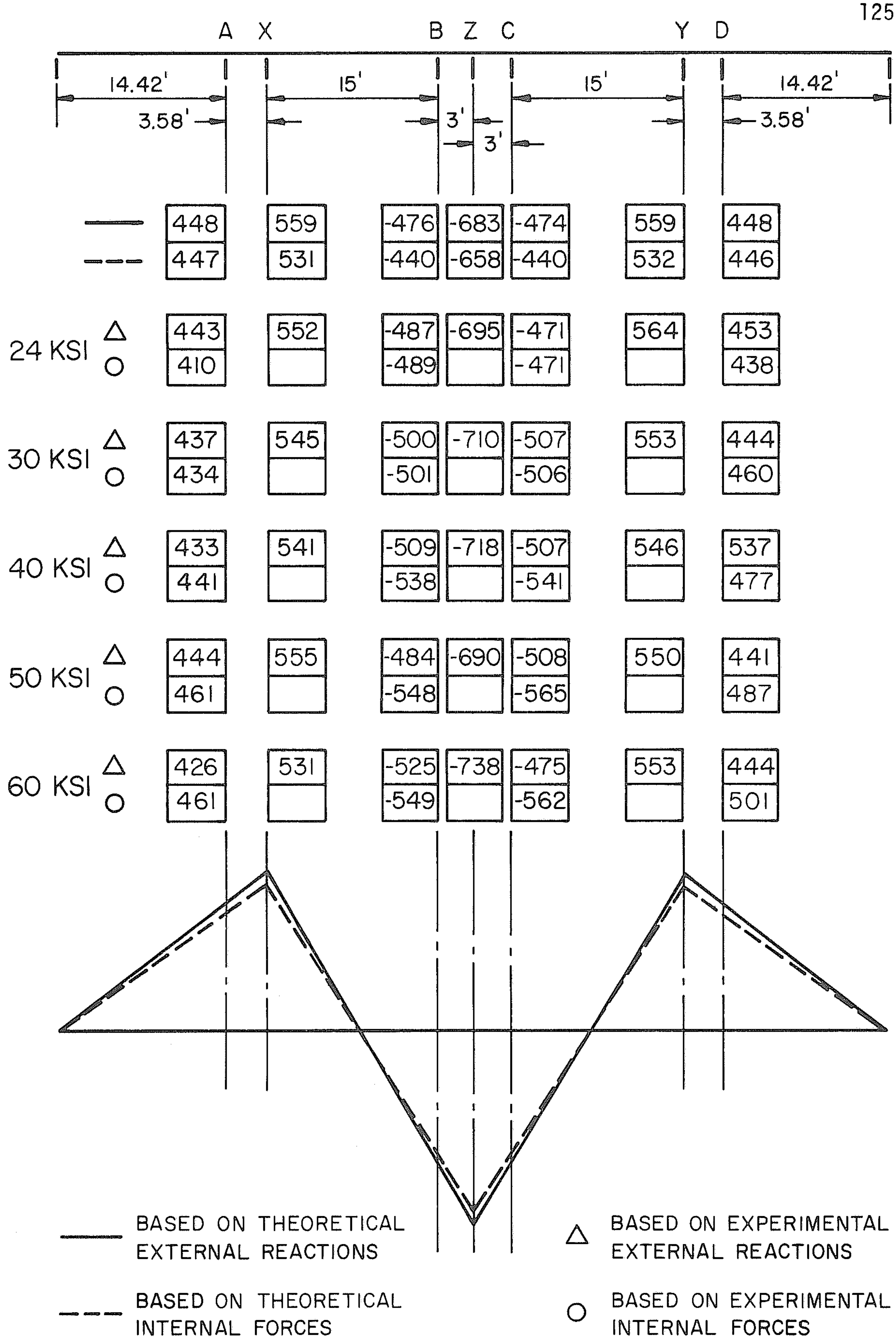

FIG. 45 TOTAL MOMENTS (FT–KIPS) FOR CONDITIONING LOADS OF 100 KIPS PER SPAN CAUSING NOMINAL MAXIMUM STEEL TENSILE STRESSES AS SHOWN

The transverse distributions of the total moments at Sections A, B, C and D are illustrated in Fig. 46. Recalling that a theoretical distribution of 16.5, 22.4, 22.4, 22.4 and 16.5% for girders 1 to 5 would be obtained for a uniform stress distribution across the entire section, it can be seen that theoretical values and experimental values for all conditioning load levels shown in Fig. 45 approach this distribution. Agreement between theory and experiment is generally within 1 to 2% of the total moment for the percentage taken by any girder. Little change in the experimental distribution occurs as the conditioning load level is increased from the 24 to the 60 ksi cases.

6.3 Results for Point Loads After Conditioning Overloads

Detailed tabulations of theoretical and experimental results related to reactions, deflections, strains and moments are given in Vol. III (Tables 21 to 23) for working stress nominal point loads of 19.4 kips at 5X, 5Y or 5X + 5Y designed to give a total maximum stress of 30 ksi in the reinforcement in each case, subsequent to the application of the conditioning loads which brought the maximum stress level to 24, 30, 40, 50 and 60 ksi. All theoretical and experimental values have been normalized for purposes of comparison to total loads of 100 kips per span.

During each of the cases of application of a total point load of 19.4 kips at 1Y following the 24, 30, 40, 50 and 60 ksi conditioning loads a special sequence was followed (See Fig. 33 of Vol. I).

(1) Take zero readings on all gages and meters.

(2) Apply load in four increments (1/4, 1/2, 3/4, 1) to reach the full load and take readings after each increment.

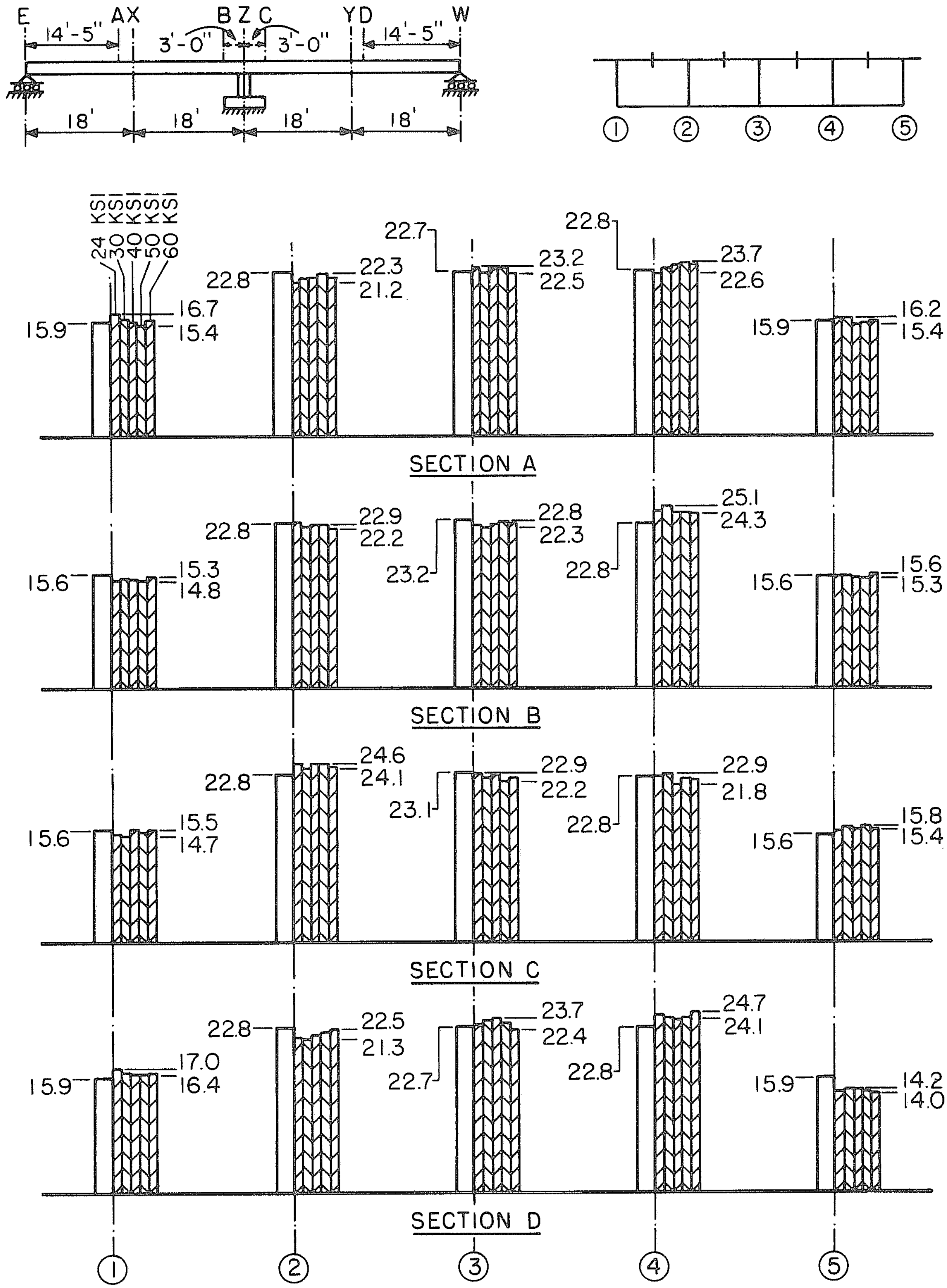

FIG. 46 PERCENTAGES OF TOTAL MOMENT AT A SECTION CARRIED BY EACH GIRDER FOR CONDITIONING LOADS (MOMENTS TAKEN ABOUT GROSS CROSS-SECTION NEUTRAL AXIS)

(3) Remove full load in one increment to reach zero load and take readings.

For the above cases of point loading at 1Y, a series of graphs are given in Figs. 47 to 58 for the total west and center reactions, deflections at 1Y and 5Y, and steel and concrete strains at 1D and 5D. Figs. 47, 48, 50, 51, 53, 54, 56 and 57 depict in separate graphs the response for each complete point load cycle after the 30, 40, 50 and 60 ksi conditioning loads. Figs 49, 52, 55 and 58 superimpose on single plots the response for all of the point load cycles.

6.3.1 Total West and Center Reactions

Figures 47 and 48 indicate that the west and center reactions are linearly related to load for all cases shown and little difference exists between the results for the cycles after 30 and 60 ksi conditioning loads.

Figure 49 shows that relation between reactions and applied point load remain essentially unchanged after all conditioning overloads up to 60 ksi. It can also be seen that theory accurately predicts the reactions.

6.3.2 Deflections at 1Y and 5Y

Figures 50 and 51 indicate that very little permanent deflection exists after each cycle of loading. Some nonlinearities in the cycles occur, especially after the higher conditioning overloads.

Figure 52 shows that due to a point load at 1Y after each higher conditioning overload an increase in deflection occurs at 1Y directly under the load while at the opposite side of the bridge at 5Y a decrease in the deflection occurs. It is interesting to compare the

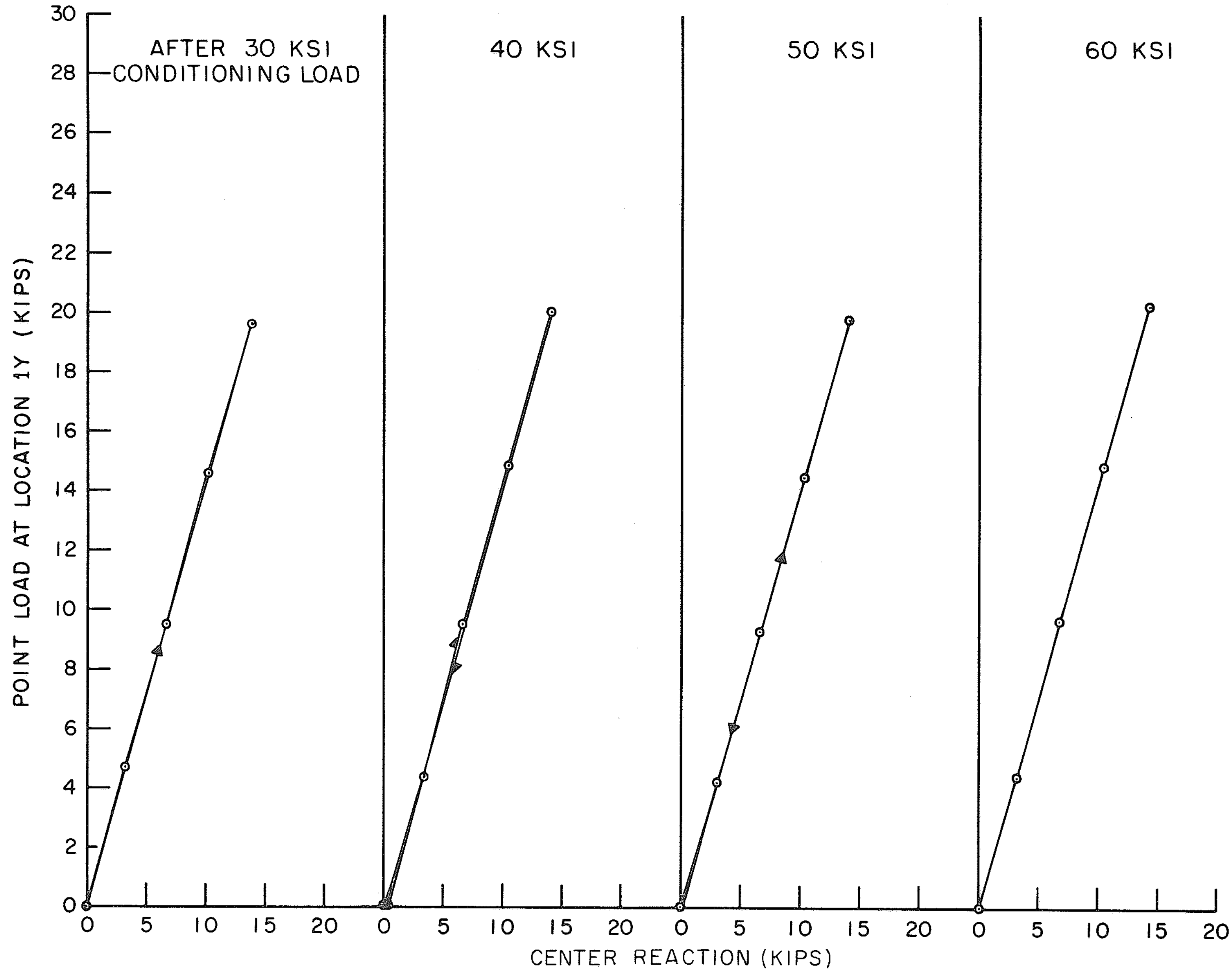

FIG. 47 EXPERIMENTAL TOTAL CENTER REACTIONS (KIPS) DUE TO POINT LOAD AT 1Y AFTER CONDITIONING LOADS

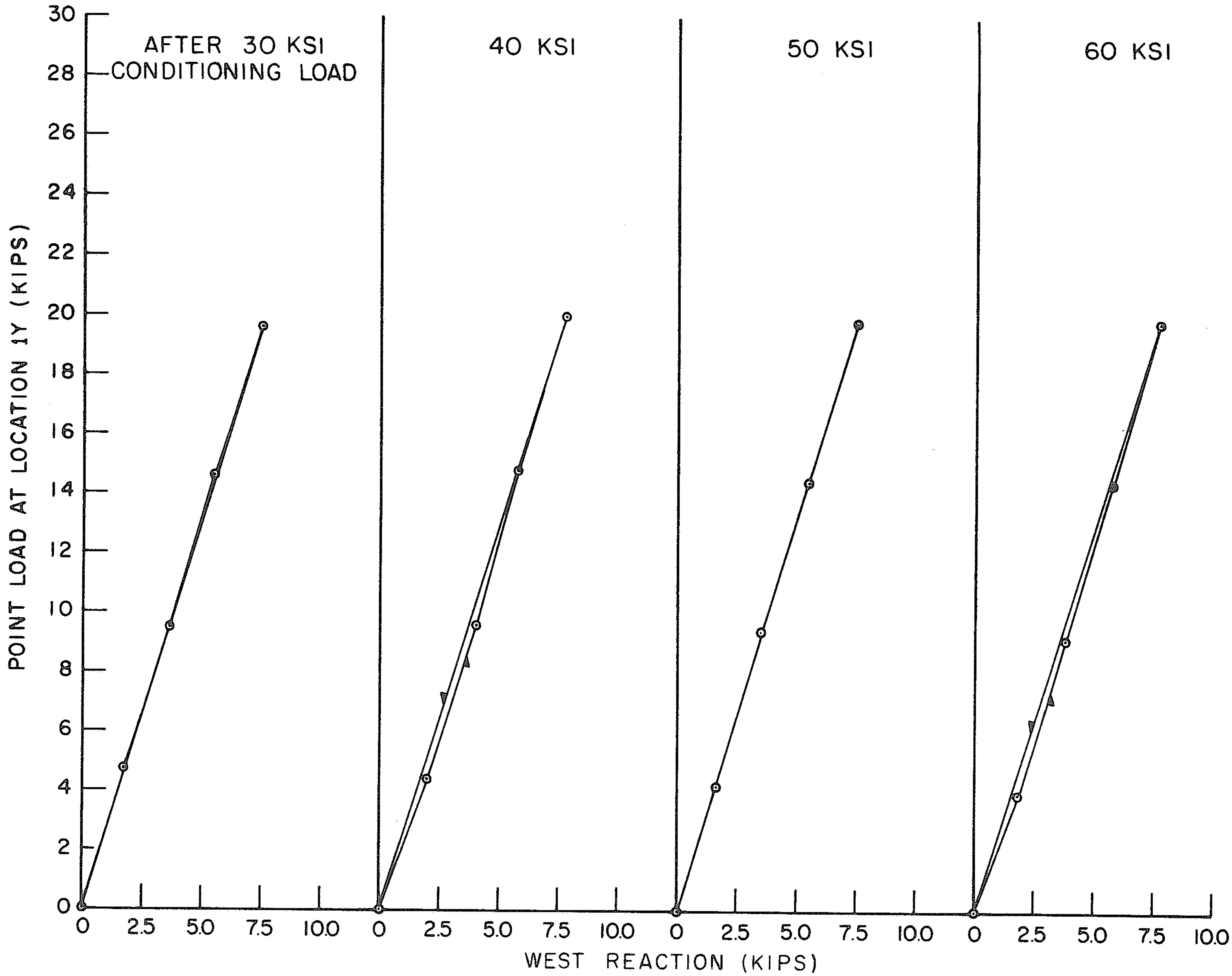

FIG. 48 EXPERIMENTAL TOTAL WEST REACTIONS (KIPS) DUE TO POINT LOAD AT 1Y AFTER CONDITIONING LOADS

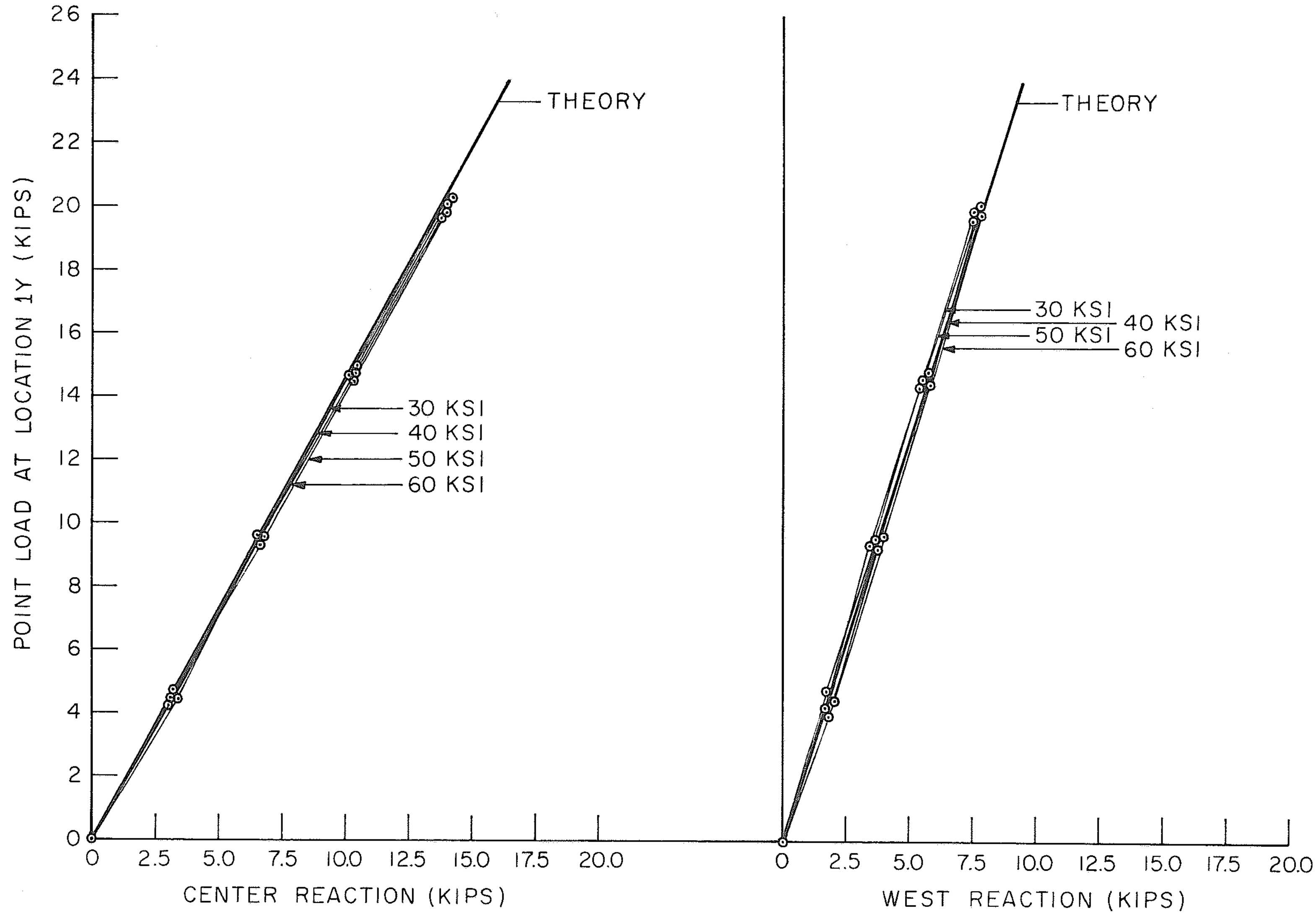

FIG. 49 CENTER AND WEST REACTIONS (KIPS) DUE TO POINT LOAD AT 1Y AFTER CONDITIONING LOADS

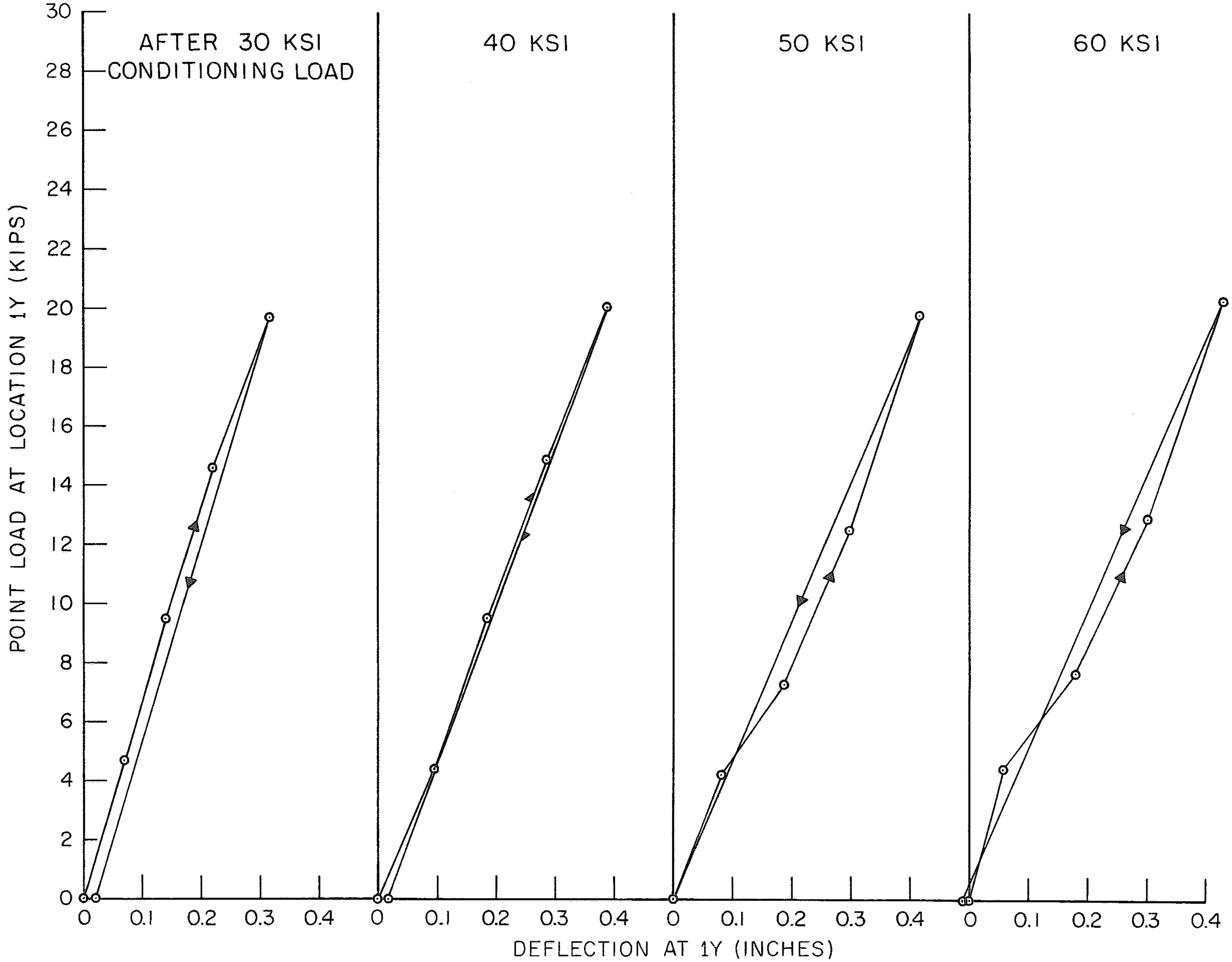

FIG. 50 EXPERIMENTAL DEFLECTIONS (INCHES) AT 1Y DUE TO POINT LOAD AT 1Y AFTER CONDITIONING LOADS

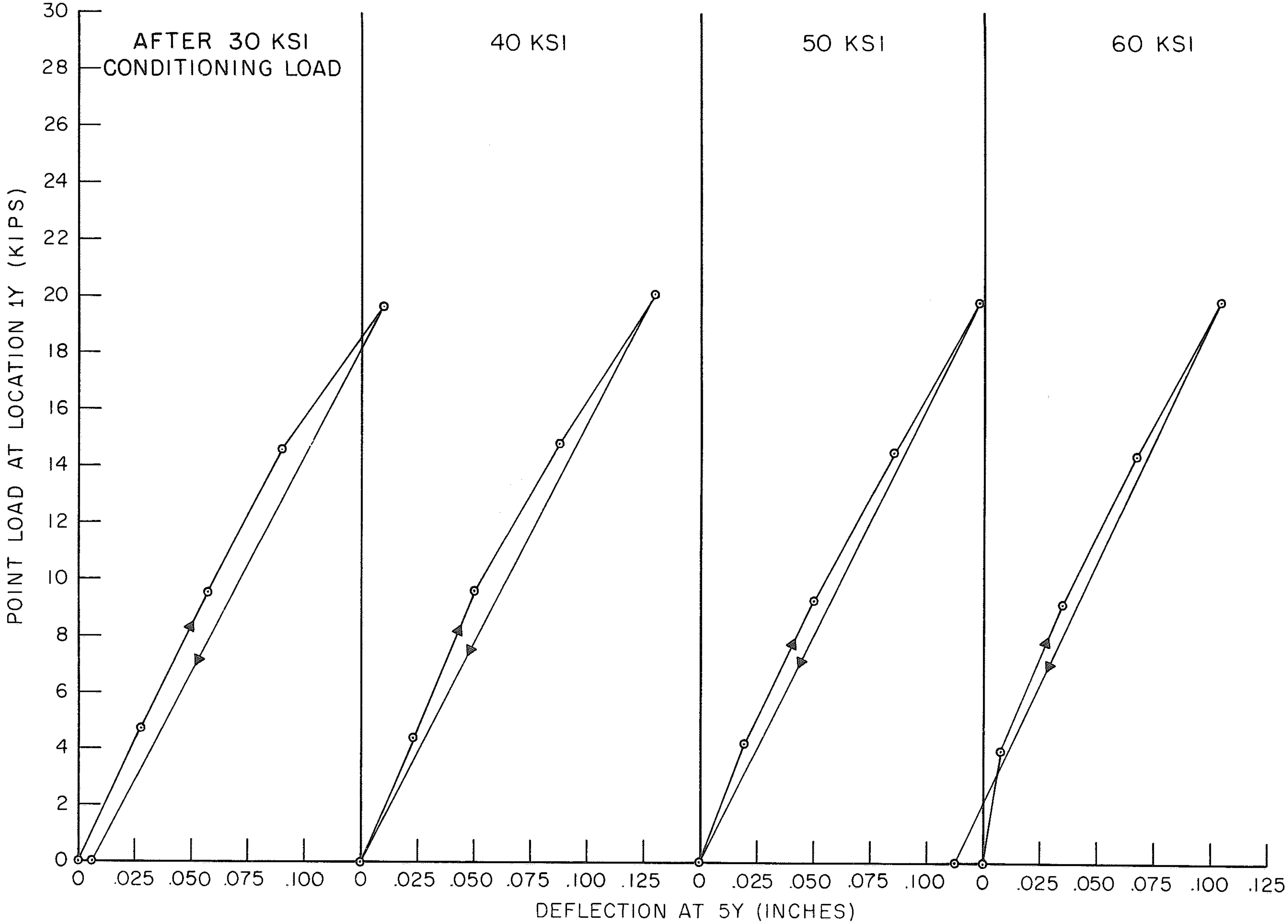

FIG. 51 EXPERIMENTAL DEFLECTIONS AT 5Y DUE TO POINT LOAD AT 1Y AFTER CONDITIONING LOADS

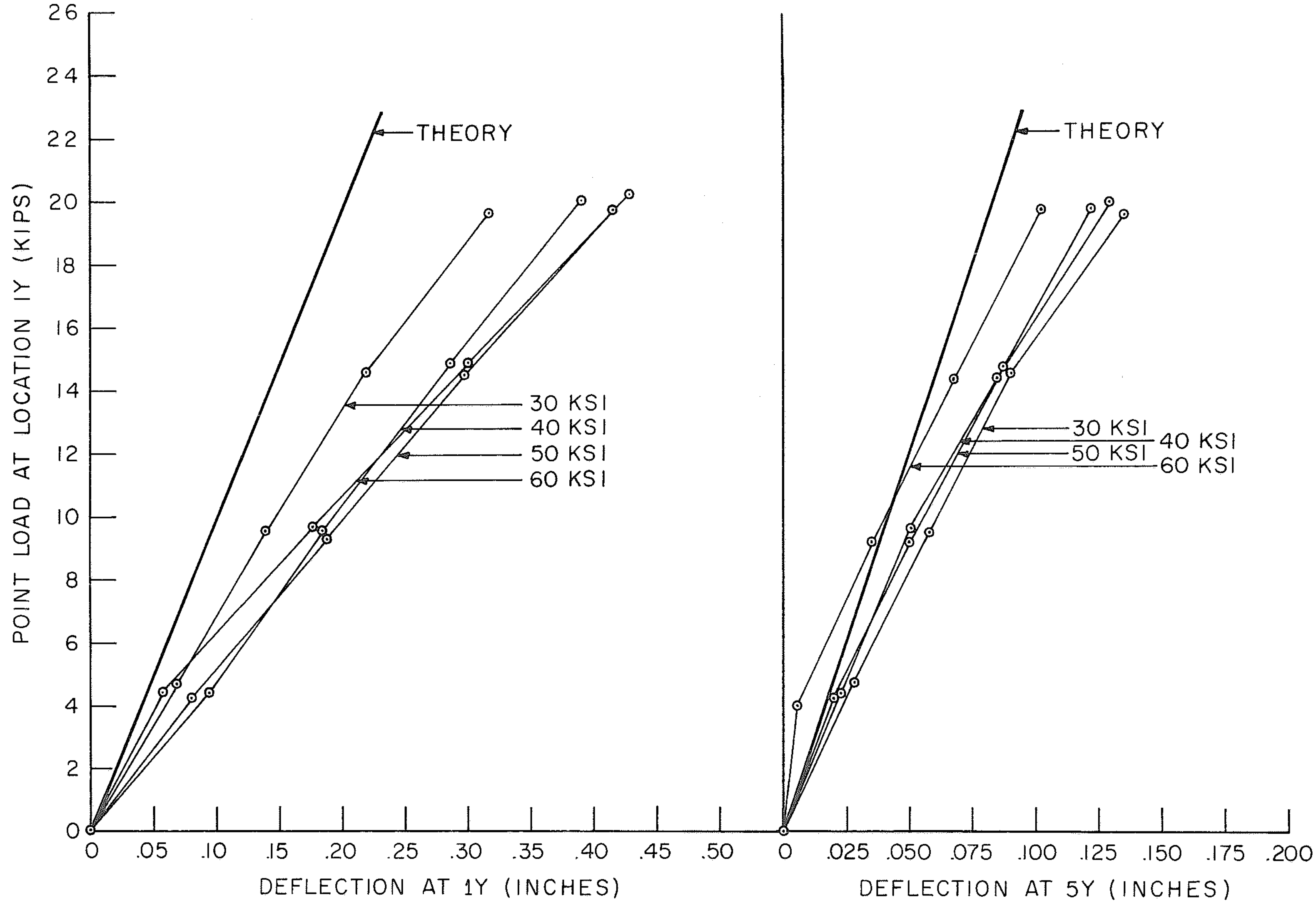

FIG. 52 DEFLECTIONS (INCHES) AT 1Y AND 5Y DUE TO POINT LOAD AT 1Y AFTER CONDITIONING LOADS

ratios of experimental to theoretical deflections at 1Y and 5Y due to the point load at 1Y after the 30 ksi conditioning load, which are respectively .320/.200 = 1.60 and .140/.084 = 1.66, with those after the 60 ksi conditioning load, which are respectively .420/.200 = 2.10 and .105/.084 = 1.25. It is evident that after the 30 ksi working stress conditioning load the theory based on an uncracked section accurately predicts the transverse distribution of deflections between 1Y and 5Y, with the experimental values being about 60% higher than theoretical. However, after higher and higher conditioning overloads, the theory can no longer be used to accurately predict the transverse distribution of deflections. As indicated above, after the 60 ksi conditioning load, the experimental deflection may be anywhere from 25% higher than theoretical values, at points some distance away from the point load, to 110% higher, at points directly under the point load.

6.3.3 Steel and Concrete Strains at 1D and 5D

For point loadings at 1Y, Figs. 53 to 58 depict the strains at 1D, near the point load, and at 5D, near the opposite edge of the bridge.

For Section 1D, near the point load at 1Y, Figs. 53 and 54 indicate that little residual deformation occurs after each load cycle except for the concrete strain after the 60 ksi conditioning load. Fig. 55 indicates that an increase in the steel strain per unit load occurs after higher conditioning loads with a continued fairly linear response for all cases. Fig. 58 shows that the concrete strain due to the first 1/4 increment of the point load at 1Y becomes larger and larger after each successively higher conditioning load is applied. However, for the remaining increments (1/2, 3/4,1) of load, the slope of the load

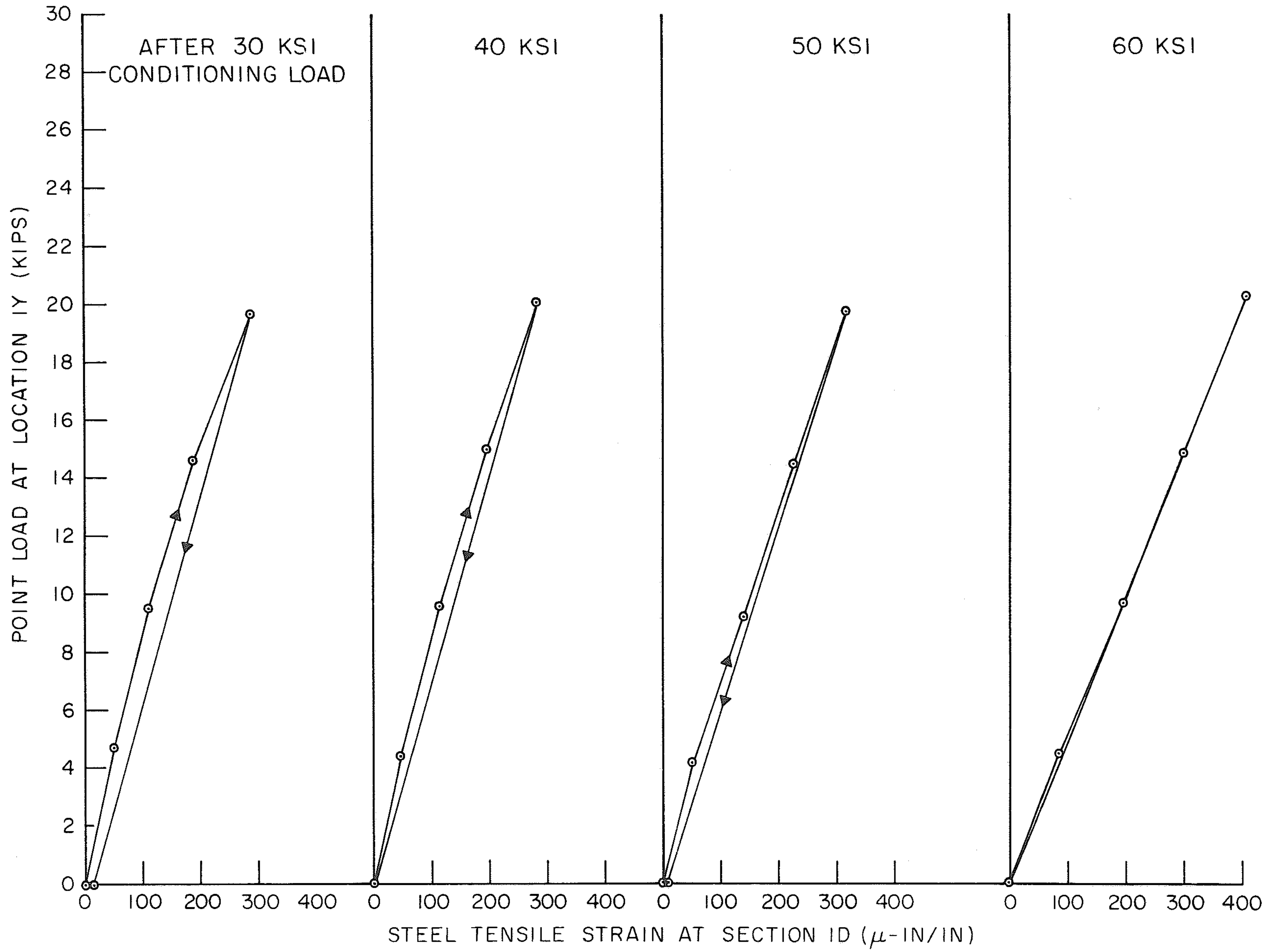

FIG. 53 EXPERIMENTAL STEEL TENSILE STRAINS (MICRO-INCH/INCH) AT 1D DUE TO POINT LOAD AT 1Y AFTER CONDITIONING LOADS

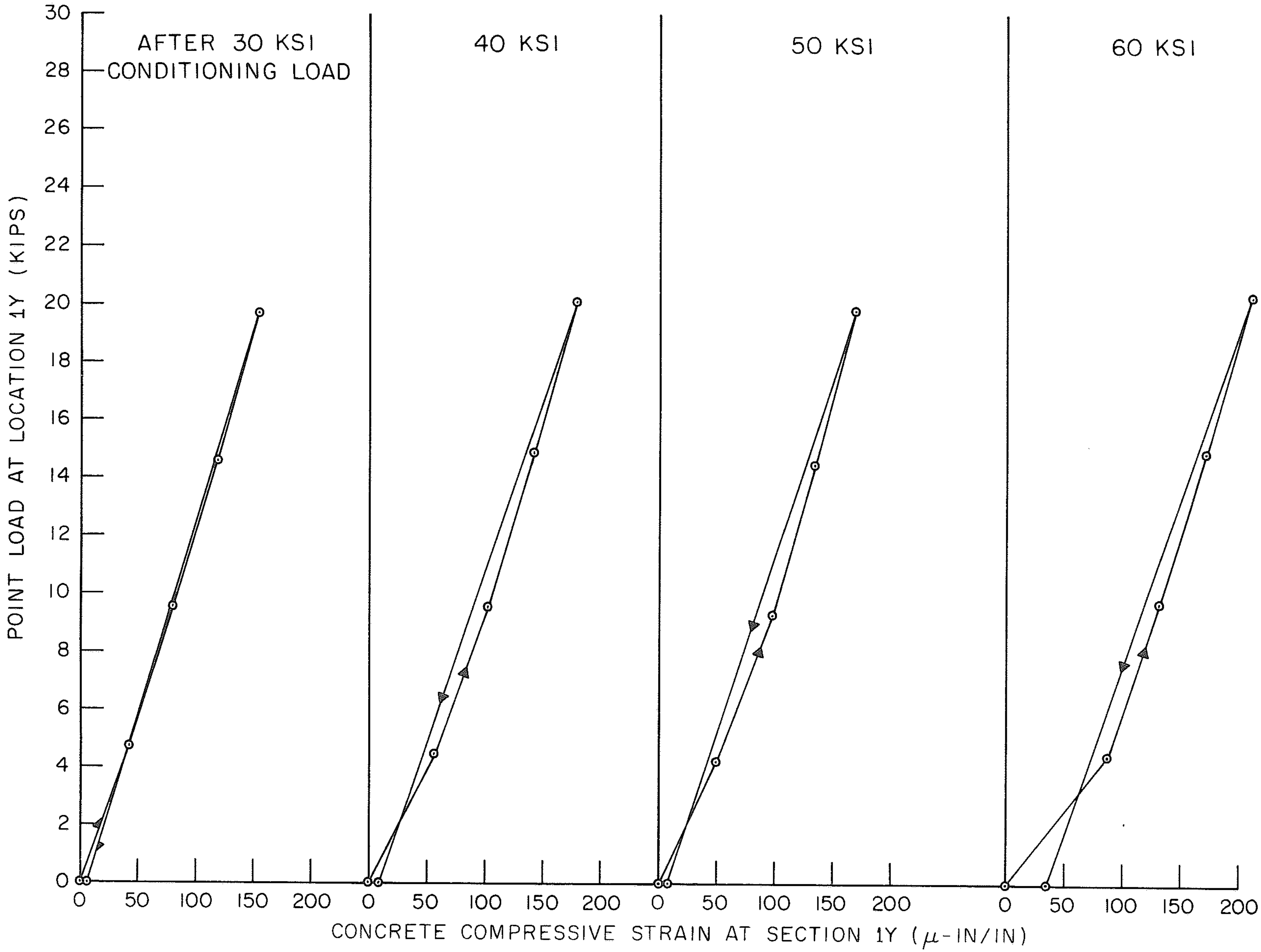

FIG. 54 EXPERIMENTAL CONCRETE COMPRESSIVE STRAINS (MICRO-INCH/INCH) AT 1D DUE TO POINT LOAD AT 1Y AFTER CONDITIONING LOADS

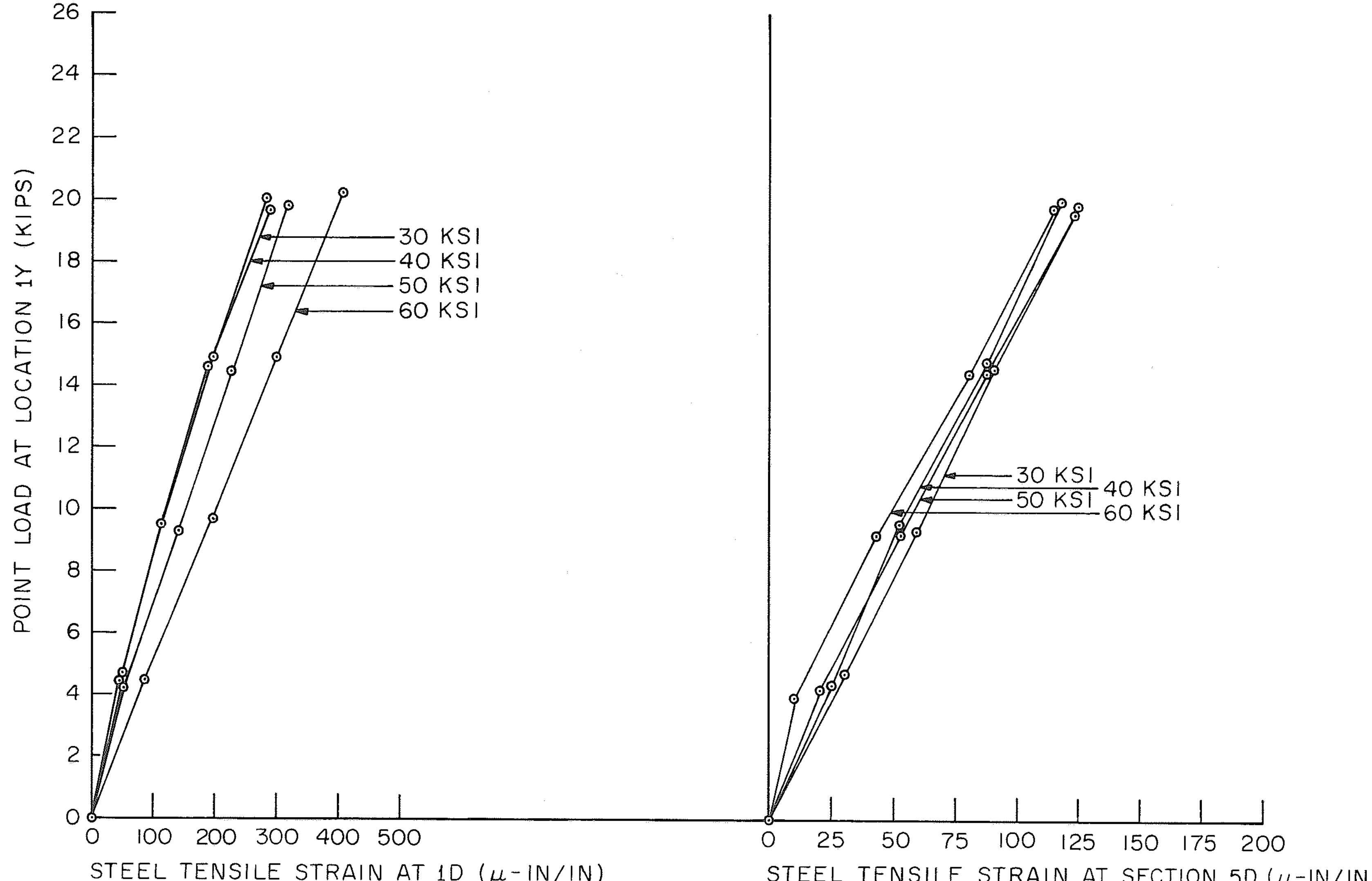

FIG. 55 EXPERIMENTAL STEEL TENSILE STRAINS (MICRO-INCH/INCH) AT 1D AND 5D DUE TO POINT LOAD AT 1Y AFTER CONDITIONING LOADS

strain curves are almost the same for all cases. This could indicate that some cracking may have existed on the compressive face which had to be initially closed during the first increment.

For Section 5D, at the opposite edge of the bridge from the point load at 1Y, the strains are much smaller. Figs. 56 and 57 indicate that some small residual deformation occur after the load cycles following the 40 ksi and 60 ksi conditioning loads. For the 30 and 50 ksi conditioning loads, essentially no residual steel or concrete strains remain after the point load cycle. Fig. 55 shows little change in load vs steel strain response, and also indicates linearity of behavior except following the 60 ksi conditioning load. For the concrete strain, linearity exists for all cases, with plots for the cases following the 40, 50 and 60 ksi conditioning loads being almost coincident.

6.3.4 Moments

A comparison is given in Fig. 59 of the theoretical and experimental longitudinal distributions of the total moments at a section for a point load at 5Y designed to give a total maximum stress of 30 ksi in the reinforcement in each case, subsequent to the application of conditioning loads which brought the maximum stress level to 24, 30, 40, 50 and 60 ksi. All values have been normalized to a 100 kip point load at 5Y. Moments obtained from both external reactions and an integration of the internal forces at a section are given.

First, comparing experimental values with theoretical values, which were obtained by FINPLA2, the agreement for moments based on external reactions is very good (generally within 1 to 5%) for all cases, except after the 60 ksi conditioning load where the differences are much

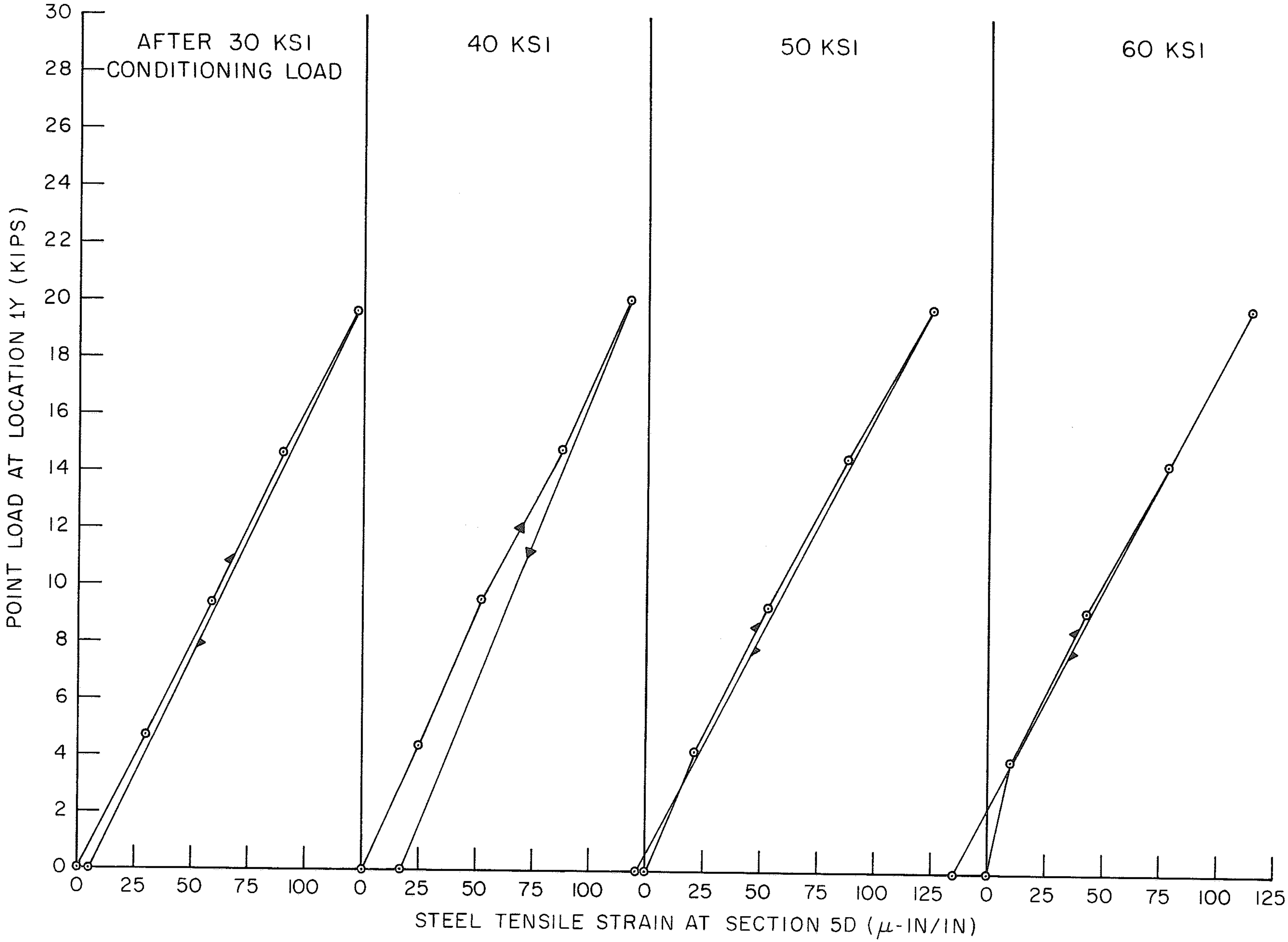

FIG. 56 EXPERIMENTAL STEEL TENSILE STRAINS (MICRO-INCH/INCH) AT 5D DUE TO POINT LOAD AT 1Y AFTER CONDITIONING LOADS

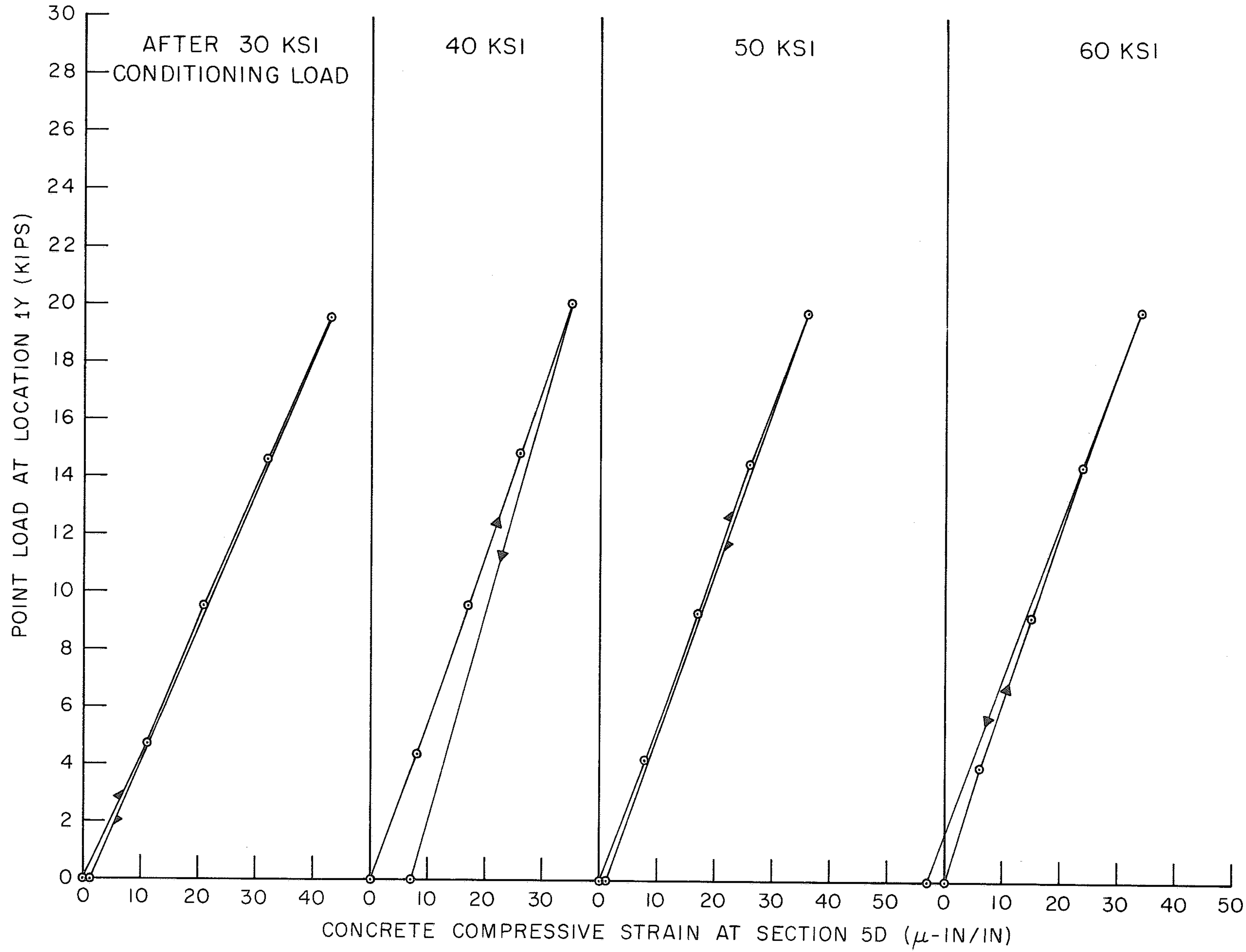

FIG. 57 EXPERIMENTAL CONCRETE COMPRESSIVE STRAINS (MICRO-INCH/INCH) AT 5D DUE TO POINT LOAD AT 1Y AFTER CONDITIONING LOADS

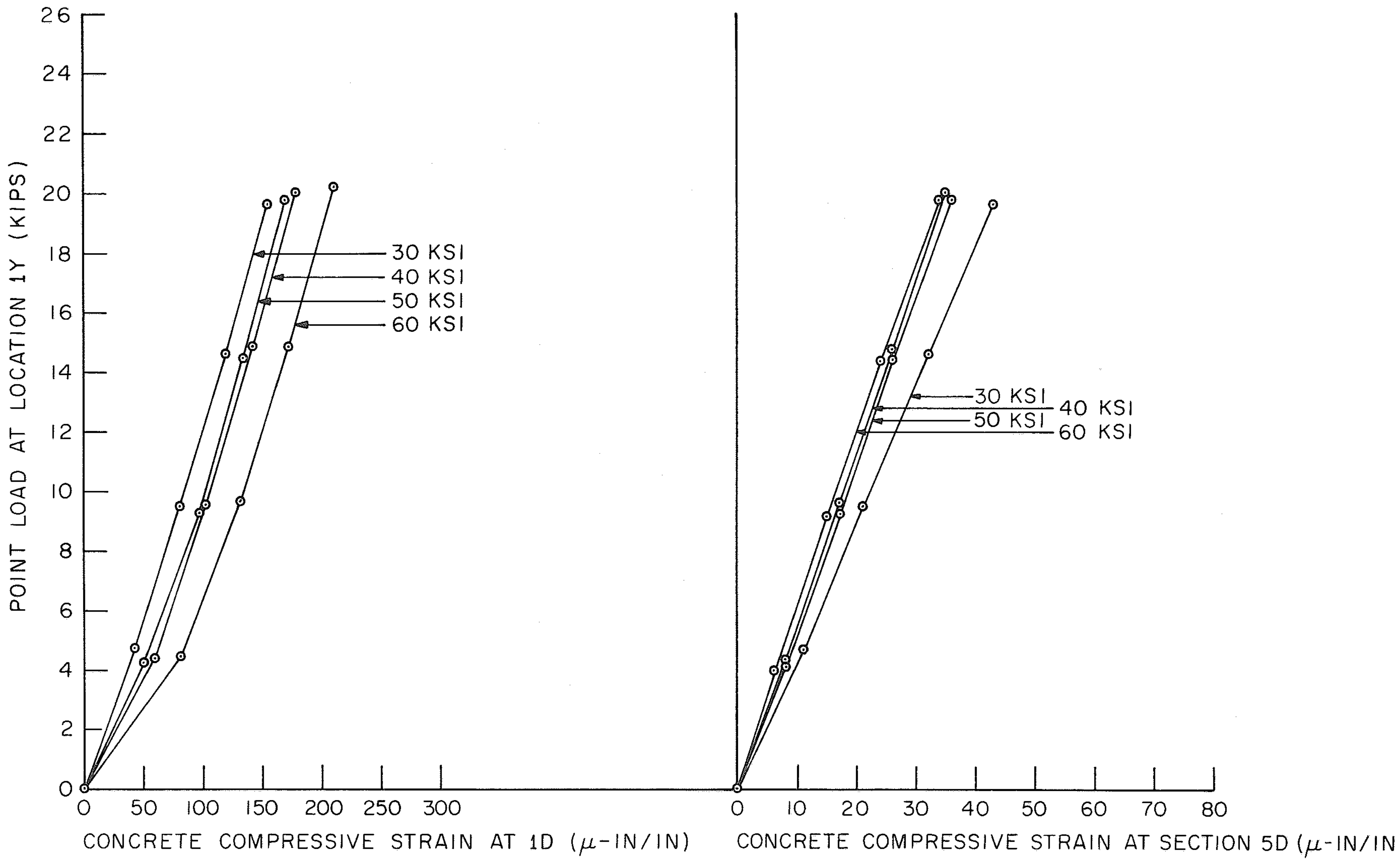

FIG. 58 EXPERIMENTAL CONCRETE COMPRESSIVE STRAINS (MICRO-INCH/INCH) AT 1D AND 5D DUE TO POINT LOAD AT 1Y AFTER CONDITIONING LOADS

larger. The agreement between experiment and theory for moments based on internal forces is within 1 to 7% at Sections A, B and D for all cases, but larger differences exist at Section C near the support in the loaded span, once again due to the low theoretical value given by the finite element solution.

Second, comparing moments based on internal forces to those based on external reactions, which should give identical results, it is seen that at Sections A, B and D the agreement is within 1% for theoretical values and within 1 to 7% for all experimental values except after the 60 ksi conditioning load. At Section C, for the theoretical values, the internal moment is about 12% less than the external moment, once again indicating a finer finite element mesh is required in this region of steep moment gradient to get accurate internal forces. For experimental values at Section C, exclusive of the 60 ksi case, where the difference are very large, the internal moments are greater than the external moments by amounts ranging from 8 to 12%, or in terms of absolute moment difference 19 to 28 ft kips. It should be emphasized, that only a 1 ft shift along the bridge in this region of steep moment gradient changes the moment by about 35 to 40 ft kips, which would eliminate the above difference.

The transverse distributions of the total moments at Sections A, B, C and D are illustrated in Fig. 60 for a point load at 5Y. At Section D, nearest the loaded midspan Section Y, the changes in the experimental distribution to each girder, after successively higher conditioning overloads, range from 2.0 to 3.9% of the total moment at the section. In terms of individual girder moments, the maximum percentage changes are 13% for interior girders and 18% for exterior

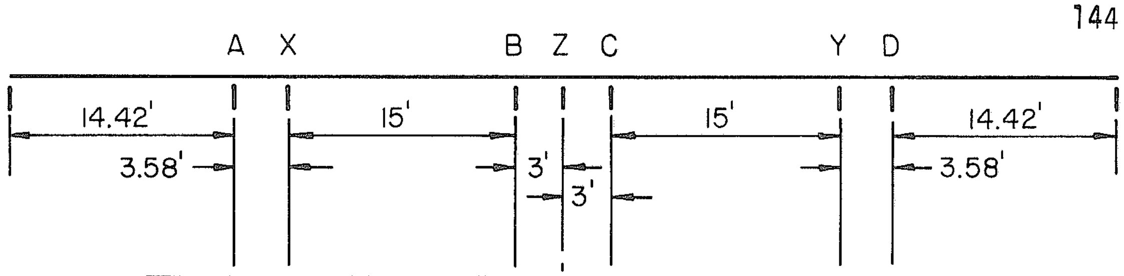

		A	X	B	C	Y	D
	———	-118	-148	-270	-208	705	565
	– – –	-117	-147	-261	-182	686	561
24 KSI	△	-123	-153	-280	-200	710	569
	○	-111		-259	-228		556
30 KSI	△	-122	-152	-278	-215	702	563
	○	-110		-244	-242		-598
40 KSI	△	-119	-148	-272	-235	690	562
	○	-112		-270	-254		610
50 KSI	△	-116	-144	-264	-230	693	563
	○	-113		-271	-257		612
60 KSI	△	-278	-344	-630	-465	-564	-453
	○	-117		-282	-289		588

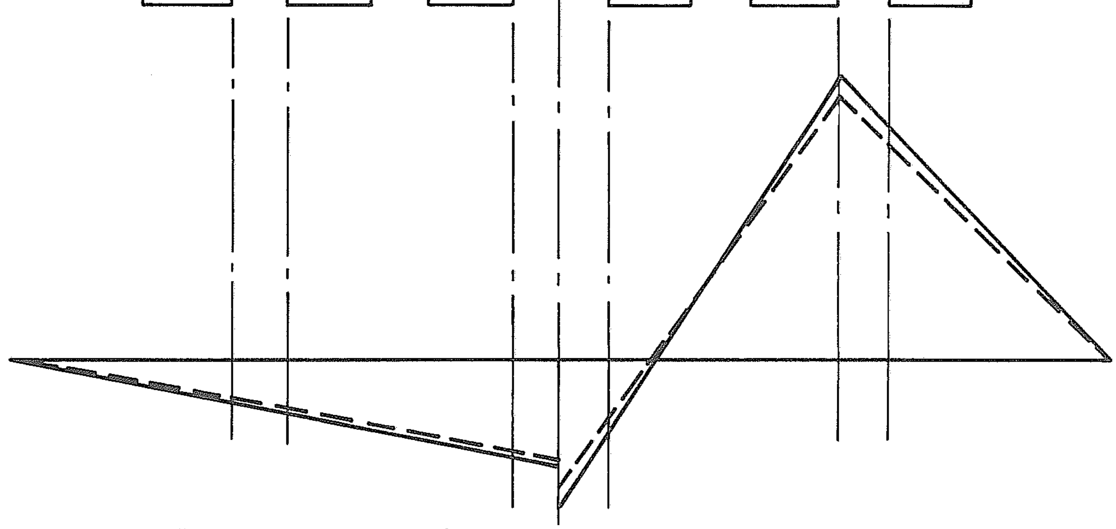

——— BASED ON THEORETICAL EXTERNAL REACTIONS

– – – BASED ON THEORETICAL INTERNAL FORCES

△ BASED ON EXPERIMENTAL EXTERNAL REACTIONS

○ BASED ON EXPERIMENTAL INTERNAL FORCES

FIG. 59 TOTAL MOMENTS (FT–KIPS) AT A SECTION FOR NORMALIZED 100 KIP LOAD AT 5Y CAUSING NOMINAL MAXIMUM STEEL TENSILE STRESSES AS SHOWN

girders. Theoretical values at Section D for girders 1, 2 and 3 are in good agreement with all experimental values, generally differing by only 1 to 2% of the total moment at the section. However, for girders 4 and 5 the maximum differences are larger, with theoretical values becoming 4.2% lower for girder 4 and 4.7% higher for girder 5. The same order of magnitude of changes in experimental values after successively higher conditioning loads and differences between theoretical and experimental values occurs in the unloaded span at Sections A and B. At Section C, in the region of the steep moment gradient, the changes in experimental values for individual girders, after successively higher conditioning loads, range from 1.9 to 4.5% of the total moment at the section. Theoretical values at Section C are larger than experimental values for girders 4 and 5 and smaller for girders 1, 2 and 3.

From Fig. 60 and the above discussion of the transverse distribution of moments after increasing conditioning loads, a general statement can be made that under a single point load the changes in distribution of the total moment to a girder will usually range from 2 to 4% of the total moment on the section or in terms of a percentage of the individual girder moment from 10 to 20%. Theoretical calculations based on FINPLA2 appear to predict the experimental values generally within about the same range as the above percentages. If one considers that the design for girder moments will be predicated on several wheel loads across the width of the bridge rather than a single load, it is apparent that the differences will be much smaller, as evidenced in the discussion of the results for the conditioning overloads in Section 6.3. Thus it would appear that for practical design purposes the theory can be used to adequately predict both the longitudinal distribution of the

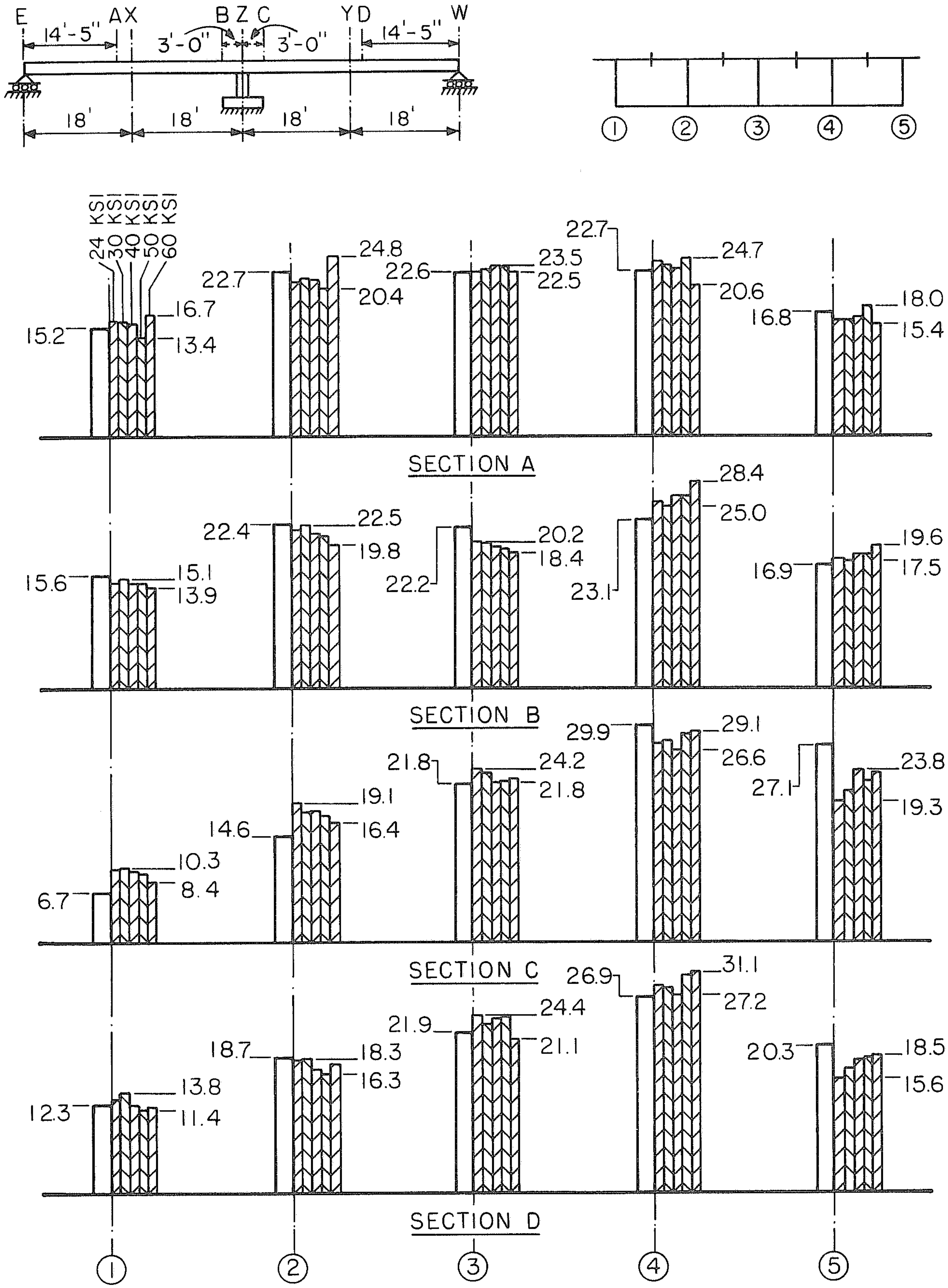

FIG. 60 PERCENTAGES OF TOTAL MOMENT AT A SECTION CARRIED BY EACH GIRDER FOR POINT LOAD AT 5Y. (MOMENTS TAKEN ABOUT GROSS CROSS-SECTION NEUTRAL AXIS)

total moments at a section and the transverse distribution of the total moment to individual girders, even after overload conditions producing stresses of 30, 40 or 50 ksi in the reinforcement.

6.4 Summary

Detailed discussions of the results for overload stress levels produced by increasing conditioning loads and for working stress point loads applied after each successively higher conditioning load have been presented. The most important conclusions are summarized below. Theoretical results were based on FINPLA2.

1. Total reactions are accurately predicted by theory for all load levels. As a consequence the total external moment at any section can be found with confidence.

2. Theory predicts the magnitude and distribution of deflections quite well for the 24 ksi and 30 ksi stress levels provided theoretical values based on an uncracked section are multiplied by a factor of about 1.5 to account for cracking.

3. At or after higher stress levels of 40, 50 or 60 ksi the deflections for a given load at some locations can increase to a value as high as 2.1 times the theoretical value. In addition, the theory can no longer be used to accurately predict the distribution of deflections under point loads. After the 60 ksi conditioning load, values ranging from 1.2 to 2.1 times the theoretical value were found for points some distance away and directly under the point load respectively.

4. An essentically linear load vs steel strain curve continues to exist for all stress levels, however, the slope of these curves increases for or after higher overload stress levels. Concrete strains exhibit greater nonlinearity with respect to load than do the steel strains.

5. The longitudinal distributions of the total moments at a section are adequately predicted by theory. Values based on external reactions are more accurate than those based on an integration of internal forces at a section. If the latter are used a refinement of the finite element mesh should be used in the region of steep moment gradients to achieve satisfactory accuracy.

6. Changes in the transverse distribution of moments under uniform loads across the width of the bridge, such as the conditioning loads, are small for all overload stress levels. These changes are much greater for single point loads applied after the above conditioning overloads and can range from 2 to 4% of total moment at the section for individual girders or in terms of the individual girder moments themselves from 10 to 20%.

7. Theoretical calculations based on FINPLA2 predict the transverse distribution of moments under uniform loads very accurately and under point loads within the same ranges as described in 6.

8. Since actual girder design moments are based on several wheel loads acting on the bridge width, total differences between theory and the actual values should be smaller than that under single point loads, and thus for design purposes the theory should be adequate for predicting design moments even at or after overload stress levels.

7. REVIEW OF STRUCTURAL RESPONSE DURING LOAD HISTORY OF BRIDGE MODEL

7.1 Strain History

With the intent of monitoring the concrete and steel strains during the construction phase up to the time the dead load was applied, strains in a number of concrete strain meters and weldable strain gages were recorded following the pouring of the bottom and top slabs. However, two weeks prior to the application of the dead load the gages had to be disconnected in order to be connected to another strain recording system. Hence, from that moment on, strain readings could no longer be related to the original zero-strain base. Results are therefore only presented for the above initial period.

It was decided to monitor concrete strain meters in only one girder, namely girder 3. Hence, two strain meters located in Sections B and C near the center support and located in the bottom slab directly under the girder 3 web were monitored almost daily after the concrete was placed. Two additional concrete strain meters were placed in the top slab, above girder 3, at the Sections A and D, located 3.5 ft from the mid-span sections. These meters were monitored after the top slab concrete had been placed.

The monitored strain data for these four meters are presented in Fig. 61. Results indicate an excellent agreement between data recorded in Sections B and C, and A and D. Initially high tensile strains developed in both support Sections B and C. However, after about 10 days these strain values reduced rapidly from about 200-250 micro-inch/inch to about 50 - 100 micro-inch/inch. During the next 40-day period the strain values reduced gradually and reached a zero strain level after about 60 days following the pouring of the bottom slab. Then a slow compressive strain increase was observed with maximum values of 100 micro in/in. Observing the recorded strains of the top slab gages located at Sections A and D (Fig. 61 c and d) one notes considerably smaller tensile strain values during the initial period following placement of the top slab concrete. It is interesting to note that all gages recorded a near zero strain value at the same instance and had reached a virtually stable strain level of about 80 micro inch/inch at the end of the monitoring period.

The recorded weldable strain gage data are presented in Fig. 62. Each graph shows the average strains for two diametrically opposite gages welded to a number of No. 4 bars. The bars selected in the bottom slab were located under the girder webs of girders 1 and 5 at Sections A and D respectively. The third graph (Fig. 62 c) reflects the No. 4 bar strain in the top slab above the web of girder 1 at Section B. The results for Sections A and D seem to indicate a fairly symmetrical behavior of the bottom slabs following placement of the concrete. Regarding both Figs. 61 and 62 one may conclude that the bottom slab seemed to have been subjected to initial tensile strains, possibly caused by differential shrinkage between the girder webs and the bottom slab.

7.2 Deflections Under Sustained Dead Load

While the pre-dead load behavior of the bridge model was monitored by means of strain data, the deterioration of the model under the sustained dead-load over the entire range from initial application of dead load to final ultimate failure was monitored by observing the span displacements versus time.

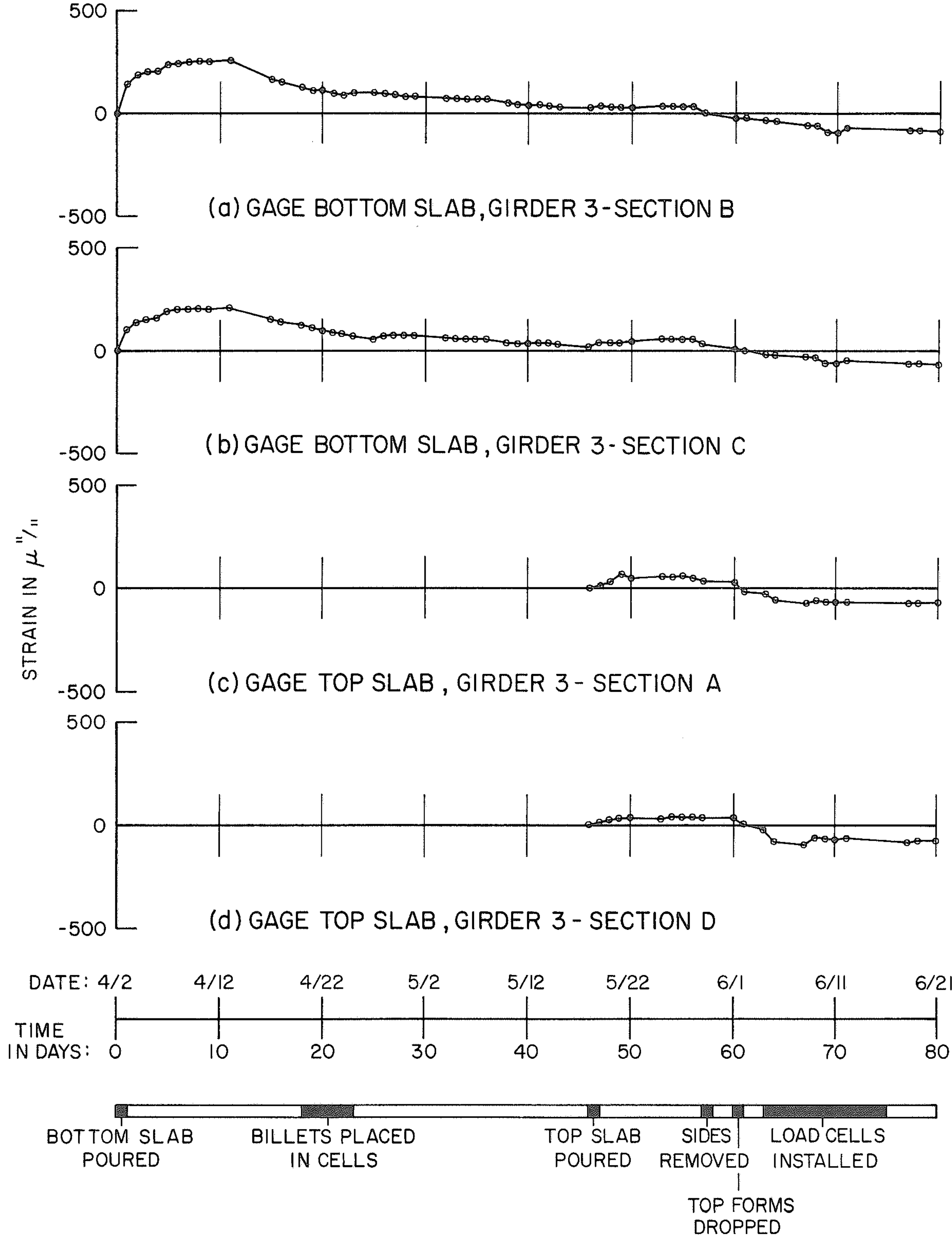

FIG. 61 STRAIN HISTORY FOR CONCRETE STRAIN METERS

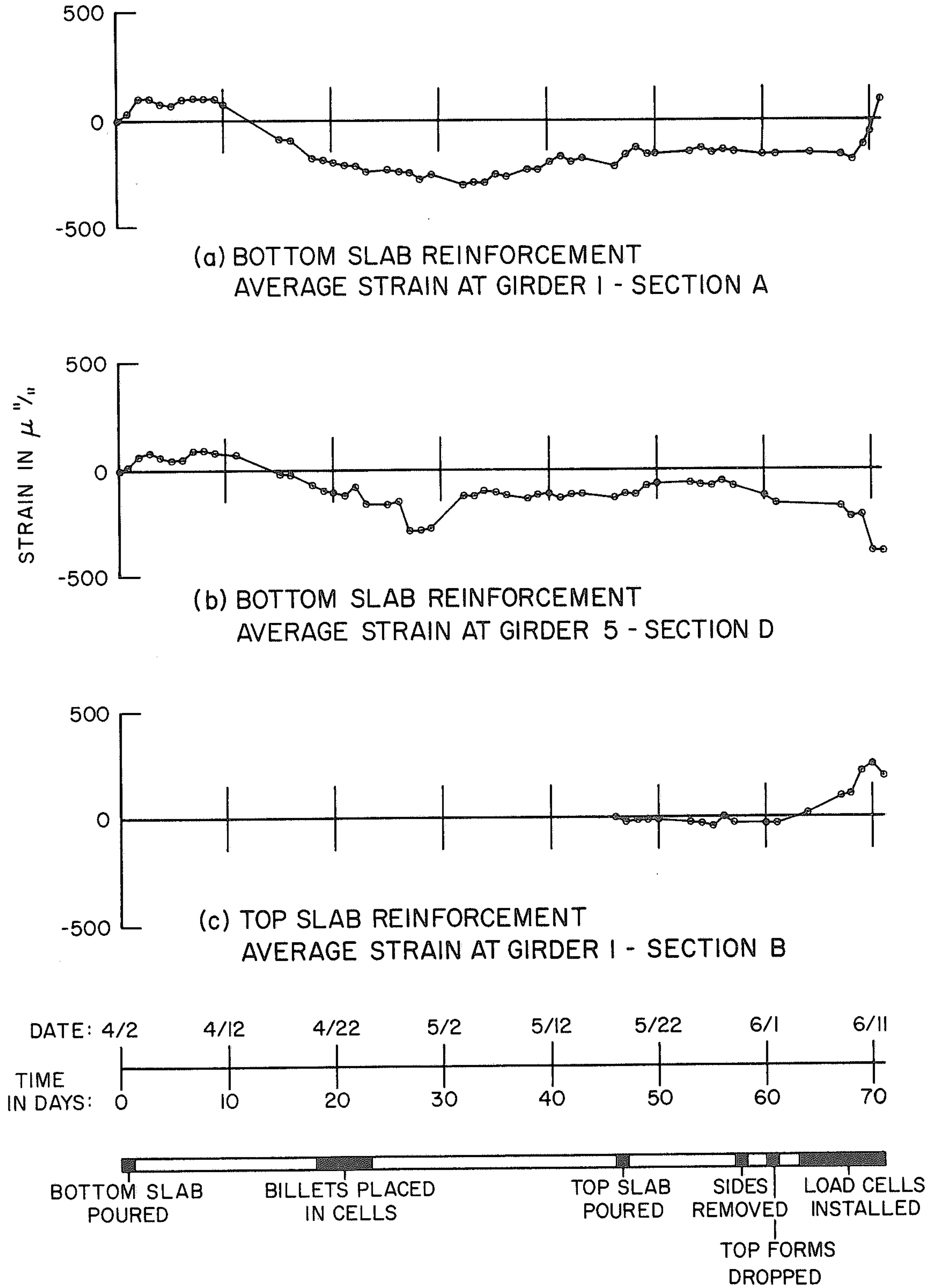

FIG. 62 STRAIN HISTORY FOR WELDABLE STRAIN GAGES

The displacement data, as derived from mirror-scale readings, and presented in Fig. 63 a and b, were recorded at the North and South face of both Spans I and II, at Sections A and D respectively. The readings reflect time dependent effects and residual deflections after conditioning and cyclic loads. The data for Span I are shown in Fig. 63 a and those for Span II in Fig. 63 b.

A general observation of both graphs clearly indicates the almost identical results for both spans. In the first 27 days, during which the bridge was readied for live load applications, creep caused a significant increase in the displacement. During the first 3 weeks the deflections increased about 50%. Following that period the deflection remained virtually constant until the conditioning live load creating a 24 ksi total stress had been applied. The application of the live load caused cracking of the structure which, in turn resulted in permanent displacements after removal of the live loads. The same phenomenon was observed each time after a conditioning live load had been applied to raise the total dead and live load stresses to subsequent values of 30 ksi, 40 ksi, 50 ksi and 60 ksi. The gradual deterioration which can be observed from the data recorded during the 5 week period following the application of the 30 ksi conditioning load must be attributed primarily to progressive cracking as a result of the many live load applications. It is further interesting to note that the permanent displacements following the 60 ksi conditioning load were significantly larger than those observed following the application of conditioning loads creating lower stress levels. This phenomenon is undoubtedly due to a partial yielding of the reinforcement. The mid-span displacements prior to the final loading to failure reflected a

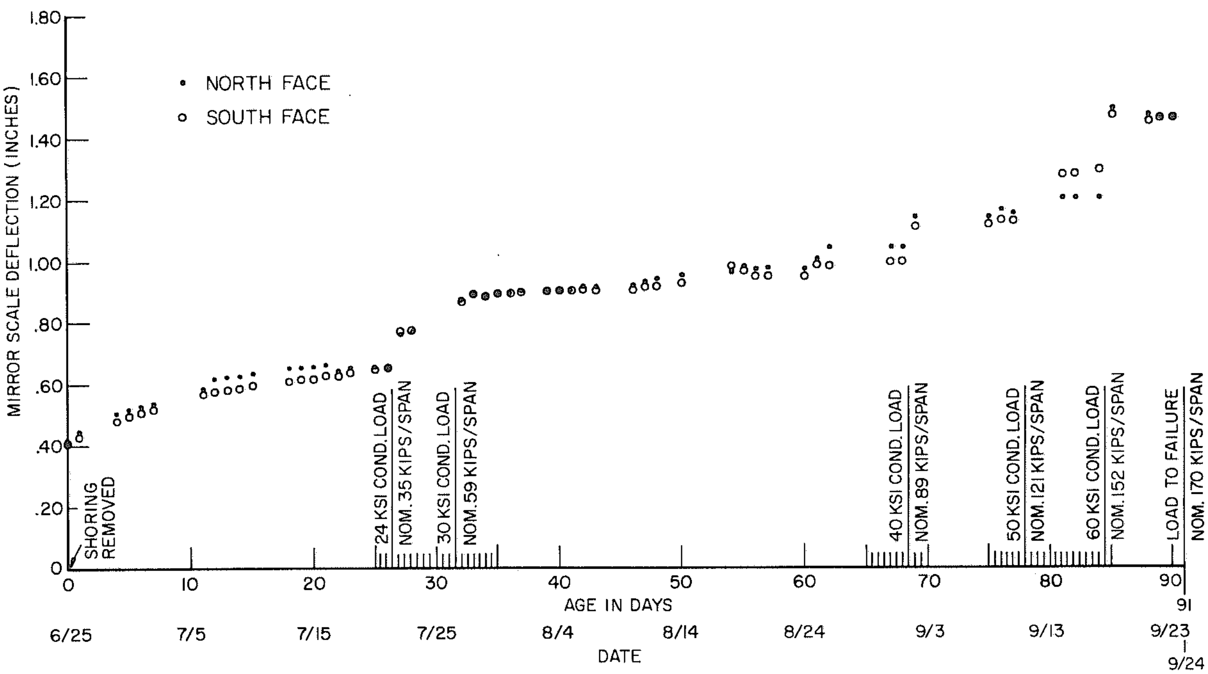

(a) SPAN I : DEFLECTION AT SECTION A, IN INCHES

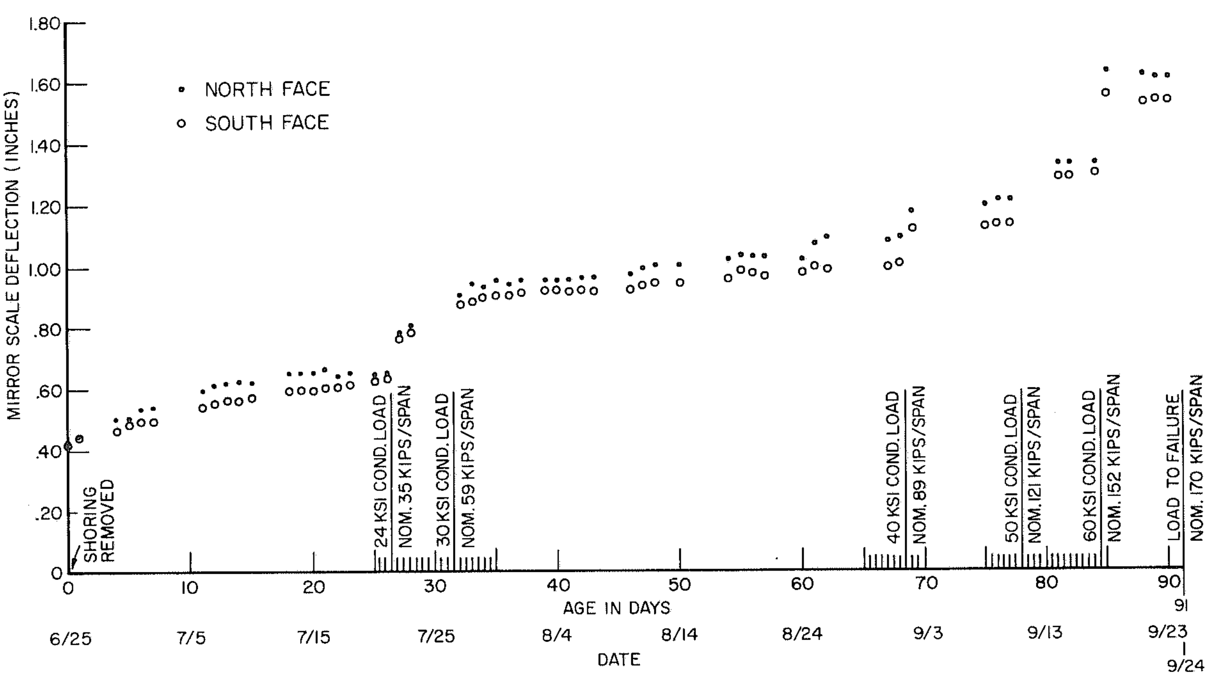

(b) SPAN II : DEFLECTION AT SECTION D, IN INCHES

FIG. 63 DEFLECTION HISTORY UNDER DEAD LOAD

permanent displacement of about 1.50 inches, or almost 4 times the initial deflections recorded immediately after removal of the shoring. With reference to the dead load deflections after the primary creep period of three weeks, the final permanent deflections show a magnification of about 2.5.

7.3 Crack Development Under Conditioning Loads

After removal of the shoring and following each application of the conditioning loads the cracks in the girders 1 and 5 (north and south side respectively) and in the top and bottom slabs were recorded and are presented in Figs. 64, 65, 66 and 67.

The crack patterns as presented for dead load, and the 24, 30, 40, 50 and 60 ksi conditioning loads are basically self explanatory. However, a couple of observations are particularly pertinent in evaluating the bridge model under design stress conditions and successively increasing overloads. Firstly, it is satisfying to note that under combined dead and design live loads, the crack pattern consisted virtually exclusively of hair-line cracks with width of less than 0.01 in.

The crack pattern in the exterior girders as presented in Figs. 64 and 65 show progressively the development of bending moment cracks from the early stages of loading, followed by the development of typical shear cracks after applications of the 30 ksi conditioning loads

An observation of the top slab crack pattern after the 24 ksi load application, as presented in Fig. 66, shows a number of cracks in the center support region. Although, as shown in Fig. 67, the bottom slab crack pattern after the 24 ksi conditioning load is rather

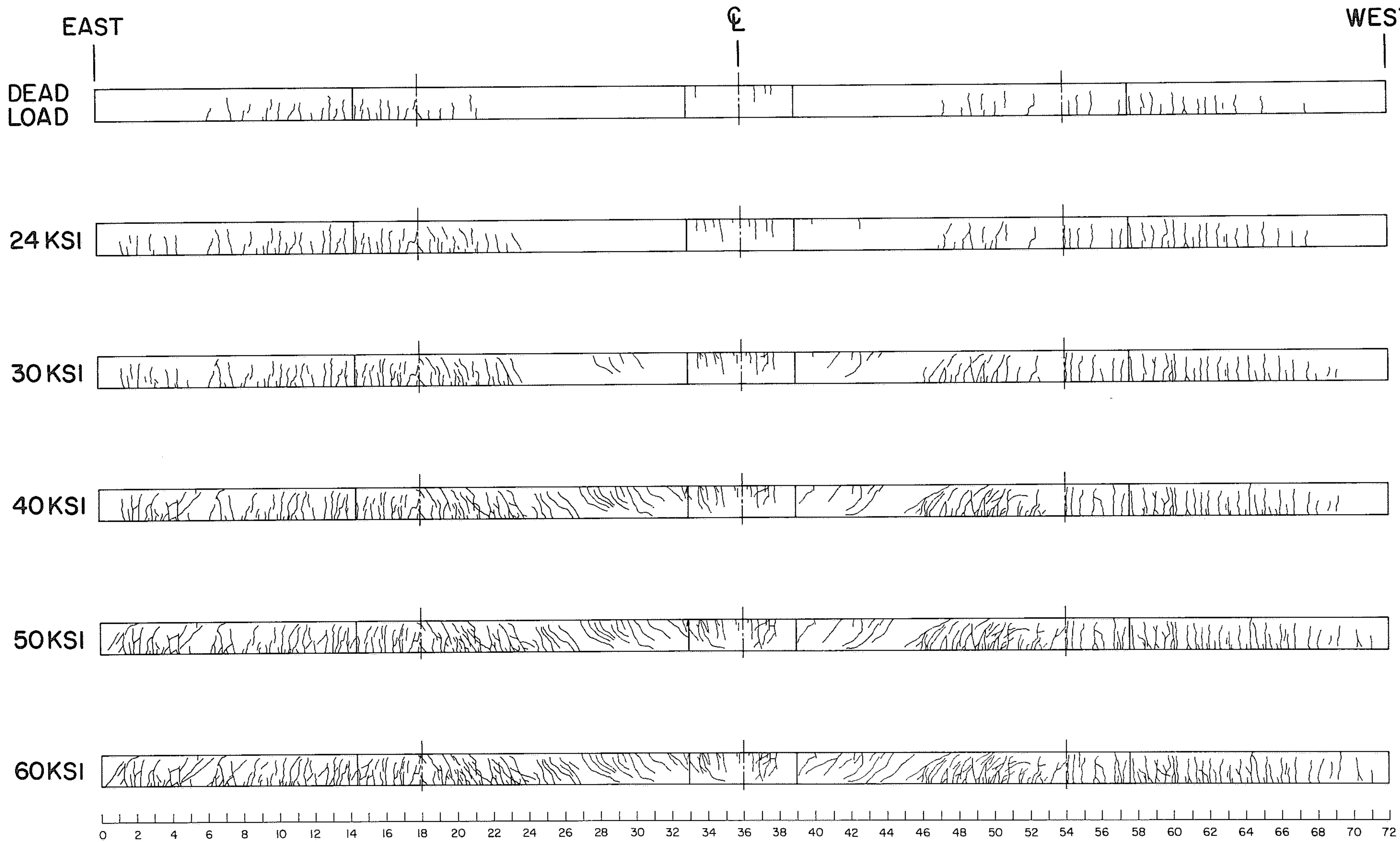

FIG. 64 CRACK HISTORY FOR GIRDER 1 (NORTH FACE)

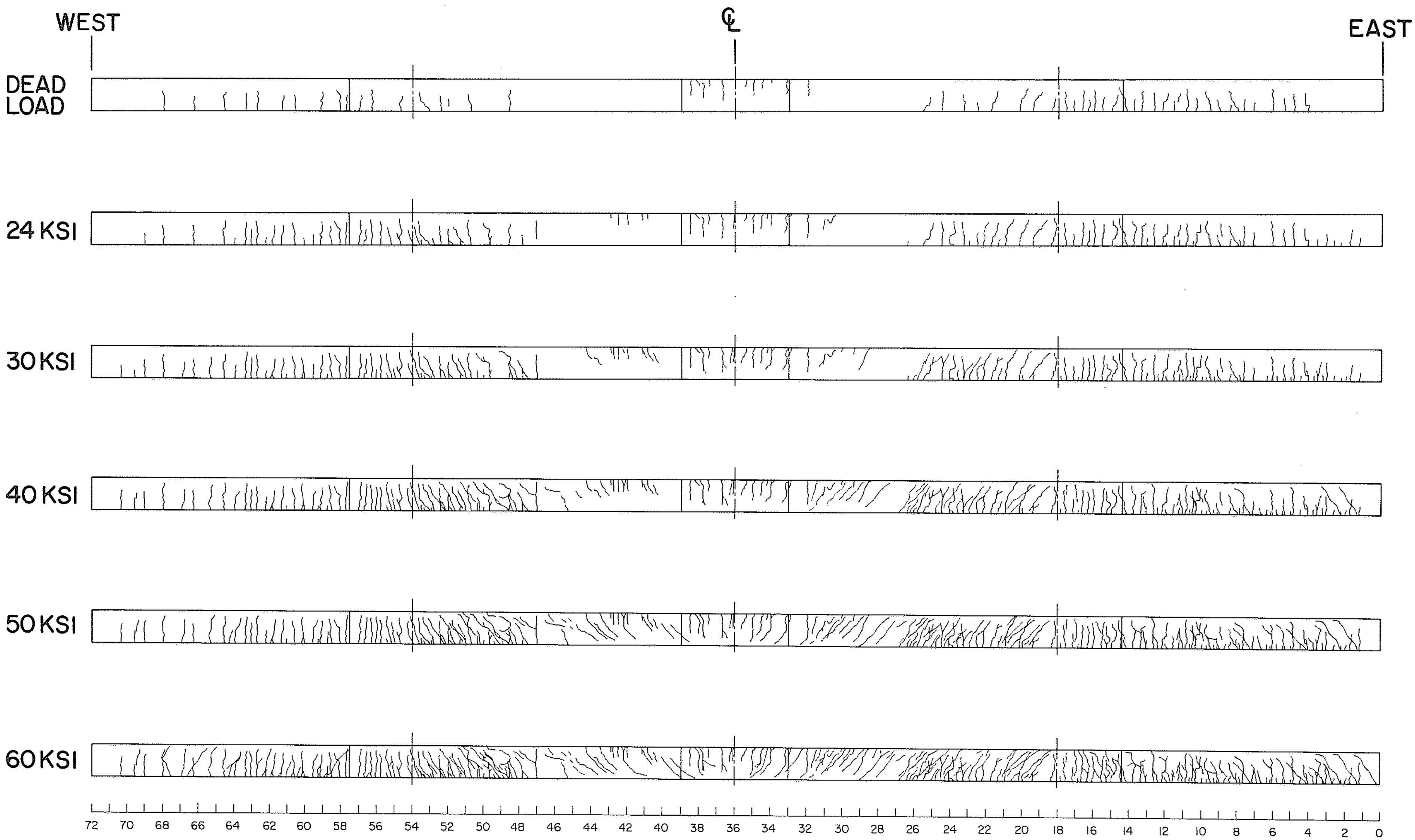

FIG. 65 CRACK HISTORY FOR GIRDER 5 (SOUTH FACE)

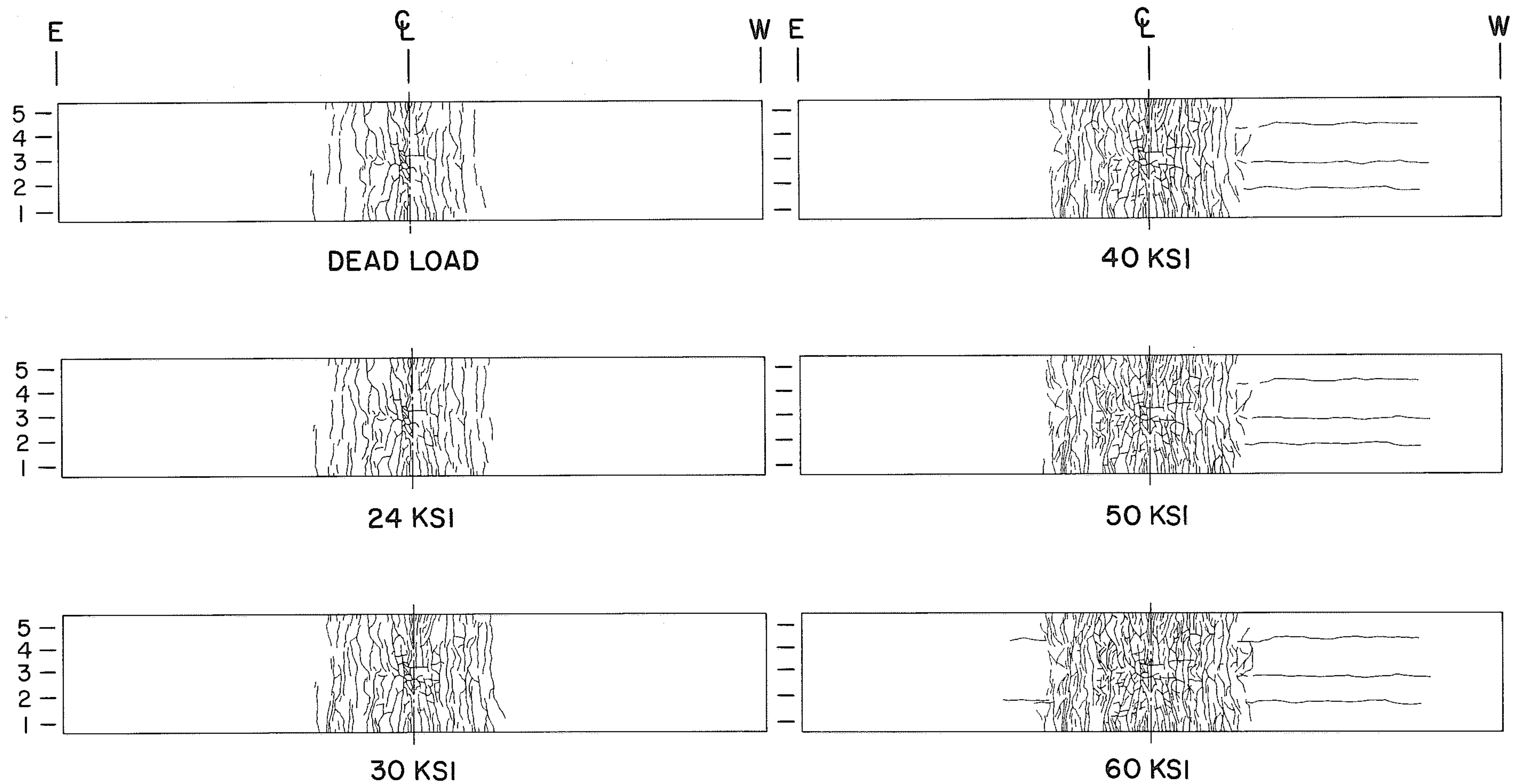

FIG. 66 CRACK HISTORY FOR TOP SLAB

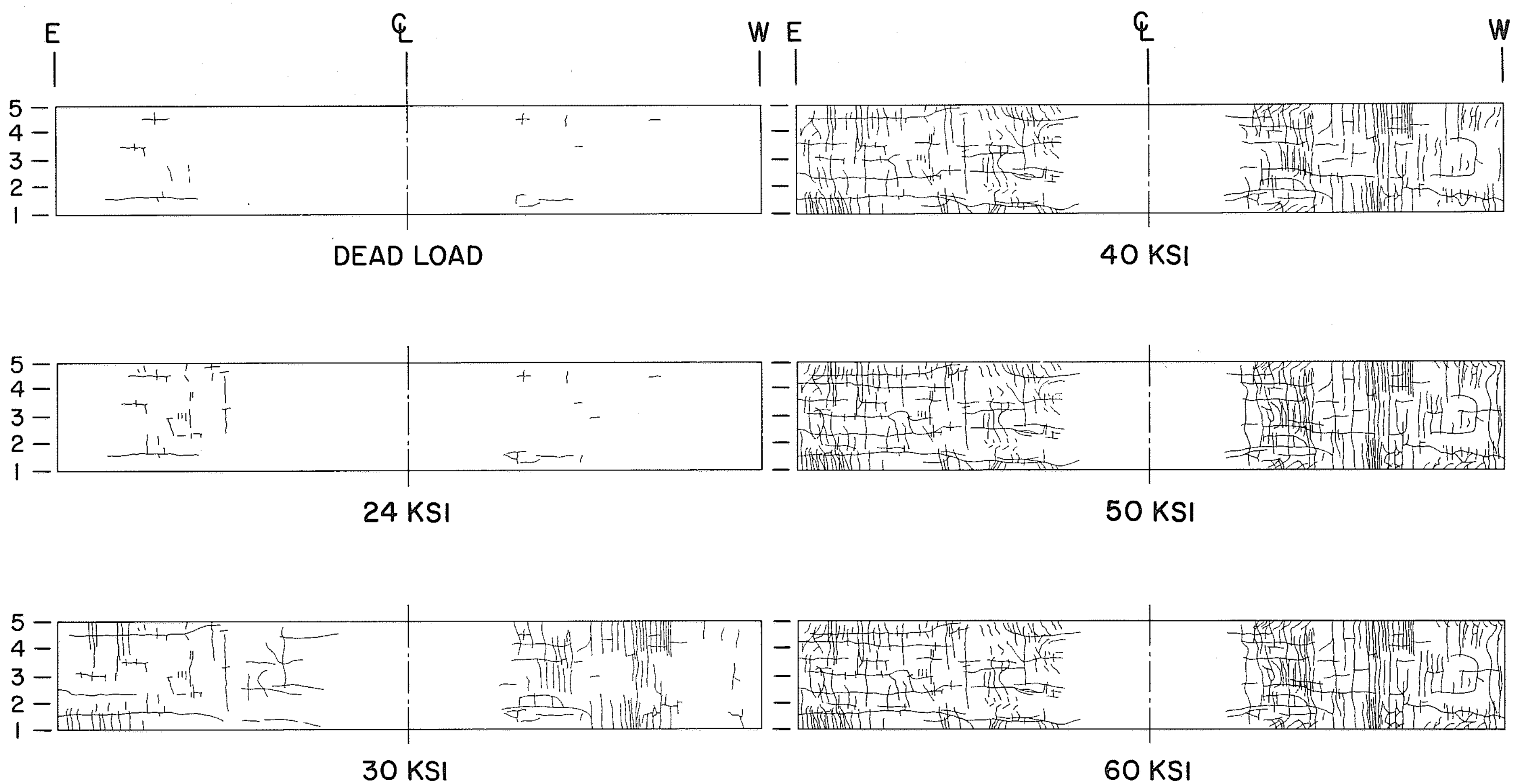

FIG. 67 CRACK HISTORY FOR BOTTOM SLAB

limited, one can be certain that a substantial number of transverse cracks must have been present in the mid span regions. However, difficulties in observation resulted in this limited record. The necessary presence of cracks in those bottom slab regions is further supported by the observed crack patterns in the exterior girders as presented in Figs. 64 and 65. A critical observation of the limited bottom slab crack pattern seems to indicate a more extensive longitudinal crack development in the undiaphragmed span as compared to the diaphragmed span. The latter development became more evident under increasing conditioning loads. Significant also at the higher load level is the development of diagonal shear cracks in the bottom slabs of the outer cells. This pattern, as shown in Fig. 67 reflects the increasing torsional action and load transfer to the other girders particularly in the undiaphragmed span.

8. LOADING TO FAILURE OF BOX GIRDER MODEL

8.1 General Remarks

To determine the bridge response under increasing loads until failure would occur, concentrated loads were applied simultaneously in both spans. Through the loading at the midspan Sections X and Y the loading arrangement was designed to develop failure through the formation of a collapse mechanism with plastic hinges at Sections X, B', C' and Y. Sections B' and C' coincided with the face of the center bent diaphram and were located approximately 1 foot from the center support. The corresponding failure load was calculated to be 170 kips in each span.

In order to provide a large measure of deformation in the bridge model, it was decided to use at each midspan two 200 kips loading rams, each with a maximum stroke of 10 inches. The rams were centered on 10 inch by 12 inch by 1 inch thick steel plates at girders 2 and 4 respectively, Fig. 68. Neoprene pads of one inch thickness were provided under the steel plates for better distribution of load. All four rams were calibrated earlier at various loads and stroke lengths and a common calibration in terms of hydraulic pump pressure in psi versus ram load in kips was obtained.

During this phase of the loading, the potentiometers mounted on stands at various transverse sections along the span of the bridge model were removed to protect them from damage. Deflections were read at the two midspan sections by means of dial gages at girder lines 1 and 5 and at other sections on scales by means of wires stretched tautly along the length of the bridge model at the level of the top slab

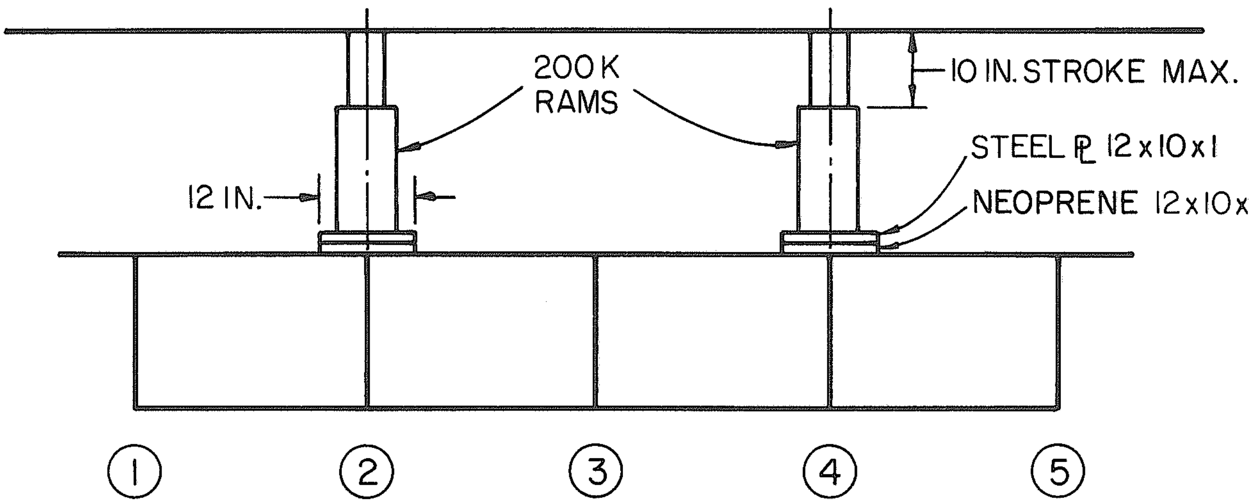

FIG. 68 LOAD ARRANGEMENT AT MIDSPANS OF SPANS I AND II FOR FINAL LOADING TO FAILURE

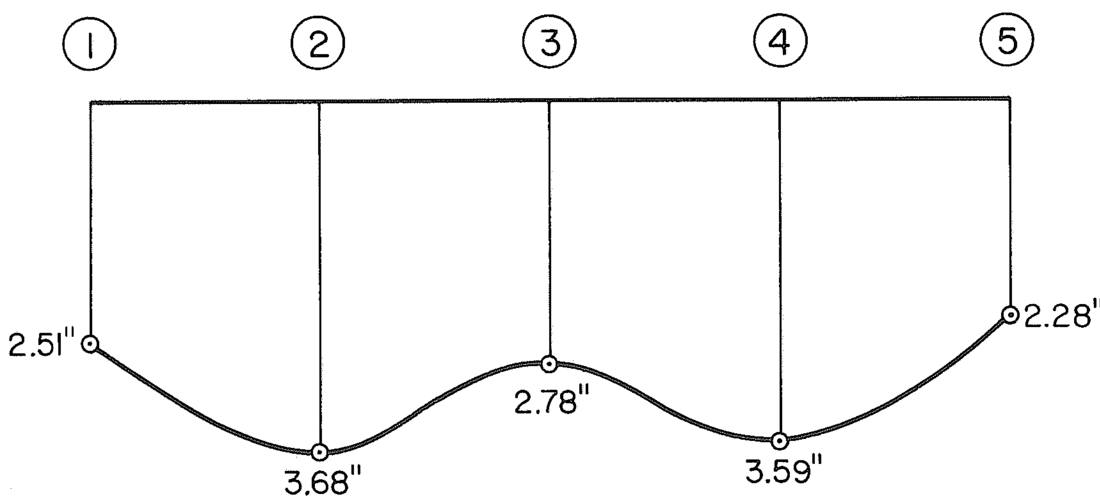

FIG. 69 GIRDER DEFLECTIONS (INCHES) AT MIDSPAN OF SPAN II AT FAILURE LOAD (170 KIPS)

mid-depth on both north and south faces, as earlier described in Vol. I.

8.2 Results Under Loading

After taking zero readings, the two rams in each span were successively loaded to provide total nominal stresses in the tensile steel at midspan sections X and Y of 24, 30, 40, 50 and 60 ksi. In each case readings were taken by means of the scanning unit. At the stress level of 60 ksi each span carried a live load of 150 kips. The next step augmented the load in each span to 160 kips causing an increase in cracking. The subsequent step called for load increased in each span to a total of 180 kips per span. However, as the load value in each span reached 170 kips, yielding of the bottom slab steel started in the undiaphragmed span at Section Y. It was observed that the yield pattern took the form of a local slab failure on either side of girder 2 at Section Y. The girder appeared to push downward causing a major crack in the bottom slab on the side near girder 1 that extended longitudinally about 5 feet in the direction towards that center bent. The transverse deflection profile of the bridge model at Section Y after this initial failure can be seen in Fig. 69. Scanner readings were taken after the load had stabilized at a value of about 160 kips per span.

Further loading was continued but the load could not be increased beyond 160 kips per span because girder 2 at Section Y continued moving downward causing further local failures in the bottom and top slabs, until finally with a clearly audible sound the ram bearing plate punched through the top slab. The load dropped to 125 kips in each span and readings were taken. A close up of the punching failure over girder 2 is shown in Fig. 70. No damage of this kind was

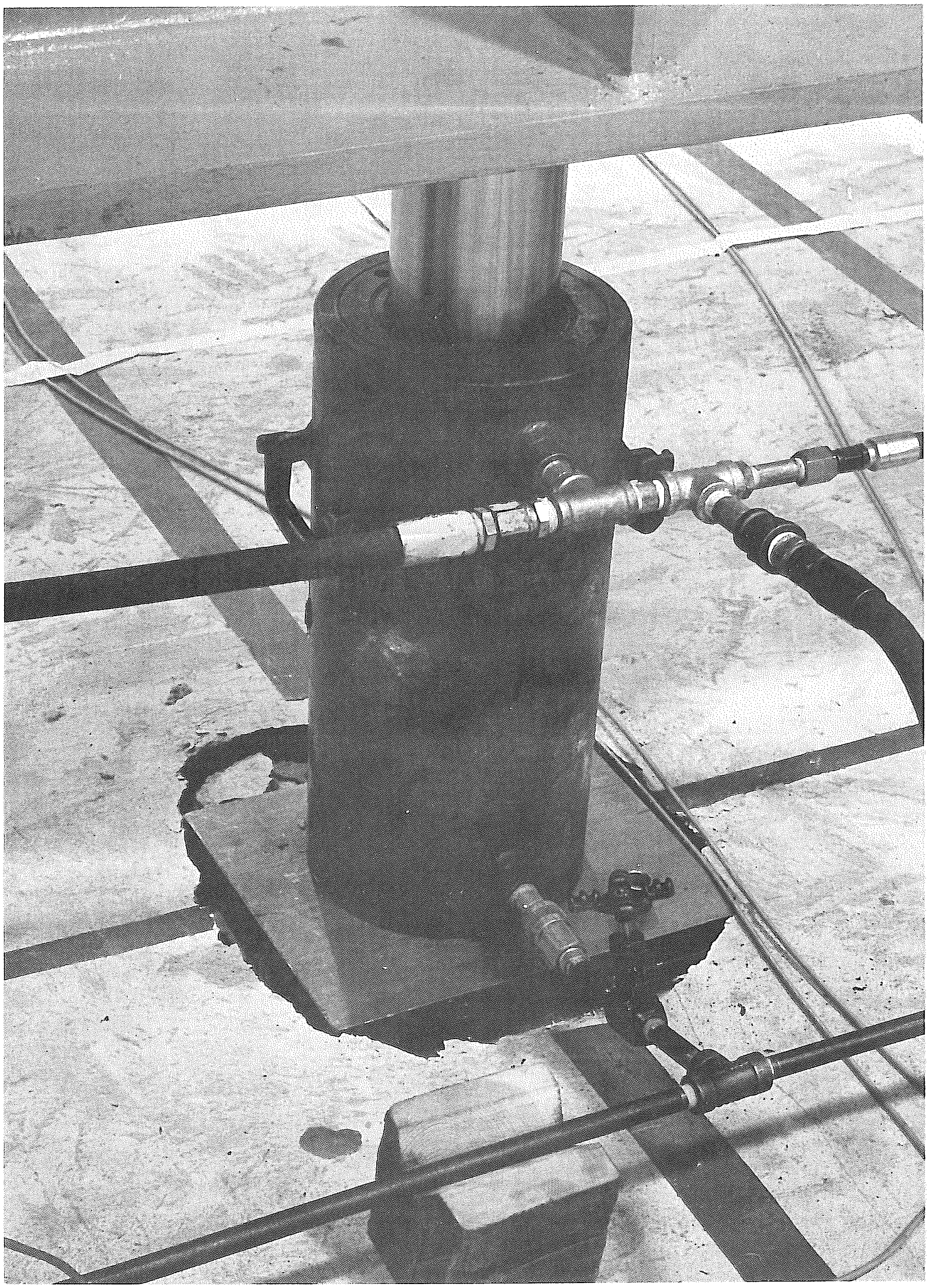

FIG. 70 PUNCHING FAILURE IN TOP SLAB AT 2Y

observed in the diaphragmed span where the behavior of the gages continued to be fairly linear. Deflections along the north and south faces of the bridge model for all load steps up to and including the punching failure are shown in Figs. 71 and 72. A general view of the bridge model,after initial failure in the undiaphragmed span had occurred,is shown in Fig. 73.

In view of the local failure at Section Y it was decided to freeze the deflection there by the insertion at girders 1, 3 and 5 of solid timber struts of 7 inch by 7 inch cross-section and heights sufficient to maintain the existing deflection at the load of 125 kips at Section Y. The rams were than unloaded and a set of zero readings taken. Subsequently, only the diaphragmed span at Section X was loaded, with readings taken at loads of 80, 100, 120, 140, 160 and 170 kips.

In the following step, the load at Section X was to be raised to 180 kips. However, as soon as the load was increased from 170 kips a seemingly uniform yielding occurred at Section X with the load gradually dropping to 160 kips. At this point, both north and south faces of the bridge model showed longitudinal shear cracks at the junction of the top slab with the girders. The maximum crack width in the tensile zone at Section X was measured as 0.125 inches. The yielding continued, with increasing deflection and widening cracks at Section X. At a midspan deflection of 3.8 inches the crack width had grown to about 0.25 inches.

No readings were taken during this period because of continuing yielding. The load further dropped gradually to 132 kips by which time the deflection at Section X was 6.47 inches and the maximum crack width in the tensile zone at Section X was 0.3 inches. When the midspan deflection was 7.40 inches and the load on the span was 108 kips concrete

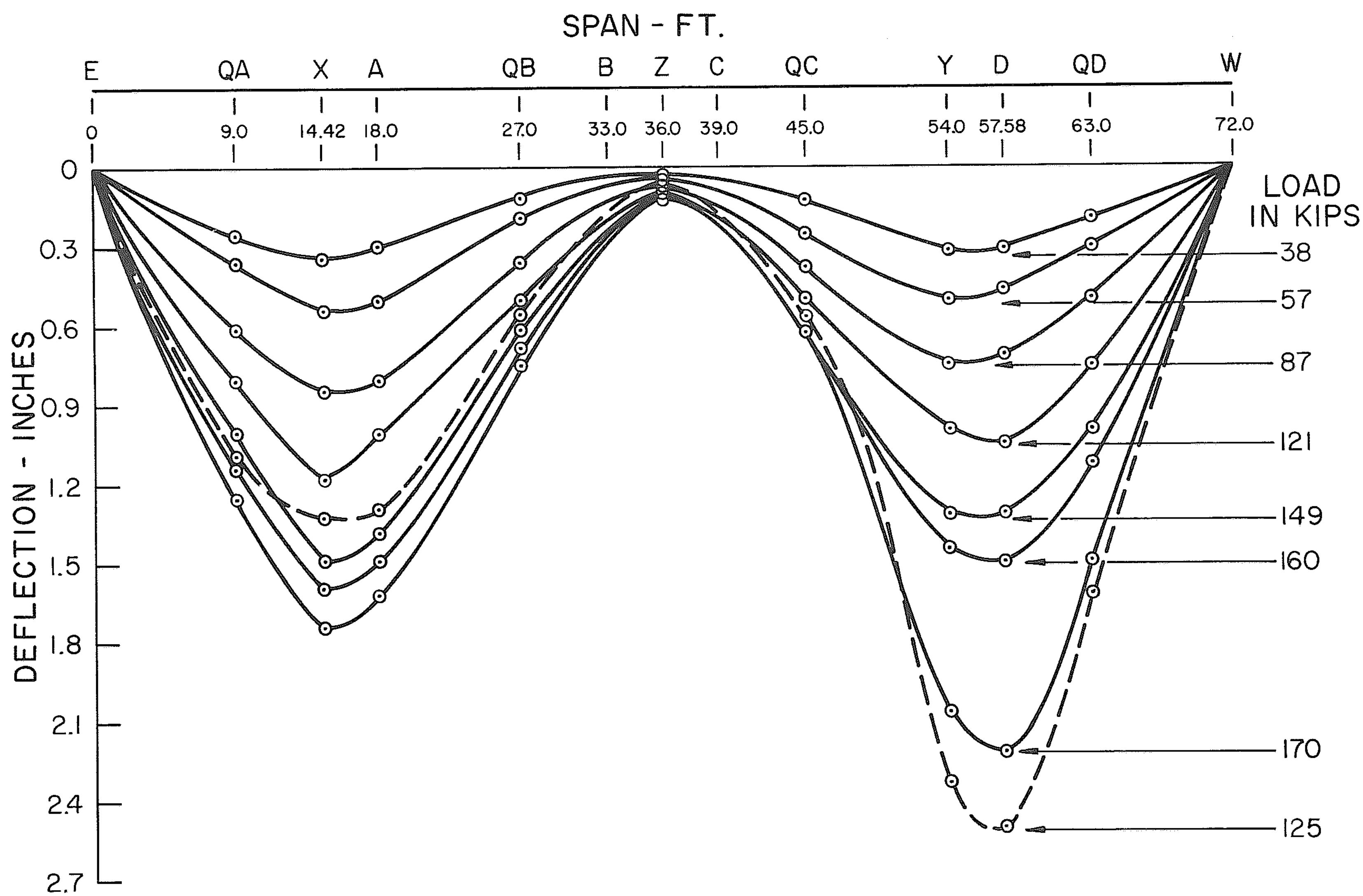

FIG. 71 DEFLECTION (INCHES) CURVES UNDER INCREASING LOADS FOR GIRDER 1

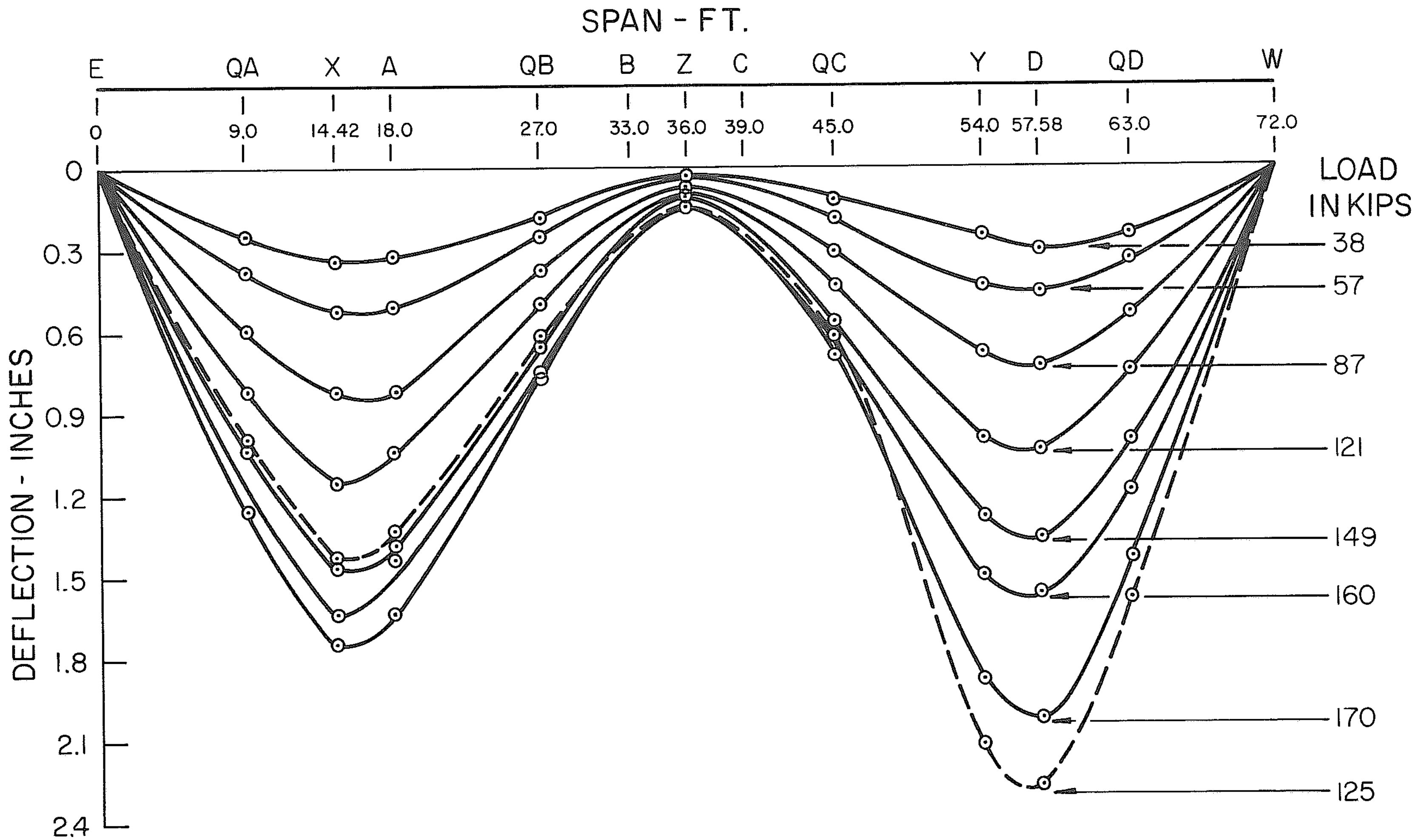

FIG. 72 DEFLECTION (INCHES) CURVES UNDER INCREASING LOADS FOR GIRDER 5

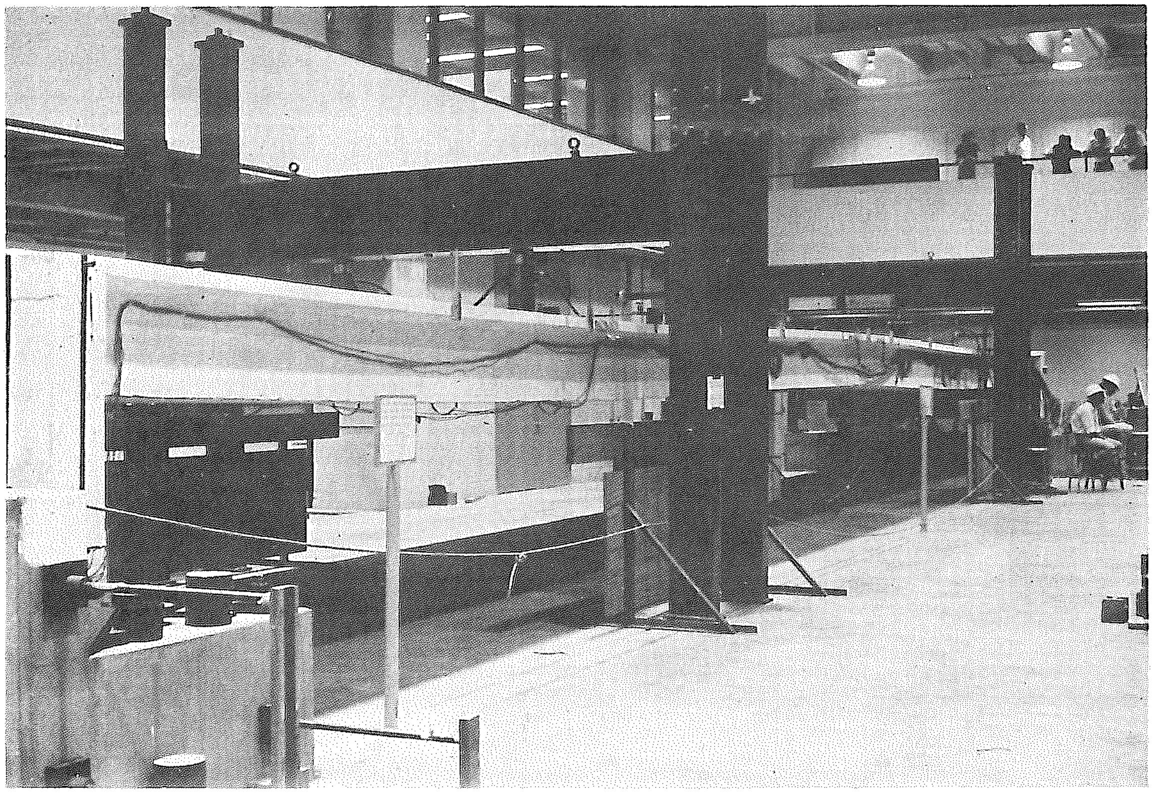

FIG. 73 BRIDGE MODEL AFTER FAILURE IN UNDIAPHRAGMED SPAN (SPAN II)

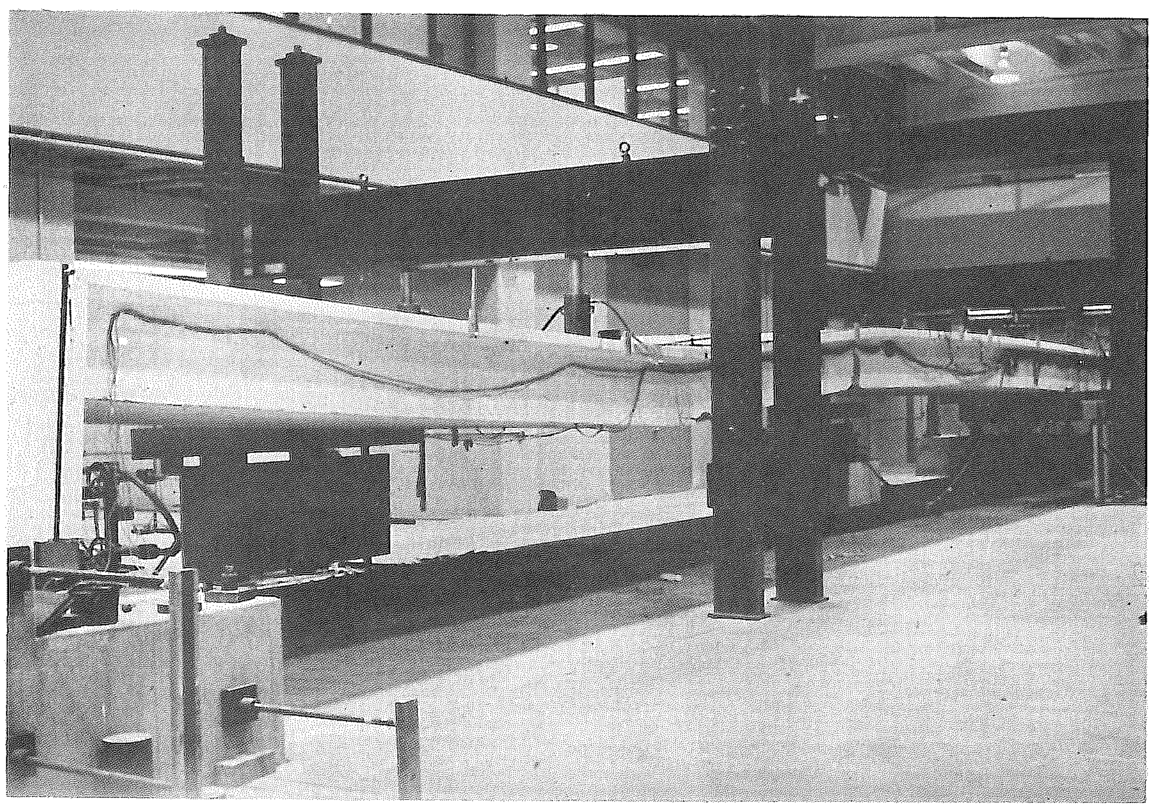

FIG. 74 BRIDGE MODEL AFTER FINAL FAILURE IN DIAPHRAGMED SPAN (SPAN I)

began spalling at about 8 feet from the center support of the bridge, i.e. near Section QB. The continuing load-midspan deflection relationship until the end of the 10 inch travel of the loading rams can be observed in Fig. 75. An overall view of the bridge model after a midspan deflection of 10 inches in the diaphragmed span had been reached is shown in Fig. 75. By this stage, the plastic collapse mechanism was fully developed, with the second hinge forming in Span I at a distance of 8 feet from the bridge center support on the north face of the bridge model (girder 1)and following a skew path to emerge at a distance of 10 feet from the center support on the south face (girder 5).

After the rams had reached the maximum stroke of 10 inches, the cylinders were retracted and steel circular disks with a total height of about 10 inches were placed on each of the cylinder rods. The diaphragmed span was loaded again. After an initial load of 80 kips the load gradually reduced under increasing center displacements (Span I). At a load of 50 kips in each span the center-span displacement was recorded as 15 inches. The load corresponding to a maximum displacement of 20 inches was 39 kips. At that instance the test was terminated. Fig. 76 shows the final deflected shape of girder 5. Photographs showing girders 1 and 5 in Span I between the first center span hinge at Section X and the second hinge which formed at a distance of 8 to 10 feet from the center support, are presented in Figs. 77 and 78 respectively. Details of the overall failure in both exterior girders 1 and 5 at the midspan hinge Section X are shown in Figs. 79 and 80, respectively. The crushing of the concrete and the buckling of the reinforcing bars in the compression zone of girder 1 at the point of the second hinge can be observed in Fig. 81.

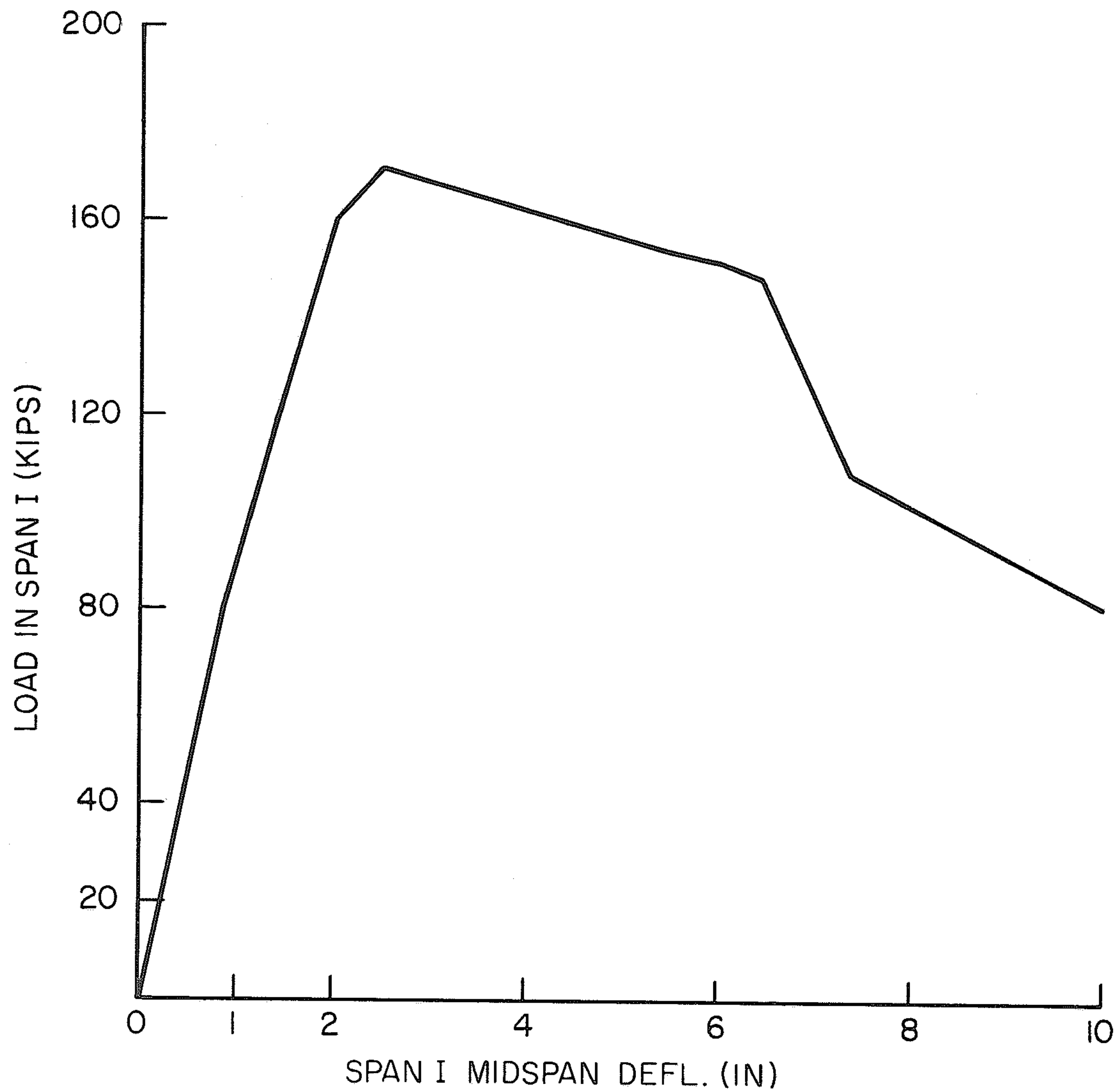

FIG. 75 LOAD-DEFLECTION RELATION FOR SPAN I

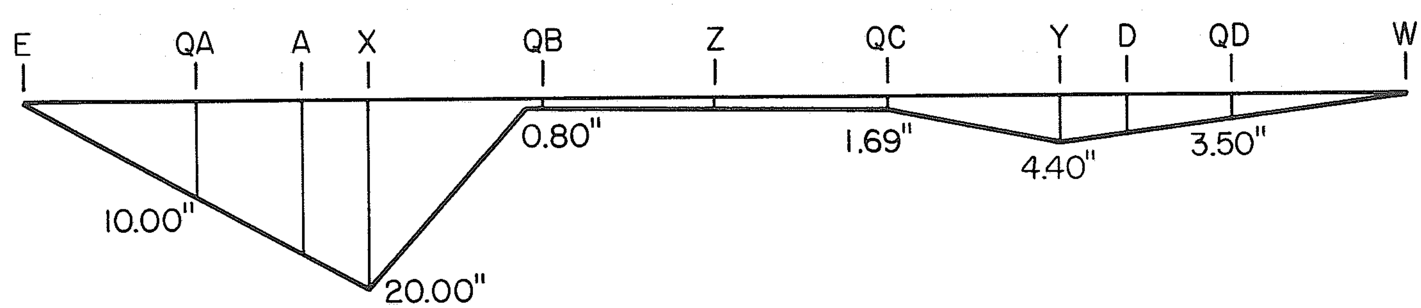

FIG. 76 FINAL DEFLECTIONS (INCHES) ALONG GIRDER 5 AFTER COMPLETION OF TEST

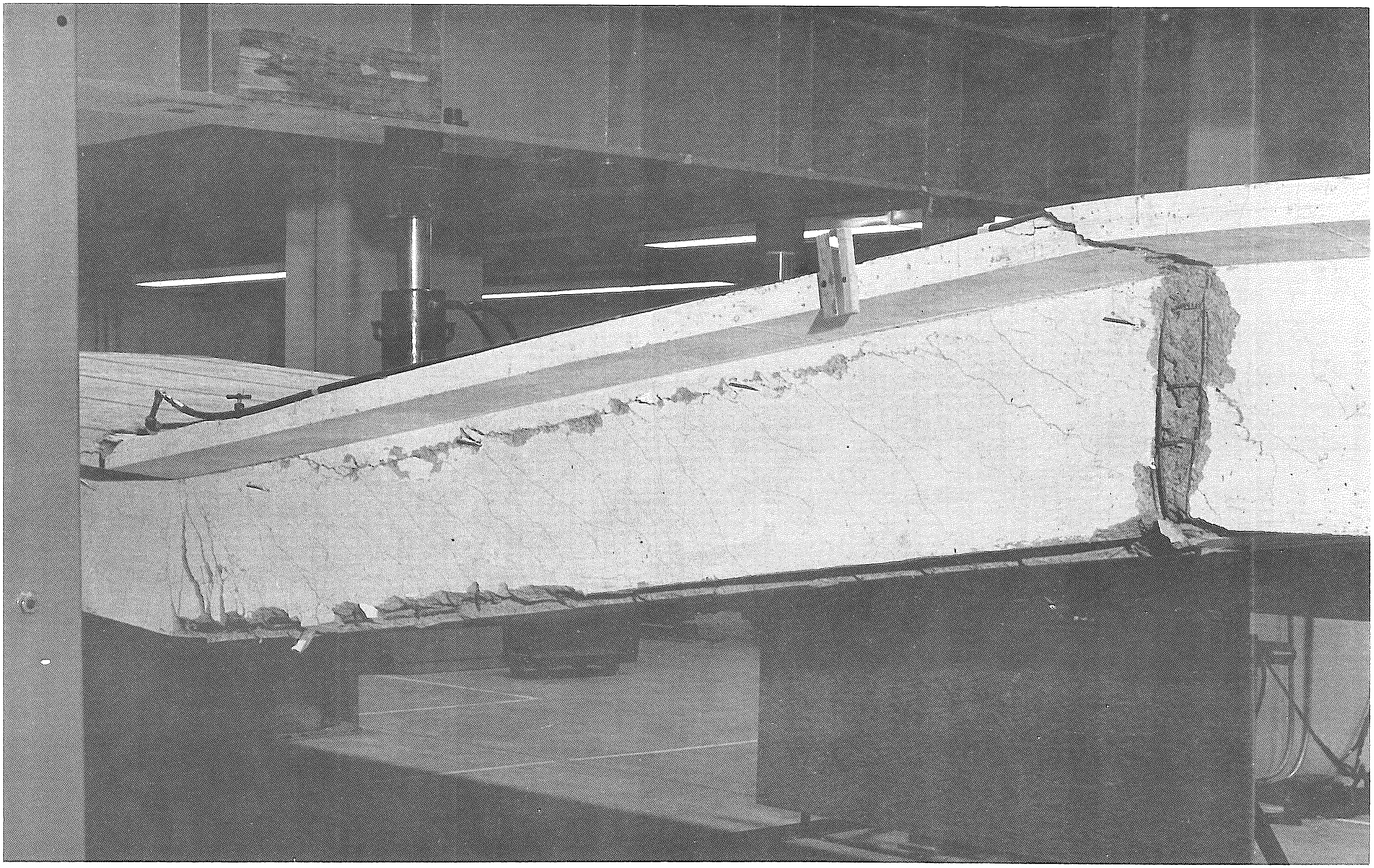

FIG. 77 FINAL DEFLECTED SHAPE AND CRACK PATTERN FOR GIRDER 1 IN SPAN I

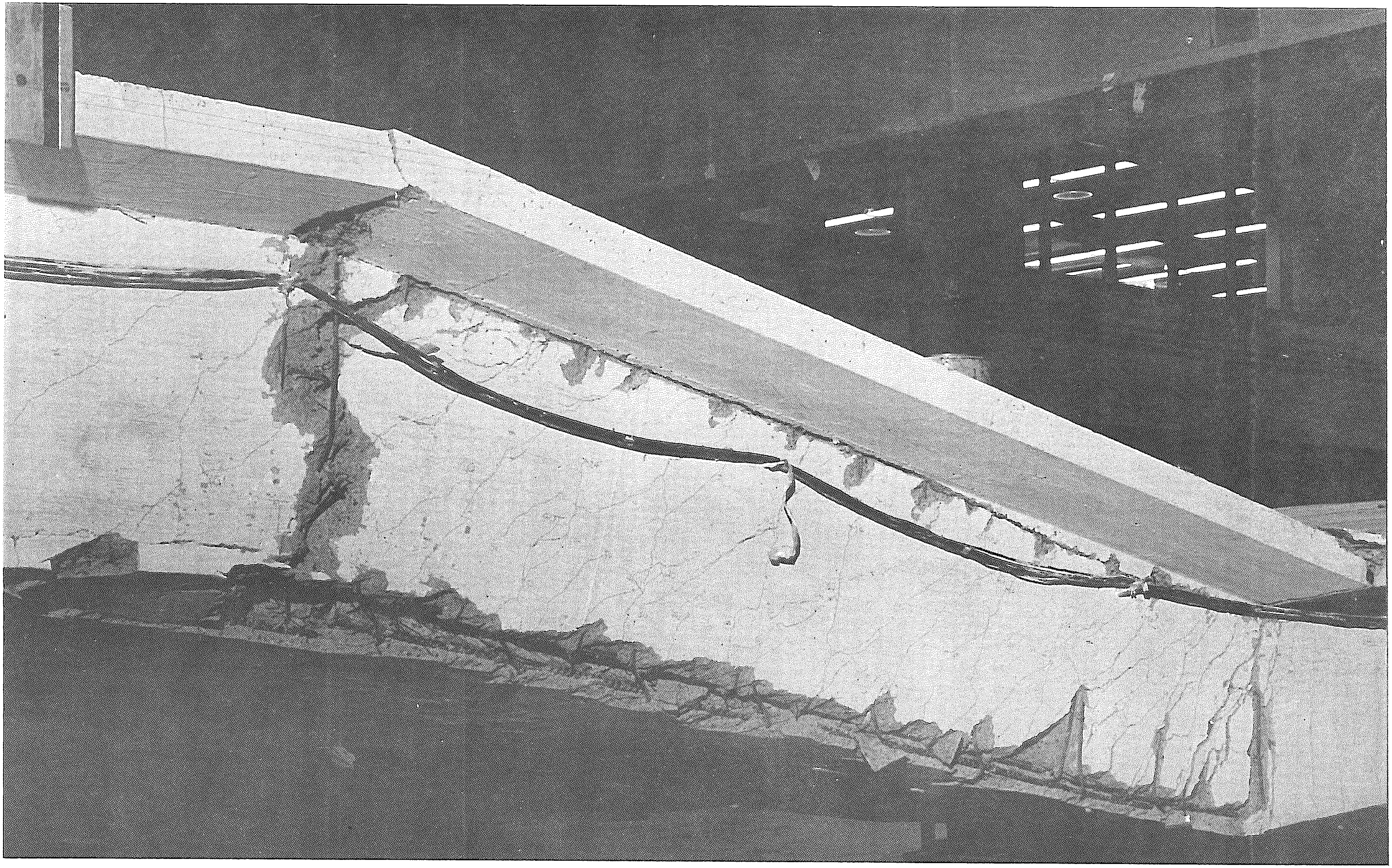

FIG. 78 FINAL DEFLECTED SHAPE AND CRACK PATTERN FOR GIRDER 5 IN SPAN I

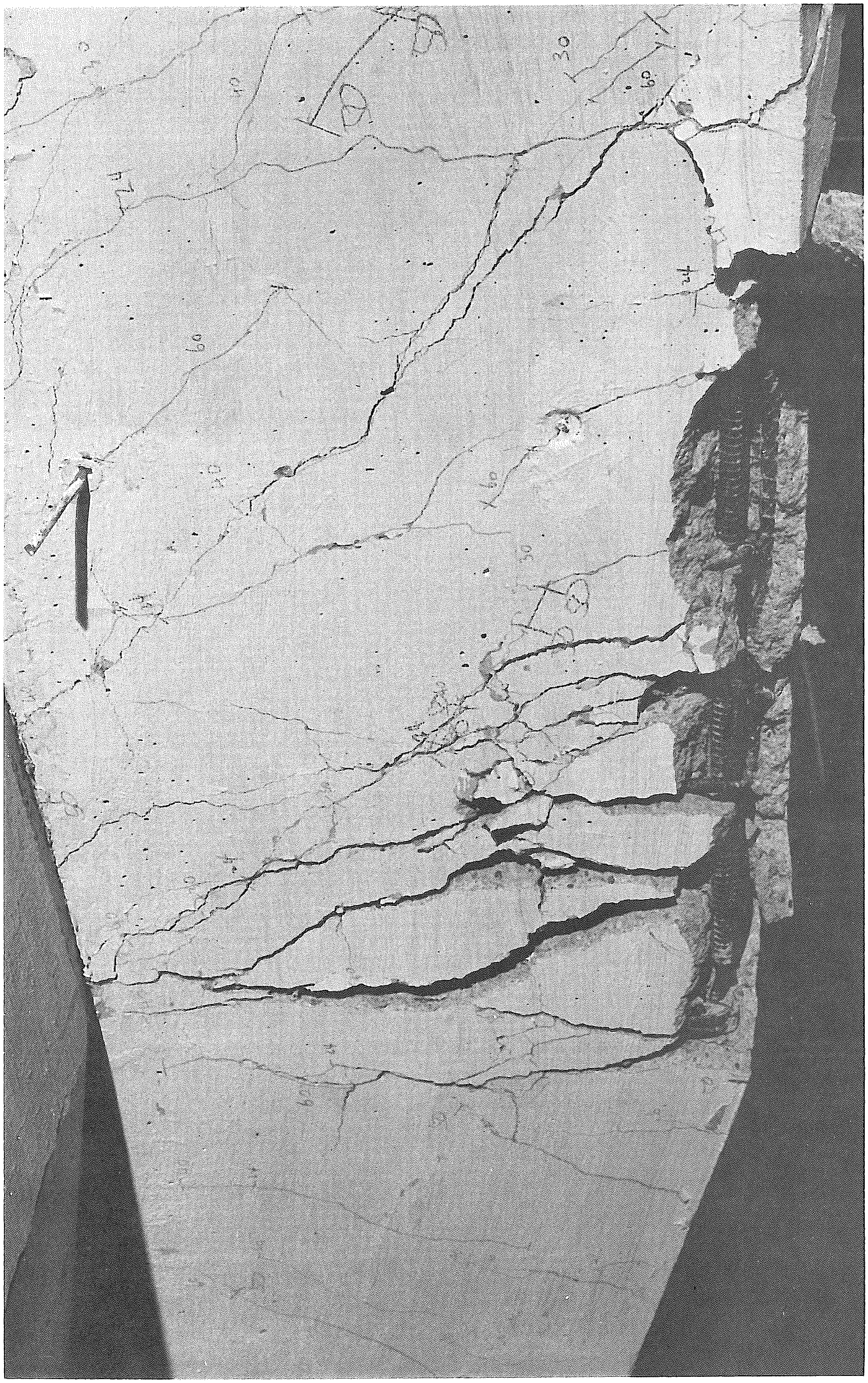

FIG. 79 FAILURE DETAILS AT 1X

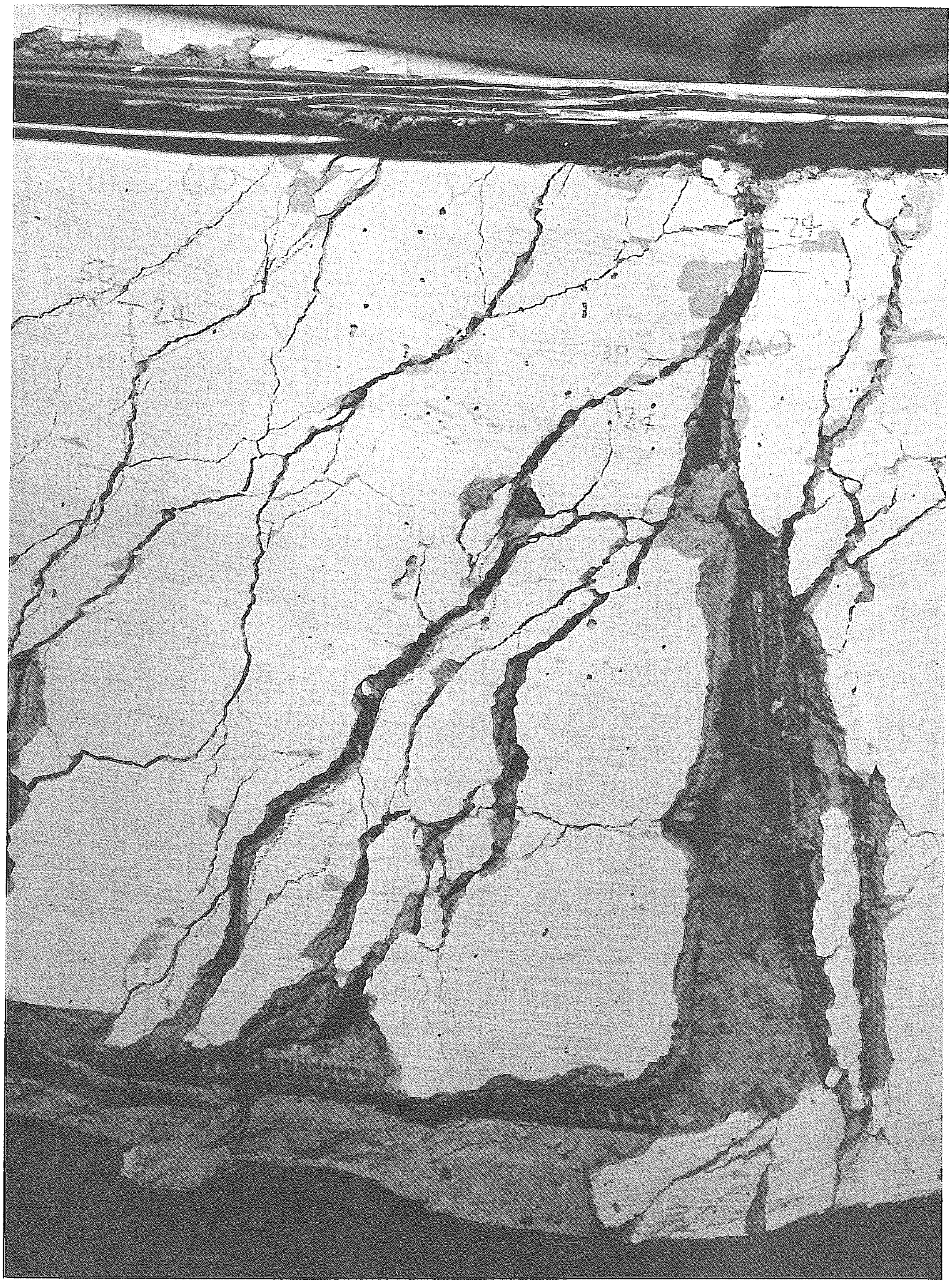

FIG. 80 FAILURE DETAILS AT 5X

FIG. 81 FAILURE DETAILS AT SECOND HINGE IN GIRDER 1

8.3 Ultimate Strength Behavior

It is of interest to review the results reported in Section 8.2 and compare for the different collapse mechanisms the experimental data with analytically predicted values.

Although the initial failure at Section Y was due to insufficient transverse load distribution in the undiaphragmed box girder section, full collapse only occurred, as will be shown later, after the full load distributing capacity of the section had been activitated and the entire cross section had reached a state of imminent yielding. An evaluation of the collapse mechanism will indicate a live-load over load capacity of better than 4. A similar conclusion will be drawn from the failure observed in Span I.

In reviewing the failure development in the undiaphragmed span II it becomes obvious that the two loads on the interior Girders 2 and 4 caused these girders to deflect more than both the exterior girders and the central interior girder (see Fig. 69). These smaller displacements of the exterior girders 1 and 5 at Section Y are misleading if compared with the mid span displacements at Section X as presented in Figs. 82 and 83 respectively. Both graphs show consistently, that, prior to failure, the displacements for the undiaphragmed span are smaller (10 - 15%) than those recorded for the diaphragmed span. This would indicate, assuming identical loads on each girder, that the undiaphragmed span is stiffer than the span without a diaphragm. In reality, however, the bending stiffness of both spans should be virtually identical. Hence, the unexpected behavior is clearly due to the poor load distribution of the undiaphragmed section resulting in the relatively limited load carried by the exterior girders in Span II. A

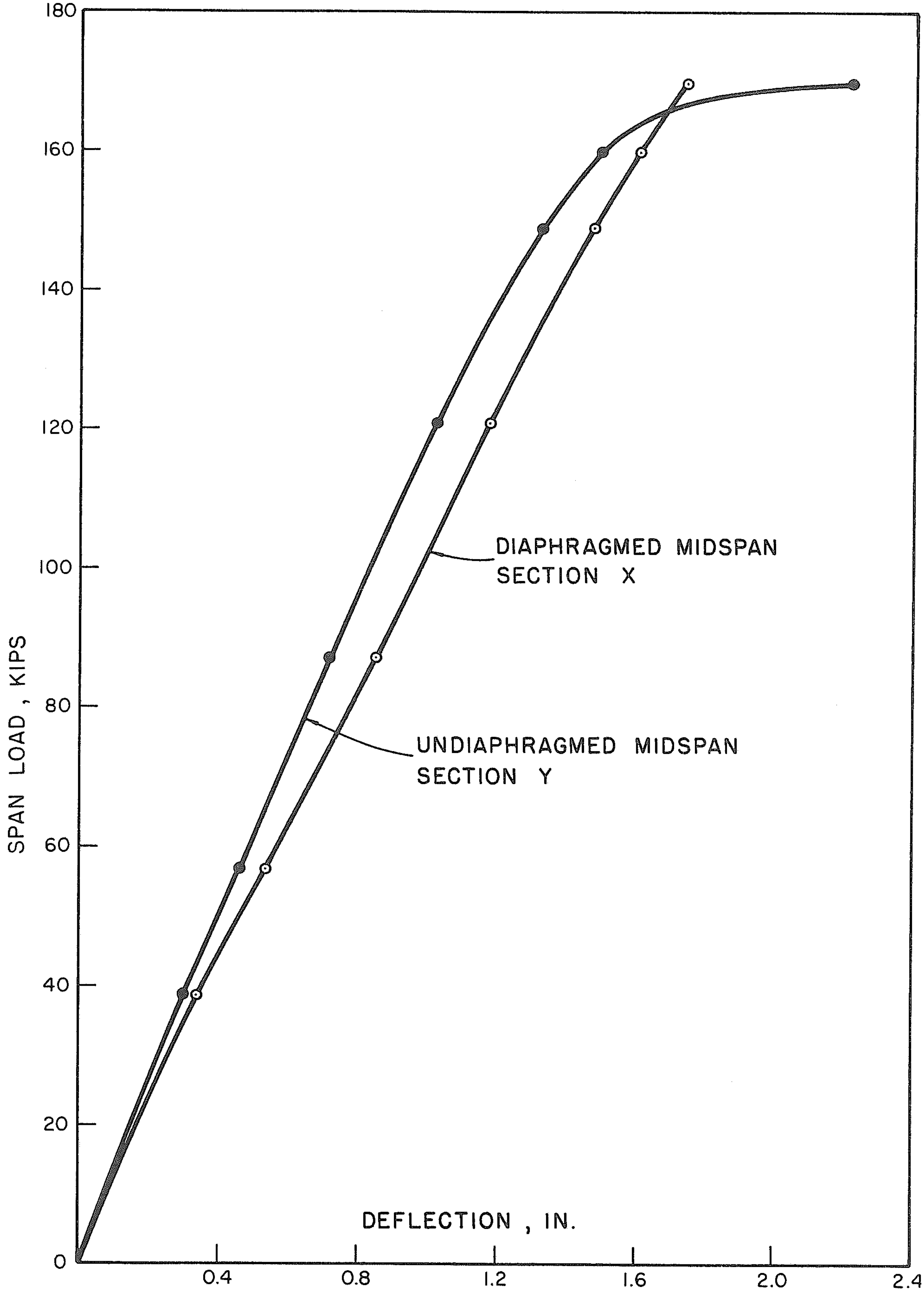

FIG. 82 LOAD-DEFLECTION GRAPHS FOR GIRDER 1 AT MIDSPAN SECTIONS DURING LOADING TO FAILURE

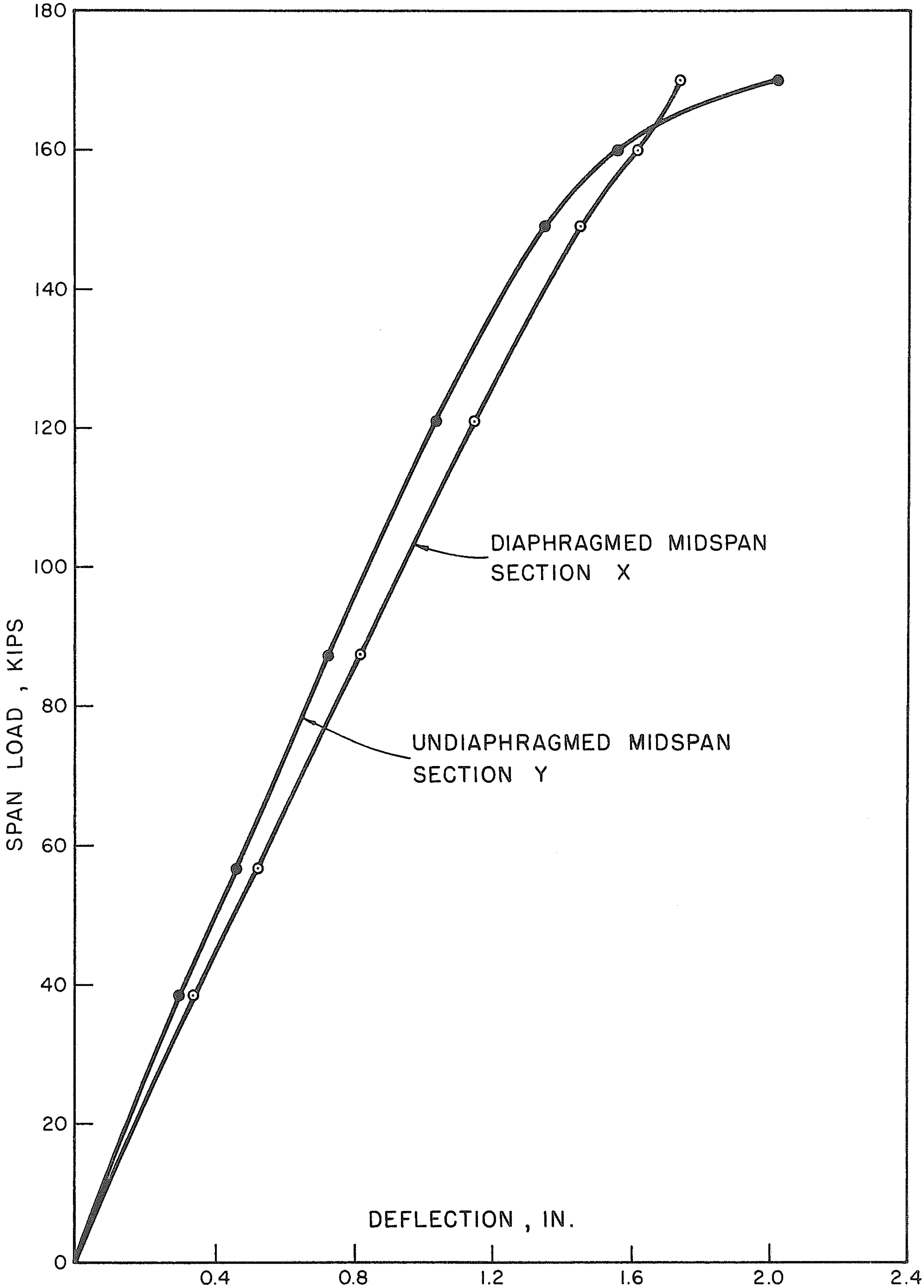

FIG. 83 LOAD-DEFLECTION GRAPHS FOR GIRDER 5 AT MIDSPAN SECTIONS DURING LOADING TO FAILURE

study of the displacements of the interior girders 2 and 4 would undoubtedly show larger displacements in Span II without a diaphragm as compared with the displacements in diaphragmed Span I.

The initial failure in Span II could in principle correspond with an incipient collapse machanism exhibiting full yield moments at both the loaded Sections X and Y and at the Sections B', and C' located at the edge of the center bent diaphragm or approximately 1 ft from the center support. However, no noticeable yielding at Section C' did occur. Therefore, a detailed investigation of the observed failure mode seems particularly interesting.

The tension steel in the midspan and support sections consisted of 55 #4 and 82 #4 bars, or 11.0 in ^{2} and 16.4 in^2 respectively.

As mentioned in the preceeding section initial failure occurred under a load of 170 kips in both spans. To compare the experimental data with analytically predicted values the dead load stress condition has to be taken into account. As reported in Vol. I, Table 1, the nominal dead load stress in the tension steel at the midspan Sections X and Y was 11.45 ksi. and at the edge of the center bent diaphragm 12.56 ksi.

Considering a yield stress f_y = 62 ksi, as based on test results (Vol. I), an internal lever arm of 1.5 ft and the above dead load stresses, the additional moments required to develop a yield moment at the midspan and support sections were 835 kip-ft and 1215 kip-ft respectively.

Analysis indicates that under increasing midspan loads the midspan yield moment was to be reached at a load of P = 156 kips. Furthermore, increasing the center span loads to 170 kips each would result in the development of the yield moments on either side of the center support diaphragm as well. Although this latter load agrees exactly with the actual test failure load, the failure mode did not indicate the complete development of a mechanism associated with the above calculated load of 170 kips. It is therefore particularly interesting to postulate the sequence of events which led to the observed failure in the undiaphragmed span. Initially, failure probably started with the development of a yield moment at midspan in girders 2 and 4. This occurred undoubtedly even before the 156 kip load, associated with the yield moment in the entire midspan section was reached. This development seems to be supported by the load-deflection graphs in Figs. 82 and 83, which show a gradually increasing midspan deflection from about 140 kips on. After having passed 156 kips and reached 160 kips the mid-span displacement rapidly increases indicating that the midspan yield moment was fully developed. Based on the displacements at failure as shown in Fig. 69 it is obvious that girder 2 and 4 must have carried a proportionally larger part of the applied load. Hence, yield moments at both the midspan and support sections did probably already occur in these girders before the failure load of 170 kips was applied to the bridge. It is in this respect particularly important to note that the transverse load-carrying capacity of the bridge model was adequate to transfer the overload on the girders 2 and 4 to the exterior and center girders (nos. 1, 5 and 3) in order to develop, as it seems, the full load-carrying capacity of the bridge cross-section. The proof of this hypothesis was unfortunately lost when the ram bearing plate above girder 2 punched through the top slab at a total midspan load of 170 kips. However, it can be assumed that overall failure in the undiaphragmed span, reflecting the earlier assumed failure mechanism, was imminent.

Based on the observed failure load and the existing yield condition at that instance one can note a substantial live load over load capacity of (62-11.45)/12.55 or 4.

In the development of the above discussed failure mode the occurence of two additional failure phenomena related to the transverse bridge action should be noted. Firstly, the development of longitudinal cracks in the bottom and top slabs in the central region of the span indicated the strained transverse load distributing action of the box girder section. Secondly, shear cracks in the bottom slab near the exterior girders on either of the midspan section and propagating under 45° towards the end and center supports signify both the horizontal shear transfer to activate the load carrying capacity of the exterior girders and the critical torsional action of the exterior cells prior to total collapse. Both crack patterns already gradually developed during the application of the previous conditioning loads. After the blocking up of Span II, the final failure in Span I, under a known load of 170 kips in Span I only was due to a yielding of the steel in the bottom slab at midspan (Section X) and probably a combined yielding of the top deck steel and a crushing of the concrete in both the bottom slab and webs at a distance between 8 feet (girder 1) and 10 feet (girder 5) from the center support. The crushing at the latter locations might well have been affected by the termination in that region of the flared portion of the web. Another aspect which contributed to the initial failure in this particular region (8 to 10 feet away from the center support) was the significant and rather abrupt reduction of the tensile reinforcing steel in the top slab, namely:

@ 7 1/2 ft = reduction 12 # 4 from 56 to 44 bars

@ 8 ft = reduction 4 # 4 to 40 bars

@ 9 ft = reduction 14 # 4 to 26 bars

@ 10 ft = reduction 8 # 4 to 18 bars

@ 11 ft = reduction 8 # 4 to 10 bars.

Furthermore, the weakness of the cantilever section of the top slab due to the serious reduction of the longitudinal tensile reinforcement near the edge might also have contributed to failure in these regions. An early failure of the cantilever portion would initiate complete failure of the overall weakened bridge cross section.

The progressive failure in the negative moment zone seems to have been due to crushing of the concrete, and buckling of the light compression reinforcement in the web followed later on by an overall separation of the bottom slab from the girder webs (see Figs. 77, 78 and 81). This failure development (loss of strength) seems to be supported by the considerable load drop off following failure, as shown in Fig. 74.

An evaluation of the failure load on the basis of full yielding of the tensile steel in the failed sections at midspan (Section X) and at points 8 to 10 feet away from the center support give some interesting results. Considering a section 8 feet from the center support with 40 #4 bars, the yield moment would be: (40 x 0.2) (62) (1.5) = 744 kip—ft. As before the yield moment at midspan can be assumed at 1025 kip—ft. In order to evaluate the failure load the dead load stresses have to be considered. With a dead load stress of 11.45 ksi at midspan the supplemental moment due to the applied load should only be (50.55/62) 1025 = 835 kip-ft. At the section 8 feet from the center support practically a zero dead load moment and stress exist. On the basis of the above conditions failure would occur under a load of 203 kips. Since failure in the negative moment zone occurred in a skew pattern, the section 10 feet away from the center support should also be considered. This section having 18 #4 bars in the top slab would yield under a moment of 335 kip-ft. Based on the same dead load stress assumptions as mentioned above the corresponding failure load would be 191 kips. Comparing the two calculated failure loads with the observed failure load of 170 kips one might conclude that the failure mechanism did not reflect complete yielding at both sections. Should one, however, assume that a one-foot bond length is insufficient to develop the full yield load in these #4 reinforcing bars the number of bars effective at the above noted sections would reduce to 26 and 10 #4 bars respectively. Hence, with the yield moments reduced to 484 kip ft and 186 kip ft respectively and assuming the same dead load stress conditions, the failure loads would reduce to 177 kips and 172 kips respectively. These values are fairly close and in relatively good agreement with the observed failure load of 170 kips in the diaphragmed span. However, it seems reasonable nevertheless to conclude that the final failure in this postion of the span was probably initiated by a crushing failure of the webs and bottom slab in the negative moment zone just prior to the full yielding of the deck slab reinforcing steel. Hence the final failure was only a partial yield mechanism as postulated before. Again it should be noted that the live load overload capacity was slightly better than 4, which is a substantial value.

8.4 Summary

Failure of the box girder bridge developed in two phases. During the first phase, with equal loads applied at the midspan locations above girders 2 and 4, an incipient yield mechanism failure occurred at Section Y of the undiaphragmed span under a load of 170 kips in each span. This implies that nominal yield stresses of 62 ksi were reached. Hence, the bridge model exhibited, with a live load factor of safety of (62 - 11.45)/12.55 = 4.0, a substantial overload capacity. This is particularly significant since the bridge cross-section was seriously strained to provide an adequate load transfer to the exterior girders. Despite significant longitudinal cracking in the top and bottom slabs, and the occurrence of diagonal shear cracks in the bottom slab as a result of the transverse load transfer, the bridge section continued to carry a load until a yield mechanism was about to be formed. Unfortunately shortly after yielding developed the load distribution pad of one of the rams punched through the deck slab and the test had to be terminated. This particular failure is virtually impossible in case of a bridge subjected to actual truck loads from several wheels, even when these trucks are substantially heavier than the standard design trucks. The two point loadings at Sections X and Y, created an extreme load condition which required the full load distributing capacity of the undiaphragmed span. That the model could withstand this loading until a point where yield moments were virtually fully developed over the entire cross-section is most remarkable and shows the strength of this type of bridge.

The second failure phase occurred while loading only the diaphragmed span and fixing the failed undiaphragmed span at a permanent displaced position. Failure in this instance was caused by reaching a yield moment at the midspan Section X of the diaphragmed span and a skewly oriented hinge mechanism in the negative moment region of the same span. This hinge traversed the deck plate from a point above girder 1 and 8 feet from the center support to a point located above girder 5 at a distance of 10 feet from the center support. This failure also occurred under a load of 170 kips. Indications are that prior to the development of a complete yield mechanism crushing of the reinforced concrete webs and bottom deck occurred. It seems safe to state that if formation of this hinge mechanism had not occurred a complete yield mechanism was imminent. Again a substantial live load over load factor of 4 should be noted.

9. CONCLUSIONS AND RECOMMENDATIONS FOR IMPLEMENTATION

A detailed presentation of the reduction, analysis and interpretation of the experimental and theoretical results obtained in testing a large scale, two span, four cell, reinforced concrete box girder bridge model has been given. Results, in terms of reactions, deflections, strains and moments, for the response of the bridge to dead load, working stress loads and at or after overload stress levels have been presented. Single or several point loads, AASHO standard truck loads, construction vehicle loads and a moving fork lift truck load have all been considered. The behavior under sustained dead load during the load history of the model has been described. Finally, the structural behavior during the final loading phase to failure has been discussed in detail.

Theoretical results referred to below were based either on FINPLA2, a finite element computer program which treats the bridge as a true three dimensional assembly of plate elements or on 1DFRAME, a computer program which treats the bridge as a simple equivalent planar frame consisting of one dimensional frame elements. Thus FINPLA2 gives transverse as well as longitudinal distributions of reactions, forces, moments and displacements, while 1DFRAME can give only the longitudinal distributions of total reactions, forces and moments and the average deflection at a transverse section. Both FINPLA2 and IDFRAME treat the bridge as an uncracked homogeneous structure.

The most important conclusions from this study are summarized below.

1. The distribution of total reactions between the east, center and west supports is accurately predicted by theory for all load levels and types of loads studied. Either FINPLA2 or 1DFRAME can be used for the theoretical solutions.

2. The transverse distribution of the total reactions at each end to individual reaction supports is highly dependent on the type and the manner of installation of the supports and is difficult to predict by theory unless the spring constant of each individual support is accurately known.

3. As a result of 1 the total external moment at any section of the bridge can be found by theory with confidence. Moments calculated from reactions are least sensitive to small errors in the values of the reactions for moments in midspan regions and most sensitive for moments over the central support bent.

4. From a study of 19 different midspan point load combinations it can be concluded that the total reactions and the total moment at any section are independent of the transverse position of the point loads.

5. The transverse distribution of the total moment at a section, in terms of percentage to each girder, can be accurately predicted by theory at working stress levels for both single point loads and uniform loads across the width of the bridge. At or after overload stress levels, agreement between theory and experiment decreases somewhat for single point loads, but remains good for uniform loads across the width of the bridge. Since actual critical girder design moments are based on

several wheel loads acting on the bridge width, the theory should be adequate for predicting design moments even at or after overload stress levels.

6. Theory predicts the magnitude and distribution of live load deflections under point loads quite well for the 24 ksi and 30 ksi steel working stress levels provided theoretical values based on uncracked sections are multiplied by a factor of about 1.5 to account for cracking. At or after higher stress levels of 40, 50 or 60 ksi the theory can no longer be used to accurately predict the distribution of deflections under point loads. After the 60 ksi conditioning load, deflections ranging from 1.2 to 2.1 times the theoretical value were found for points some distance away and directly under the point load respectively.

7. Midspan dead load deflections immediately after removing the shoring generally ranged from 0.38 to 0.44 inches which were 1.5 to 1.7 times theoretical values respectively. During the following three weeks the deflections under sustained dead load increased 50% after which they remained constant until the application of live load. Subsequent application of live loads causing increasingly higher steel stresses of 24, 30, 40, 50 and 60 ksi produced additional cracking and permanent deflections so that at a time 3 months after removal of the shoring and just prior to loading to failure, the sustained dead load midspans deflections had increased to 1.50 inches or about 4 times the initial dead load deflection.

8. Comparing the effects of torsional support restraints at the center bent with the normal restraint case, the differences in results were small and could be ignored in practical design problems with similar center bent configurations. The differences were much larger however, where longitudinal restraints at the bottom of the end diaphragms were introduced and this effect should be considered in design if it exists.

9. Both theoretical and experimental results show that for the bridge tested the AASHO empirical formula $N_{WL} = S/7$ over-estimates the actual value of the girder moment slightly for a two lane truck loading but underestimates it by as much as 23% for the three lane truck loading on the bridge.

10. The final loading to failure demonstrated that this type of bridge has an excellent overload capacity of 4 on the live load and has the ability, through its high torsional strength, to transfer loads laterally almost up to failure.

11. Differences between the behavior of Span I with a disphragm and Span II without a diaphragm were not significant at working stress levels, but became more pronounced at very high over-stress levels and during the final loading to failure.

On the basis of the above conclusions it appears that the theoretical methods and computer programs previously developed at the University of California for straight multi-cell box girder bridges [1, 2, 5] can be used as accurate methods of analysis in unusual design cases not covered in standard AASHO specifications and also they can be used to develop an improved simplified design method which might replace the present AASHO method. A report [3] containing detailed analytical studies in this regard and preliminary recommendations was published in 1969. It is now recommended that for implementation, a joint effort be made by representatives of the State of California Bridge Department and the faculty investigators at the University of California to develop a final recommendation for a simplified design method for straight box girders, which will include all important parameters, but yet be practical enough for use in the design office.

10. ACKNOWLEDGEMENTS

The planning, preparation, construction, supervision, testing, control, analysis and data reduction for a research project of the scope and size of the box girder bridge model of the present study necessitate the cooperative assistance and teamwork of all involved.

From the State of California Division of Highways, Mr. G. D. Mancarti, Supervising Bridge Engineer, Mr. R. E. Davis, Senior Bridge Engineer, and their staff maintained a close and keen interest in the project in all its stages.

Mr. R. M. Stephen, S.E.M. Laboratory Manager, actively participated in the preliminary planning, design, instrumentation and construction of the box girder bridge model, and deserves special thanks for his assistance and interest.

The various Research Assistants, Students and Staff working for different periods on the box girder bridge model from its inception to its completion -- Messrs. F. Aksel, B. Atalay, A. Kanaan, O. Küstü, D. Lee, R. Loew, A. Oyekan and B. Sarkar -- deserve sincere thanks for their hard work and enthusiasm. Mr. D. Ngo gave much help in organizing the vast mass of experimental data, and Mr. C. S. Lin was of assistance with the theoretical analyses. Mr. A. Kabir participated extensively in the preparation of the figures and tables in Volumes II and III.

Finally, acknowledgement is due to the draftsman, Mr. A. Klash, and the typist, Mrs. S. Edwards for their share in the production of the report.

The work described in this report was part of a continuing research project in the Department of Civil Engineering, University of California at Berkeley, under the sponsorship of the Division of Highways, Department of Public Works, State of California, and the Bureau of Public Roads, Federal Highway Administration, United States Department of Transportation. The opinions, findings and conclusions expressed in this report are those of the authors and not necessarily those of the sponsors.

11. REFERENCES

1. Scordelis, A. C., "Analysis of Simply Supported Box Girder Bridges," Structural Engineering and Structural Mechanics Report No. 66-17, University of California, Berkeley, October 1966 (PB 175 646).

2. Scordelis, A. C. "Analysis of Continuous Box Girder Bridges," Structural Engineering and Structural Mechanics Report No. 67-25, University of California, Berkeley, November 1967 (PB 178 355).

3. Scordelis, A. C., and C. Meyer, "Wheel Load Distribution in Concrete Box Girder Bridges," Structural Engineering and Structural Mechanics Report No. 69-1, University of California, Berkeley, January 1969 (PB 183 923).

4. Willam, K. J., and A. C. Scordelis, "Analysis of Orthotropic Folded Plates with Eccentric Stiffeners," Structural Engineering and Structural Mechanics Report No. 70-2, University of California, Berkeley, February 1970 (PB 191 051).

5. Meyer, C., and A. C. Scordelis, "Computer Program for Prismatic Folded Plates with Plate and Beam Elements," Structural Engineering and Structural Mechanics Report No. 70-3, February 1970 (PB 191 050).

6. Meyer, C., and A. C. Scordelis, "Analysis of Curved Folded Plate Structures," Structural Engineering and Structural Mechanics Report No. 70-8, University of California, Berkeley, June 1970 (PB 193 535).

7. Willam, K. J., and A. C. Scordelis, "Computer Program for Cellular Structures of Arbitrary Plan Geometry," Structural Engineering and Structural Mechanics Report No. 70-10, University of California, Berkeley, September 1970 (PB 196 143).

8. Meyer, C., "Analysis and Design of Curved Box Girder Bridges," Structural Engineering and Structural Mechanics Report No. 70-22, University of California, Berkeley, December 1970 (PB 197 289).

9. Bouwkamp, J. G., Scordelis, A. C., and Wasti, S. T., "Structural Behavior of a Two Span Reinforced Concrete Box Girder Bridge Model," UCSESM Report No. 71-5, University of California, Berkeley, April, 1971 (PB 199 187).